

CLIMATOGRAPHY
OF THE
IDAHO NATIONAL
ENGINEERING
LABORATORY

2nd Edition

December 1, 1989

Kirk L. Clawson
G. E. Start
Norman R. Ricks
Editors

U. S. Department of Commerce
National Oceanic and Atmospheric Administration
Environmental Research Laboratories
Air Resources Laboratory
Field Research Division
Idaho Falls, ID 83402

NOTICE

This report was prepared as an account of work sponsored by an agency of the United States Government. Neither the United States Government nor any agency thereof, or any of their employees, makes any warranty, expressed or implied, or assumes any legal liability or responsibility for any third party's use, or the results of such use, of any information, apparatus product or process disclosed in this report, or represents that its use by such third party would not infringe privately owned rights.

GENERAL PREFACE

The primary goal of the Air Resources Laboratory is to advance the state of knowledge of the transport, dispersion, and removal of those materials in the atmosphere usually regarded as pollutants. Progress toward this goal is sought by studies of both mean and turbulent atmospheric flow characteristics on all scales of motion, and by studies of the history of a wide variety of tracers incidentally or purposefully introduced into the atmosphere. The Laboratory works closely with the U. S. Department of Energy, the U. S. Environmental Protection Agency, the U. S. Department of Defense, and a multitude of other federal and local agencies in an advisory or participating capacity on programs dealing with pollution from a variety of single and multiple source configurations from both urban and rural complexes. The programs may involve studies of pollutant materials which are found in the friction layer, the upper troposphere, or the stratosphere.

PREFACE

Numerous research and climatological reports have been published about the Idaho National Engineering Laboratory (INEL) by the Field Research Division of the Air Resources Laboratory, or the various agency names under which this office has operated. Several preliminary reports were prepared in the late 1940's which described the expected climatology of the INEL. The first series of reports using meteorological data acquired on-site was published during the time period from 1958 to 1960 (IDO-12003, IDO-12004, and IDO-12015). A major addition to that original body of climatological literature was the first edition of the "Climatology of the National Reactor Testing Station" (IDO-12048). Each of these reports were written primarily to: 1) provide engineers, health physicists, scientists, and other researchers with a source of meteorological information pertinent to designing, locating, and operating nuclear reactors and support facilities, and 2) provide insight into the atmospheric aspects of health physics.

Following the publication of the first edition of the INEL climatology, many specialized research studies of atmospheric transport and diffusion at the INEL have been conducted and reported. Additional climatological data have also been acquired in the intervening years. It is, therefore, appropriate that the climatology of the INEL be revised, updated, and enhanced with these sources of information.

This second edition of the INEL climatology builds significantly on the material found in its predecessor. It is not, however, intended to be a replacement of all preceding climatological documents. It also does not provide guidance describing methods whereby the climatological data are to be utilized. Nevertheless, most of the meteorological and climatological information needed for the purpose of assessing the location, the design, and the operation of facilities within the setting of the INEL are provided.

This publication is identified as DOE/ID-12118 and is the second edition of IDO-12048 which was issued in 1966. It updates chapters I (Introduction), II (Climatological Data and Studies), III (Calculation of Atmospheric Dispersion from Sources at the NRTS), and V (Atmospheric Transport). It also includes a partial update of chapter IV (Persistence and Extreme Values). This edition provides averages and extreme values for most of the various meteorological parameters monitored by the Field Research Division of the Air Resources Laboratory (ARLFRD). The only analysis of these data appears in the atmospheric transport and diffusion chapter. Further analyses will appear as separate volumes. These volumes will be prepared from the climatological data sets of DOE/ID-12118 and subsequently acquired data sets. The volumes will be prepared as requested to aid in the analysis of proposed project sites or in support of ongoing operations.

K. L. Clawson
G. E. Start
N. R. Ricks

ACKNOWLEDGEMENTS

This edition of the "Climatology of the Idaho National Engineering Laboratory" is the culmination of the efforts of various personnel (both past and present) employed by the Field Research Division of the Air Resources Laboratory (ARLFRD), and the efforts of others funded by special supporting contracts. The material presented herein contains a portion of the texts prepared by those individuals.

The talent and efforts of Mr. G. A. DeMarrais, author of the initial series of climatological reports, is greatly appreciated. His articles set the foundation upon which all succeeding reports have been built.

The endeavors of Messrs. G. R. Yanskey, E. H. Markee, Jr., and A. P. Richter, authors of the first edition of the INEL climatology, are greatly appreciated. The format of this second edition is closely patterned after their original text. A significant amount of their original material is also included in this edition.

Recognition is also given to the Morrison-Knudson Environmental Services Division, Boise, Idaho, which prepared the revised statistics, figures, tables, and supporting text of the initial draft of this document.

The contribution of Kay Taylor of EG&G in the preparation of the INEL regional maps is greatly appreciated.

Recognition is given to Mr. C. Ray Dickson, Director, ARLFRD, under whose guidance this report was completed. The contributions of the present staff of the ARLFRD is gratefully acknowledged. Messrs. J. F. Sagendorf, N. F. Hukari, and G. R. Ackermann helped with data archiving, computer programming, data base management, figure and table preparation, and also contributed through helpful discussions and suggestions. The efforts of Mrs. Dianne Hoover, desk-top publisher and proofreader, are also greatly appreciated.

Funding for this project was provided by the U. S. Department of Energy, Idaho Operations Office.

TABLE OF CONTENTS

I. INTRODUCTION	1
II. AREA PHYSIOGRAPHIC DESCRIPTION	3
III. METEOROLOGICAL OBSERVATION NETWORK	5
IV. GENERAL CLIMATOLOGY	11
V. SPECIFIC CLIMATOLOGY	13
A. Wind	13
On-site Near-surface Wind Flow Patterns	14
On-site Wind Averages and Maximums	27
Regional Near-surface Wind Flow Patterns	28
Winds Aloft	37
B. Air Temperatures	47
Daily Near-Surface Characteristics	47
Monthly and Annual Near-Surface Characteristics	53
Surface Spatial Variations	54
Specific Temperatures	56
Upper Air General Characteristics	62
Profile Characteristics to 250 ft. AGL	63
Profile Characteristics Above 250 ft	63
C. Soil Temperatures	71
Soil Surface Characteristics	71
Subsoil Characteristics	73
D. Precipitation	76
General Characteristics	76
Frequency and Duration Characteristics	76
Snow	80
E. Atmospheric Moisture	87
Wet Bulb Temperature	87
Relative Humidity	87
Dew Point Temperature	91
Mixing Ratio	91
Pan Evaporation	91
F. Solar and Terrestrial Radiation	94
Sunrise and Sunset Times	94
Solar Radiation	94
Net Radiation	94
Sky Cover	97
G. Atmospheric Pressure	97
Station Pressure	97
Air Density	98

H. State of the Ground	99
I. Special Phenomena	100
Dew	100
Thunderstorms	100
Lightning	100
Hail	101
Airborne Dust and Sand	101
Dust Devils	101
Blowing Snow	101
Icing	101
Tornadoes	102
VI. ATMOSPHERIC TRANSPORT AND DIFFUSION	105
A. Atmospheric Transport	105
Winds Aloft and Synoptic Forcing	105
Topographic Influences	106
Diurnal Wind Cycles	106
Mesoscale Winds at the INEL and Regional Trajectories	107
B. Atmospheric Diffusion	114
The Diffusion Equation	114
Evaluation of Parameters in the Diffusion Equation	115
Measured Diffusion Parameters	116
Available Mathematical Models	124
Vertical Diffusion	124
Horizontal Diffusion	125
Facility Influences and Source Configurations	126
Structure Wake Effects	126
Source Elevation	127
Plume Rise	127
Effects of Cooling Towers and Ponds	128
Removal Processes and Transformations	128
Deposition	128
Decay	128
Precipitation Scavenging	128
C. Normalized Dispersion Concentration Fields	129
REFERENCES	133
APPENDICES	
1. Surface Air Temperature Extremes	137
2. Precipitation Extremes	149
3. Snow Fall Extremes	151
4. Snow Depth Extremes	153

LIST OF FIGURES

Figure II-1. Location of the INEL in relation to regional state boundaries	3
Figure II-2. Topographic depiction of the INEL and surrounding area	4
Figure III-1. Geographic location of 26 of the 27 active INEL meteorological monitoring stations (TRA is located approximately 3 mi. west-southwest of GRD3)	8
Figure A-1. Annual and seasonal wind roses for the 20 ft. level at CFA from January 1950 through May 1962	15
Figure A-2. Annual and seasonal wind roses for the 20 ft. level at CFA under lapse conditions from January 1950 through May 1962	16
Figure A-3. Annual and seasonal wind roses for the 20 ft. level at CFA under inversion conditions from January 1950 through May 1962	17
Figure A-4. Annual and seasonal wind roses for the 250 ft. level at CFA from July 1951 through May 1962	18
Figure A-5. Annual and seasonal wind roses for the 250 ft. level at CFA under lapse conditions from July 1951 through May 1962	19
Figure A-6. Annual and seasonal wind roses for the 250 ft. level at CFA under inversion conditions from July 1951 through May 1962	20
Figure A-7. TAN 20 ft. level wind roses, November 1952 through May 1962	21
Figure A-8. Annual and seasonal wind roses for the 20 ft. level at TAN under lapse conditions from November 1952 through May 1962	22
Figure A-9. Annual and seasonal wind roses for the 20 ft. level at TAN under inversion conditions from November 1952 through May 1962	23
Figure A-10. Annual and seasonal wind roses for the 150 ft. level at TAN from May 1956 through May 1962	24
Figure A-11. Annual and seasonal wind roses for the 150 ft. level at TAN under lapse conditions from May 1956 through May 1962	25
Figure A-12. Annual and seasonal wind roses for the 150 ft. level at TAN under inversion conditions from May 1956 through May 1962	26
Figure A-13a. Regional INEL wind flow patterns indicated by off-site and some on-site meteorological monitoring stations	31
Figure A-13b. Local INEL wind flow patterns indicated by wind roses from on-site meteorological monitoring stations	32
Figure A-14. Joint wind speed and direction frequency distributions for Aberdeen (ABN), Argonne National Laboratory-West (ANL), Arco (ARC), Blue Dome (BDM), Blackfoot (BLK), and Big Southern (BSN) during 1980 through 1982	33
Figure A-15. Joint wind speed and direction frequency distribution for CFA, Dubois (DBS), Dunes (DUN), GRD3 32.8 ft. level (GRDL), GRD3 200 ft. level (GRDU), and Hamer (HMR) during 1980 through 1982 (1981 through 1982 for GRD3)	34
Figure A-16. Joint wind speed and direction frequency distributions (wind roses) for Howe (HOW), Idaho Falls (IDF), Kettle Butte (KTB), Minidoka (MIN), Montevieu (MTV), and the Naval Reactor Facility (NRF) during 1980 through 1982	35
Figure A-17. Joint wind speed and direction frequency distributions (wind roses) for Power Burst Facility (PBF), Roberts (RBT), Richfield (RCH), Rover (ROV), Radioactive Waste Management Center (RWMC), and St. Anthony (STA) during 1980 through 1982	36

Figure A-18. Joint wind speed and direction frequency distributions (wind roses) for the Loss of Fluid Test 32.8 ft. level (TANL), Loss of Fluid Test 150 ft. level (TANU), Tabor (TBR) and Terreton (TRN) during 1980 through 1982	37
Figure A-19. Joint wind speed and direction frequency distributions (wind roses) stratified by air temperature stability class (A-F) for 32.8 ft. level at Grid 3 (GRD3) during 1981 and 1982	38
Figure A-20. Joint wind speed and direction frequency distributions (wind roses) stratified by air temperature stability class (A-F) for the 200 ft. level at Grid 3 (GRD3) during 1981 and 1982	39
Figure A-21. Upper air wind roses obtained from pibal soundings for the winter season (December-February) during 1950 through 1965	40
Figure A-22. Upper air wind roses obtained from pibal soundings for the spring season (March-May) during 1950 through 1965	41
Figure A-23. Upper air wind roses obtained from pibal soundings for the summer season (June-August) during 1950 through 1965	42
Figure A-24. Upper air wind roses obtained from pibal soundings for the fall season (September-November) during 1950 through 1965	43
Figure A-25. Upper air wind roses obtained from pibal soundings for the combined for all seasons during 1950 through 1965	44
Figure A-26. Seasonal and annual average upper air wind speeds obtained from pibal observations during 1950 through 1965	45
Figure A-27. Example upper air wind speed and direction profiles during conditions of strong pressure gradients (24 December 1964), weak pressure gradients (11 January 1965) and air temperature inversions (12 December 1964)	46
Figure B-1. Mean weekly minimum, average, and maximum air temperatures at CFA from January 1950 through December 1988	52
Figure B-2. Normalized daily maximum, average, and minimum air temperatures at TAN from 1930 through 1959	52
Figure B-3. Average time of onset and dissipation of the nocturnal inversion as a function of time of year	66
Figure B-4. Typical winter season (December-February) air temperature profiles (solid line) as a function of time of day plotted together with the dry adiabatic lapse rate (dashed line). Data were obtained above both a bare and a snow covered surface	67
Figure B-5. Typical spring (March-May) season air temperature profiles (solid line) as a function of time of day plotted together with the dry adiabatic lapse rate (dashed line). Data were obtained above both a bare and a snow-covered surface	68
Figure B-6. Typical summer (June-August) season air temperature profiles (solid line) as a function of time plotted together with the dry adiabatic lapse rate (dashed line). Data were obtained above a bare surface	69
Figure B-7. Typical fall (September-October) season air temperature profiles (solid line) as a function of time of day plotted together with the dry adiabatic lapse rate (dashed line). Data were obtained above a bare surface	70
Figure B-8. Typical high-level air temperature soundings for the summer and winter seasons taken near sunrise (thick solid line) and approximately 6 hours later (dashed line) and plotted together with the dry adiabatic lapse rate (thin solid line)	71
Figure C-1. Average monthly subsoil temperatures beneath a bare soil surface.	73
Figure C-2. Average monthly subsoil temperatures beneath an asphalt surface	74
Figure C-3. Selected average monthly soil temperature profiles beneath asphalt (top) and bare sandy soil (bottom) surfaces	74

Figure D-1. Average weekly total precipitation for CFA from January 1950 through December 1988	79
Figure D-2. Average weekly total snow fall for CFA from January 1950 through December 1988	84
Figure D-3. Average weekly snow depths for CFA from January 1950 through December 1988	86
Figure E-1. Seasonal and annual cumulative frequency distributions of wet bulb temperatures	89
Figure E-2. Average hourly relative humidity for winter, spring, summer, and fall seasons represented by data from January, April, July, and October, respectively	90
Figure E-3. Estimated CFA pan evaporation utilizing a regression analysis of data from southeastern Idaho. Dashed lines indicate the 99% confidence limit about the mean	93
Figure F-1. Annual traces of maximum daytime, average daytime, 24-hour, and nocturnal total daily net radiation	96
Figure I-1. Tornado sightings in the ESRP according to National Severe Storms Forecast Center Statistics from 1950 through 1987	103
Figure VI-1. Example trajectory for type A, characterized by sustained northeasterly winds	107
Figure VI-2. Example trajectories for types E (top), B (bottom left), and I (bottom right), characterized by sustained southerly or southwesterly winds	108
Figure VI-3. Example trajectories for types G (top) and H (bottom), characterized by localized wind recirculations	109
Figure VI-4. Example trajectories for types C (top), D (bottom left), and L (bottom right), characterized by diurnal wind reversals from a down-valley to an up-valley flow	110
Figure VI-5. Example trajectories for types J (top) and K (bottom), characterized by diurnal wind reversals and synoptic frontal passages	111
Figure VI-6. Example trajectory for type F, characterized by sustained wind flow along a shear line	112
Figure VI-7. σ_y versus downwind distance as a function of stability class for a 3 to 15 minute release time (Hilsmeier and Gifford, 1962)	118
Figure VI-8. σ_z versus downwind distance as a function of stability class for a 3 to 15 minute release time (Hilsmeier and Gifford, 1962)	119
Figure VI-9. Relative axial concentration versus downwind distance as a function of stability class for a 3 to 15 minute release time (Hilsmeier and Gilford, 1962)	120
Figure VI-10. σ_y versus downwind distance as a function of stability class for a 15 to 60 minute release time (Markee 1963). The dashed portions of each line represent extrapolations according to data from Fugway et al., 1963)	121
Figure VI-11. σ_z versus downwind distance as a function of stability class for a 15 to 60 minute release time (Markee, 1963). The dashed portions of each line represent extrapolations according to data from Fugway et al., 1963)	122
Figure VI-12. Relative axial concentration versus downwind distance as a function of stability class for a 15 to 60 minute release time (Markee, 1963). The dashed portions of each line represent extrapolations according to data from Fugway et al., 1963)	123
Figure VI-13. Monthly averages of the maximum daily mixed layer depth	125
Figure VI-14. 95% level, fourth-order curves of frequency of normalized concentration versus scaled distance	127
Figure VI-15. Annual normalized total integrated concentration ($\text{h}^2/\text{m}^3 \times 10^{-9}$) for ICPP from 1974 through 1983	130
Figure VI-16. Annual normalized total integrated concentration isopleths ($\text{h}^2/\text{m}^3 \times 10^{-9}$) for ICPP during 1988	131

LIST OF TABLES

Table III-1. Active INEL meteorological monitoring stations, as of December 31, 1988, together with identification codes and periods of record for air temperature, precipitation, and wind speed and direction	6
Table III-2. Active INEL meteorological monitoring stations co-located with National Climatic Data Center (NCDC) stations, accompanied with NCDC identification codes and NCDC periods of record for air temperature and precipitation	7
Table III-3. Discontinued INEL meteorological monitoring stations, together with identification codes and periods of record for air temperature, precipitation, and wind speed and direction	9
Table IV-1. Compilation of National Climatic Data Center (NCDC) temperature and precipitation records for observation stations on and surrounding the INEL from the years 1981-1985. N/A indicates that the data is not available for a given station. Normals are average data from the 30 year period of 1951 - 1980	12
Table A-1. Average monthly and annual wind speeds for CFA at 20 and 250 ft. AGL together with the highest hourly average wind speed and the concurrent direction of occurrence	28
Table A-2. Average monthly and annual wind speeds for TAN at 20 and 150 ft. AGL together with the highest hourly average wind speed and the concurrent direction of occurrence	29
Table A-3. Monthly and period of record peak wind gusts with concurrent wind directions for CFA at 20 and 250 ft. AGL and for TAN at 20 and 150 ft. AGL	30
Table B-1. Average daily air temperature (Mean), daily air temperature range (RNG), and daily heating degree-days (Heat.DGD) for CFA from January 1950 through December 1988	48
Table B-2. Normalized average daily air temperature (Mean), daily air temperature range (RNG), and daily heating degree-days (Heat.DGD) for TAN from 1930-1959	50
Table B-3. Average (or normal) and maximum daily air temperature ranges summarized by month for CFA and TAN	53
Table B-4. Daily air temperature extremes summarized by month for CFA and TAN	54
Table B-5. Monthly and annual air temperature averages and extreme averages for CFA	55
Table B-6. Monthly and annual air temperature averages and extreme averages for TAN	55
Table B-7. Spatial variability in air temperature on and surrounding the INEL on the days with the highest maximum (20 July 1960) and the lowest minimum (23 December 1983) at CFA	56
Table B-8. Monthly and annual average number of days (%) when the maximum daily air temperature was at or below 32 °F and at or above 90 °F at CFA and TAN	57
Table B-9. Monthly and annual average number of days (%) when the minimum daily air temperature was at or below 0 °F and at or above 90 °F at CFA and TAN	57
Table B-10. Dates of the last recorded minimum air temperature of 24, 28, and 32 °F in the spring and the first occurrence of these temperatures in the fall together with the number of days between those dates for CFA	59
Table B-11. Dates of the last recorded minimum air temperature of 24, 28, and 32 °F in the spring and the first occurrence of these temperatures in the fall together with the number of days between those dates for TAN	60
Table B-12. Monthly and annual summary of daily freeze/thaw cycles for CFA and TAN.	61
Table B-13. Monthly and annual average and extreme heating degree days (HDD) for CFA and normalized average and extreme heating degree days for TAN	61
Table B-14. Monthly and annual average and extreme cooling degree days (CDD) for CFA	62

Table B-15. Seasonal and annual distribution (% of time) of air temperature stability classes for CFA, TAN, and GRD3	64
Table B-16. Average onset and dissipation times of inversion and lapse air temperature profiles together with intensity values for CFA	65
Table C-1. Monthly averages and extremes of surface soil and air temperatures from copper and black colored probes. Paired temperatures indicate soil/air temperature. Unpaired values are soil temperature	72
Table C-2. Monthly subsoil temperature extremes (maximum/minimum) at various depths under asphalt and bare soil surfaces..	75
Table D-1. Average total monthly and annual precipitation (water equivalent) for CFA	77
Table D-2. Average total monthly and annual precipitation (water equivalent) for TAN. The annual average includes only years with 12 months of observations	77
Table D-3. Occurrences of precipitation amounts equal to or greater than one inch per day for CFA and TAN	78
Table D-4. Greatest 1-hour and 24-hour precipitation amounts for CFA and TAN	78
Table D-5. Monthly and annual average number of days (%) on which measurable precipitation was recorded at CFA and TAN	79
Table D-6. Monthly and annual probabilities of one or multiple days of continuous precipitation (amounts equal to or greater than 0.01 in.) expressed as a percent of occurrence for CFA	81
Table D-7. Monthly and annual probabilities of one or multiple days of continuous precipitation (amounts equal to or greater than 0.01 in.) expressed as a percent of occurrence for TAN	81
Table D-8. Monthly and annual probabilities of one or more continuous days of no measurable precipitation (including trace amounts) expressed as a percent of occurrence for CFA	82
Table D-9. Monthly and annual probabilities of one or more continuous days of no measurable precipitation (excluding also trace amounts) expressed as a percent of occurrence for TAN	83
Table D-10. Monthly and annual snow fall totals and monthly and daily extreme totals for CFA	84
Table D-11. Monthly and annual average number of days (%) and extreme number of days with snow fall amounts, of equal to or greater than 0.1, 1.0, and 3.0 in. for CFA	85
Table D-12. Monthly and annual average snow depths on the ground and extreme snow depths for CFA	86
Table E-1. Monthly and annual averages and extremes of hourly wet bulb temperatures for CFA	88
Table E-2. Monthly and annual averages of daily maximum and minimum wet bulb temperatures for CFA	88
Table E-3. Monthly and annual relative humidity averages and extremes for CFA	91
Table E-4. Monthly and annual averages of dew point temperatures and corresponding air (dry bulb) and wet bulb temperatures for CFA	92
Table E-5. Monthly and annual mixing ratio averages and extremes for CFA	92
Table F-1. Sunrise (S.R.) and sunset (S.S.) times at CFA	95
Table F-2. Estimated monthly and annual averages of total daily solar radiation (global, normally oriented direct, and diffuse) for the INEL	96
Table F-3. Average daily opaque sky cover for the INEL based on regional NWS observations	97
Table G-1. Monthly and annual atmospheric pressure averages and daily pressure extremes for CFA	98

Table H-1. State of the ground coding scheme	99
Table H-2. Monthly and annual classification summary of the state or condition of the ground surface (% of observations) for CFA	99
Table I-1. Funnel clouds and tornado sightings observed on the INEL by NOAA or other INEL personnel	102
Table VI-1. Atmospheric stability estimates using time of day, wind speed, and cloud cover for the INEL (Markee, 1963)	117
Table VI-2. Estimated seasonal and annual mixing depths for mornings and afternoons at the INEL	124
Table VI-3. NRC stability classification system	125

NOTES

Chapter I INTRODUCTION

In 1949, the U. S. Weather Bureau, by agreement with the Reactor Development Division of the Atomic Energy Commission, established a Weather Bureau station with a complete complement of meteorologists and technicians at the National Reactor Testing Station (NRTS). The staff was responsible for a full range of hourly and daily climatological observations, including balloon soundings, which were transmitted onto the National Weather Service (NWS) observations network.

After 15 years of operation, the first complete climatology of the area was published (Yanskey et al., 1966). Regular observation functions related solely to synoptic forecasting were thereafter reduced to allow for more intense research on area transport and diffusion characteristics. Basic meteorological observations of the renamed Idaho National Engineering Laboratory (INEL) were, however, continued in order to satisfy the requirements of the site operator, the Department of Energy (DOE). The Air Resources Laboratory Field Research Division (ARLFRD) of the

National Oceanic and Atmospheric Administration (NOAA) continues to furnish forecast and emergency support while reporting only basic climatological parameters to the National Climatic Data Center (NCDC).

After the printing of the first complete climatology of the INEL, numerous studies were conducted to evaluate several aspects of the meteorology and diffusion likely to occur in the area. These studies included numerous field experiments using sophisticated gas sampling systems and radar-tracked balloons. Additional basic climatological observations have also been collected. All of these efforts have contributed significantly to the INEL climatological data base, but are not found in one convenient publication. This edition of the INEL climatology is based on an assemblage of five previous reports (DeMarrais, 1958a and 1958b; DeMarrais and Islitzer, 1960; Johnson and Dickson, 1962; and Yanskey et al., 1966) combined with new information acquired since that time.

NOTES

Chapter II AREA PHYSIOGRAPHIC DESCRIPTION

The climatology of the INEL cannot be fully understood without an understanding of the topography and some of the geological features of the site itself and the surrounding area. The INEL is located along the western edge of the Eastern Snake River Plain (ESRP) in southeastern Idaho (Figure II-1). The ESRP is the eastern segment of the Snake River Plain that extends from about Twin Falls, Idaho, to the Yellowstone Plateau as shown in Figure II-2. Lying at the foot of the Lost River, Lemhi and Bitterroot-Centennial Mountain Ranges, the INEL occupies an 890 square mile area. These mountains rise to approximately 11,000 ft. above mean sea level (m.s.l.). The general orientation of the entire mountain range complex which borders the ESRP is northeast to southwest. Long, deep mountain valleys bordering the INEL

immediately to the northwest, however, are oriented in a northwest-southeast direction.

The general surface of the INEL, like that of the entire Snake River Plain, is rolling to broken. The average elevation of the INEL is about 5000 ft. above m.s.l. (Figure II-2). A broad, low, volcanic ridge extends from the Craters of the Moon National Monument along the southern edge of the INEL and northeastward through the eastern INEL to the south and east of the Mud Lake area. Two buttes, located in the southeast corner of the INEL, rise approximately 1400 and 1600 ft. above the surface of the valley floor. Just a few miles south of the INEL is Big Southern Butte. This butte has an elevation of 7576 ft. above m.s.l. and is a major landmark.

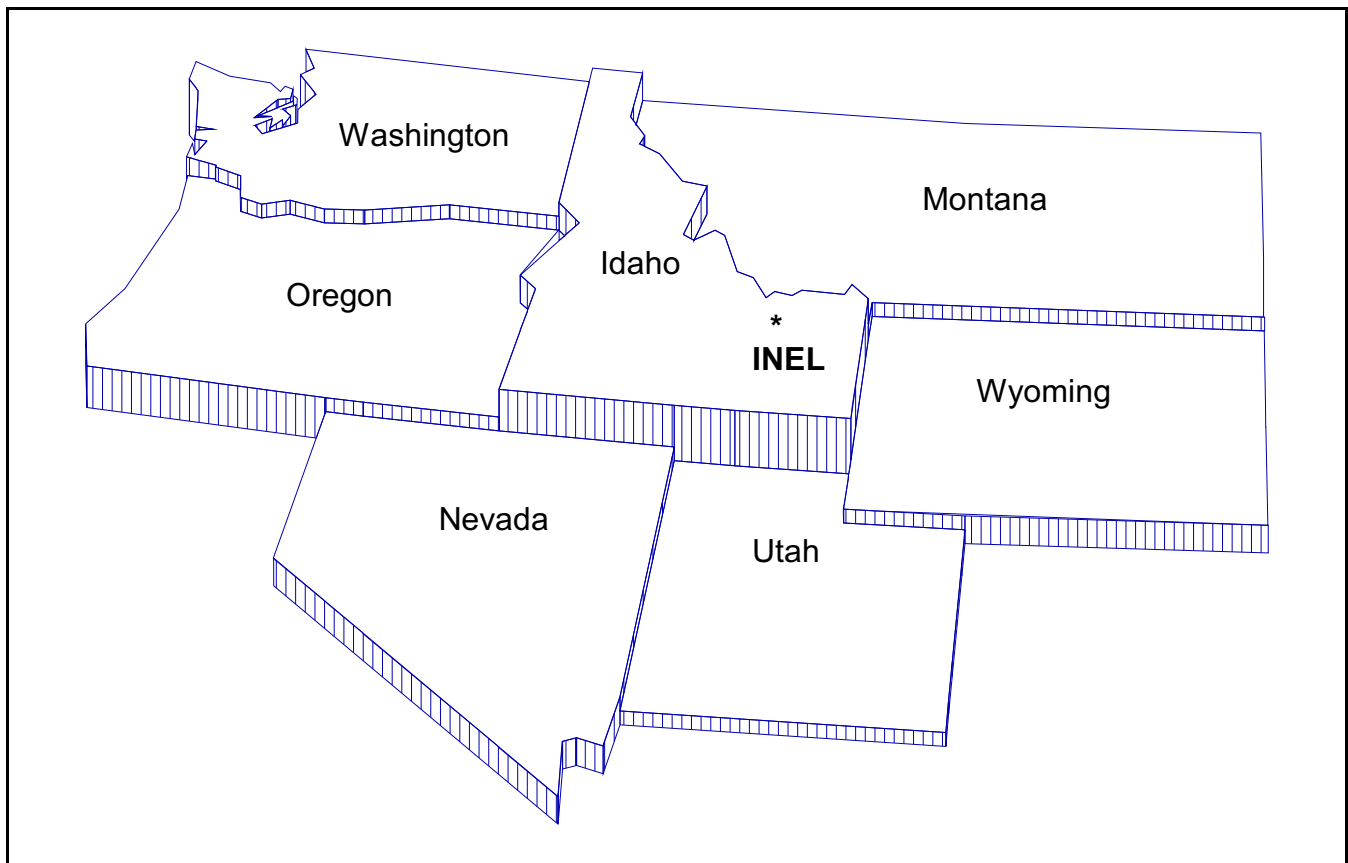


Figure II-1. Location of the INEL in relation to regional state boundaries.

Three streams enter the ESRP from the northwest and flow through the INEL across alluvial fans into playas or sinks. Due to seepage, evaporation, and substantial upstream water diversion for irrigation, the streams in the INEL are often dry during the warm months of the year.

The two principal surface materials at the INEL, according to the U. S. Geological Survey (Nace et al., 1975) are loess and olivine basalt. Other surface materials are sand, black basalt,

playa deposit, alluvial-fan deposits, slope wash and talus, and lake bed sediments with associated beach and bar deposits. Plant life consists primarily of sagebrush and various grasses.

The meteorological effects of these physiographic features will be clarified in later chapters as they relate to wind fields, transport and diffusion, air temperatures, and other atmospheric parameters.

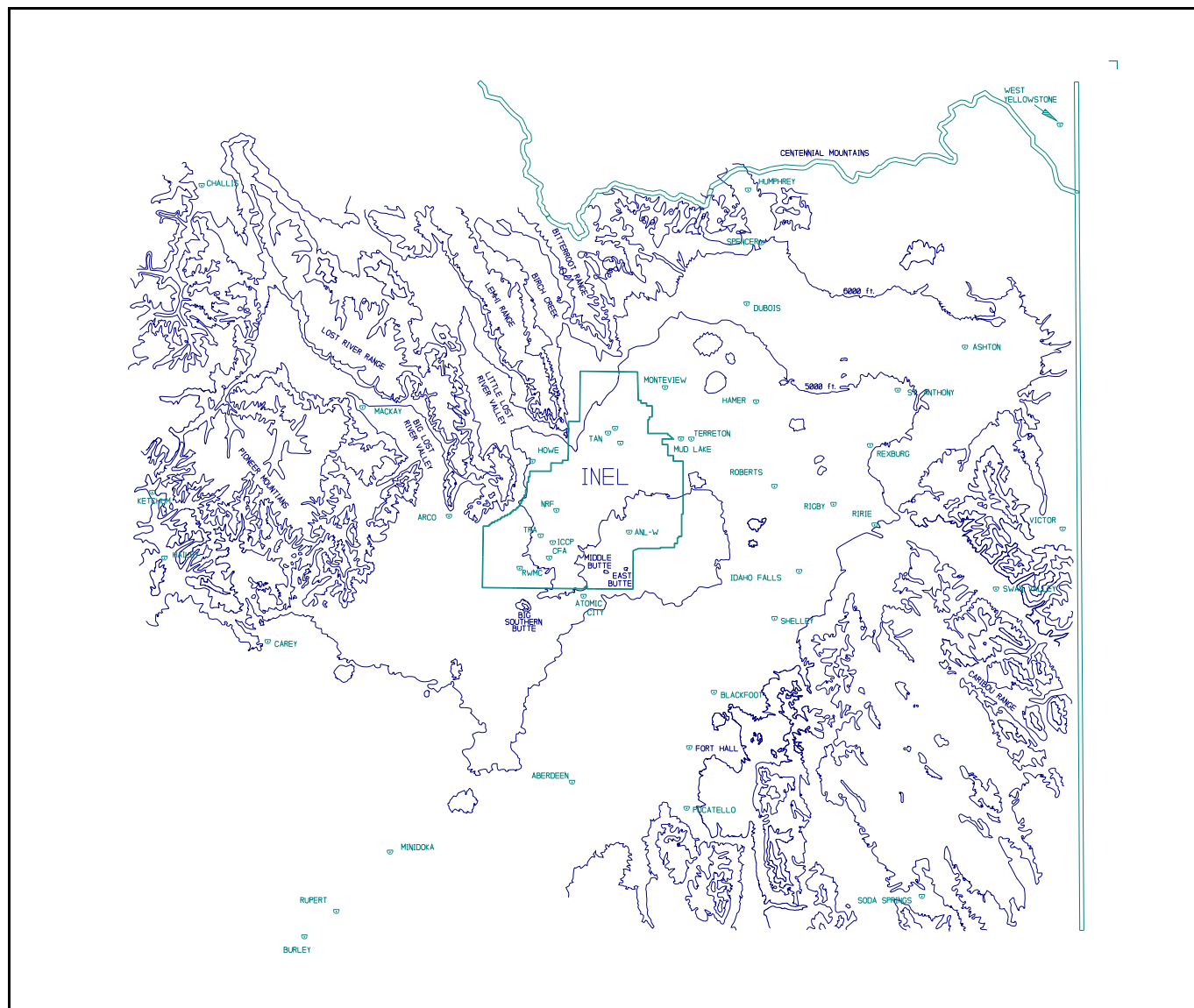


Figure II-2. Topographic depiction of the INEL and surrounding area.

Chapter III

METEOROLOGICAL OBSERVATION NETWORK

There were 27 meteorological observation stations in operation at and surrounding the INEL as of 31 December, 1988. The type of data being collected, the period of record of these data, and the three- or four-letter location code for each of these stations are given in Table III-1. Occasionally, the observation station is located at or near a NCDC weather station. These stations and the NCDC location designation together with the period of record of that weather station are given in Table III-2. The physical location of each active observation station in relation to the INEL is shown in Figure III-1.

Wind measurements (both speed and direction) are currently being observed at all monitoring stations, normally at 50 ft. above ground level. Air temperature is also recorded at some of these stations normally at the 5 ft. level. Three stations are "primary" observation stations, i.e., GRD3, ANL, and LOFT, and are intensely instrumented. Tall towers at these stations are equipped to measure winds and air temperatures at multiple levels (up to 250 ft.). Atmospheric humidity is also currently recorded at CFA and ANL, while precipitation is monitored at CFA. All of these data are continuously being added to the INEL climatological data base.

Meteorological data have been collected at more than 45 locations on and near the INEL. The weather station at the Central Facilities Area (CFA), established in 1949, was the first meteorological observation station established solely in support of the INEL. It is also the only on-site station with over 35 years of record for air temperature and precipitation. The data from this station have been, since its inception, included in the NCDC records under the designation "Idaho Falls 46 W." The data from the TAN station were also, at one time, included in the NCDC records under the designation

"Idaho Falls 42 NW" (Table III-2). The original monitoring stations established in 1950 and 1951, together with the current station ID, if appropriate, comprised the following:

R	-->	Arco
WBO	-->	Central Facilities Area
P	-->	East Perimeter
H	-->	Howe
M	-->	Midway
T	-->	Terreton

The Midway, East Perimeter and Terreton stations have all been discontinued. These three stations and all other abandoned stations are listed in Table III-3 together with the type and period of record of the meteorological data collected at each station. The Arco, Central Facilities Area, and Howe stations are still operational and are currently designated ARC, CFA, and HOW, respectively. Additional details about these stations are more completely discussed in Yanskey et al., 1966.

Some confusion may arise when using climatological data from old and/or discontinued stations. Many of the old stations have been known by more than one name, which was usually a one-letter location designation as given above. For example, instrumentation at Test Area North (TAN) has, at different times, been known as: 1) Idaho Falls 42 NW, 2) ANP, 3) WXA-2, 4) LOFT, and 5) IET. At the present time, the LOFT station is also known as TAN. The location of a few stations has also been changed. For example, the current Terreton (TRN) site is not located at the original Terreton (T) site. Furthermore, several monitoring stations have been combined into one station, as in the case of STR #1, #2, #3, and #4 into NRF. Therefore, care must be exercised when working with older data.

Table III-1. Active INEL meteorological monitoring stations, as of December 31, 1988, together with identification codes and periods of record for air temperature, precipitation, and wind speed and direction.

<u>LOCATION</u>	<u>CODE</u>	<u>WIND SPEED & DIRECTION</u>	<u>AIR TEMPERATURE</u>	<u>PRECIPITATION</u>
ON-SITE STATIONS				
Argonne National Lab-West ^{a,b}	ANL ^b	1964-present ^c	1964-present ^c	none
Central Facilities ^a	CFA	1950-present	1949-present	1950-present
Grid 3	GRD3	1957-present ^{c,e}	1979-present ^c	none
Loss of Fluid Test	LOFT ^d	1953-present ^{c,e}	1987-present ^c	none
Naval Reactor Facility	NRF	1956-present	none	none
Power Burst Facility	PBF	1964-present	none	none
Radioactive Waste Management Complex	RWMC	1977-present	none	none
Rover	ROV	1972-present	none	none
Sand Dunes	DUN	1956-present	none	none
Test Reactor Area	TRA	1971-present	none	none
OFF-SITE STATIONS				
Aberdeen	ABN	1968-present	none	none
Arco	ARC	1968-present	none	none
Big Southern Butte	BSN	1968-present	none	none
Blackfoot	BLK	1968-present	1971-present	none
Blue Dome	BDM	1968-present ^e	1954-present ^c	1954-1955
Dubois	DBS	1968-present	1971-present	none
Hamer	HMR	1971-present	none	none
Howe	HOW	1950-present ^e	1971-present	none
Idaho Falls	IDF	1968-present	none	none
Kettle Butte	KTB	1968-present	none	none
Minidoka	MIN	1968-present	1972-present	none
Monteview	MTV	1955-present ^e	1955-present ^c	1955-1963
Richfield	RCH	1968-present	1972-present	none
Roberts	RBT	1968-present	none	none
St. Anthony	STA	1968-present	1972-present	none
Taber	TBR	1968-present	none	none
Terreton	TRN ^e	1950-present ^e	1958-1961	1958-1961

- a. Instrumentation includes dew point temperature (period of record is from 1978 for CFA and 1978 for ANL).
- b. Station code is also referred to as EBR2.
- c. Meteorological variable is measured at multiple levels.
- d. Station code is frequently identified as TAN.
- e. Station was not operational for the entire period of record.

Table III-2. Active INEL meteorological monitoring stations co-located with or near National Climatic Data Center (NCDC) stations, accompanied with NCDC identification codes and NCDC periods of record for air temperature and precipitation.

<u>LOCATION</u>	<u>NATIONAL CLIMATE DATA CENTER</u>	<u>AIR TEMPERATURE</u>	<u>PRECIPITATION</u>
Aberdeen	Aberdeen Exp. Station ^{a,b}	1915-present	1914-present
Arco	Arco 3 SW	1935-present	1922-present
Blackfoot	Blackfoot 2 SSW	1907-present	1905-present
Central Facilities	Idaho Falls 46 W	1954-present	1954-present
Dubois	Dubois Exp. Station	1931-present	1931-present
Hamer	Hamer 4 NW	1950-present	1948-present
Howe	Howe	1958-present	1936-present
Idaho Falls (airport)	Idaho Falls FAA AP ^b	1930-present	1930-present
Idaho Falls (residential)	Idaho Falls 2 ESE	1956-present	1952-present
Minidoka	Minidoka 10 WNW	1966-present	1966-present
Richfield	Richfield	1925-present	1924-present
St. Anthony	St. Anthony 1 WNW	1944-present	1943-present
Test Area North	Idaho Falls 42 NW	1954-1970	1954-1970

- a. Climate record also includes pan evaporation.
b. Climate record also includes soil temperature.

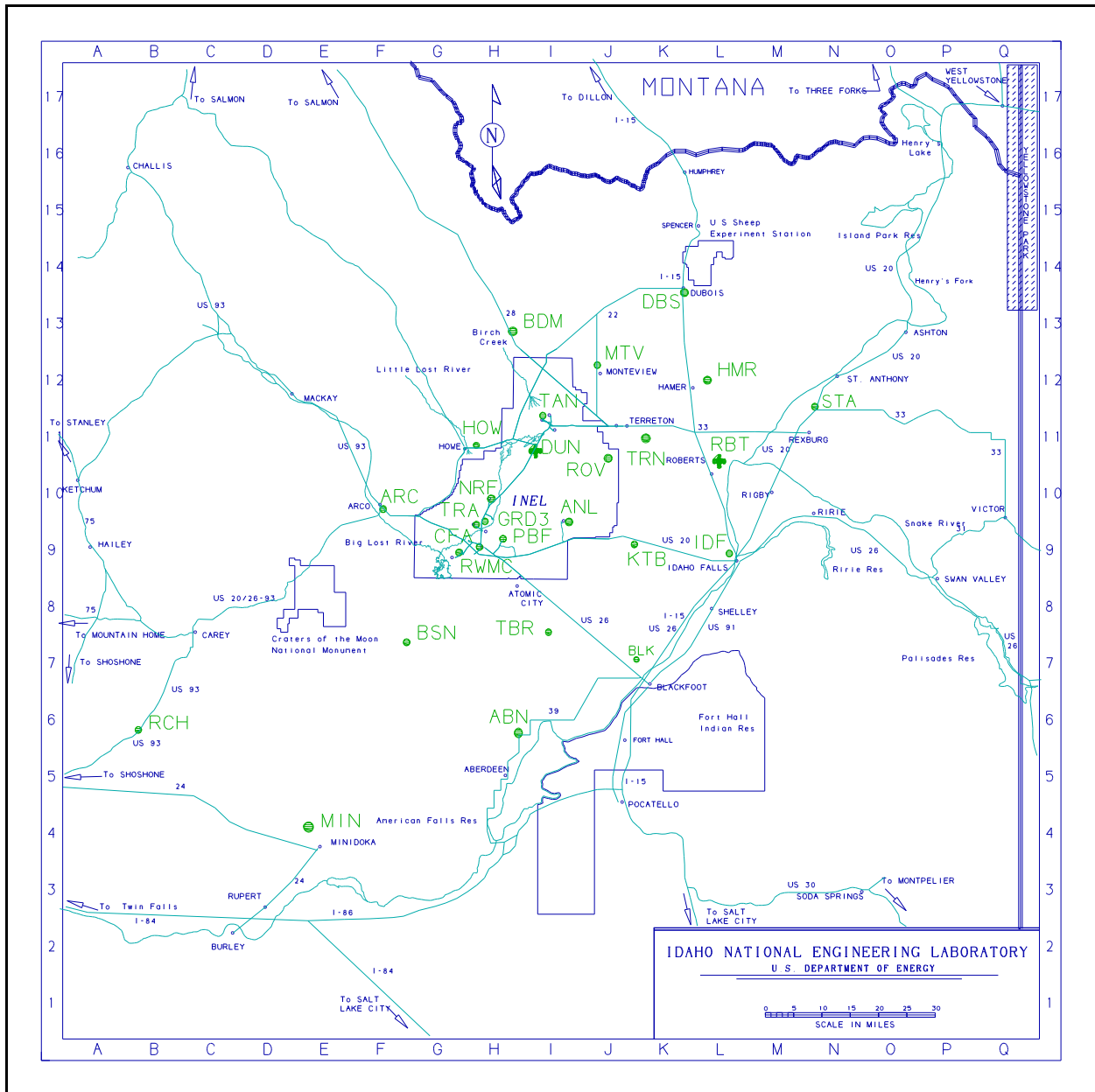


Figure III-1. Geographic location of the 27 active INEL meteorological monitoring stations.

Table III-3. Discontinued INEL meteorological monitoring stations, together with identification codes and periods of record for air temperature, precipitation, and wind speed and direction.

<u>LOCATION</u>	<u>CODE</u>	<u>WIND SPEED & DIRECTION PRECIPITATION</u>	<u>AIR TEMPERATURE</u>	
ON-SITE STATIONS				
Arco	A	1950-1952	1950-1952	1950-1952
Birch Creek	BC	1955-1961	1955-1961	1955-1961
CERT (Dairy Farm)	CERT	1962-1970	1962-1970	none
East Butte	EB	1954-1960	1954-1955	none
East Perimeter	P ^a	1951-1954	1951-1954	1951-1954
Experimental Breeder Reactor 1	EBR1	1964-1977	1964-1977	none
Midway	M	1950-1952	1950-1952	1950-1952
Naval Reactor Facility	STR 1b	1951-1954	none	none
	STR 2b	1953-1954	1953-1954	none
	STR 3 ^b	1956-1958	none	none
	STR 4 ^b	1956-1958	none	none
Prickly Pear Flats	PP	1953-1954	1953-1954	none
SPERT	SPERT	1964-present	1955	1955
Test Area North	ANP ^c	1955-1987	1955-1966	1955-1966
	IET	1950-1987	1950-1987	1954-1970
	WXA-1	1952-1955	1952-1955	1952-1955
Well 21	WXA-2 ^c	1952-1970	1967-1969	1966-1969
	Well 21	1956-1958	none	none
X	X	1955-1956	none	none
Y	Y	1956-1958	1956-1958	1956-1958
Z	Z	1955-1956	none	none
OFF-SITE STATIONS				
Craters of the Moon	NPS	1961-1963	1961-1963	none
Howe	H	1950-1953	1950-1953	1950-1953
Raft River	RFR	1976-1981	1976-1981	1979-1981
Rexburg	RB	1959-1962	none	none

- a. Station code was also designated E.
b. Stations designated as STR were also called NRF.
c. Station code was also designated TSF and in National Climate Data Center records as Idaho Falls 42 NW.

NOTES

Chapter IV GENERAL CLIMATOLOGY

The location of the INEL in the ESRP, including its altitude above sea level, its latitude, and its inter-mountain setting, affects the climate of the site. Air masses crossing the ESRP have first traversed a mountain barrier and precipitated a large percentage of inherent moisture. Annual rainfall at the INEL is, therefore, light and the region is classified as arid to semi-arid. The relatively dry air and infrequent low clouds permit intense solar heating of the surface during the day and rapid radiational cooling at night. These factors combine to give a large diurnal range of temperature near the ground.

The moderating influence of the Pacific Ocean produces a climate which is usually warmer in the winter and cooler in summer than is found at locations with similar latitudes in the more continental regions of the United States to the east of the Continental Divide. The Centennial and Beaverhead Mountain Ranges act as an effective barrier to movement of most of the intensely cold winter air masses passing to the south out of Canada toward the ESRP. Occasionally, however, cold air spills over the mountains and is trapped in the ESRP. The INEL

then experiences below normal temperatures for periods lasting usually a week to 10 days.

The mountains bordering the ESRP also act to channel the prevailing west winds into a southwesterly flow. This is due to the northeast-southwest orientation of the ESRP between the bordering mountain ranges. The second most frequent wind direction is from the northeast.

A summary of recent climatological data from 14 NCDC stations on and surrounding the INEL (U. S. Department of Commerce, 1980-1985) is given in Table IV-1. The data have been compiled for a common time period (January 1981 through December 1985) to facilitate a climatological comparison of these sites. The data include average annual statistics for air temperature and precipitation. Normal annual air temperatures and precipitation levels, which are an average of the 30 year period of 1951-1980, are also provided, when they are available. Data listed under the heading "Upper Snake River Plains Division", is an average of all NCDC stations in the ESRP and represents the average regional climate.

Table IV-1. Compilation of National Climatic Data Center (NCDC) temperature and precipitation records for observation stations on and surrounding the INEL from the years 1981-1985. N/A indicates that the data is not available for a given station. Normals are average data from the 30 year period of 1951-1980.

National Climatic Data Center ID	Elevation (ft. m.s.l.)	Absolute Temperature (°F)		Annual Average Temperature (°F)		Annual Average (Normal) Cooling Degree Days (DGD/yr)		Annual Average (Normal) Heating Degree Days (DGD/yr)		Absolute Maximum Daily Precipitation (in.)		Annual Average (Normal) Precipitation (in.)	
		Maximum	Minimum	Average	Temperature	Days	Days	Days	Days	Maximum	Average	Maximum	Average
Aberdeen Exp. Station	4405	98	-38 ^a	42.9 ^a (44.8)	247 ^a (269)	7975 ^a (7633)	0.76 ^a	N/A	10.23 ^a (8.81)				
Arco 3 SW	5328	97	-45 ^b	40.9 ^d	217 ^b (204)	7286 ^c (8613)	1.64 ^c	N/A	14.35 ^b				
Blackfoot 2 SSW	4487	97	-24 ^b	43.6 ^d	409 ^d	6144 ^a	1.36 ^d	N/A	10.20 ^c (10.70)				
Craters of the Moon	5897	95	-37	42.4 ^c	355 ^c	7751	2.00 ^c	121.9 ^a	17.71 ^a				
Dubois Exp. Station	5450	98	-25	42.4(42.7)	335(301)	8250(8424)	1.25	50.9	16.05(11.74)				
Hamer 4 NW	4791	98	-46 ^a	38.7 ^d (42.5)	116 ^c (262)	8352 ^a (8441)	0.81 ^c	31.8	11.49 ^a (8.46)				
Howe	4820	97 ^a	-38 ^a	43.0 ^c	244 ^c	7890	2.02 ^c	19.8	10.16 ^c (8.85)				
Idaho Falls 2 ESE	4765	98 ^a	-34 ^b	45.0 ^c	393 ^b	7480 ^a	1.13 ^c	39.1 ^c	16.39 ^b				
Idaho Falls FAA AP	4730	100	-38	42.8(43.8)	309(288)	8094(7995)	0.97	43.5	12.89(9.77)				
Idaho Falls 46 W	4938	99	-47	40.7(42.0)	272(253)	8840(8626)	1.51	28.3	10.31(8.62)				
Minidoka 10 WNW	4290	105 ^c	-30 ^c	40.3 ^d	343 ^c	7551 ^c	1.95 ^d	N/A	10.73 ^c				
Rexburg Ricks College	4920	97 ^a	-31 ^b	43.7 ^b	310 ^b	7948(7443)	1.40 ^c	75.1	17.39 ^b				
Richfield	4306	100	-28	44.4(45.4)	369(332)	7546(8398)	1.36	39.5	14.51(11.09)				
St. Anthony 1 WNW	4950	95	-39	41.6 (42.2)	104 ^b (146)	8297 ^a	1.14 ^b	N/A	14.50 ^a				
Upper Snake River Plains	N/A	N/A	N/A	43.1(43.9)	N/A(N/A)	N/A(N/A)	N/A	N/A	14.62(11.21)				

a. Data is missing for all or part of 1 year.

b. Data is missing for all or part of 2 years.

c. Data is missing for all or part of 3 years.

d. Data is missing for all or part of 4 years.

Chapter V SPECIFIC CLIMATOLOGY

The climatological data base of the INEL is comprised of several types of measurements. The wind regime on and around the INEL has been monitored in detail for many years. These data comprise the largest portion of the INEL climatological data base. Air temperature has also been monitored in detail for many years and these data comprise the second largest portion of the data base. Both of these parameters are currently monitored at many locations both on- and off-site (Table III-1). Precipitation and atmospheric moisture content also comprise a portion of the climatological data base. These parameters are

currently being measured at a few sites on the INEL.

Other parameters which have been measured in the past, but for which observations have been discontinued include: 1) soil temperature, 2) solar and terrestrial radiation, 3) atmospheric pressure, and 4) state or condition of the ground. Other special atmospheric phenomenon have been observed and are found in the climatological data base. Descriptions and summaries of each of these types of data are found in the following sections.

Section A Wind

Wind speed and direction (always recorded as the direction from which the wind is blowing) have been continuously monitored at a large number of stations on and surrounding the INEL since 1950. The network of wind stations supporting operational requirements at the INEL has been expanded considerably since the installation of the original 6 stations. These original stations were upgraded and new sites established during the 1964-1970 period to form an expanded observational network using 50 ft. towers. The original strip chart recording system was replaced during the 1969-1970 period with radio-telemetry equipment. Knowledge of the general wind flow patterns on the INEL is based on these data records.

The wind pattern over the INEL can, at times, be quite complex. The orientation of the bordering mountain ranges, as well as the general orientation of the ESRP, play an important part in determining the wind regime. The INEL is in the belt of prevailing westerly winds which are normally

channeled within the ESRP. This channeling usually produces a west-southwest or southwest wind. When the prevailing westerlies at the gradient level (approximately 5000 ft. above the surface) are strong, the winds channeled across the ESRP between the mountains become very strong. Some of the highest wind speeds at the INEL are observed under these meteorological conditions. The greatest frequency of this wind is in the spring.

Local mountain and valley features exhibit a strong influence on the wind flow under other meteorological conditions as well. When the winds above the gradient level are strong and from a direction a little north of west, channeling in the ESRP usually continues to produce southwesterly winds over most of the INEL. At the mouth of Birch Creek however, the northwest to southeast orientation of this valley channels strong north-northwest winds into the TAN area. This "Birch Creek" wind may equal the strongest southwesterly winds recorded at other locations on the INEL.

Drainage winds also contribute to the overall wind flow over the INEL. On clear or partly cloudy nights with only high thin clouds, the valley experiences rapid surface radiational cooling. This results in a simultaneous cooling of the air near the surface which, in turn, causes the air to become stable and less turbulent. However, air along the slopes of the mountains cools at a faster rate than the air at the same elevation located aloft over the valley. Consequently, it becomes more dense and flows or sinks toward the valley floor forming a down-slope wind. When this wind reaches the valley, it still flows toward lower elevations and becomes a down-valley wind. The main nocturnal down-valley flow is the second most frequent wind observed over the INEL and flows primarily out of the north-northeast.

A reverse flow, opposite in direction to that of the drainage wind, occurs during the daytime when the air along the mountain slopes is heated more rapidly than air at the same elevation over the valley. The air rises along the slopes as it becomes less dense. This up-slope wind, in turn, contributes to the production of an up-valley wind. This up-valley wind is seldom detectable as a separate component of the wind until the synoptic pressure gradient becomes quite weak. Although the mountain and valley winds are predominantly "fair weather" phenomena, they can also occur under other sky cover conditions.

In addition to the relatively local drainage winds, a somewhat stronger wind has occasionally been observed. It develops during an outbreak of cold air east of the Continental Divide during the winter and behaves in the same manner as the down-valley wind. If the cold air becomes deep enough, it spills over the Continental Divide and flows down across the ESRP. The result of this phenomenon is valley winds from the northeast.

Pressure gradient forces related to passing synoptic weather systems, as well as local storms, all affect the winds of the INEL. These storms alter the local flow regime such that winds from any direction can be observed. The frequency of

occurrence of these types of wind flow patterns is very small, however.

On-site Near-surface Wind Flow Patterns

The characteristics of the near-surface wind regime at the INEL can best be described using a graphical display called a wind rose. Wind roses are graphs which display the frequency (in percent) of the occurrence of winds from various direction sectors for selected speed classes and calm periods. This is an effective method of showing joint wind speed and direction frequency distributions at a glance. The differences between stations, seasons, sensor levels, stability classes, etc., are easily seen.

Wind roses for CFA and TAN are illustrated in Figures A-1 through A-12. These two locations are representative of wind flow patterns over the south and north ends of the INEL, respectively. The figures show wind roses as a function of season, air temperature, stability class and sensor height (for a discussion of stability classes, see section B). Data for CFA were obtained from the 20 and 250 ft. levels. Data for TAN was obtained from the 20 and 150 ft. levels. Some specific conclusions based on the data from CFA are as follows:

1. A distinct channeling effect of the wind is apparent. The directions with the highest percentages of occurrence are the west-southwest to southwest and north-northeast to northeast quadrants.
2. A very small percentage of the wind direction originates from the southeast and northwest quadrants.
3. A higher frequency of calm periods occurs during the winter months while the lowest frequency of calm periods occurs during the spring months.
4. Much higher wind speeds are observed during lapse conditions (usually daytime) than during inversion conditions.
5. Higher wind speeds and hence, a smaller frequency of calms, are observed at the 250 ft. level.

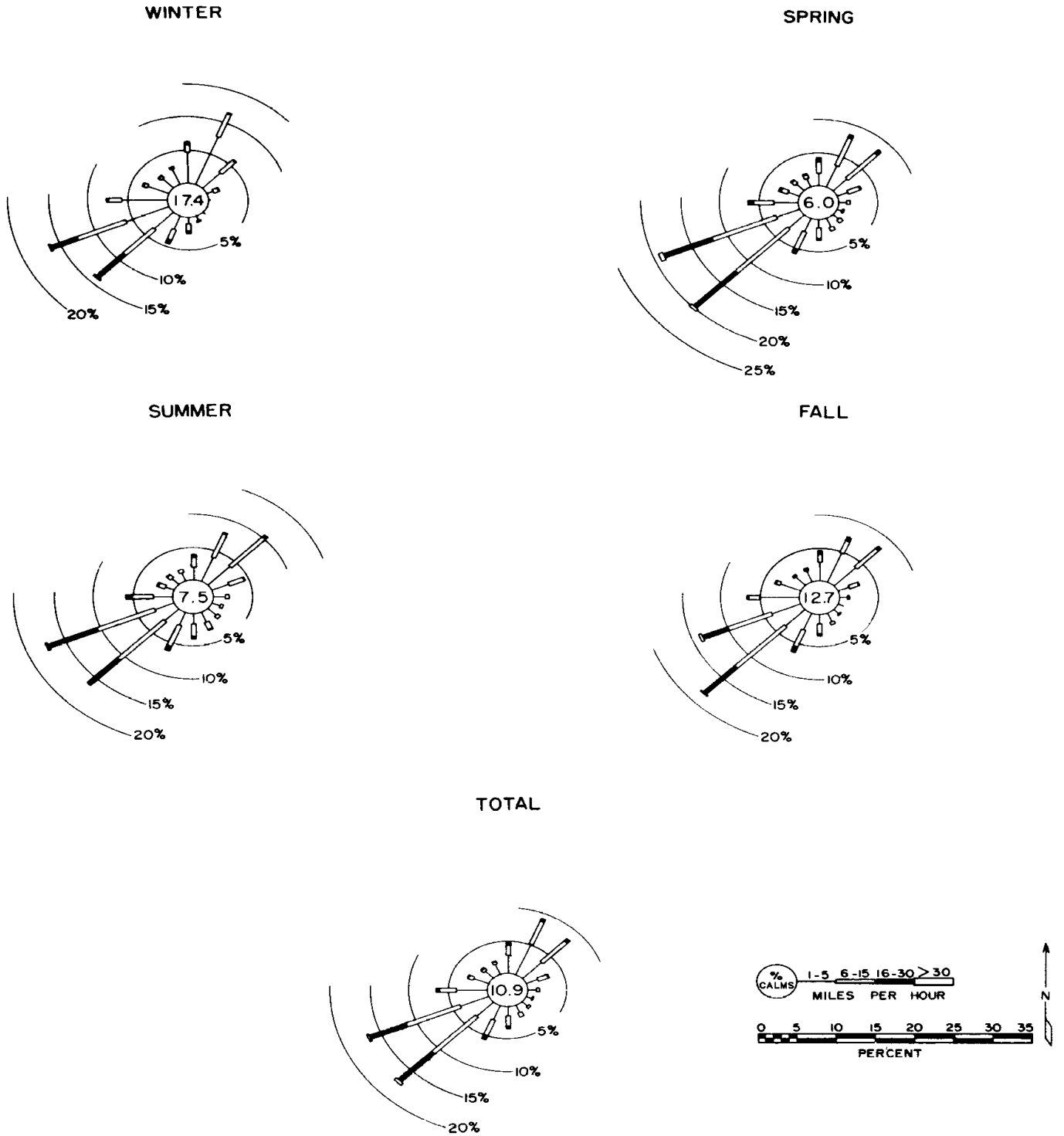


Figure A-1. Annual and seasonal wind roses for the 20 ft. level at CFA from January 1950 through May 1962.

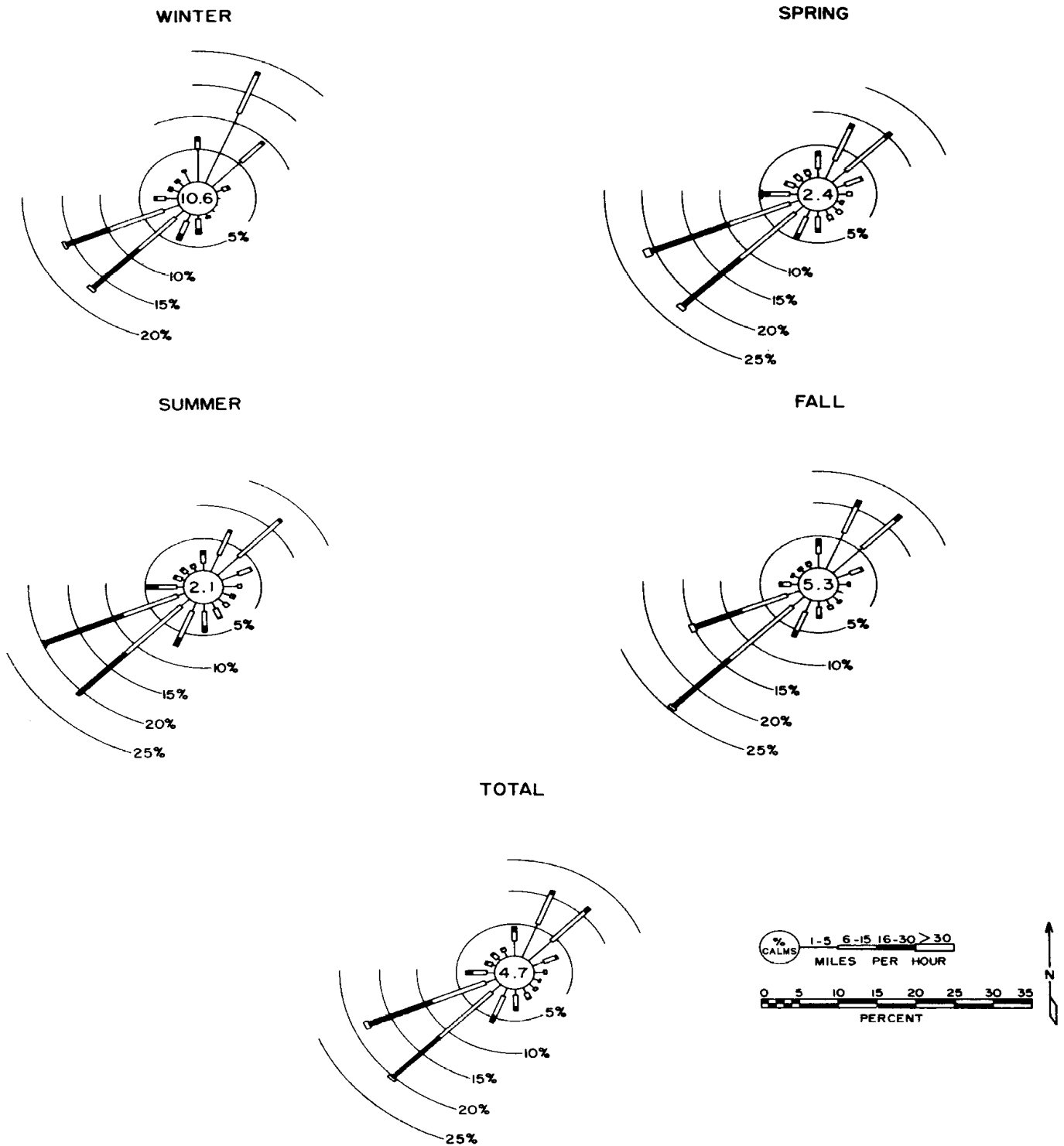


Figure A-2. Annual and seasonal wind roses for the 20 ft. level at CFA under lapse conditions from January 1950 through May 1962.

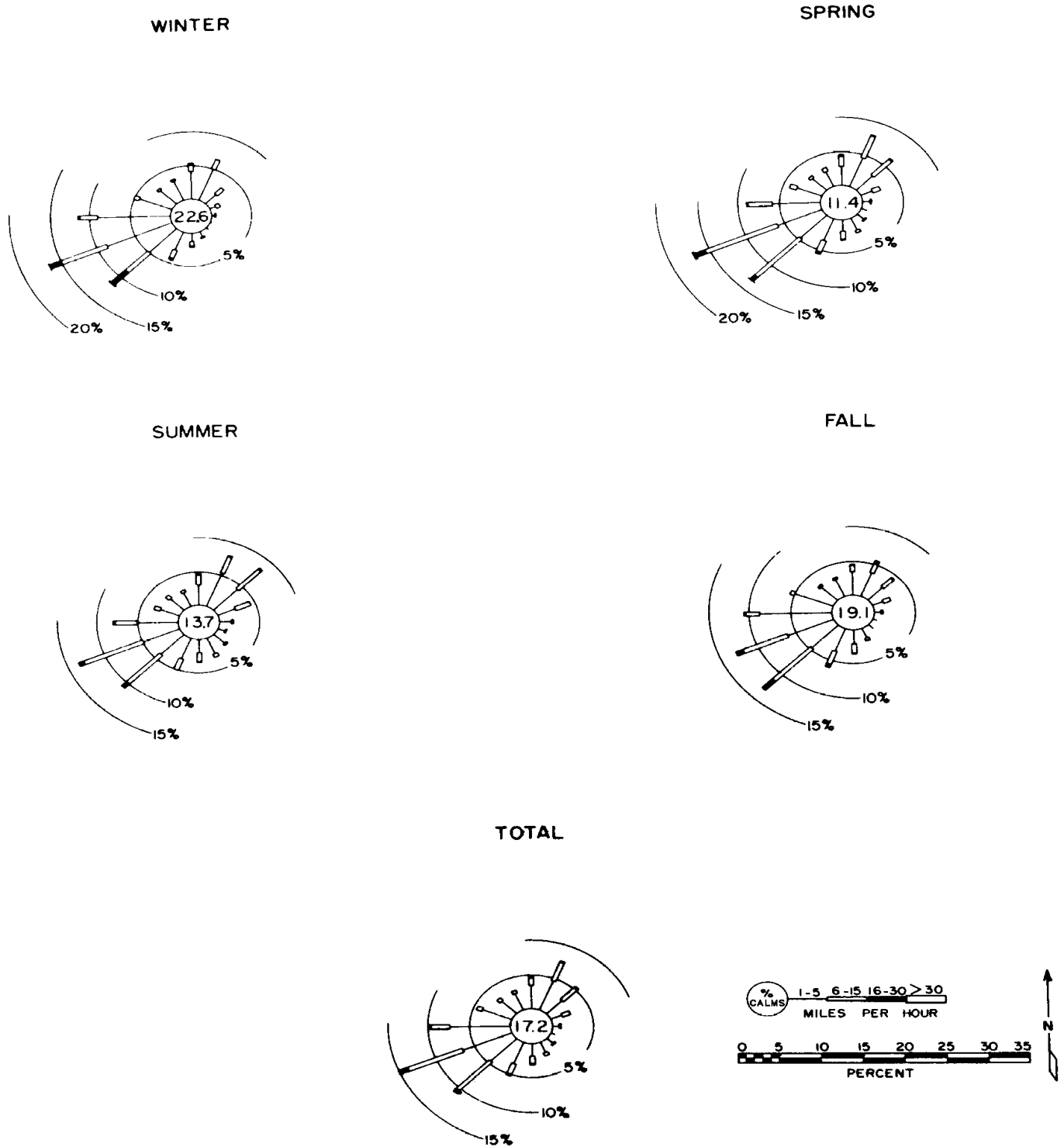


Figure A-3. Annual and seasonal wind roses for the 20 ft. level at CFA under inversion conditions from January 1950 through May 1962.

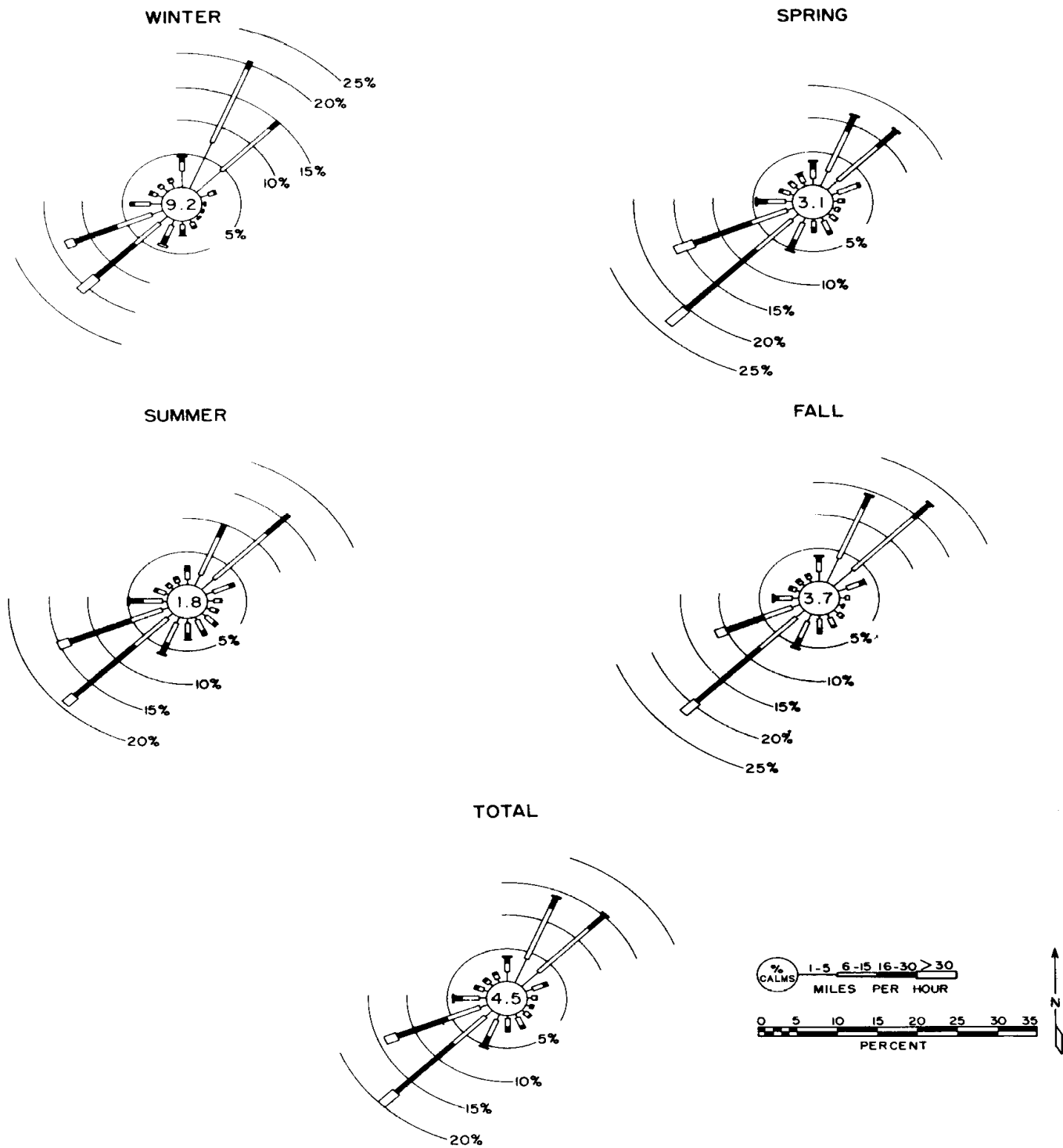


Figure A-4. Annual and seasonal wind roses for the 250 ft. level at CFA from July 1951 through May 1962.

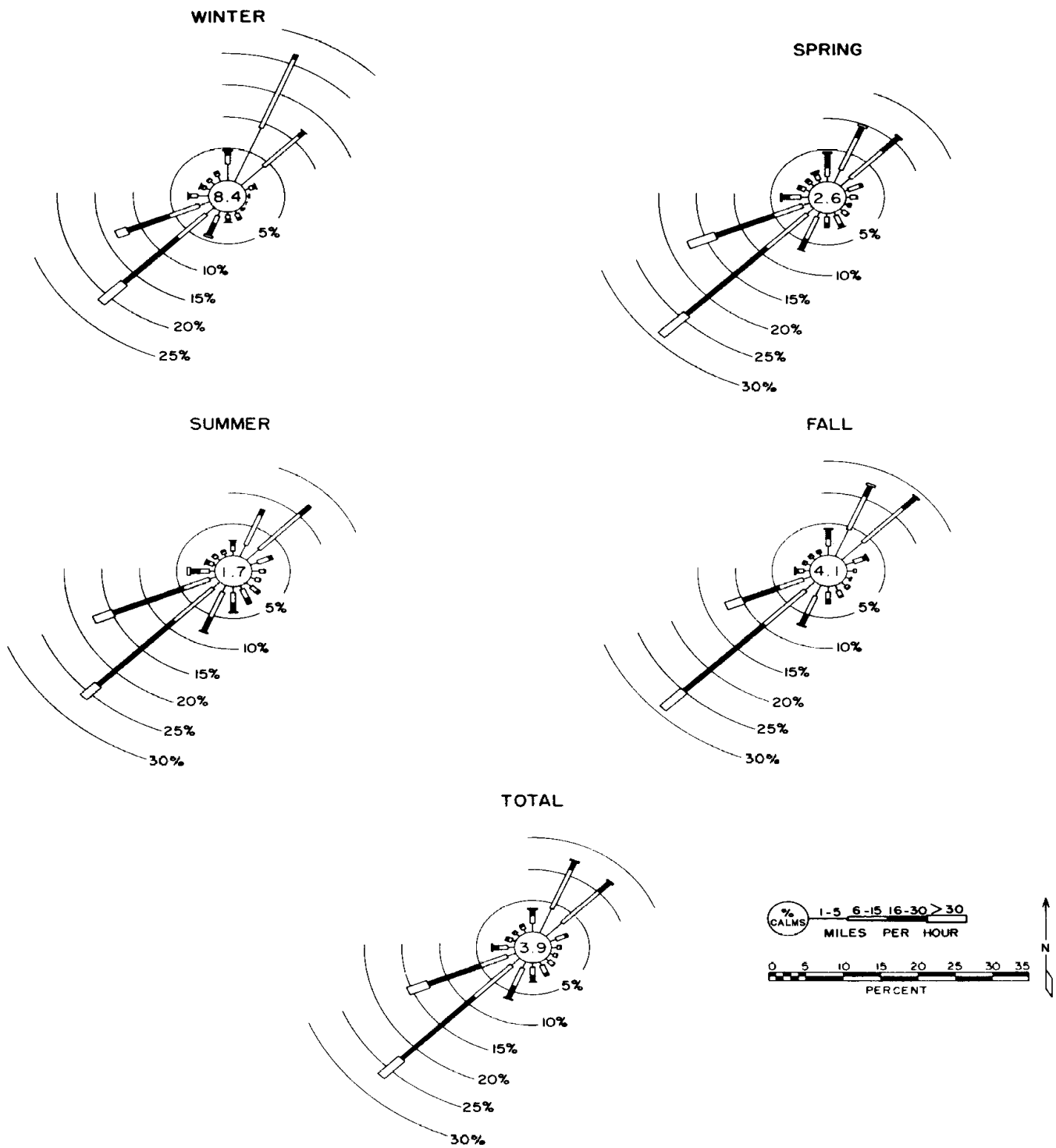


Figure A-5. Annual and seasonal wind roses for the 250 ft. level at CFA under lapse conditions from July 1951 through May 1962.

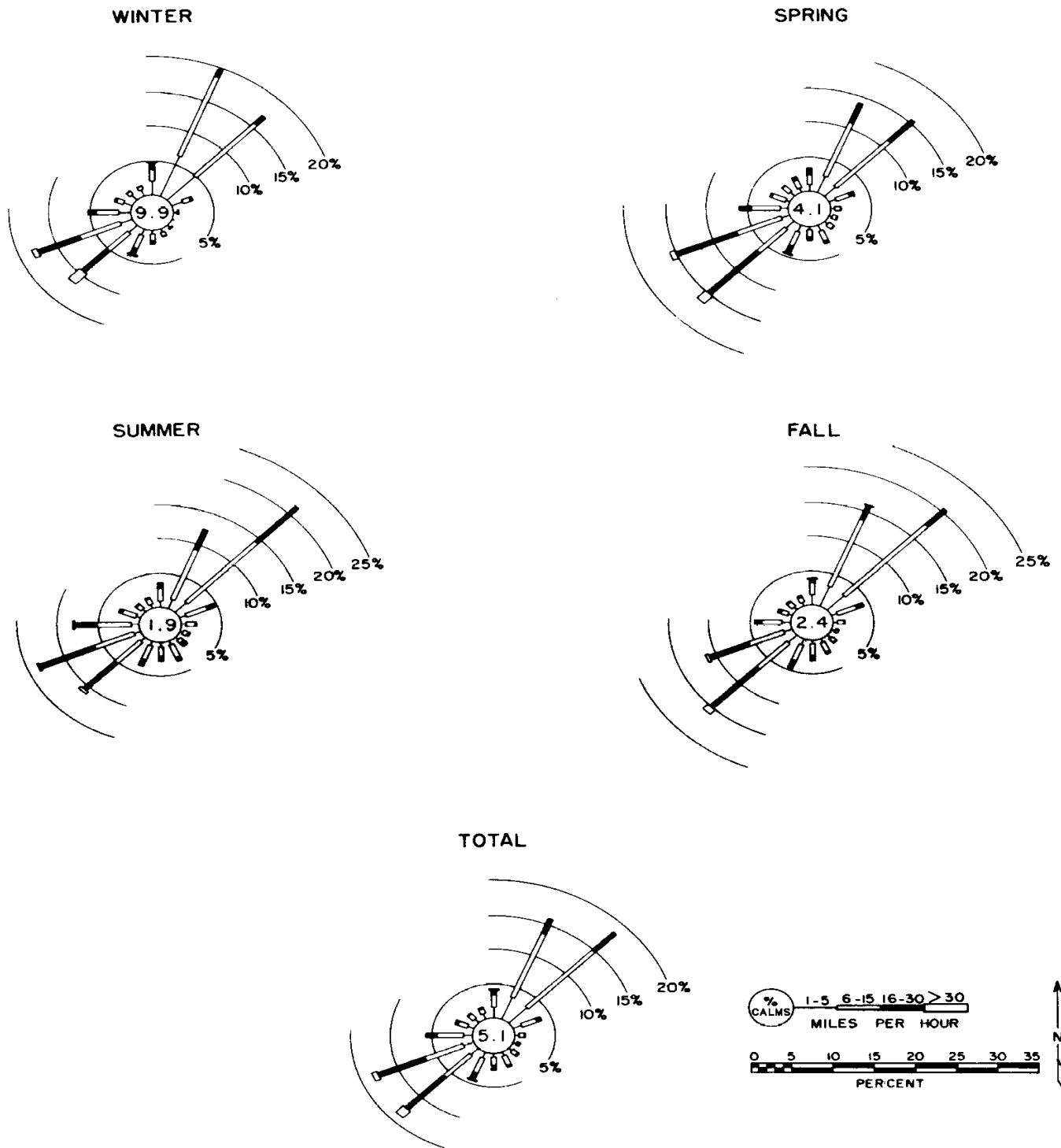


Figure A-6. Annual and seasonal wind roses for the 250 ft. level at CFA under inversion conditions from July 1951 through May 1962.

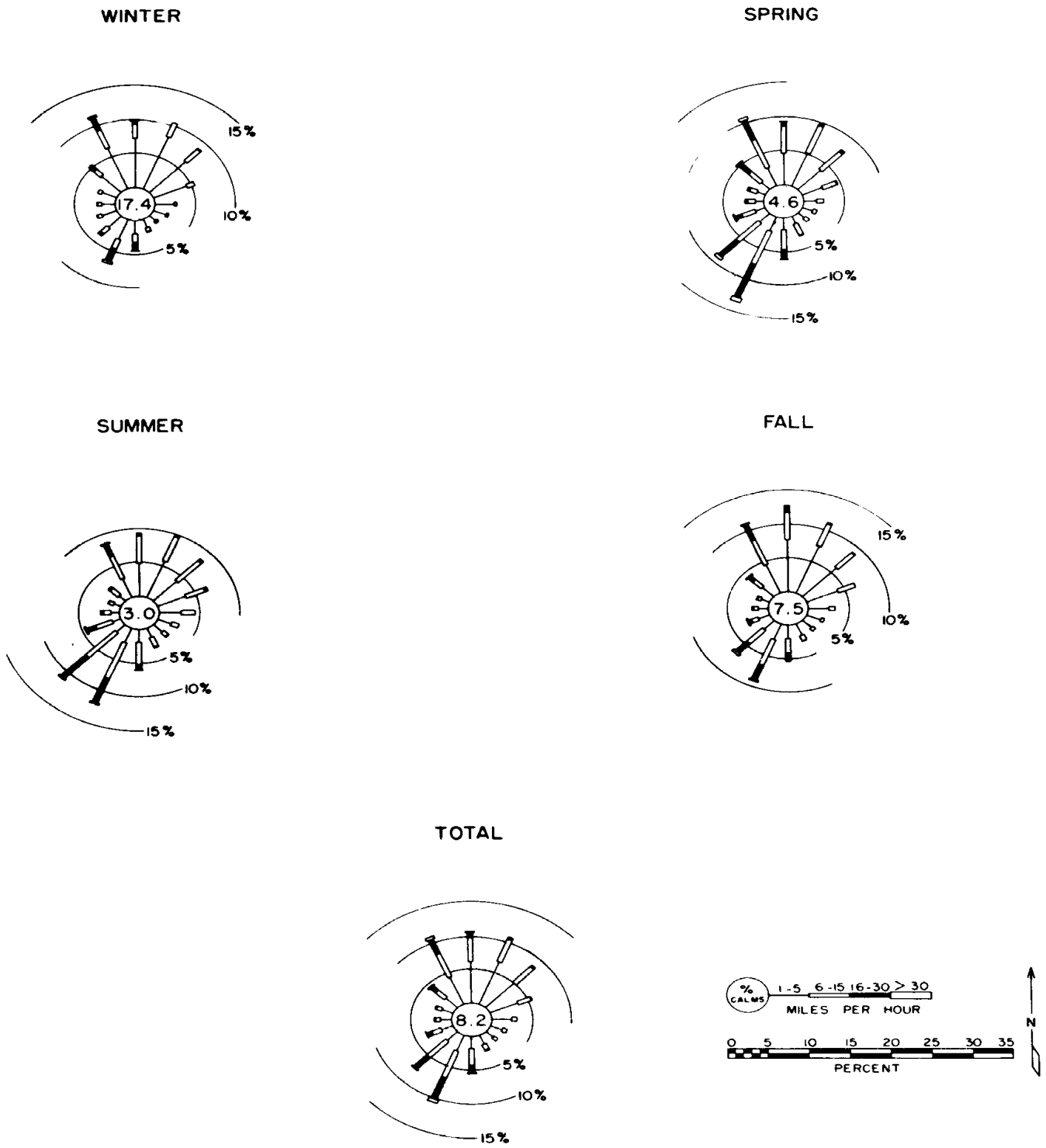


Figure A-7. TAN 20 ft. level wind roses, November 1952 through May 1962.

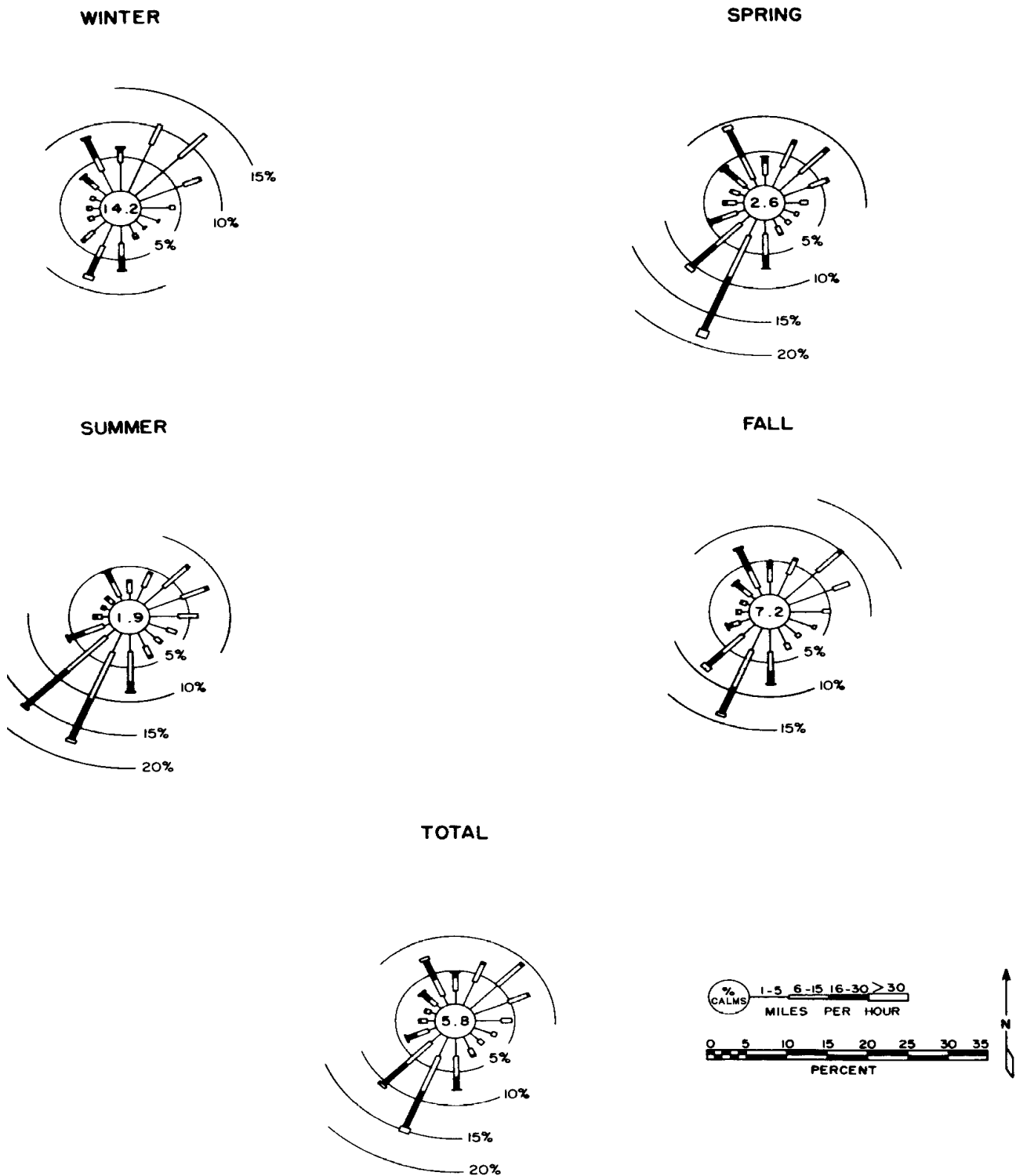


Figure A-8. Annual and seasonal wind roses for the 20 ft. level at TAN under lapse conditions from November 1952 through May 1962.

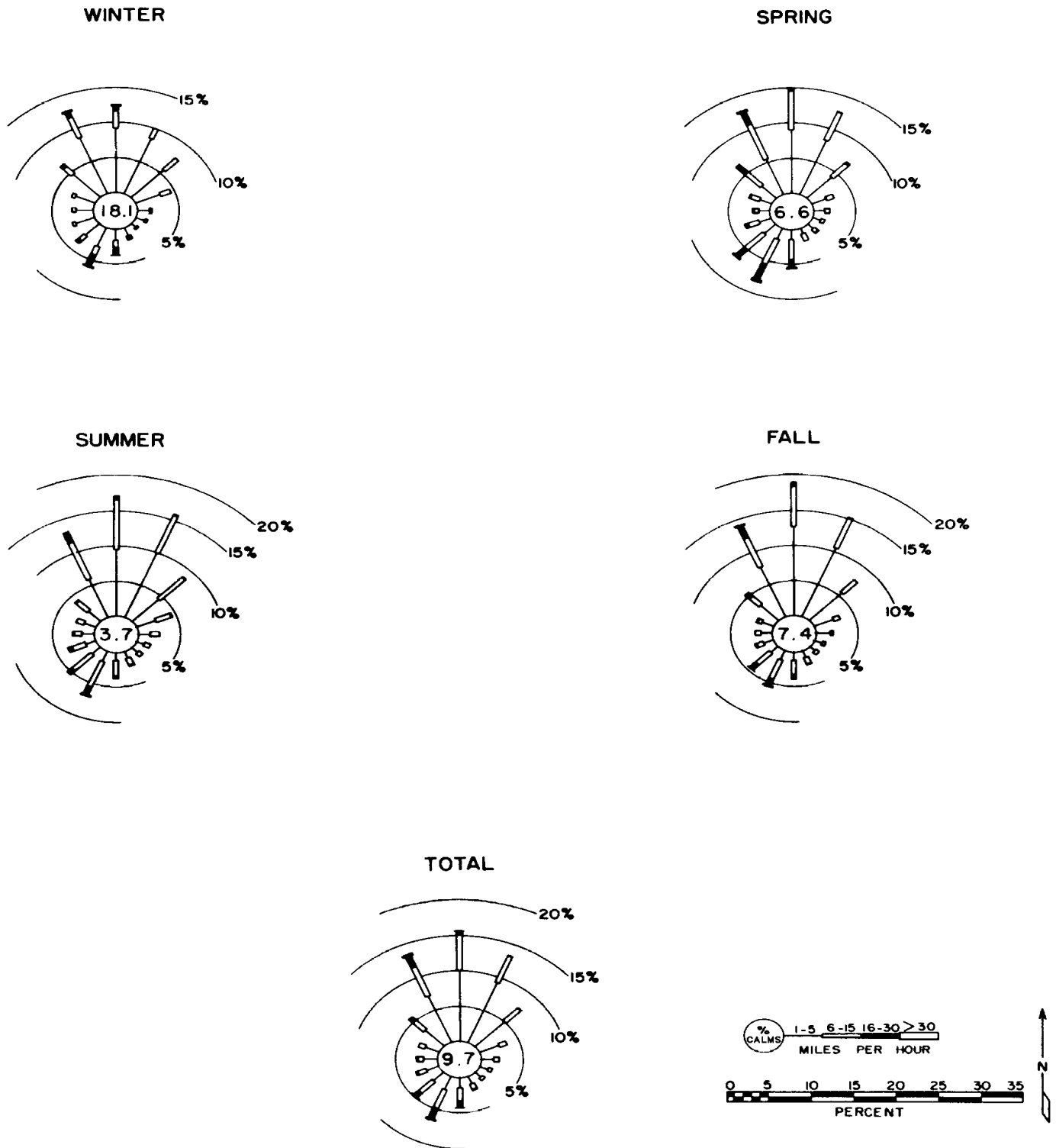


Figure A-9. Annual and seasonal wind roses for the 20 ft. level at TAN under inversion conditions from November 1952 through May 1962.

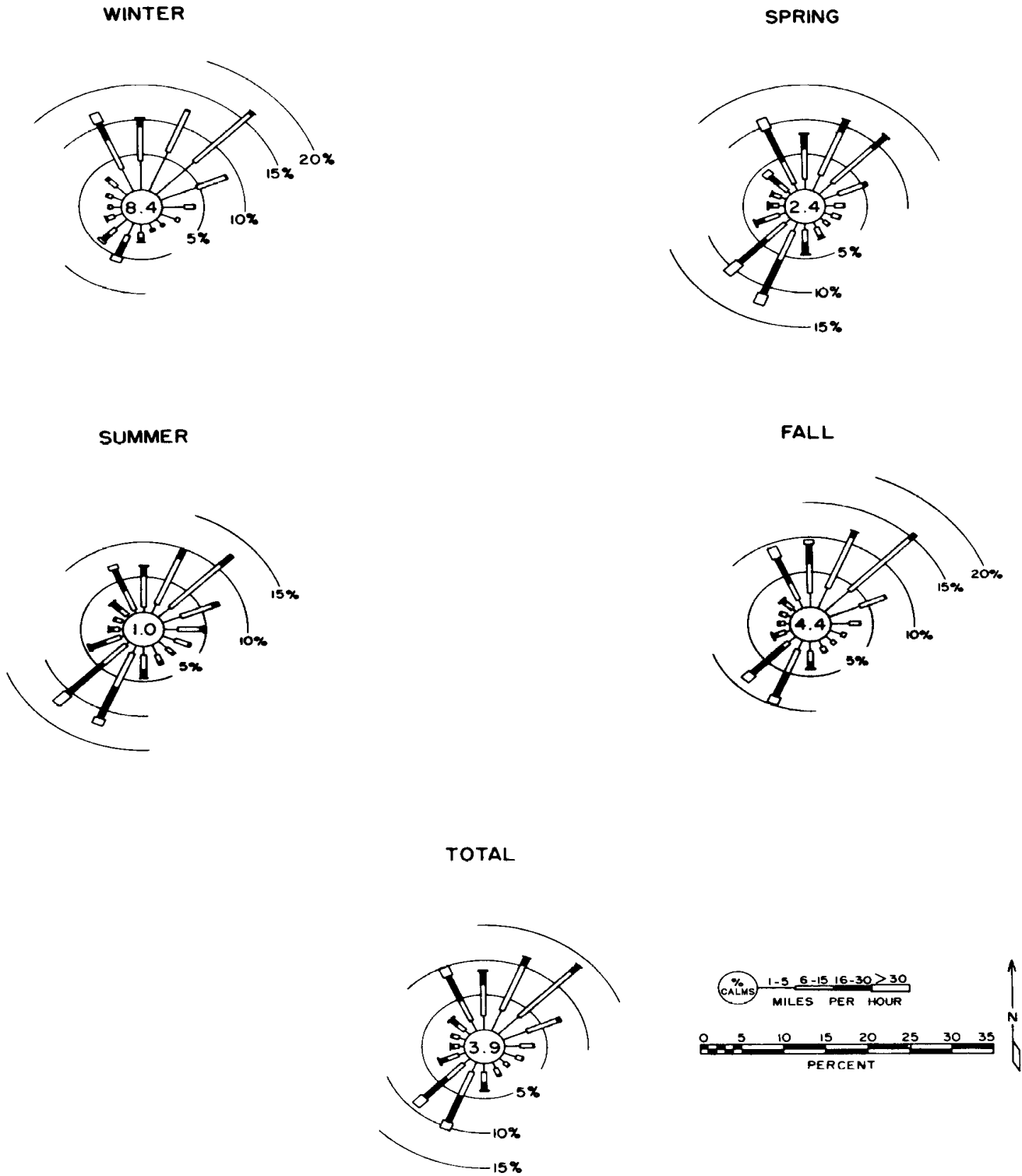


Figure A-10. Annual and seasonal wind roses for the 150 ft. level at TAN from May 1956 through May 1962.

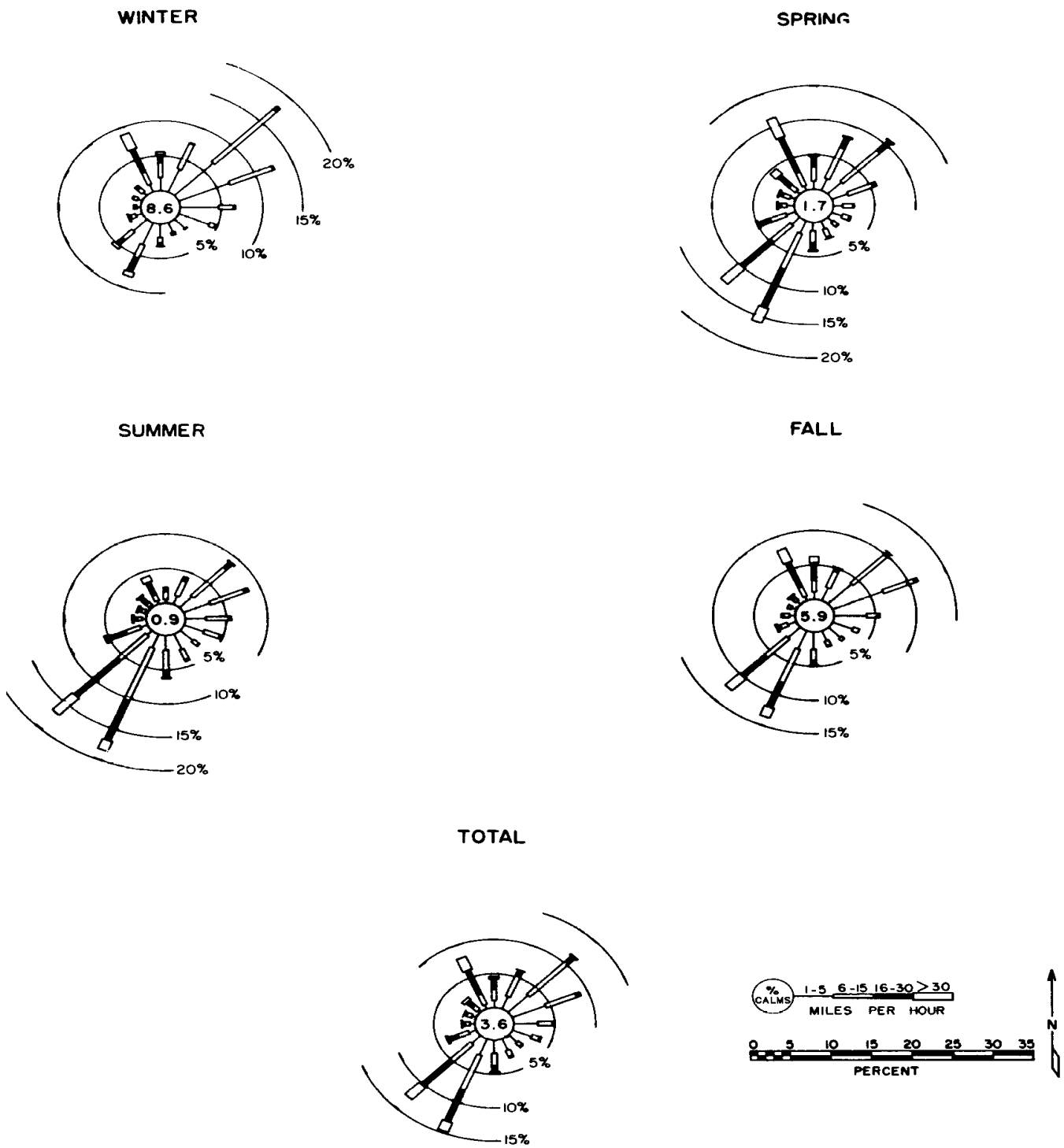


Figure A-11. Annual and seasonal wind roses for the 150 ft. level at TAN under lapse conditions from May 1956 through May 1962.

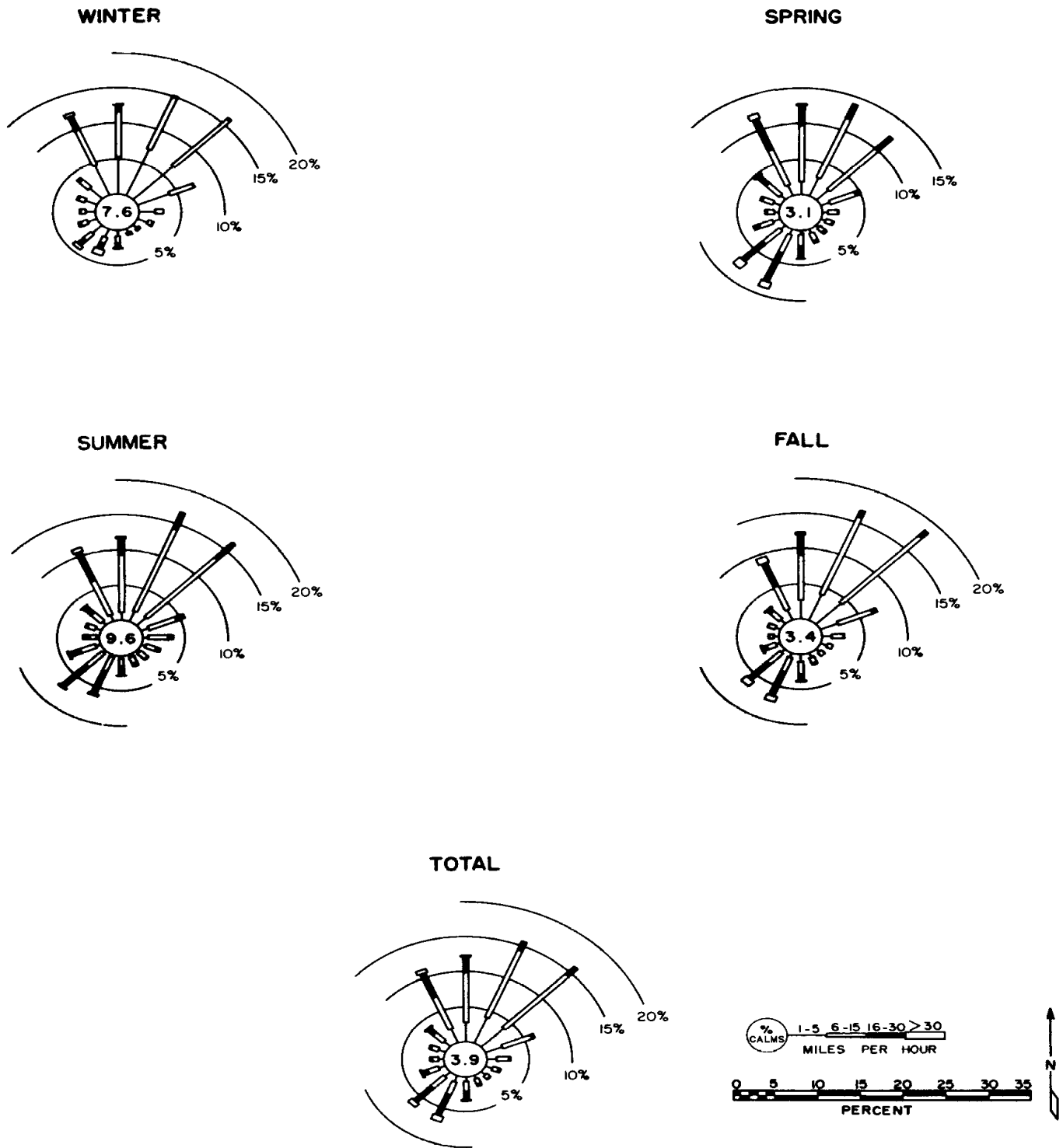


Figure A-12. Annual and seasonal wind roses for the 150 ft. level at TAN under inversion conditions from May 1956 through May 1962.

Some specific conclusions based on the data from TAN are as follows:

1. A distinct channeling effect of the wind is apparent. The directions with the highest percentages of occurrence are the south to southwest and northwest to northeast quadrants.
2. A very small percentage of the wind direction originates from the west and southeast quadrants.
3. A much higher frequency of calm periods occurs during the winter months, approximately 2.5 times as often as for any other season. The lowest frequency of calm periods occurs during the summer season (June - August).
4. Higher wind speeds are observed during lapse conditions than during inversion conditions.
5. Higher wind speeds and hence, a smaller frequency of calms are observed at the 150 ft. level.
6. A greater diversity of wind direction is observed at TAN as compared to CFA.

A distinct diurnal trend is also evident in the data from both locations. There is a tendency for an increase in the frequency of winds from the northeast quadrant during the nighttime hours at CFA. The increase is not large, however, and is due to the lag of the diurnal shift of the wind direction after the temperature stability class has changed from lapse to inversion near sunset, and back sometime after sunrise. Thus, southwest winds can continue to blow for some hours after sunset. Conversely, the northeast winds associated with down-valley drainage conditions can continue to blow in the morning after the inversion has dissipated near the ground. There is also a tendency for shallow southwest drainage winds to occur at CFA (often less than 500 ft. deep). This is due to the local sloping of the terrain from southwest to northeast.

The shift of wind direction with a change from lapse to inversion is much more pronounced at TAN than at CFA. This is evidenced by the

increase in the percentage of northeast winds at night at TAN. The distribution indicates that, for a certain fraction of time, there exists an opposing wind direction between CFA and TAN. Winds from the southwest at CFA and from the northeast at TAN can be observed simultaneously. Indeed, the predominate wind direction at TAN in the winter season is from the northeast and Birch Creek, while at CFA it is from the southwest.

On-site Wind Averages and Maximums

Monthly average wind speeds and corresponding directions at the 20 and 250 ft. levels, together with the highest hourly average wind speeds and corresponding directions for a given month at CFA are listed in Table A-1. The same type of information for the 20 and 150 ft. levels at TAN is listed in Table A-2. The month with the highest average wind speed at the 20 ft. level at both CFA and TAN is April. The speed values are 9.3 and 9.5 mph, respectively. The month with the lowest average wind speed at the 20 ft. level at both CFA and TAN is December. The speed values are 5.1 and 4.6 mph, respectively.

Both the monthly and hourly wind speeds at the two stations are similar in magnitude. The highest hourly average wind speeds for CFA and TAN are 67 and 62 mph, respectively. The wind directions for all of the highest hourly speeds listed for CFA are from the west-southwest and southwest. This is not always true at TAN, however, where strong winds are often channeled towards TAN from Birch Creek located to the northwest.

Some months show a difference in direction between levels at the same station for the highest hourly wind speed. These differences are mostly an artifact caused by the difference in the period of record, or by periods of missing data when only one level was operational. However, strong winds from either the north through northwest or southwest directions may be observed at TAN.

Table A-1. Average monthly and annual wind speeds for CFA at 20 and 250 ft. AGL together with the highest hourly average wind speed and the concurrent direction of occurrence.

	Monthly Average		Highest Hourly Average			
	20-ft. ^a	250-ft. ^b	20-ft Level ^c		250-ft Level ^d	
	Level (mph)	Level (mph)	Speed (mph)	Direction (quad.)	Speed (mph)	Direction (quad.)
January	5.6	9.7	48	WSW	65	SW
February	6.9	11.3	36	SW	52	WSW
March	8.7	13.8	51	WSW	67	WSW
April	9.3	14.6	39	WSW	49	WSW-SW
May	9.3	14.3	41	SW	47	WSW-SW
June	8.9	14.2	36	SW	46	WSW-SW
July	8.0	13.5	35	WSW	47	WSW
August	7.7	13.1	40	WSW	54	SW
September	7.2	12.8	42	WSW	56	WSW
October	6.8	12.3	44	WSW	58	WSW
November	6.4	11.6	40	WSW	54	WSW
December	5.1	9.6	43	SW	56	SW
ANNUAL	7.5	12.6	51	WSW	67	WSW

- a. Data period of record spans April 1950 through October 1964.
- b. Data period of record spans July 1951 through October 1964.
- c. Data period of record spans April 1950 through October 1983.
- d. Data period of record spans July 1951 through October 1983.

Peak wind gusts stratified by month and observed at CFA and TAN are given in Table A-3. The measurement levels are the same as those given previously. The maximum instantaneous gust recorded at CFA at the 20 Ft. level was 78 mph from the west-southwest. The maximum gust at the same level at TAN was 67 mph from the south. Higher gusts occur at greater heights on each of the towers. Winds gusts at the INEL may be a result of either pressure gradients from large-scale systems, or the result of local thunderstorms. Most gusts from pressure gradients are channeled from the southwest. However, gusts from thunderstorms can be expected from any direction since they may form in any location and move in any direction.

Regional Near-surface Wind Flow Patterns

Hourly-averaged historical wind data have been used to assemble an INEL and vicinity map containing wind roses from each of the meteorological monitoring stations (Figure III-1). This map is illustrated in Figure A-13a with the wind rose from each off-site station and representative on-site stations presented its relative geographical position. A wind rose map of the INEL containing only data from on-site stations, with the exception of TRA, is presented in Figure A-13b. The GRD3 wind rose is representative of TRA. Data from a two or three-year period (usually January 1980 through December 1982)

Table A-2. Average monthly and annual wind speeds for TAN at 20 and 150 ft. AGL together with the highest hourly average wind speed and the concurrent direction of occurrence.

	Monthly Average		Highest Hourly Average			
	20-ft. ^a	150-ft. ^b	20-ft Level ^a		150-ft Level ^b	
	Level (mph)	Level (mph)	Speed (mph)	Direction (quad.)	Speed (mph)	Direction (quad.)
January	4.7	7.0	41	SSW	48	SSW
February	5.9	8.8	46	SSW	48	SW
March	8.3	11.7	50	M ^c	59	SW
April	9.5	14.9	50	NW	62	NW
May	8.9	13.8	43	SW	55	SSW
June	8.9	13.6	40	SW	51	SW
July	8.1	12.9	38	SSW	47	SW
August	7.4	12.3	35	WSW	49	SSW
September	6.8	11.5	42	SW	53	SSW
October	6.3	11.1	40	NW	51	NNW
November	5.7	9.6	43	SW	57	N
December	4.6	7.1	41	SSE	53	NNW
ANNUAL	7.1	11.2	50	NW	62	NW

- a. Data period of record spans July 1950 through October 1964.
b. Data period of record spans April 1956 through October 1964.
c. Direction data is missing.

were used to produce the wind roses. Each separate wind rose is presented in an expanded view in Figures A-14 through A-18. A number of features are readily apparent upon inspection of the figures.

First, the predominate southwest/northeast flow direction of the ESRP is evident in most of the wind roses. This predominance is a result of the orientation of the ESRP when convective heating couples the surface winds with the persistent westerly winds aloft. Prefrontal winds are also invariably southwesterly. Nocturnal drainage winds are from the northeast at most stations. The monitoring stations which exhibit these phenomena are Idaho Falls (IDF), Kettle Butte (KTB), and St. Anthony (STA).

Second, subtle terrain features adjacent to individual stations considerably affect the overall southwest/northeast flow. These features modify the wind direction when a low wind speed prevails, particularly during inversion conditions. The Argonne National Lab-West (ANL), Rover (ROV), and Terreton (TRN) stations have considerably broadened northwest/southeast components due to drainage winds moving northwest from elevated terrain located to the south and east of these stations. The Power Burst Facility (PBF) has an augmented southerly component which results from slightly higher terrain located to the south. Both Hamer (HMR) and Dubois (DBS) have significant distributions of easterly winds caused by terrain blockage of the airflow at the north end of the ESRP.

Table A-3. Monthly and period of record peak wind gusts with concurrent wind directions for CFA at 20 and 250 ft. AGL and for TAN at 20 and 150 ft. AGL.

	CFA				TAN			
	20-ft. Level ^a		250-ft. Level ^b		20-ft. Level ^c		150-ft. Level ^d	
	Direction (quad.)	Speed (mph)	Direction (quad.)	Speed (mph)	Direction (quad.)	Speed (mph)	Direction (quad.)	Speed (mph)
January	SW	78	S	75	S	58	NNW	64
February	WSW	60	SW	66	N and SSW	62	SW	59
March	WSW	78	SW	84	N	65	SW	73
April	S	67	SW	62	SSW	60	NW	76
May	SW	62	SSW	67	NNW	60	NNW	66
June	SSW	60	SSW	75	S	67	SW	76
July	N	68	S	66	W	60	W	73
August	WSW	62	SW	72	SSW	64	WSW	68
September	WSW	61	WSW	70	SSW	54	W	73
October	WSW	66	WSW	76	NNW	63	NW	64
November	WSW-SW	60	WSW	70	SW	59	NNW	78
December	SW	64	SSW	80	NNW	62	NNW	68
Period Of Record	WSW	78	SW	84	S	67	NNW	78

- a. Data period of record spans April 1950 through October 1964.
- b. Data period of record spans July 1951 through October 1964.
- c. Data period of record spans July 1950 through April 1961.
- d. Data period of record spans April 1956 through April 1961.

Third, channeled canyon cold air drainage dominates the wind distributions at stations located at the boundaries of mountain valleys and the ESRP. Arco (ARC), Blue Dome (BDM), Montevue (MTV) and TAN (particularly the lower level) are dominated by this flow pattern. The Dunes (DUN), the Naval Reactor Facility (NRF), and Rover (ROV) stations have augmented northwesterly winds which result from the influence of these canyon winds as they flow out onto the ESRP. The other monitoring stations not specifically enumerated above exhibit some or all of the main flow characteristics given in the preceding discussion.

An analysis of wind speed and direction distributions at a given station under specific meteorological conditions enhances understanding of the wind flow regime. Wind roses for the 33 and 200 ft. levels on the Grid 3 (GRD3) tower have been prepared for a two-year period (January 1981 through December 1982). The data were categorized into Pasquill-Gifford stability classes, using measured temperature gradients as defined by the U.S. Nuclear Regulatory Commission (U.S. NRC, 1972). These wind roses are illustrated in Figures A-19 and A-20.

Several conclusions can be drawn from the data stratified in this manner. First, in neutral

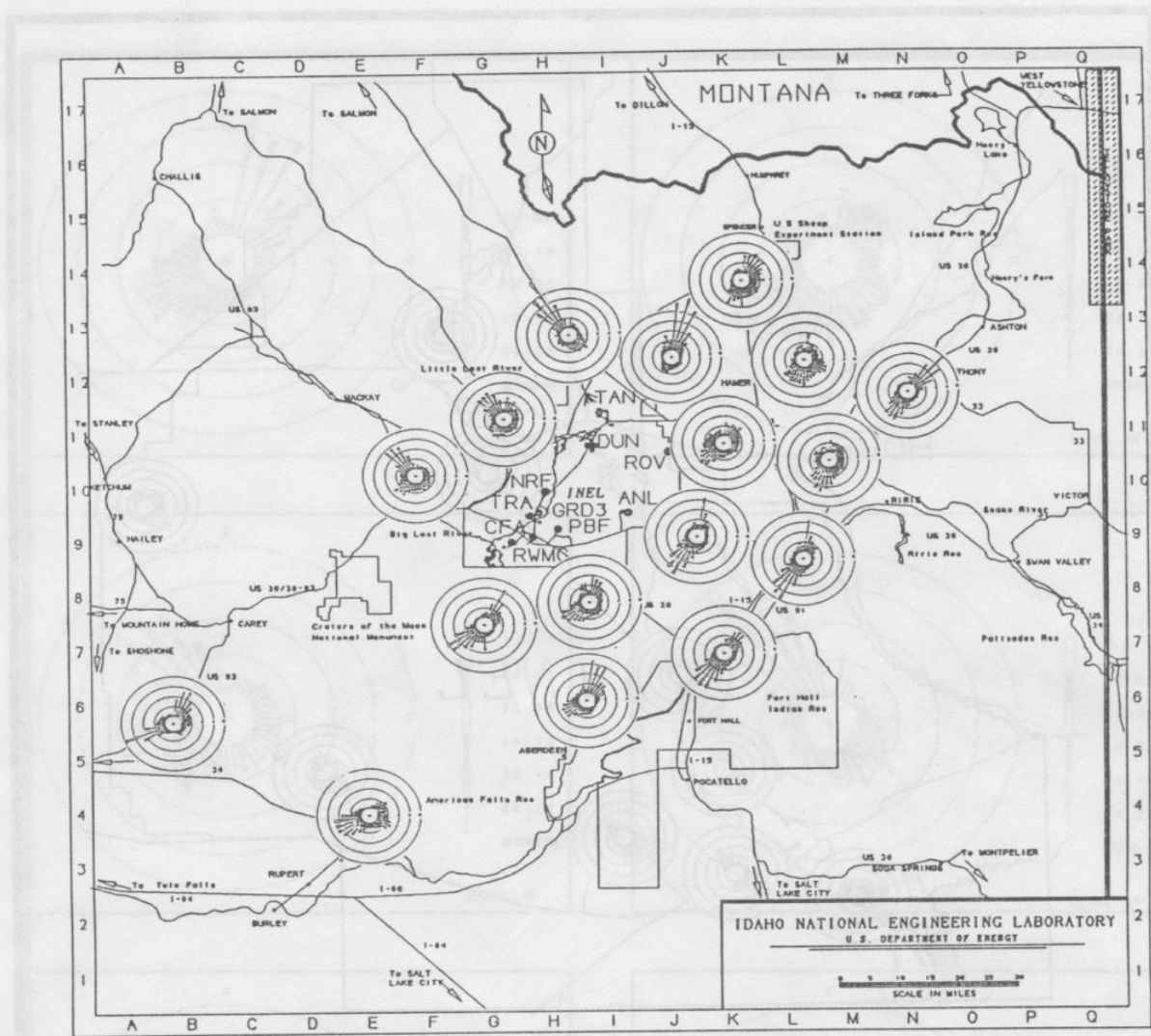


Figure A-13a. Regional INEL wind flow patterns indicated by off-site meteorological monitoring stations.

conditions, i.e., stability class D, the upper and lower levels show very similar characteristics. No large wind shears are evident. Stability class D is common when the atmospheric thermal gradient is near adiabatic due to high wind speeds with strong mechanical turbulence or during heavy overcast conditions when the net radiation flux is very small. Under high wind conditions, the possibility

of a large directional shear with height is minimized.

Second, in stable conditions, i.e., stability classes E and F, the flow near the surface becomes decoupled from the winds aloft. Stability classes

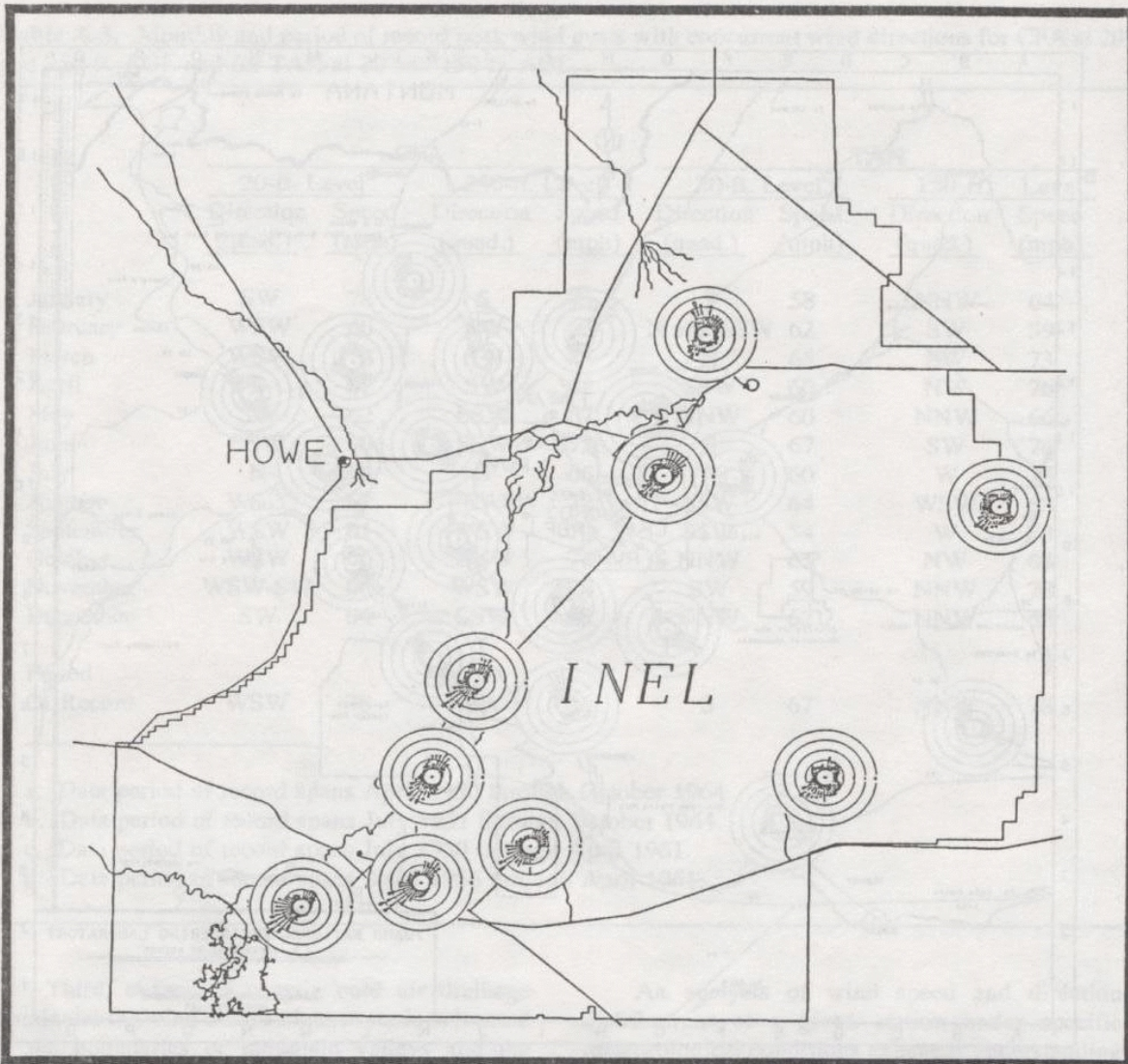


Figure A-13b. Local INEL wind flow patterns indicated by wind roses from on-site meteorological monitoring stations. TRA is represented by GRD3 wind rose.

E and F indicate the presence of temperature inversions. Large shears in wind direction between the upper and lower levels are manifest under these conditions. Additionally, the surface wind exhibits a large variability in direction (meander) during conditions of low wind speeds.

Third, during unstable conditions, i.e., stability classes A, B, and C, winds at both the upper and lower levels are influenced by buoyant eddies which rise as air is warmed at the surface. Stability classes A-C are common when solar heating is strong. The buoyant eddies tend to broaden the directional distribution which would

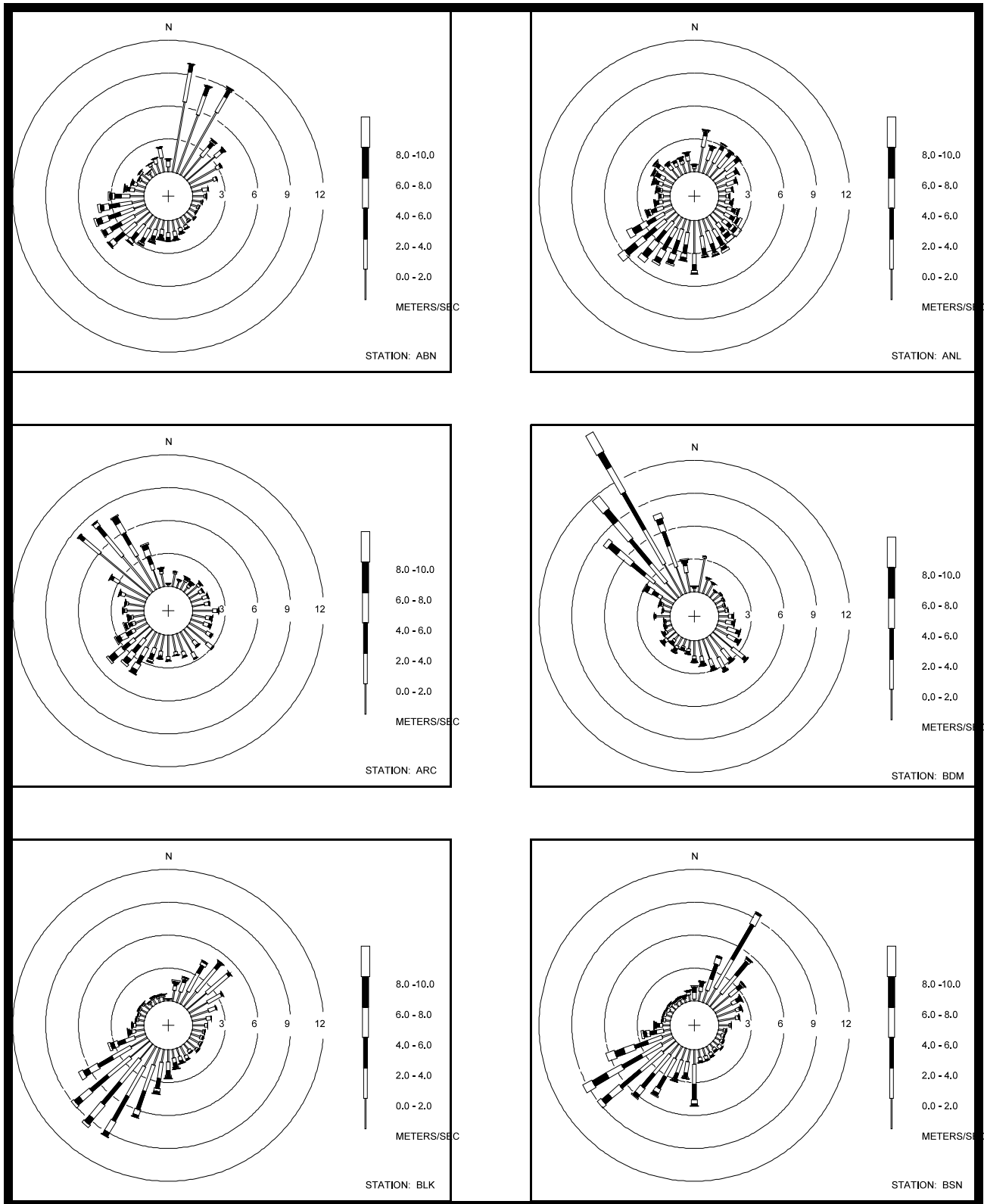


Figure A-14. Joint wind speed and direction frequency distributions for Aberdeen (ABN), Argonne National Laboratory-West (ANL), Arco (ARC), Blue Dome (BDM), Blackfoot (BLK), and Big Southern (BSN) during 1980 through 1982.

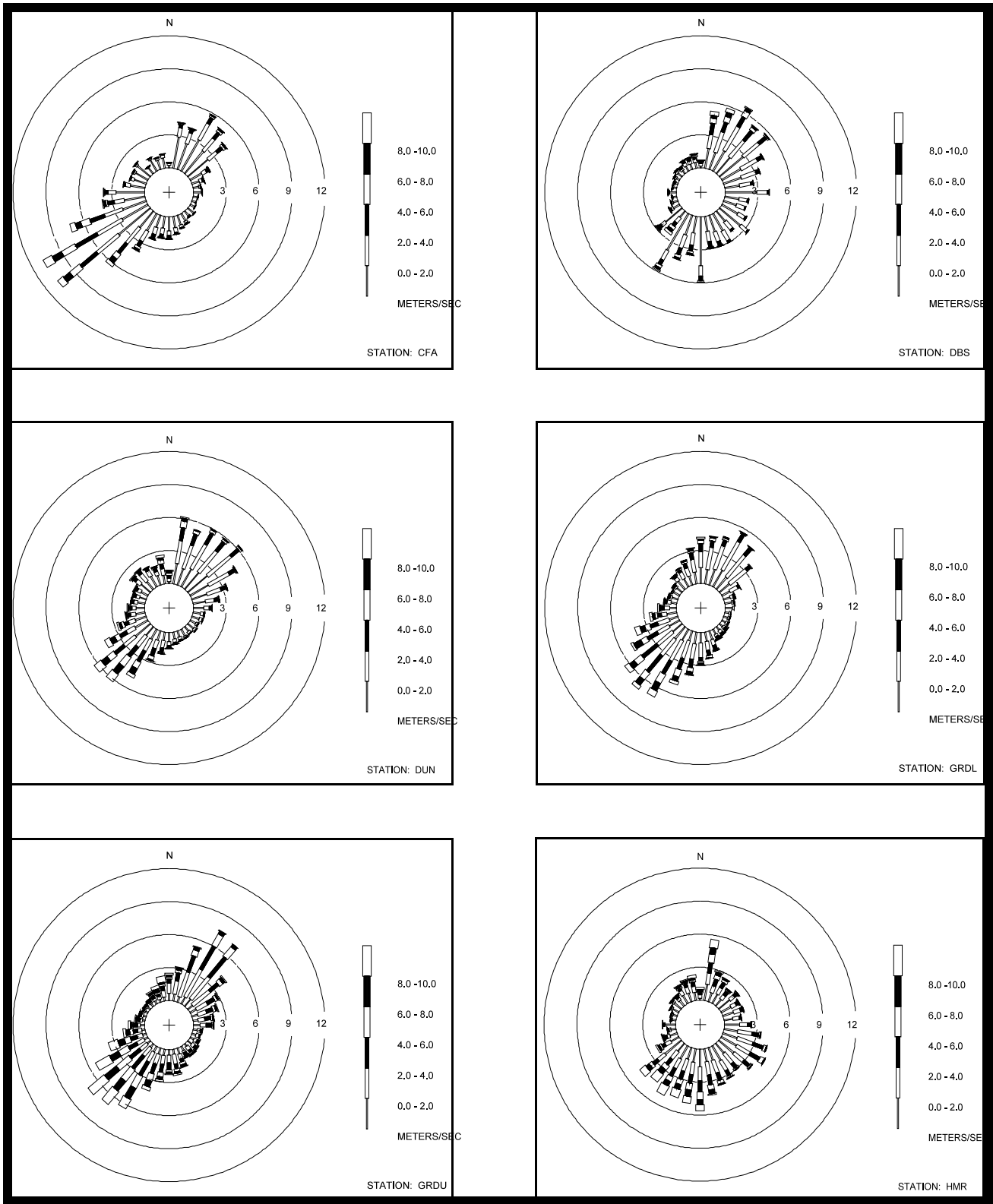


Figure A-15. Joint wind speed and direction frequency distribution for CFA, Dubois (DBS), Dunes (DUN), GRD3 32.8 ft. level (GRDL), GRD3 200 ft. level (GRDU), and Hamer (HMR) during 1980 through 1982 (1981 through 1982 for GRD3).

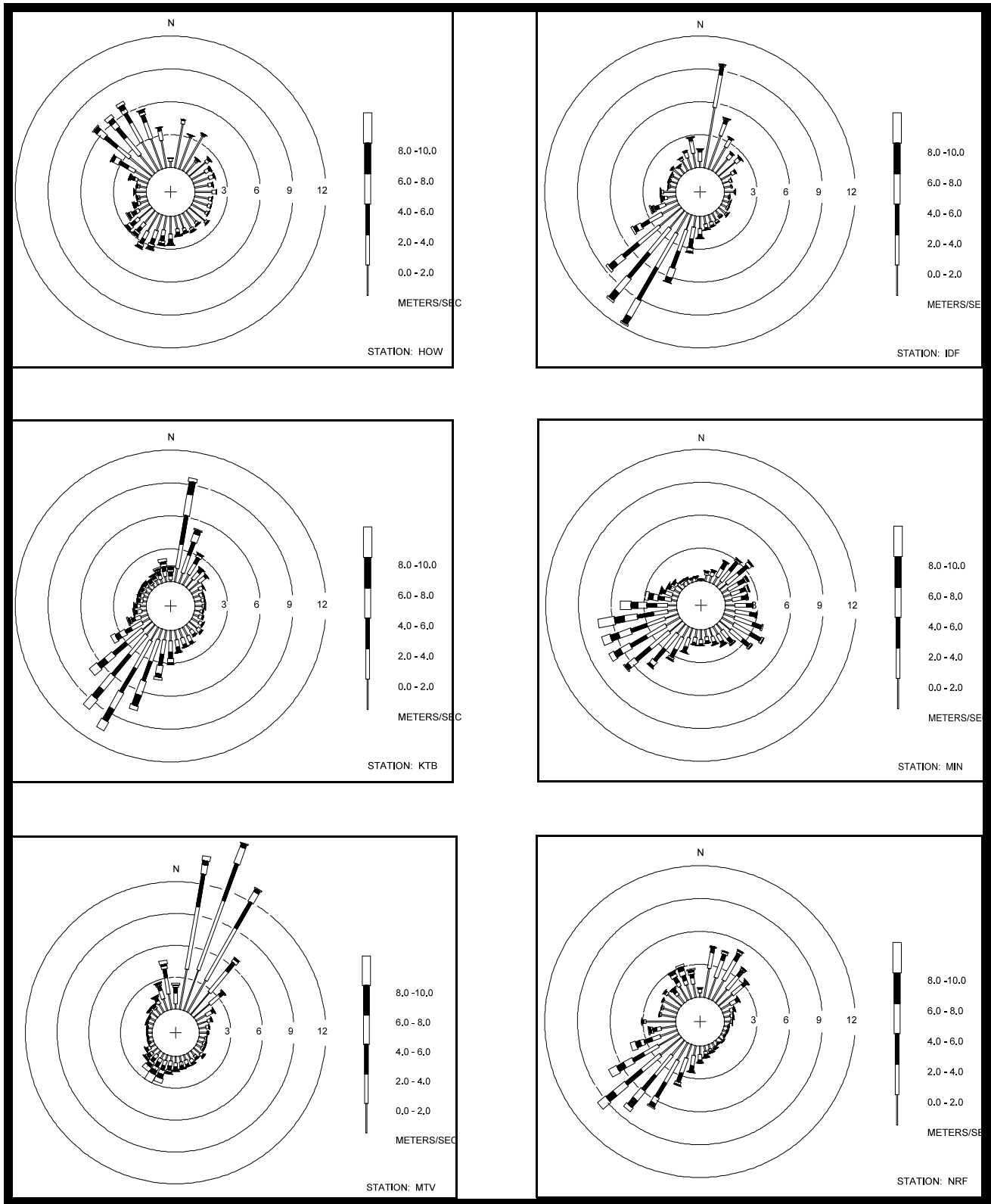


Figure A-16. Joint wind speed and direction frequency distributions (wind roses) for Howe (HOW), Idaho Falls (IDF), Kettle Butte (KTB), Minidoka (MIN), Monteview (MTV), and the Naval Reactor Facility (NRF) during 1980 through 1982.

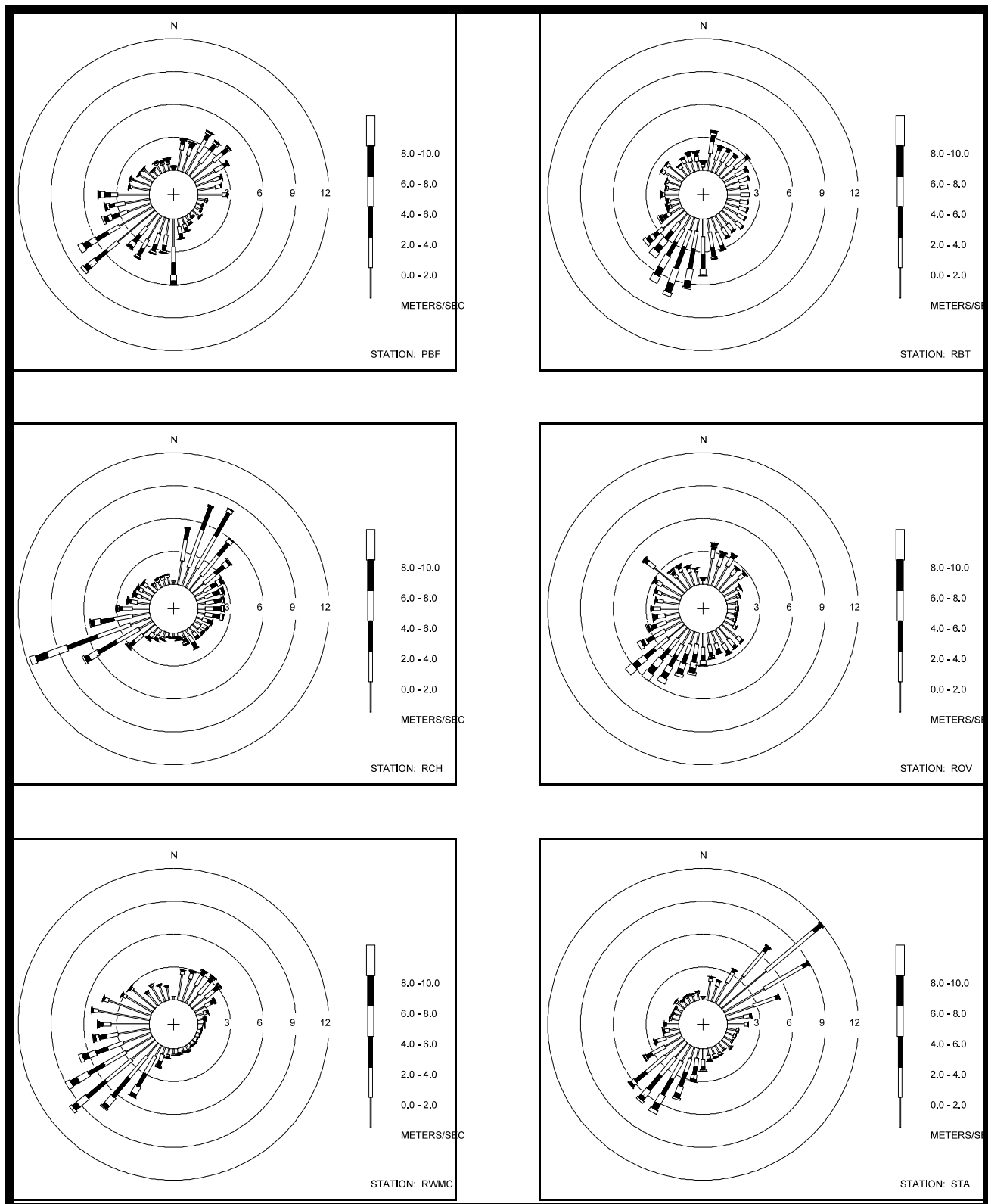


Figure A-17. Joint wind speed and direction frequency distributions (wind roses) for Power Burst Facility (PBF), Roberts (RBT), Richfield (RCH), Rover (ROV), Radioactive Waste Management Center (RWMC), and St. Anthony (STA) during 1980 through 1982.

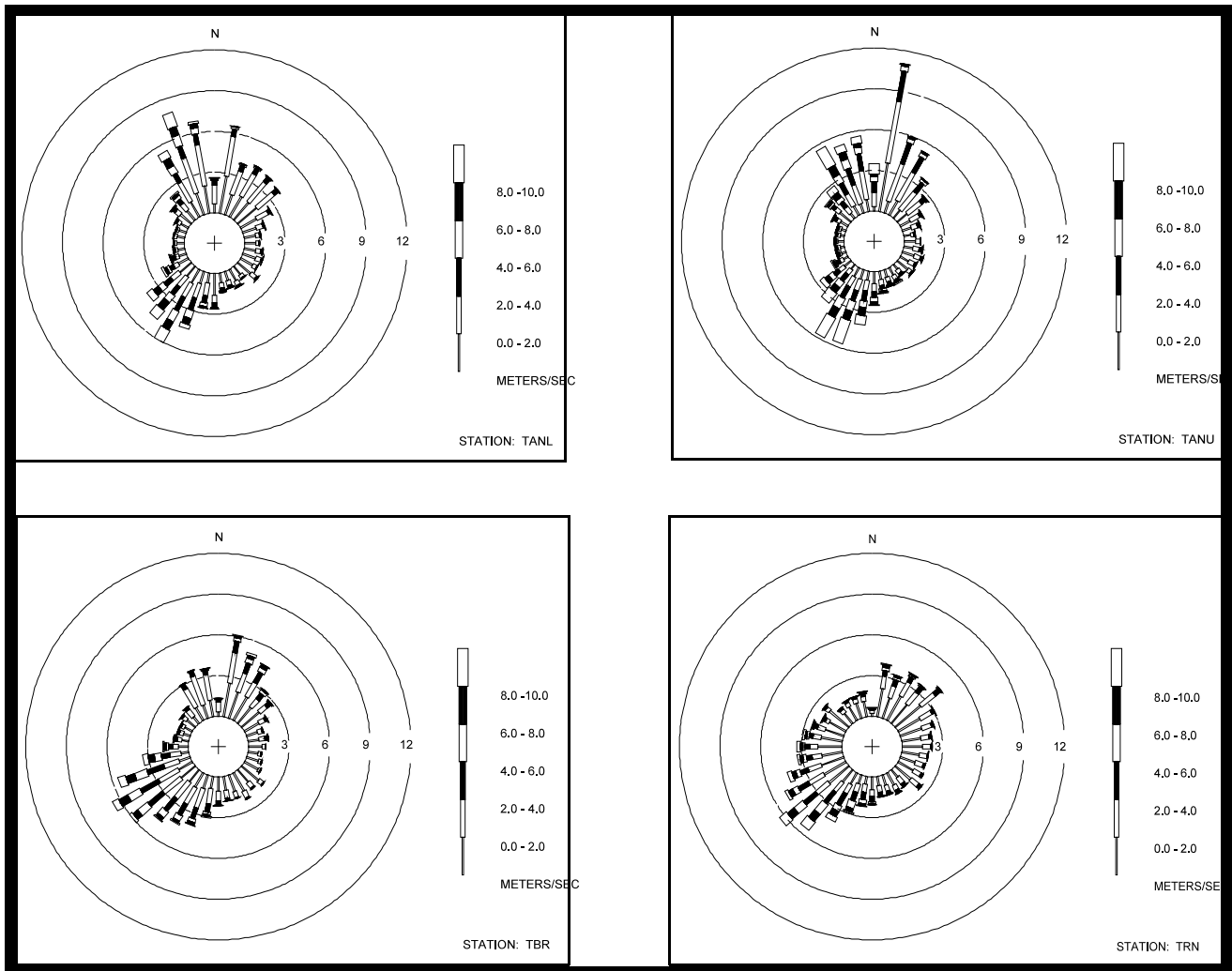


Figure A-18. Joint wind speed and direction frequency distributions (wind roses) for the Loss of Fluid Test 32.8 ft. level (TANL), Loss of Fluid Test 150 ft. level (TANU), Tabor (TBR), and Terreton (TRN) during 1980 through 1982.

otherwise exist, because they are somewhat randomly distributed spatially. This disruption is weakest at the upper level where, due to a reduction of friction effects the winds are stronger.

Winds Aloft

An extensive record of upper air observations has been assembled from routine pibal (pilot balloon) observations for the period from 1950 through 1965. A pibal was released every morning at CFA during those years between 0800 and 1000

hours in order to obtain the wind speed and direction at selected levels above the surface. These balloons were tracked up to heights of 14,000 ft. m.s.l. The primary purpose of these soundings was to provide information for short-term forecasts in support of INEL operations. However, a detailed wind rose analysis of the compiled data set is helpful in understanding the INEL wind regime.

Wind roses for the winter, spring, summer, and fall seasons are shown in Figures A - 21

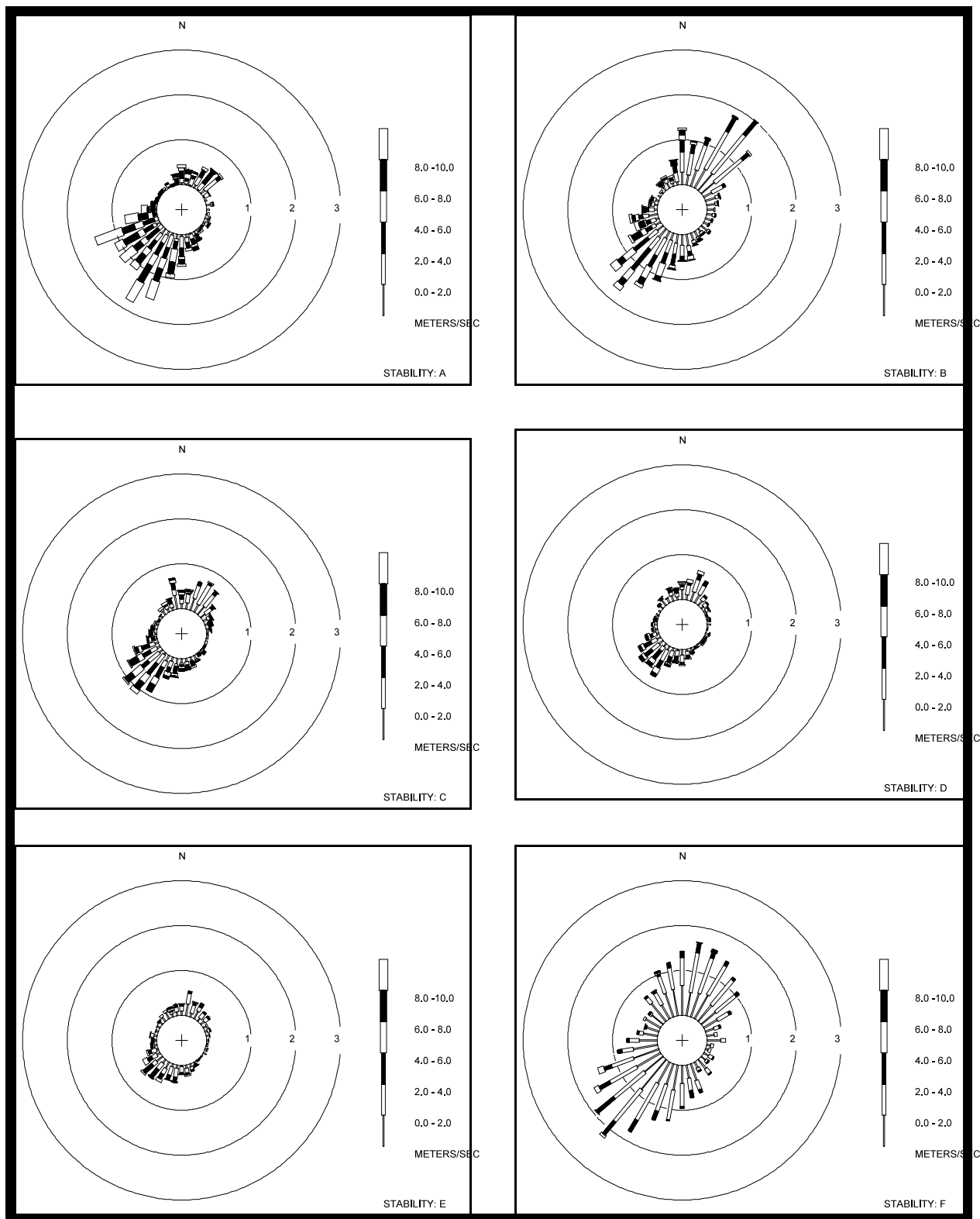


Figure A-19. Joint wind speed and direction frequency distributions (wind roses) stratified by air temperature stability class (A-F) for the 32.8 ft. level at GRD3 during 1981 and 1982.

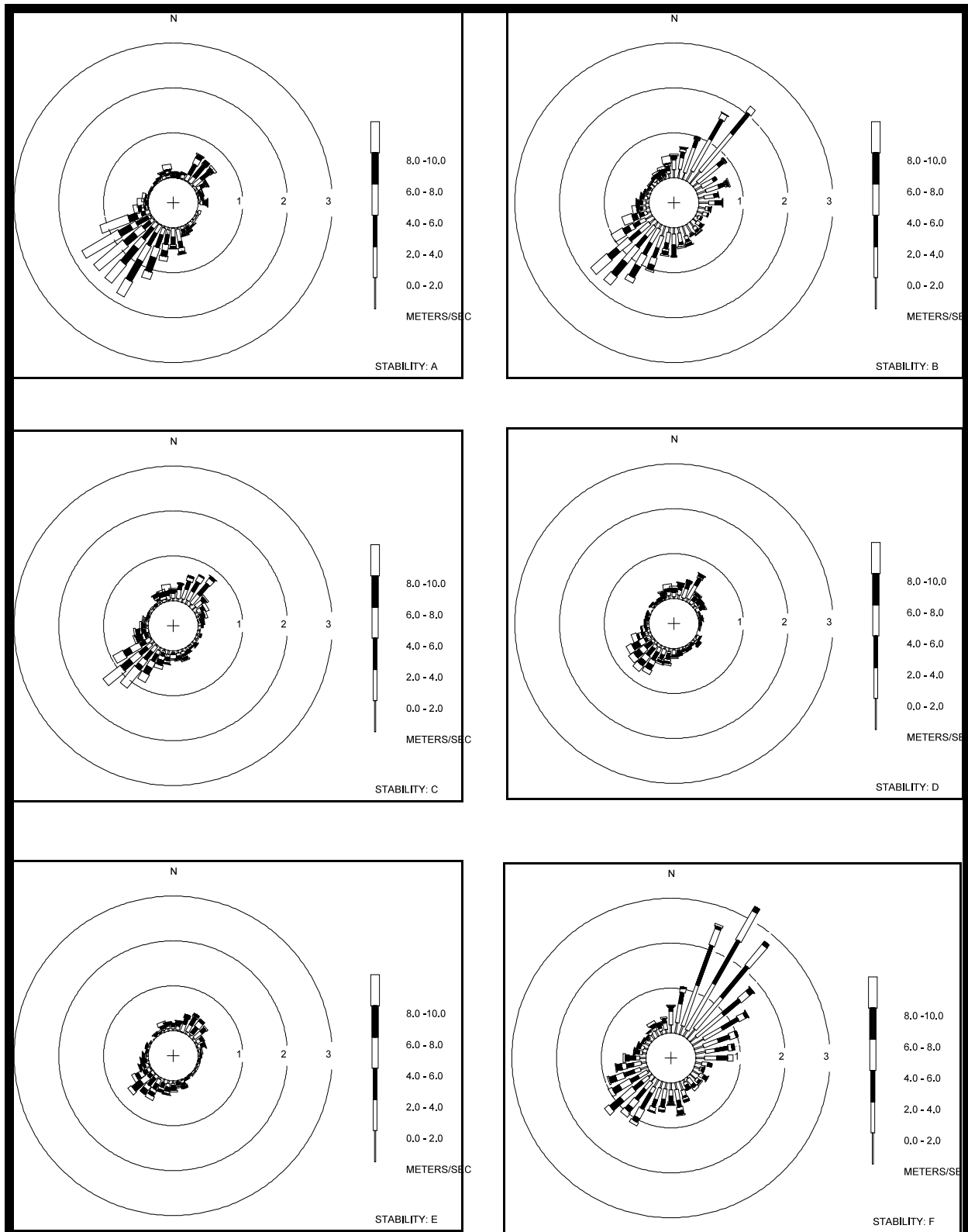


Figure A-20. Joint wind speed and direction frequency distributions (wind roses) stratified by air temperature stability class (A-F) for the 200 ft. level at GRD3 during 1981 and 1982.

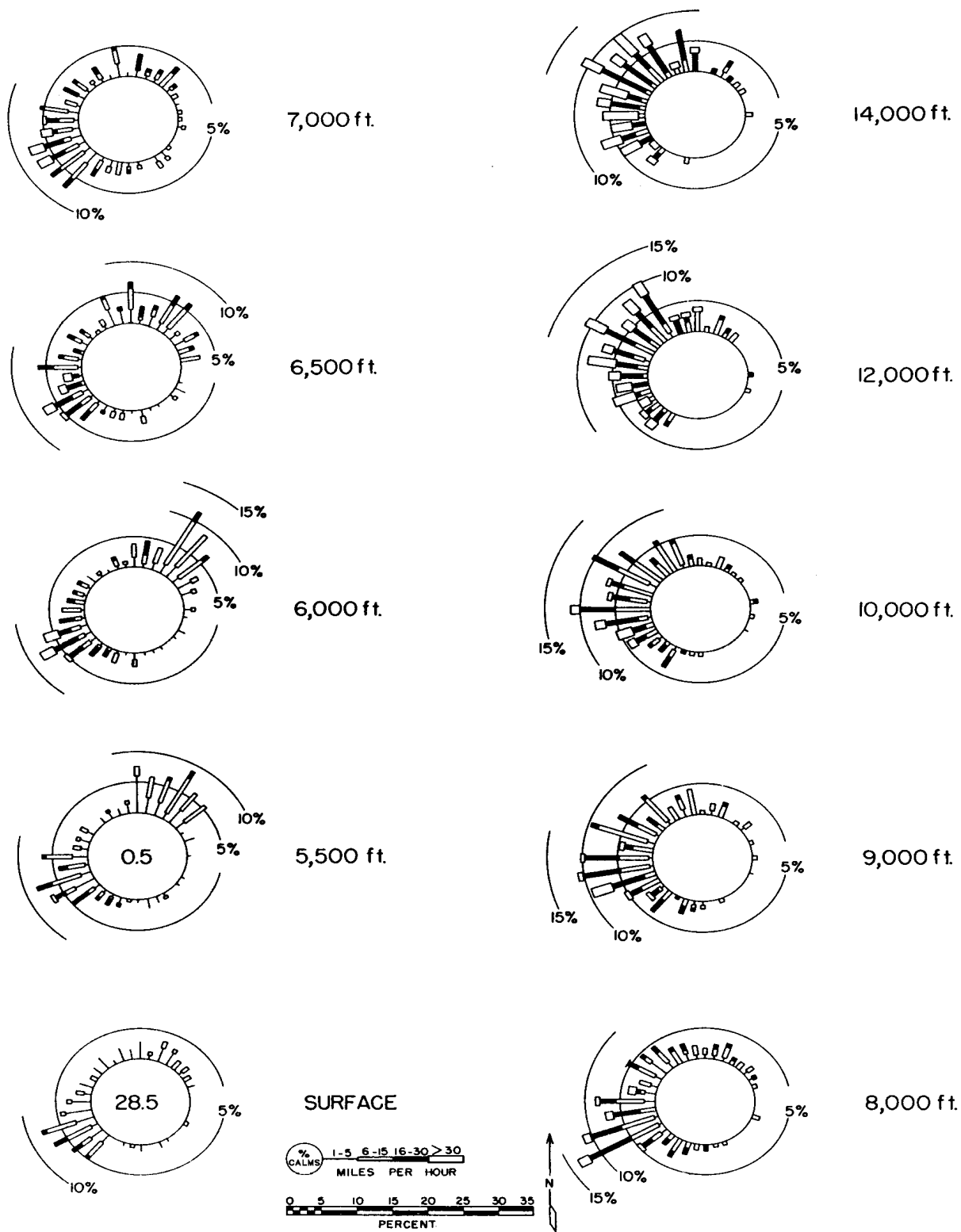


Figure A-21. Upper air wind roses obtained from pibal soundings for the winter season (December-February) during 1950 through 1965.

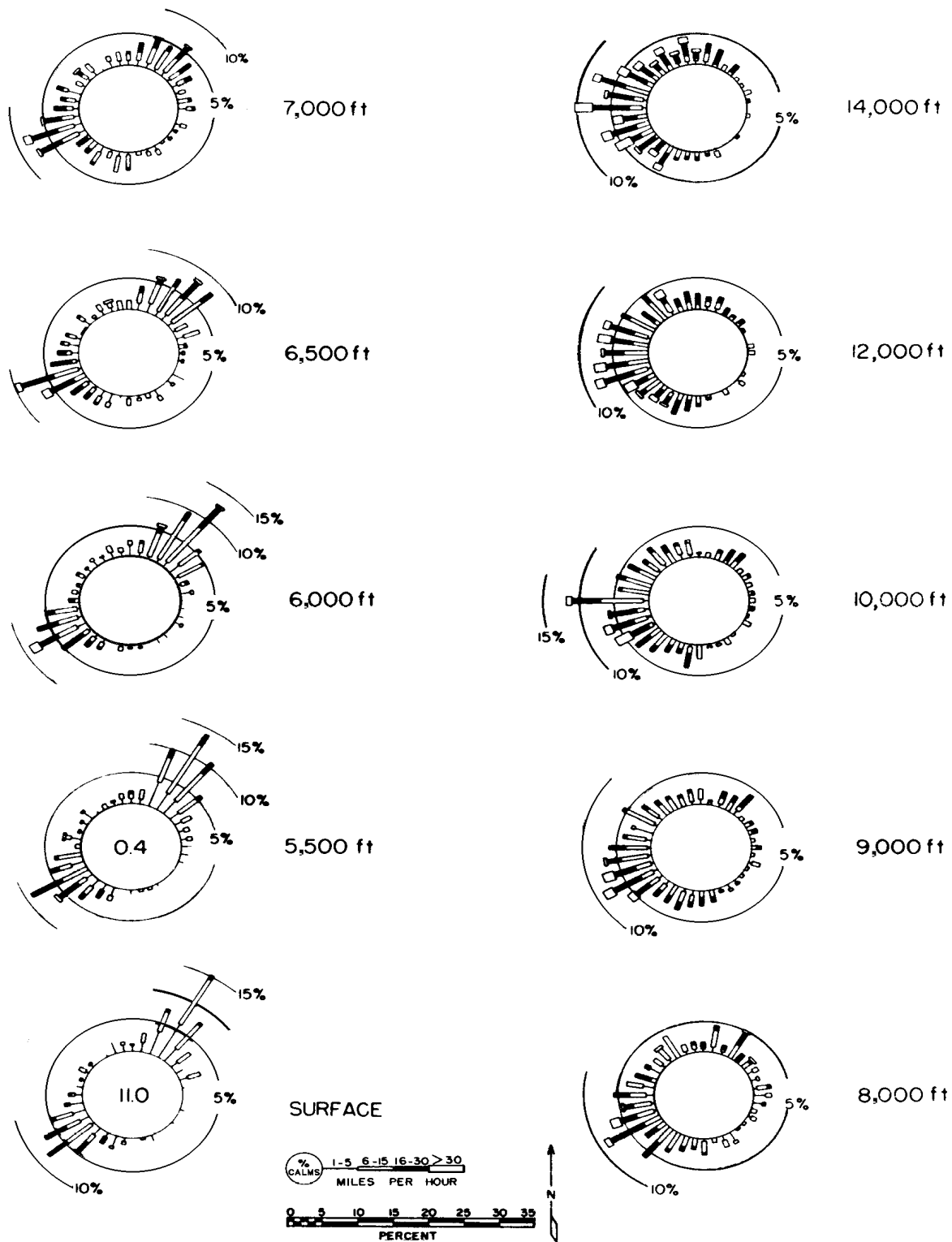


Figure A-22. Upper air wind roses obtained from pibal soundings for the spring season (March-May) during 1950 through 1965.

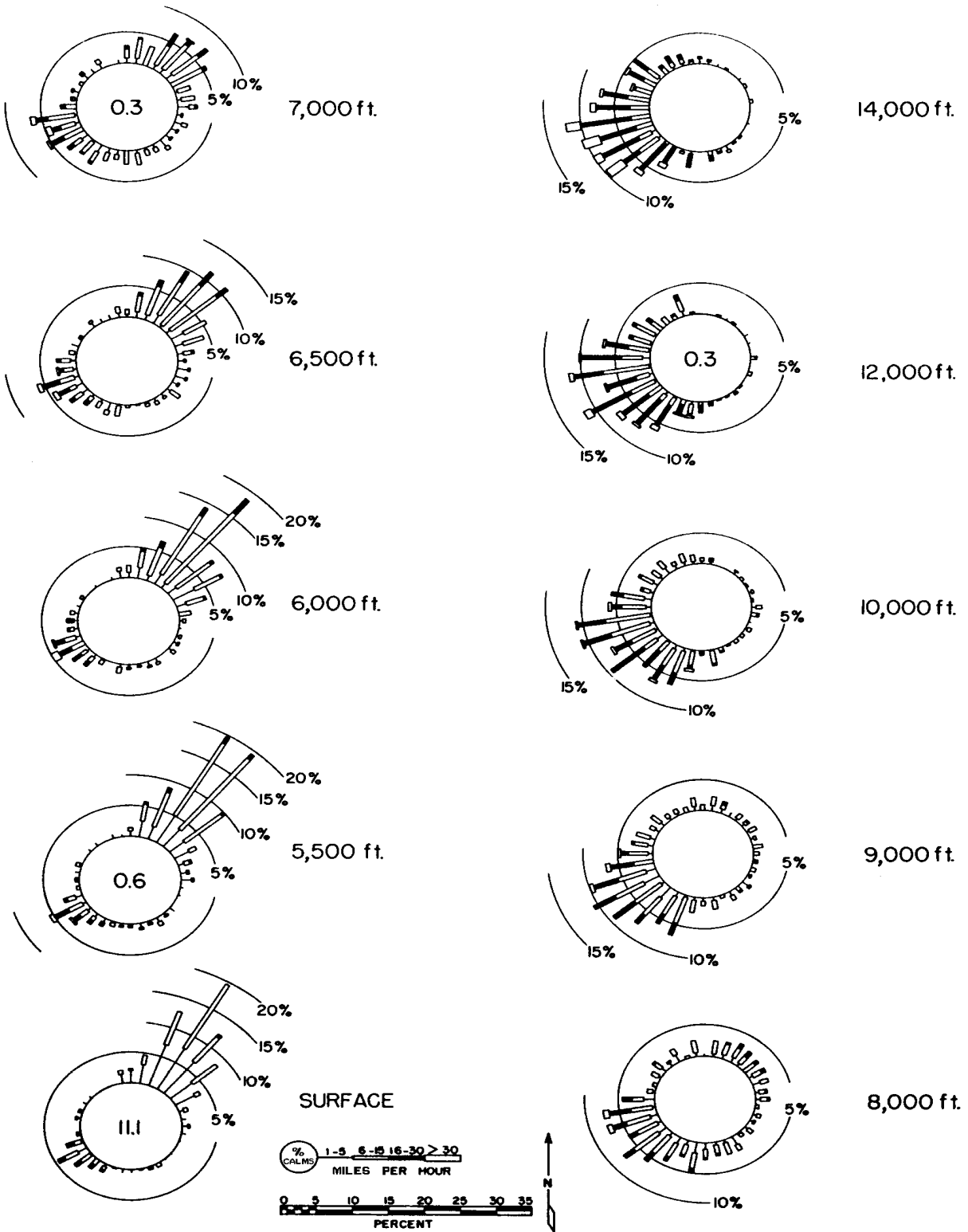


Figure A-23. Upper air wind roses obtained from pibal soundings for the summer season (June-August) during 1950 through 1965.

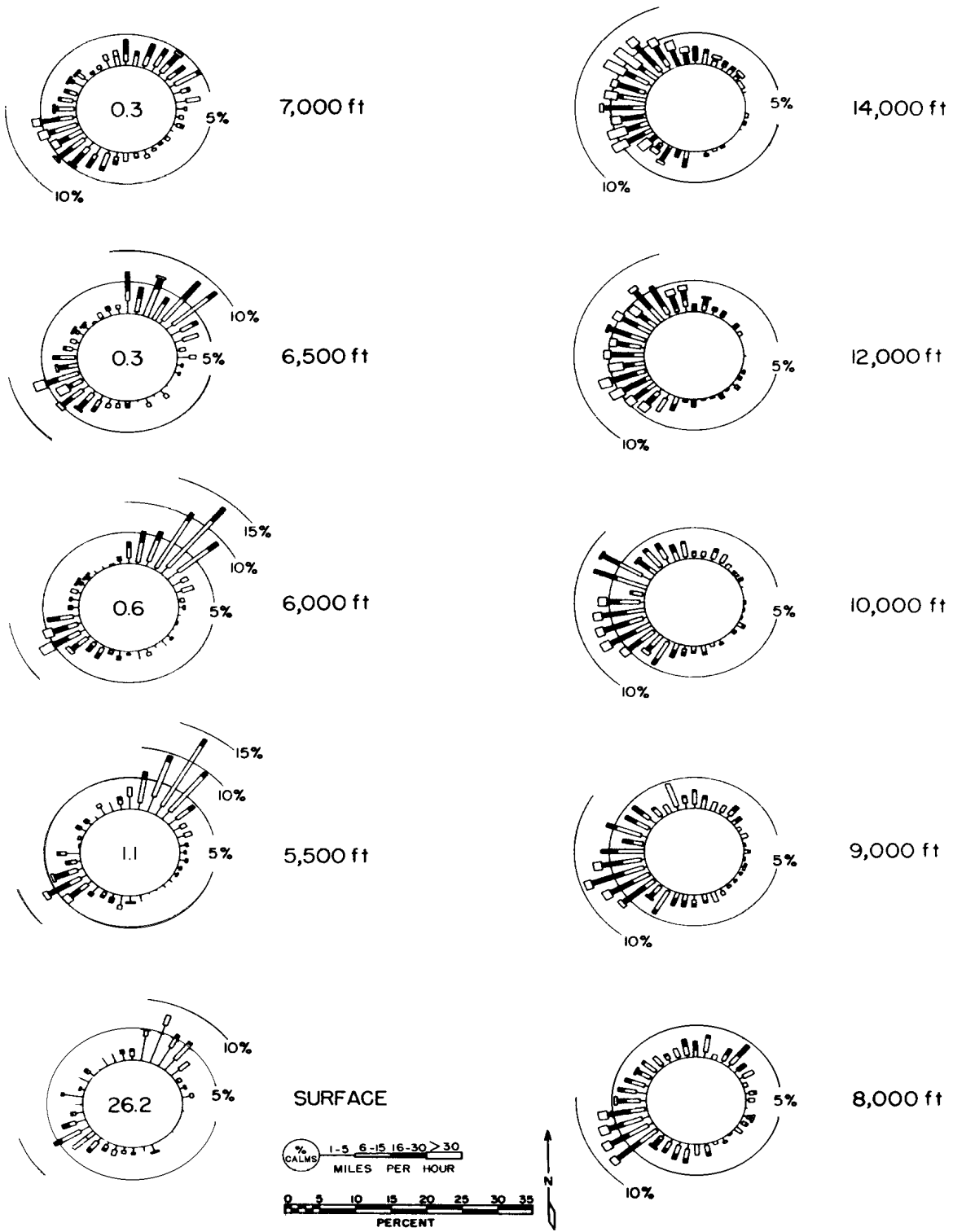


Figure A-24. Upper air wind roses obtained from pibal soundings for the fall season (September-November) during 1950 through 1965.

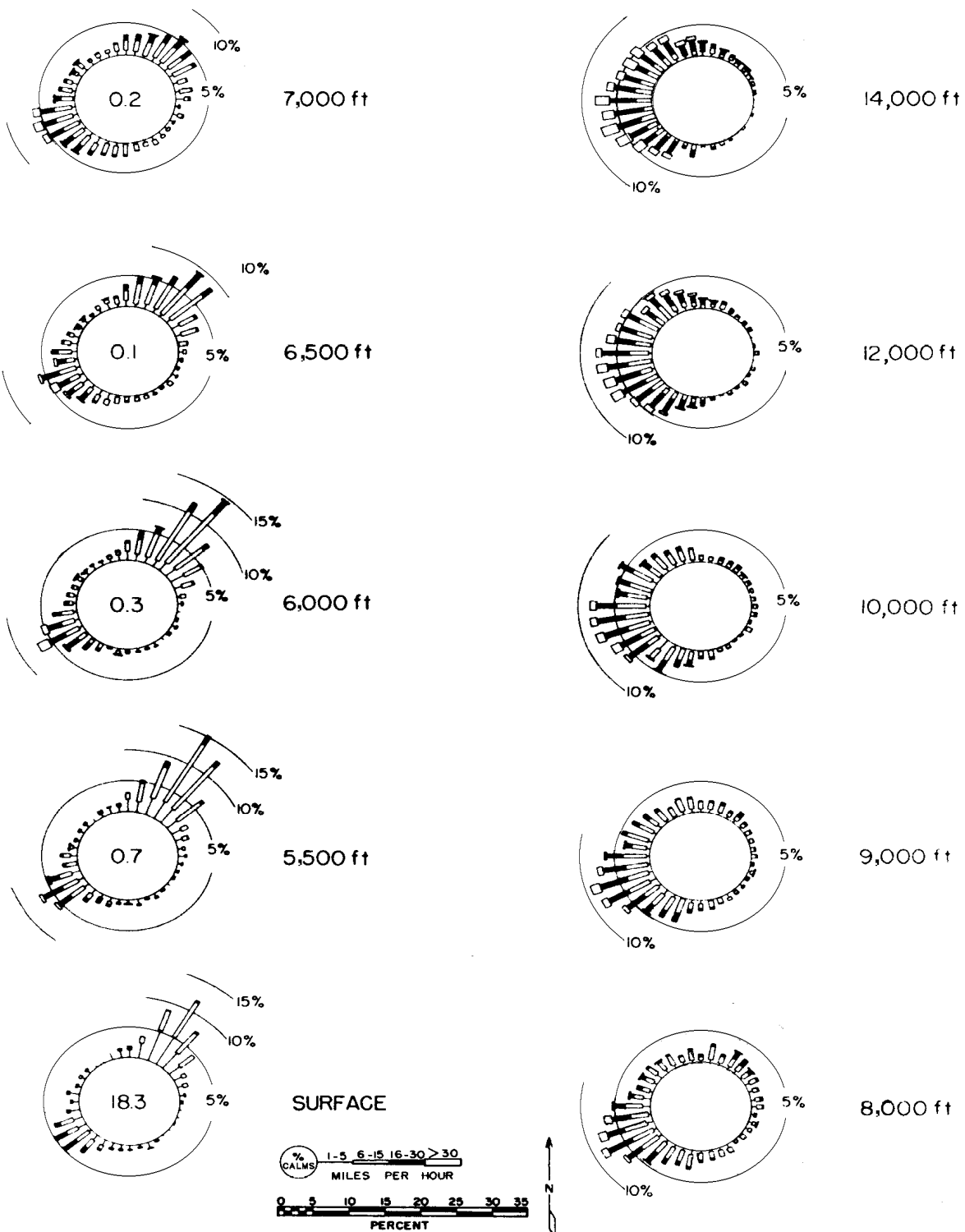


Figure A-25. Upper air wind roses obtained from pibal soundings combined for all seasons during 1950 through 1965.

through A-24. A combined wind rose from all seasons is shown in Figure A-25. These wind roses illustrate several features of the wind speed and direction variation with height above the INEL. A higher frequency of the northeast drainage winds near the surface at the lower levels is apparent during the morning hours in every season of the year. This is particularly noticeable during the spring and summer months. A higher frequency of calms or light winds occurs in the winter and the fall seasons also near the surface at the lower levels. Winter exhibits the shallowest layer of northeast drainage winds, while the deepest layer is observed in the fall. The frequency of northeast winds decreases and the frequency of west-southwest winds increases with height in every season of the year. The presence of the prevailing westerlies at and above the general mountain tops (10,000 ft. m.s.l.) is also seen in every season of the year. However, the predominant direction in the winter is northwest,

shifting to west in the spring, southwest in the summer, and back to northwest in the fall.

The effects of various synoptic patterns on the upper level winds over the INEL during the different seasons can be seen in the assemblage of data shown in Figure A-26. This figure is a graph of mean wind speed with height as a function of season. Since sunrise is earlier in the summer than in the winter, the pibals observed in the winter were usually made when the temperature inversion was at its peak strength. The observations made in the summer were usually obtained after the inversion layer had begun to dissipate.

The higher wind speeds observed in the winter at the upper levels (Figure A-26) are due to intense pressure systems prevalent during that season of the year. The low wind speeds observed in the summer at the higher levels are due to the flat pressure gradients prevalent during that season of the year. The relatively light wind speeds seen

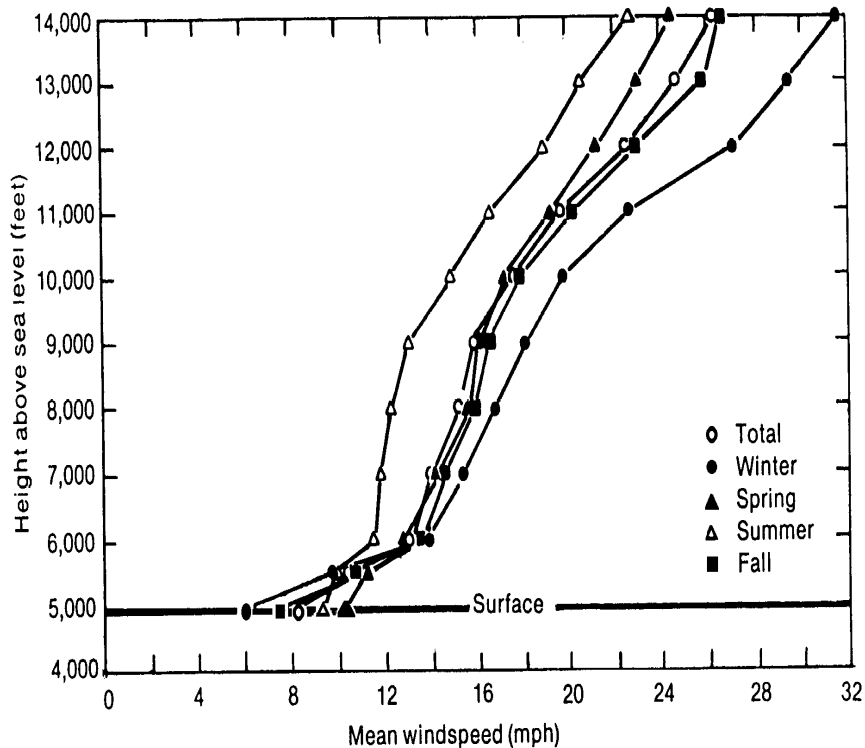


Figure A-26. Seasonal and annual average upper air wind speeds obtained from pibal observations during 1950 through 1965.

during the fall and winter near the surface are the results of the effects of strong stability. The stronger winds in the summer and spring at the lower levels are the result of less stratification. Hence, the greater wind speeds aloft more readily affect the speeds at lower levels.

Three typical pibal observations are illustrated in Figure A-27. These soundings are representative of the 3 most commonly observed wind speed and direction profiles. Although these data are from the winter season, they nevertheless illustrate the general profile features possible in any season. The sounding from 24 December 1964 shows a very strong southwest flow at all

observation levels due to the presence of a strong pressure gradient. The sounding from 11 January 1965 is an example of an extremely weak pressure gradient which causes wide direction variations and light wind speeds. The sounding from 12 December 1964 shows moderate southwest winds at the higher levels which do not extend to the surface due to the presence of an inversion layer at the surface. The northeasterly surface drainage winds gradually turn easterly, then southeasterly, then southerly, and finally southwesterly with increasing height inside this stable layer. This type of sounding occurs with extreme regularity in the absence of strong frontal or low pressure systems.

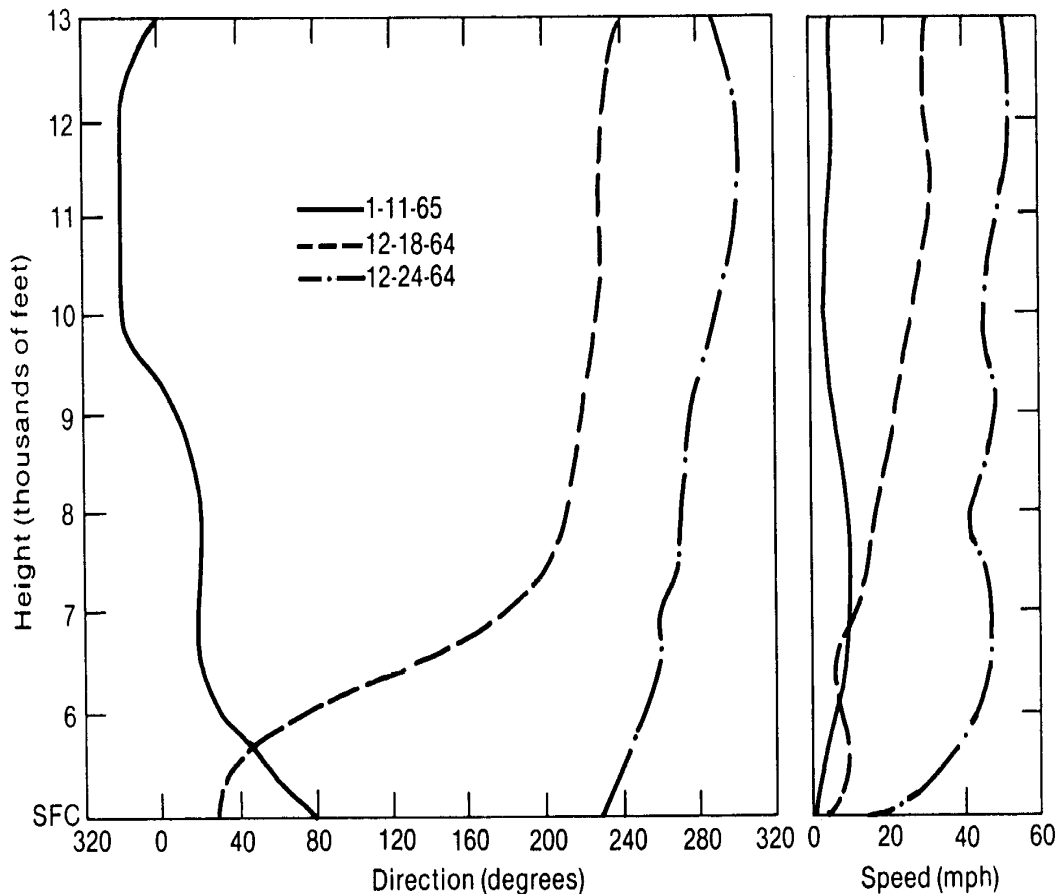


Figure A-27. Example upper air wind speed and direction profiles during conditions of strong pressure gradients (24 December 1964), weak pressure gradients (11 January 1965) and air temperature inversions (12 December 1964).

Section B Air Temperatures

A knowledge of air temperatures is necessary for an appropriate facility design. Perhaps just as important is a knowledge of the daily, monthly, and annual air temperature characteristics for forecasting and for airborne effluent dispersion calculations.

Surface air temperatures at the INEL are best characterized by two stations: CFA and TAN. A third regime is known to exist around the ANL area. The ANL air temperature data base is not extensive enough, however, to fully define its characteristics at this time. Average CFA temperature parameters reported here are based on the full (over 35-year) period of record in the archive. The existing 14- to 15-year period of record for TAN is too short to establish a traditional 30-year average as reported by the NCDC. The actual TAN records have been normalized to a 30-year period using the records from surrounding stations with full 30 year records according to standard NCDC procedures.

Daily Near-Surface Characteristics

The average (maximum plus minimum divided by 2) daily air temperatures for CFA and the normalized average daily air temperatures for TAN are listed in Tables B-1 and B-2, respectively. Heating degree-days are also listed in Tables B-1 and B-2, and are discussed later. These data are presented graphically in Figures B-1 and B-2 for CFA and TAN, respectively. The data indicate that the average daily air temperature for the 39-year period of record at CFA ranges from a low of 10 °F on 02 January, to a high of 70 °F on several days in late July. The 30-year normalized average daily air temperature at TAN ranges from a low of 13 °F during mid January to a high of 70 °F during the latter half of July. The apparent time difference in the occurrence of the winter minimum air temperature between the two sites is caused

by the normalization routine for the data at TAN.

The average daily air temperature ranges (difference between maximum and minimum) for CFA and TAN are also listed in Tables B-1 and B-2 and illustrated in Figures B-1 and B-2, respectively. The smallest average daily air temperature range at CFA occurs on 14 January, with a value of 20 °F. The largest average daily air temperature range at CFA occurs on 09 July and 04 September with a value of 41 °F. The normalized average daily air temperature ranges for TAN are the smallest in December and January with a value of about 26 °F. The largest normalized average daily air temperature range occurs in July and August at TAN with a value of approximately 40 °F. As can be seen, the smallest daily air temperature range occurs in the winter, while the largest daily air temperature range occurs in the summer. This phenomenon is more easily seen in the monthly summary of the daily air temperature ranges given in Table B-3. July and August have average daily air temperature ranges of 38 °F, while December and January have average daily air temperature ranges of 23 °F at CFA. Table B-3 also shows that the largest daily air temperature ranges ever recorded at CFA and TAN were 59 and 62 °F, respectively. Thus, large daily air temperature ranges can be expected at either CFA or TAN, and at any other location on the INEL.

The daily extremes of temperature for CFA from 1950 through 1988 are given in Appendix 1 and summarized in Table B-4. A summary of the actual extremes for TAN is also provided in this table. The highest maximum air temperature ever recorded at CFA is 101 °F, while the coldest minimum is -47 °F. The highest maximum and coldest minimum air temperatures ever recorded for TAN are 103 and -49 °F, respectively.

Table B-1. Average daily air temperature (Mean), daily air temperature range (RNG), and daily heating degree-days (Heat. DGD) for CFA^a.

Day	January		February		March		April		May		June	
	Mean (F)	RNG (F)										
1	11	28	17	23	27	22	37	24	47	30	55	30
2	10	26	16	23	25	23	37	24	47	30	56	32
3	12	25	16	26	24	23	37	26	48	32	57	32
4	12	22	17	27	25	26	39	29	48	30	57	32
5	13	23	18	25	26	24	40	31	48	32	58	31
6	14	22	17	28	27	24	40	27	49	28	59	30
7	14	25	20	26	28	23	39	26	49	28	57	28
8	14	25	20	27	29	25	38	30	50	28	56	29
9	16	22	20	27	30	24	40	28	50	29	58	30
10	16	22	20	25	29	23	40	28	49	29	57	30
11	15	24	20	27	28	22	40	29	49	27	59	33
12	17	23	23	24	28	24	40	31	49	31	59	32
13	18	21	22	24	29	23	42	32	50	32	59	31
14	19	20	22	23	28	24	42	31	50	32	59	33
15	19	21	23	21	30	25	42	30	51	31	59	31
16	20	21	24	21	30	23	43	32	51	29	60	31
17	19	21	24	21	30	23	43	30	52	32	60	33
18	19	21	23	23	31	23	43	27	52	31	61	35
19	18	23	24	22	31	24	41	28	53	31	63	35
20	18	23	23	25	30	26	42	28	53	30	63	33
21	17	24	23	23	32	25	43	29	53	28	62	32
22	16	23	23	24	34	25	44	30	53	30	62	32
23	17	23	24	23	34	25	45	29	54	31	64	34
24	17	23	25	24	34	25	44	28	54	29	62	33
25	18	22	25	24	34	26	44	27	54	30	62	35
26	18	22	24	25	35	25	44	25	54	32	63	35
27	17	22	25	24	35	23	44	28	55	32	64	35
28	16	23	26	25	34	24	45	29	55	32	64	37
29	16	25	22	26	35	26	45	28	55	32	63	34
30	16	23	22	26	36	26	45	30	55	29	62	38
31	17	23	37	26	37	26	45	30	54	32	62	38

Table B-1. (Continued).

Day	July			August			September			October			November			December		
	Mean (°F)	RNG (°F)	Heat. DGD															
1	64	37	1	69	38	0	60	38	5	50	36	15	36	30	29	23	24	42
2	64	36	1	68	38	0	62	37	3	49	37	16	35	30	30	24	24	41
3	65	36	0	69	37	0	60	39	5	49	37	16	35	30	30	25	22	40
4	65	39	0	68	39	0	61	41	4	48	38	17	36	30	29	23	24	42
5	66	38	0	68	38	0	61	39	4	49	38	16	36	29	29	21	22	44
6	67	36	0	68	38	0	62	38	3	49	39	16	36	28	29	21	22	44
7	67	36	0	68	38	0	62	38	3	48	35	17	36	27	29	22	23	43
8	67	40	0	68	37	0	61	34	4	47	36	18	33	27	32	17	23	48
9	68	41	0	67	40	0	59	38	6	48	34	17	33	28	32	18	21	47
10	68	35	0	69	39	0	58	35	7	47	36	18	33	27	32	19	22	46
11	67	36	0	68	39	0	58	33	7	48	33	17	34	23	31	18	23	47
12	68	37	0	67	38	0	56	34	9	46	31	19	33	22	32	19	20	46
13	68	37	0	67	38	0	56	35	9	46	32	19	32	22	33	17	24	48
14	69	38	0	66	37	0	55	34	10	44	34	21	30	22	35	17	24	48
15	69	40	0	66	38	0	54	36	11	44	34	21	28	22	37	18	26	47
16	69	39	0	66	37	0	55	36	10	44	36	21	27	24	38	19	24	46
17	69	36	0	67	38	0	55	35	10	43	37	22	28	23	37	19	24	46
18	69	38	0	66	38	0	54	36	11	43	37	22	28	22	37	19	23	46
19	69	38	0	66	36	0	54	35	11	44	35	21	27	21	38	19	24	46
20	69	38	0	65	36	0	51	30	14	43	35	22	28	21	37	20	21	45
21	68	37	0	65	36	0	51	32	14	42	33	23	26	22	39	20	24	45
22	68	38	0	64	38	1	51	37	14	41	32	24	27	21	38	19	23	46
23	70	39	0	64	39	1	52	38	13	41	31	24	26	22	39	17	22	48
24	69	39	0	64	39	1	52	37	13	40	31	25	28	22	37	18	23	47
25	70	38	0	64	38	1	52	37	13	41	32	24	27	23	38	18	21	47
26	70	39	0	64	38	1	52	37	13	40	32	25	25	22	40	16	23	49
27	70	37	0	63	36	2	51	37	14	38	33	27	23	24	42	16	25	49
28	69	38	0	63	37	2	51	35	14	38	33	27	24	22	41	15	23	50
29	70	35	0	63	37	2	50	36	15	38	32	27	23	24	42	14	22	51
30	69	38	0	62	37	3	50	36	15	37	30	28	23	24	42	14	23	51
31	69	37	0	61	36	4	50	36	15	37	30	28	23	24	42	13	23	52

a. Data period of record spans January 1950 through December 1988.

Table B-2. Normalized 30-year (1930-1959) average daily air temperature (Mean), daily air temperature range (RNG), and daily heating degree-days (Heat. DGD) for TAN^a.

Day	January			February			March			April			May			June		
	Mean (°F)	RNG (°F)	Heat. DGD															
1	16	26	49	15	27	50	25	27	40	36	27	29	50	32	15	55	32	10
2	15	26	50	15	27	50	25	27	40	36	28	29	50	32	15	55	32	10
3	15	26	50	15	27	50	25	26	40	37	29	28	51	33	14	55	32	10
4	15	27	50	15	26	50	25	26	40	37	28	28	51	32	14	56	32	9
5	14	26	51	16	27	50	26	26	39	38	29	27	51	32	14	56	32	9
6	14	26	51	16	26	49	26	26	39	38	28	27	51	32	14	56	32	9
7	14	26	51	16	26	49	26	26	39	39	29	26	52	33	13	57	33	8
8	14	26	51	17	27	48	27	25	38	40	29	25	52	33	13	57	32	8
9	14	26	51	17	27	48	27	26	38	40	29	25	52	32	13	57	32	8
10	13	26	52	17	26	48	27	26	38	41	29	24	52	32	13	58	33	7
11	13	26	52	18	27	47	28	26	37	41	30	24	52	32	13	58	33	7
12	13	26	52	18	26	47	28	26	37	42	29	23	52	32	13	59	33	6
13	13	26	52	18	26	47	28	26	37	42	30	23	53	32	12	59	33	6
14	13	26	52	19	27	46	28	26	37	43	31	22	53	33	12	59	33	6
15	13	26	52	19	26	46	29	26	36	43	30	22	53	32	12	59	34	6
16	13	26	52	20	27	45	29	26	36	44	31	21	53	32	12	60	34	5
17	13	27	52	20	27	45	29	26	36	44	30	21	53	32	12	60	34	5
18	13	27	52	21	27	44	30	26	35	45	31	20	53	32	12	61	35	4
19	13	27	52	21	27	44	30	26	35	46	31	19	53	32	12	61	34	4
20	13	27	52	21	26	44	30	26	35	46	31	19	53	32	12	62	35	3
21	13	27	52	22	27	43	31	26	34	46	32	19	53	32	12	62	36	3
22	13	27	52	22	27	43	31	26	34	47	31	18	53	32	12	63	35	2
23	13	27	52	22	26	43	32	27	33	47	32	18	54	31	11	63	36	2
24	13	27	52	23	27	42	32	26	33	48	31	17	54	32	11	63	36	2
25	13	26	52	23	26	42	32	26	33	48	32	17	54	32	11	64	37	1
26	13	26	52	24	27	42	33	27	32	48	32	17	54	32	11	64	36	1
27	13	26	52	24	27	42	33	26	32	49	33	16	54	32	11	65	37	0
28	13	26	52	25	27	41	34	27	31	49	32	16	54	32	11	65	37	0
29	13	26	52	25	27	41	34	28	31	49	32	16	55	32	10	65	37	0
30	14	27	51	25	27	41	35	27	30	50	32	15	55	32	10	66	37	0
31	14	26	51	35	28	30	35	28	30	50	32	15	55	32	10	66	37	0

Table B-2. (Continued).

Day	July		August		September		October		November		December				
	Mean °F	RNG Heat. DGD	Mean °F	RNG Heat. DGD	Mean °F	RNG Heat. DGD	Mean °F	RNG Heat. DGD	Mean °F	RNG Heat. DGD	Mean °F	RNG Heat. DGD			
1	66	0	69	40	62	39	3	51	37	36	31	29	22	25	43
2	67	0	69	40	62	39	3	51	37	36	31	29	22	25	43
3	67	0	69	40	61	40	4	50	37	35	31	30	22	25	43
4	68	0	69	40	61	39	4	50	37	34	30	31	21	24	44
5	68	0	69	40	60	40	5	49	38	33	30	32	21	24	44
6	69	0	69	40	60	39	5	49	37	33	30	32	21	25	44
7	69	0	69	41	60	39	5	49	37	33	30	32	21	25	44
8	69	0	69	41	59	40	6	48	37	33	29	32	21	25	44
9	69	0	68	40	59	39	6	48	37	32	29	33	20	26	45
10	69	0	68	40	58	40	7	47	36	31	29	34	20	26	45
11	69	0	68	40	58	39	7	46	36	30	29	35	20	25	45
12	69	0	68	40	58	39	7	46	36	30	29	35	20	25	45
13	69	0	68	41	57	40	8	46	36	29	28	36	20	25	45
14	70	0	67	40	57	39	8	45	36	28	28	37	20	25	45
15	70	0	67	40	57	39	8	45	35	28	28	37	19	24	46
16	70	0	67	40	57	39	8	45	35	28	27	37	19	25	46
17	70	0	67	40	56	39	9	45	35	27	27	38	19	25	46
18	70	0	66	40	55	38	10	44	35	27	27	38	19	25	46
19	70	0	66	40	55	39	10	43	34	26	26	39	19	25	46
20	70	0	66	40	55	39	10	43	35	26	27	39	18	24	47
21	70	0	65	40	54	38	11	42	34	25	26	40	18	25	47
22	70	0	65	40	54	39	11	42	35	25	26	40	18	25	47
23	70	0	65	40	53	38	12	41	34	24	24	41	18	25	47
24	70	0	64	40	53	38	12	41	33	24	24	41	18	25	47
25	70	0	64	40	53	38	12	40	34	24	24	41	17	26	48
26	70	0	64	40	52	38	13	40	33	23	23	42	17	26	48
27	70	0	64	39	52	38	13	39	33	23	26	42	17	25	48
28	70	0	63	40	52	37	13	38	32	23	25	42	17	25	48
29	70	0	63	39	51	38	14	38	32	23	25	42	17	25	48
30	70	0	62	40	51	37	14	37	32	23	25	42	16	26	49
31	70	0	62	40	51	37	14	37	31	23	25	42	16	26	49

a. Data period of record spans April 1950 through December 1964.

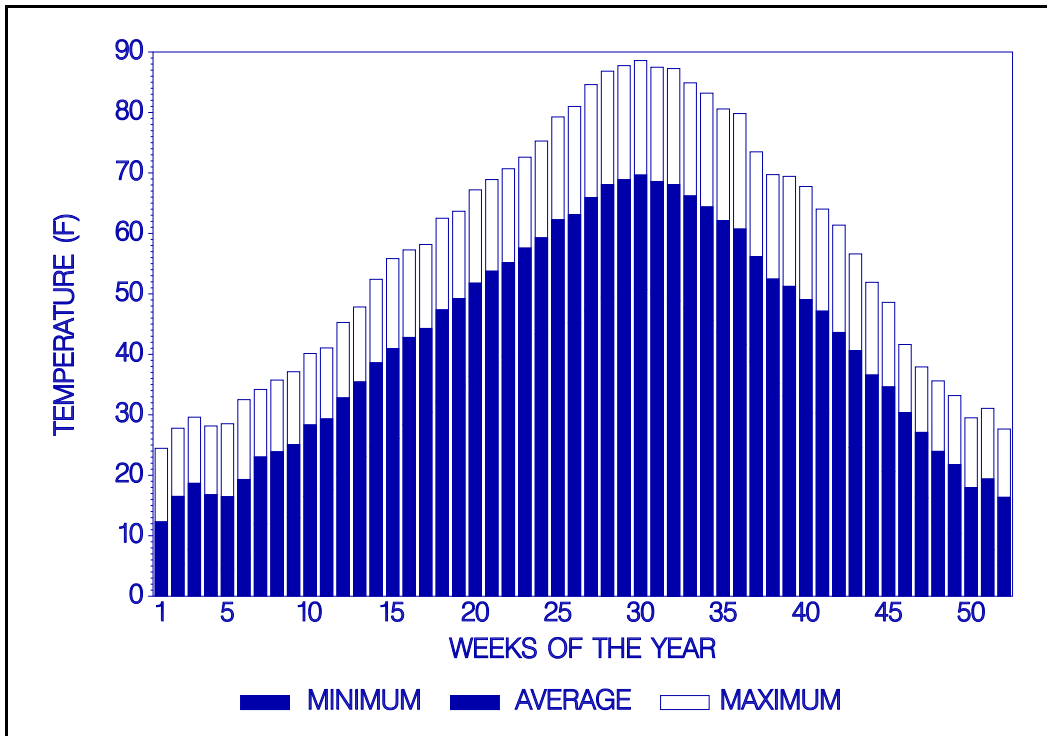


Figure B-1. Mean weekly minimum, average, and maximum air temperatures at CFA from January 1950 through December 1988.

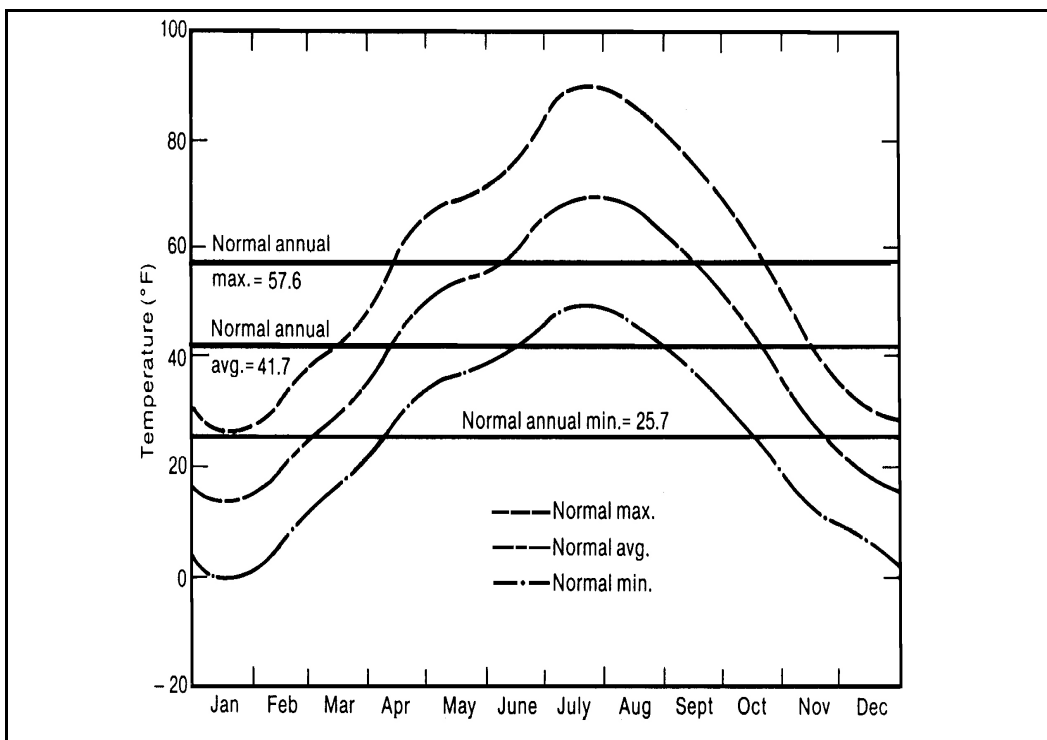


Figure B-2. Normalized daily maximum, average, and minimum air temperatures at TAN from 1930 through 1959.

Table B-3. Average (or normal) and maximum daily air temperature ranges summarized by month for CFA and TAN.

	CFA ^a		TAN	
	Mean (°F)	Maximum (°F)	Normal ^b (°F)	Maximum ^c (°F)
January	23	52	26	50
February	24	50	27	53
March	24	53	26	62
April	28	57	30	57
May	30	55	32	55
June	33	55	34	51
July	38	56	50	58
August	38	59	40	60
September	36	58	39	59
October	34	59	35	58
November	24	52	28	49
December	23	54	25	45
ANNUAL	30	59	32	62

a. Data period of record spans January 1950 through December 1988.

b. Normalized temperatures adjusted to a 30-year period, spanning 1931 through 1960.

c. Data period of record spans April 1950 through December 1964.

Monthly and Annual Near-Surface Characteristics

Monthly and annual average air temperatures for CFA and TAN are given in Tables B-5 and B-6, respectively. These tables also include the monthly and annual temperature maximums and minimums, together with the extreme averages. The large year to year variability of average monthly temperatures can be readily seen in these tables. For example, the highest monthly average air temperature at CFA has been 30.0 °F in January, while the lowest monthly average air temperature in that same month has been 7.0 °F. The difference in this particular instance is 23 °F and indicates a rather large deviation in monthly average air temperature from year to year.

The largest within month differences are observed for the minimum air temperatures in the winter, and particularly in January. The differences for CFA and TAN are 31.2 °F and 36.1 °F, respectively. The smallest within month differences are observed also for the minimum air temperatures during the spring, summer and fall months. The smallest differences for CFA and TAN are 7.1 and 5.1 °F, respectively.

The annual air temperature extremes listed in Tables B-5 and B-6 are much smaller than the within month extremes. A variation of about 5 to 7 °F is apparent for the period of record.

The air temperature trace for CFA (Figure B-1) can be used to describe the average annual temperature progression. The trace exhibits a

Table B-4. Daily air temperature extremes summarized by month for CFA^a and TAN^b.

	Highest Daily Maximum		Lowest Daily Minimum		Highest Daily Average		Lowest Daily Average	
	CFA	TAN	CFA	TAN	CFA	TAN	CFA	TAN
	(°F)	(°F)	(°F)	(°F)	(°F)	(°F)	(°F)	(°F)
January	51	46	-40	-43	44	38	-20	-23
February	59	59	-36	-35	44	44	-23	-15
March	73	69	-28	-38	54	47	-6	-7
April	82	84	6	10	63	61	23	22
May	91	93	13	16	71	72	30	34
June	100	97	23	25	83	76	40	40
July	101	103	28	32	83	80	50	51
August	99	100	28	25	83	81	46	48
September	96	99	12	18	74	71	30	36
October	85	83	3	0	64	64	22	20
November	67	67	-24	-20	52	48	-9	-5
December	51	51	-47	-32	44	42	-28	-16
ANNUAL	101	103	-47	-49 ^c	83	81	-28	-23

- a. Data period of record spans January 1950 through December 1988.
- b. Data period of record spans April 1950 through December 1964.
- c. Estimated for the day when the coldest air temperature of -47 °F was measured at CFA.

secondary maximum during the third week in January. A winter thaw has been observed to occur on a number of occasions during this period, followed by more cold weather. The CFA air temperature trace also exhibits a long spring and summer temperature increase from the first week in January until the third week in July. The duration of the fall and winter decline in air temperature is much shorter than the spring and summer rise. The time span from the winter minimum to the summer maximum is approximately 7 months. Conversely, the time span from the summer maximum to the winter minimum is approximately 5 months.

The normalized annual air temperature trace for TAN is shown in Figure B-2. Since the data is normalized to surrounding stations, the trace is

somewhat different from CFA. Traces from both stations show an annual maximum in late July. TAN shows a minimum in late January, approximately 3 weeks later than CFA. It is expected that, if the period of record for TAN coincided with that of CFA, the traces would show a greater similarity.

Surface Spatial Variations

INEL air temperatures may be highly variable from place to place for short periods of time. Simultaneous observations at CFA and TAN have occasionally shown temperature differences in excess of 25 °F during the winter. The spatial variation in the summer is usually not as large, however.

Table B-5. Monthly and annual air temperature averages and extreme averages for CFA^a.

	Average			Maximum			Minimum		
	Average (°F)	High (°F)	Low (°F)	Average (°F)	High (°F)	Low (°F)	Average (°F)	High (°F)	Low (°F)
January	16.1	30.0	7.0	27.5	37.9	19.5	4.6	22.4	-8.8
February	21.7	34.1	7.1	33.8	45.9	21.2	9.5	22.3	-7.1
March	30.5	40.4	18.4	42.6	54.1	31.4	18.4	26.6	4.5
April	41.6	49.3	35.4	55.8	68.6	46.1	27.4	32.0	22.5
May	51.2	58.2	45.3	66.3	76.1	59.9	36.1	40.7	30.2
June	60.0	67.5	55.3	76.3	86.4	69.9	43.6	49.7	39.5
July	68.0	72.0	64.9	86.8	92.9	82.3	49.2	53.6	46.5
August	66.0	70.2	60.3	84.8	90.2	75.4	47.2	53.4	43.0
September	55.5	61.0	48.6	73.6	81.2	64.1	37.5	45.2	31.9
October	44.0	51.0	38.2	61.0	71.7	53.7	26.9	32.7	21.2
November	29.9	36.3	20.3	42.1	50.7	30.8	17.6	24.3	9.5
December	18.7	26.9	9.3	30.2	37.0	20.8	7.1	17.6	-3.0
ANNUAL	42.0	44.7	37.7	56.9	61.0	52.4	27.2	29.9	22.9

a. Data period of record spans January 1950 through December 1988.

Table B-6. Monthly and annual air temperature averages and extreme averages for TAN.

	Average			Maximum			Minimum		
	Average (°F)	High (°F)	Low (°F)	Average (°F)	High (°F)	Low (°F)	Average (°F)	High (°F)	Low (°F)
January	13.6	28.8	3.3	26.7	35.2	18.8	0.3	22.4	-13.7
February	20.4	32.3	7.4	32.8	45.5	23.3	7.9	19.4	-9.1
March	28.1	33.8	16.6	41.3	48.6	31.2	14.8	21.1	1.9
April	42.1	45.2	37.5	57.0	61.4	51.1	27.1	29.0	23.9
May	51.9	58.3	46.5	66.6	77.3	60.7	36.1	39.9	31.3
June	60.0	66.5	56.8	76.8	86.3	70.4	43.2	46.7	38.7
July	68.7	72.4	65.5	88.4	92.9	83.5	48.9	51.9	45.1
August	65.8	70.6	63.5	85.6	90.5	81.4	46.0	51.1	43.4
September	56.2	60.6	50.0	75.4	81.6	64.2	37.1	43.4	34.7
October	44.2	48.5	39.9	61.9	69.5	54.8	26.5	30.2	22.5
November	28.4	35.0	22.3	42.1	49.5	35.8	14.5	20.7	6.3
December	18.7	25.8	11.4	30.9	35.2	22.6	6.5	16.4	0.2
ANNUAL	42.2	44.0	38.2	57.4	59.4	54.2	26.0	29.1	22.3

a. Data period of record spans January 1950 through December 1964.

b. Data period of record spans January 1950 through August 1964.

Air temperatures from several locations on and surrounding the INEL on the days when the extreme highest maximum and extreme lowest minimum air temperatures were observed are given as an example of the spatial air temperature variability in Table B-7. The data are from NCDC recording stations co-located with INEL meteorological monitoring stations (Table III-2). On the day the highest maximum air temperature was recorded at CFA (20 July 1960), the temperatures varied from 96 °F at Richfield to 105 °F at Hamer. On the day the lowest minimum air temperature was recorded (23 December 1983), the temperatures ranged from -23 °F at Blackfoot to -49 °F at TAN. These data show that, in general, the area near TAN has the lowest minimum and the highest maximum air temperatures.

Specific Temperatures

The occurrences of specific temperatures are frequently of interest in the analysis of climate. The average, highest, and lowest number of days per month or per year (expressed as a percentage) when the air temperature maximum was less than or equal to 32 °F or greater than or equal to 90 °F are presented in Table B-8 for both CFA and TAN. These data show that the air temperature on approximately 2/3 of the days in January usually remains below freezing at both CFA and TAN. However, the air temperature has remained below freezing during the entire month of February for at least one year at both locations. The air temperature has also risen above freezing on every day in February for at least one year at both

Table B-7. Spatial variability in air temperature from NCDC observation stations on and surrounding the INEL on the days with the highest maximum (20 July 1960) and the lowest minimum (23 December 1983) at CFA.

NATIONAL CLIMATE DATA CENTER ID	Highest Maximum (°F)	Lowest Minimum (°F)
Aberdeen Exp. Station	101	-30
Arco 3 SE	102	-45
Blackfoot 2 SSW	101	-23
Dubois Exp. Station	100	-25
Hamer 4 NW	105	-40
Howe	102	M ^a
Idaho Falls 2 ESE	100	-28
Idaho Falls FAA AP	101	-30
Idaho Falls 46 W (CFA)	101	-47
Idaho Falls 42 NW (TAN)	103	-49 ^b
Richfield	96	-27
St. Anthony 1 WNW	97	-32

a. Data are missing.
b. Data are estimated.

locations. At the other end of the spectrum, the air temperature usually rises above 90 °F about 45% of the time during July at CFA and TAN. The frequency of occurrence of this phenomenon at CFA has been as large as 84%, or as small 10%.

Table B-9 is similar to Table B-8 in that it lists the average, highest, and lowest number of days per month or per year (expressed as a percentage) when the minimum air temperature was less than or equal to 32 °F and less than or equal to 0 °F. These data indicate that the air temperature has dropped to freezing or below at least one time during every month of the year, including the summer months at both CFA and TAN. The minimum air temperature at both locations is also, on the average, at or below freezing nearly every day during December, January, February, and March. The minimum air

Table B-8. Monthly and annual average number of days (%) when the maximum daily air temperature was at or below 32 °F and at or above 90 °F at CFA^a and TAN^b.

	Number of Days with Maximum ≤ 32 °F						Number of Days with Maximum ≥ 90 °F					
	Average		Highest		Lowest		Average		Highest		Lowest	
	CFA (%)	TAN (%)	CFA (%)	TAN (%)	CFA (%)	TAN (%)	CFA (%)	TAN (%)	CFA (%)	TAN (%)	CFA (%)	TAN (%)
January	67	68	97	100	23	29	0	0	0	0	0	0
February	42	46	100	100	0	0	0	0	0	0	0	0
March	14	23	61	58	0	0	0	0	0	0	0	0
April	0	0	0	3	0	0	0	0	0	0	0	0
May	0	0	0	0	0	0	0	0	3	6	0	0
June	0	0	0	0	0	0	10	10	43	47	0	0
July	0	0	0	0	0	0	40	48	84	74	10	19
August	0	0	0	0	0	0	31	32	68	61	10	19
September	0	0	0	0	0	0	4	7	23	23	0	0
October	0	0	6	3	0	0	0	0	0	0	0	0
November	17	17	73	37	0	0	0	0	0	0	0	0
December	56	52	94	87	19	23	0	0	0	0	0	0
ANNUAL	16	17	35	28	9	9	7	8	16	13	3	4

a. Data period of record spans January 1950 through December 1988.

b. Data period of record spans April 1950 through August 1964.

Table B-9. Monthly and annual average number of days (%) when the minimum daily air temperature was at or below 32 °F and at or below 0 °F at CFA^a and TAN^b.

	Number of Days with Minimum ≤ 32 °F						Number of Days with Minimum ≤ 0 °F					
	Average		Highest		Lowest		Average		Highest		Lowest	
	CFA (%)	TAN (%)	CFA (%)	TAN (%)	CFA (%)	TAN (%)	CFA (%)	TAN (%)	CFA (%)	TAN (%)	CFA (%)	TAN (%)
January	99	100	100	100	94	100	39	52	77	90	0	0
February	99	100	100	100	89	93	27	32	89	93	0	0
March	96	100	100	100	81	94	8	13	42	39	0	0
April	75	73	97	97	53	63	0	0	0	0	0	0
May	31	29	65	48	3	10	0	0	0	0	0	0
June	6	7	17	20	0	0	0	0	0	0	0	0
July	0	0	3	3	0	0	0	0	0	0	0	0
August	2	3	16	6	0	0	0	0	0	0	0	0
September	26	27	57	43	0	0	0	0	0	0	0	0
October	76	77	97	94	39	58	0	0	0	0	0	0
November	93	97	100	100	73	90	0	10	23	0	0	0
December	98	100	100	100	84	90	0	32	68	0	0	3
ANNUAL	58	59	64	63	52	53	9	11	24	18	3	4

a. Data period of record spans January 1950 through December 1988.

b. Data period of record spans April 1950 through August 1964.

temperature during February has also been at or below 0 °F up to 93% of the time at TAN and up to 89% of the time at CFA.

The dates at which the last recorded minimum air temperatures of 32, 28, and 24 °F are observed in the spring and the first occurrence of these temperatures in the fall are oftentimes required for construction work and biological studies. Tables B-10 and B-11 contain these dates for both CFA and TAN, respectively. The number of days between the various dates is also listed. The average frost-free period at CFA is 89 days, while at TAN that value is 86 days. The shortest frost-free period has been 43 and 64 days at CFA and TAN, respectively. The year-to-year variation in the number of days between temperature thresholds varies by a factor of approximately three for both the 32 and 28 °F temperatures categories and by a factor of approximately 1.5 for the 24 °F temperature category.

The length of time between spring and fall 28 and 32 °F air temperature events over the same 14 year period (1950-1964) is longer at CFA than at TAN. The length of time for the 24 °F air temperature event is nearly identical. Differences between CFA and TAN in the last occurrence of the 28 and 32 °F minimum air temperatures in the spring and the first occurrence of these temperatures in the fall are probably the result of localized cold air drainage and pooling in the TAN area. A temperature drop to 24 °F at both locations is probably the result of a large scale synoptic weather system, and not local effects.

A measure of the amount of weathering various materials may be exposed to is the frequency at which daily freeze/thaw cycles occur. A freeze/thaw cycle in this instance is defined as a day on which the maximum air temperature exceeds 32 °F and the minimum air temperature falls to or below 32 °F. The temperatures used for this purpose are measured at a height of 5 ft. AGL. As such, the air temperature at 5 ft. may be cooler during the day and warmer at night than at ground level. Therefore, the actual number of daily freeze/thaw cycles nearer to the ground surface

would probably be greater than what may be determined using this calculation procedure.

The summary of freeze/thaw cycles for CFA and TAN is contained in Table B-12. The greatest number of cycles occur, as expected, in the spring and fall seasons. Freeze/thaw cycles have occurred every day during February and March at CFA and during March and November at TAN. Conversely, the air temperature has remained below freezing for the entire month of January at TAN and February at CFA, resulting in no freeze/thaw cycles. On the average, however, 42% of the days in a year contain a freeze/thaw cycle.

Another unit of measure based on a specific air temperature is the degree-day. The degree-day concept can be applied to either heating or cooling and is used as a basis for establishing heating and cooling energy requirements and building design considerations. A single heating degree-day is accumulated for each degree the average daily air temperature is less than 65 °F for one day. Conversely, a single cooling degree day is accumulated for each degree the average daily air temperature is greater than 65 °F.

A summary of daily heating degree-days for CFA and TAN is given in Tables B-1 and B-2, respectively. The largest daily average heating degree-day at CFA occurs on 02 January with a value of 55 degree-days. The lowest daily average heating degree day at CFA is 0 degree-days and occurs during most of July and the early part of August. TAN is also similar with the largest normalized heating degree-day of 52 on several days during the third week in January and the smallest value of 0 degree-days in the later part of July and the first part of August.

The daily trends are evident in the monthly and annual summaries as well (Table B-13). January has the highest degree-day total of 1517 and July has the lowest total of 29 at CFA. Heating degree-day totals at TAN for the same months are 1,600 and 16, respectively. Monthly heating degree-day totals as large as 1,726 and 1,912 have been recorded at CFA and TAN,

Table B-10. Dates of the last recorded minimum air temperature of 24, 28, and 32 °F in the spring and the first occurrence of these temperatures in the fall together with the number of days between those dates for CFA.

Year	Last Spring Occurrence		First Fall Occurrence		Number of Days Between	
	Minimum of 24 F or Below	Minimum of 28 F or Below	Minimum of 32 F or Below	Minimum of 28 F or Below	Last Spring and First Fall Occurrence 28 F	32 F
1950	May 20	Jun 30	Sep 12	Sep 27	130	115
1951	May 14	Jun 8	Sep 12	Sep 27	135	95
1952	Apr 22	Apr 30	Sep 13	Sep 14	145	136
1953	May 22	May 23	Sep 5	Sep 25	133	124
1954	May 2	Jun 2	Aug 27	Sep 19	139	85
1955	May 28	May 28	Sep 22	Sep 22	116	116
1956	May 1	May 15	Aug 31	Sep 6	143	113
1957	Apr 27	Apr 28	Sep 11	Sep 14	147	138
1958	Apr 30	May 3	Sep 16	Sep 25	164	144
1959	May 7	May 21	Sep 22	Sep 22	144	123
1960	May 19	May 19	Aug 25	Oct 3	147	136
1961	May 3	May 8	Sep 3	Sep 24	151	138
1962	Apr 30	Jun 7	Aug 31	Sep 9	131	93
1963	Apr 24	Apr 28	Oct 10	Oct 24	182	169
1964	May 7	May 9	Aug 29	Sep 3	134	116
1965	May 18	May 18	Aug 31	Sep 17	122	121
1966	Jun 25	Jun 25	Sep 27	Oct 1	107	97
1967	May 13	May 26	Sep 12	Sep 13	144	109
1968	May 9	May 16	Sep 17	Oct 3	152	139
1969	Apr 30	Apr 30	Sep 31	Sep 15	156	137
1970	May 14	May 31	Sep 9	Sep 10	119	101
1971	May 18	May 19	Sep 15	Sep 18	123	121
1972	May 12	May 13	Sep 7	Sep 14	135	123
1973	May 27	Jun 18	Sep 15	Sep 17	129	91
1974	May 16	May 30	Sep 2	Sep 14	121	106
1975	May 26	May 26	Sep 2	Sep 3	117	99
1976	Apr 30	Jun 14	Sep 9	Oct 5	158	112
1977	May 28	May 30	Aug 31	Sep 9	127	101
1978	May 31	Jun 20	Aug 15	Aug 18	111	59
1979	Jun 8	Jun 9	Sep 11	Sep 12	118	155
1980	Apr 17	Apr 19	Sep 1	Sep 22	183	155
1981	Apr 17	May 13	Sep 20	Sep 20	162	85
1982	May 5	May 20	Sep 29	Oct 6	154	73
1983	May 14	May 16	Sep 6	Sep 10	129	92
1984	May 17	Jun 2	Sep 7	Sep 22	130	117
1985	May 13	May 14	Sep 20	Sep 20	133	112
1986	May 23	May 24	Jul 6	Sep 23	121	129
1987	Apr 20	Jun 2	Aug 17	Sep 17	151	43
1988	May 3	May 20	Sep 15	Sep 18	138	107
Average	May 13	May 21	Sep 1	Sep 9	128	111
Longest	Apr 17	Apr 28	Sep 11	Oct 15	183	169
Shortest	Jun 25	May 24	Jul 6	Jul 6	107	43

Table B-11. Dates of the last recorded minimum air temperature of 24, 28, and 32 °F in the spring and the first occurrence of these temperatures in the fall together with the number of days between those dates for TAN.

Year	Last Spring Occurrence		First Fall Occurrence		Number of Days Between	
	Minimum of 24 °F or Below	Minimum of 28 °F or Below	Minimum of 32 °F or Below	Minimum of 28 °F or Below	Last Spring and First Fall Occurrence	28 °F
1951	Apr 23	Jun 9	Aug 31	Sep 12	156	94
1952	Apr 22	Jun 13	Aug 28	Sep 14	144	92
1953	May 22	Jun 25	Sep 21	Sep 25	146	124
1954	May 2	Jun 18	Aug 22	Sep 18	139	102
1955	May 4	Jul 2	Sep 12	Sep 16	141	110
1956	Apr 19	Jun 22	Aug 31	Aug 31	155	69
1957	Apr 27	Apr 28	Sep 11	Sep 11	147	135
1958	Apr 30	May 3	Sep 21	Oct 2	154	130
1959	May 8	May 29	Sep 3	Sep 9	136	94
1960	May 18	Jun 21	Aug 25	Aug 29	113	68
1961	May 8	May 19	Sep 3	Sep 3	128	117
1962	Apr 30	Jun 7	Aug 24	Aug 31	130	84
1963	May 2	Jun 2	Oct 7	Oct 14	167	164
1964	Apr 28	May 24	Aug 30	Sep 3	151	101
Average	May 2	Jun 1	Sep 6	Sep 12	143	107
Longest	May 2	May 2	Sep 21	Oct 14	167	164
Shortest	May 18	Jun 21	Aug 25	Aug 29	113	68

Table B-12. Monthly and annual summary of daily freeze/thaw cycles for CFA^a and TAN^b.

	Average Number of Cycles		Maximum Number of Cycles		Minimum Number of Cycles	
	CFA	TAN	CFA	TAN	CFA	TAN
	(%)	(%)	(%)	(%)	(%)	(%)
January	33	32	74	71	3	0 ^c
February	58	54	100	96	0 ^c	4
March	82	77	100	100	39	42
April	75	73	97	93	53	57
May	31	29	65	48	3	6
June	6	3	17	20	0	0
July	0	0	3	3	0	0
August	2	3	16	6	0	0
September	26	23	57	43	0	0
October	76	77	97	90	39	58
November	76	80	97	100	27	67
December	43	48	81	87	6	16
ANNUAL	42	42	54	53	23	31

a. Data period of record spans January 1950 through December 1988.

b. Data period of record spans April 1950 through August 1964.

Table B-13. Monthly and annual average and extreme heating degree days (HDD) for CFA^a and normalized average and extreme heating degree-days for TAN^b.

	Average		Highest		Lowest		Daily Extremes			
	CFA	TAN	CFA	TAN	CFA	TAN	Highest		Lowest	
	(HDD)	(HDD)	(HDD)	(HDD)	(HDD)	(HDD)	CFA	TAN	CFA	TAN
January	1,517	1,600	1,709	1,912	1,086	1,122	85	88	22	27
February	1,226	1,291	1,623	1,666	865	909	88	80	21	21
March	1,069	1,107	1,446	1,493	764	964	71	72	11	18
April	702	657	889	815	471	595	43	87	2	4
May	428	388	610	567	234	226	35	31	0	0
June	183	192	299	279	44	51	25	25	0	0
July	29	16	90	57	1	0	16	14	0	0
August	54	40	192	112	4	0	20	17	0	0
September	291	282	493	444	142	140	36	29	0	0
October	652	648	832	778	433	503	44	45	2	1
November	1,055	1,107	1,342	1,281	860	894	74	70	14	17
December	1,436	1,432	1,726	1,662	1,181	1,215	93	81	21	23
ANNUAL	8,640	8,760	10,268	10,024	7,623	7,699	93	88	0	0

a. Data period of record spans January 1950 through December 1988.

b. Data period of record spans April 1950 through December 1964.

respectively. Table B-13 also shows that the highest single heating degree-day at CFA and TAN has been 93 and 88 respectively. On the average, the locations on the INEL can expect to record approximately 8,700 degree-days annually.

A monthly and annual summary of the cooling degree-days at CFA is presented in Table B-14. The TAN data, although not given, are similar as evidenced in the heating degree-day tables. Cooling is usually not required except during the months of June, July, and August. However, a significant accumulation of cooling degree-days has been observed in both May and September. Conversely, there has been at least one time when the accumulation of cooling degree-days in May and September has been 0. On the average, an annual total of 247 cooling degree-days accumulates at CFA.

The daily extremes of cooling degree-days given in Table B-14 yields further information on cooling equipment design capacity requirements. The largest single cooling degree-day value ever observed has been 18. This has been recorded in the months of July and August.

Upper Air General Characteristics

The vertical variation of temperature above the ground surface is extremely important for evaluating atmospheric dispersion characteristics. These data are needed to properly evaluate

Table B-14. Monthly and annual average and extreme cooling degree-days (CDD) for CFA^a.

	Average (CDD)	Highest (CDD)	Lowest (CDD)	Daily Extremes	
				Highest (CDD)	Lowest (CDD)
January	0	0	0	0	0
February	0	0	0	0	0
March	0	0	0	0	0
April	0	0	0	0	0
May	1	24	0	0	0
June	31	137	3	6	0
July	123	224	58	18	0
August	85	174	32	18	0
September	6	32	0	0	0
October	0	0	0	9	0
November	0	0	0	0	0
December	0	0	0	0	0
ANNUAL	247	472	125	18	0

a. Data period of record spans January 1954 through December 1988.

potential reactor sites, as well as for determining the location, height, and design of chimneys and monitoring stations. A discussion of the vertical temperature variation and its relationship to dispersal of effluents will not be undertaken here, but is deferred to Chapter 6. However, a brief discussion of stability categories follows.

The following definitions are used to classify air temperature profiles into stability categories:

1. Inversion (or inverted profile): Air temperature warms with increasing altitude.
2. Lapse: Air temperature cools with increasing altitude.
3. Isothermal: Air temperature is constant with increasing altitude.
4. Dry adiabatic lapse rate: A special case of the lapse profile where air temperature cools with increasing altitude at the

specific rate of 5.5 °F/1,000 ft. This cooling effect is due solely to the unsaturated expansion cooling process.

5. Average environmental lapse rate: Another special case of the lapse profile where the average actual lapse rate is 3.5 °F/1,000 ft.

The terms inversion and lapse are further categorized as weak or strong, depending on the air temperature rate of change with height.

Profile Characteristics to 250 ft. AGL

Detailed studies of the air temperature structure from the surface to 250 ft. have been conducted for several years using air temperatures measured on tall towers at various locations on the INEL. From these studies, stability categories have been calculated as a function of season. These data are presented in Table B-15 for CFA, TAN, and GRD3.

The data trends indicate that inversion conditions were more prevalent at TAN (54%) than at either CFA (48%) and GRD3 (46%). The reverse is true for lapse conditions at CFA and GRD3. Weak lapse conditions occurred with nearly identical frequency (11%) at all 3 sites. This was also the case for weak inversion conditions (25%). Strong inversions were observed more frequently at TAN, while strong lapse conditions were observed more frequently at CFA and GRD3. These differences are due primarily to the lower elevation of TAN, the close proximity of TAN to the mountains, and the more frequent occurrence of afternoon clouds at TAN in the summer as compared to either the GRD3 or CFA locations.

A summary of the diurnal shift from a daytime air temperature lapse to a nighttime air temperature inversion was derived from eight years of record at CFA (Johnson and Dickson, 1962). The data were compiled as the air temperature difference between that measured at 5 and 250 ft. AGL. An attempt was made to eliminate from the data set those cases where the

formation or dissipation of the inversion was obviously controlled by factors other than incoming solar or outgoing terrestrial radiation. These data are presented in Table B-16 and illustrated graphically in Figure B-3.

The dependence of the nocturnal inversion formation and dissipation on the time of sunset and sunrise is readily apparent in the data. The nocturnal inversion does not dissipate for more than 1 to 2 hours after sunrise and reforms usually at about sunset. The more intense inversions also occur during the winter months. However, a nocturnal inversion can be expected to form on almost every day of the year (96.2% of the time). Similar conditions are expected to exist at all other locations on the INEL.

Profile Characteristics Above 250 ft. AGL

Two studies have been made of the air temperature profiles above 250 ft. at CFA. The first study made use of tethered blimps with accompanying thermistor elements to obtain air temperature soundings to a height of approximately 1,000 ft. AGL. Profile measurements were obtained every 2-3 hours throughout the day during the four different seasons. A series of typical profiles were extracted from these data and are shown in Figures B-4 through B-7. During the winter and spring seasons, air temperature profiles obtained above both bare ground and snow cover are shown.

The data readily show the formation and dissipation of the nocturnal inversion caused by surface heating and cooling, although the effects of wind slightly modified some of the profiles. The winter nocturnal inversions tend to be rather shallow, while the spring and summer inversions tend to be rather deep. The air temperature difference from the bottom to the top of the inversion has been as large as 18 °F.

The second study measured temperature profiles with T-sondes. A T-sonde contains a

Table B-15. Seasonal and annual distribution (% of time) of air temperature stability classes^a for CFA^b, TAN^c, and GRD3^d.

CFA				
Season	Strong Lapse (%)	Weak Lapse (%)	Weak Inversion (%)	Strong Inversion (%)
Winter	28.1	14.0	31.1	26.8
Spring	48.2	11.3	16.5	24.0
Summer	53.1	6.1	22.3	18.6
Fall	40.4	8.4	31.8	19.5
Annual	42.1	10.0	25.6	22.3
Annual Lapse: 52.1			Annual Inversion: 47.9	
TAN				
Season	Strong Lapse (%)	Weak Lapse (%)	Weak Inversion (%)	Strong Inversion (%)
Winter	16.7	17.3	32.7	33.3
Spring	39.0	14.3	15.9	30.8
Summer	42.9	10.4	21.7	25.0
Fall	28.2	13.4	29.6	28.8
Annual	32.1	13.7	24.9	29.3
Annual Lapse: 45.8			Annual Inversion: 54.2	
GRD3				
Season	Strong Lapse (%)	Weak Lapse (%)	Weak Inversion (%)	Strong Inversion (%)
Winter	30.8	13.0	28.9	26.4
Spring	48.3	12.6	26.8	12.3
Summer	50.7	6.9	22.1	20.3
Fall	50.0	6.1	26.2	17.7
Annual	44.0	10.1	26.3	19.6
Annual Lapse: 54.1			Annual Inversion: 45.9	

a. Stability categories are defined as follows for CFA, TAN, and GRD3:

	CFA (250'-5') $\Delta^\circ\text{F}$	TAN (150'-5') $\Delta^\circ\text{F}$	GRD3 (200'-35') $\Delta^\circ\text{F}$
Strong Lapse	<-1.0	<-1.0	<-1.0
Weak Lapse	-1.0 to -0.1	-1.0 to -0.1	-1.0 to -0.1
Weak Inversion	0.0 to 5.0	0.0 to 4.0	0.0 to 4.0
Strong Inversion	>5.0	>4.0	>4.0

b. Data period of record spans January 1953 through December 1960.

c. Data period of record spans January 1953 through December 1960.

d. Data period of record spans September 1980 through May 1983.

Table B-16. Average onset and dissipation times of inversion and lapse air temperature profiles together with intensity values for CFA^a.

	Inversion Formation		Inversion Dissipation		Inversion	
	Average Time of Onset (MST)	Average Deviation before Sunset (Minutes)	Average Time of Dissipation (MST)	Average Deviation after Sunrise (Minutes)	Average # of Hours Per Day	Maximum Number of Hours Recorded Per Day
January	1657	23	0959	116	17.0	24
February	1740	22	0919	108	15.7	23
March	1836	02	0805	80	13.5	18
April	1919	-04	0704	74	11.8	14
May	1941	09	0626	78	10.8	15
June	2000	15	0614	84	10.2	13
July	1950	21	0630	85	10.7	15
August	1919	17	0700	83	11.7	14
September	1839	04	0729	78	12.8	15
October	1746	03	0805	79	14.3	17
November	1706	02	0851	85	15.1	21
December	1646	10	0933	96	16.8	24
	Inversions			Lapse		
	Maximum Intensity (°F)	Longest Period of Duration (Hours)	Average Number of Days Without Inversion	Maximum Intensity (°F)	Longest Period of Duration (Hours)	
January	33.8	46	1	7.0	84	
February	33.7	24	1	9.4	81	
March	24.9	20	2	7.7	94	
April	24.5	14	2	9.6	77	
May	24.4	13	1	12.4	67	
June	22.5	15	1	8.7	61	
July	23.2	15	1	9.8	37	
August	23.6	14	1	9.9	42	
September	28.5	18	1	9.8	58	
October	27.1	17	1	7.4	67	
November	24.3	21	1	8.1	105	
December	33.4	66	1	6.9	62	

a. Data period of record spans January 1953 through December 1960.

small radio transmitter combined with a thermistor, which transmits a temperature modulated signal to a ground receiving station. The T-sondes were attached to free-lift balloons and tracked by double theodolites. Typical temperature profiles from the winter and summer seasons up to heights of 1.2 mi. are shown in Figure B-8. A pair of profiles for

each season is presented, one from near sunrise and the other obtained approximately 6 hours later.

The profiles show that the nocturnal inversion during the winter dissipated near the surface during the day due to surface heating, but persisted at the higher levels throughout the day. The profile taken

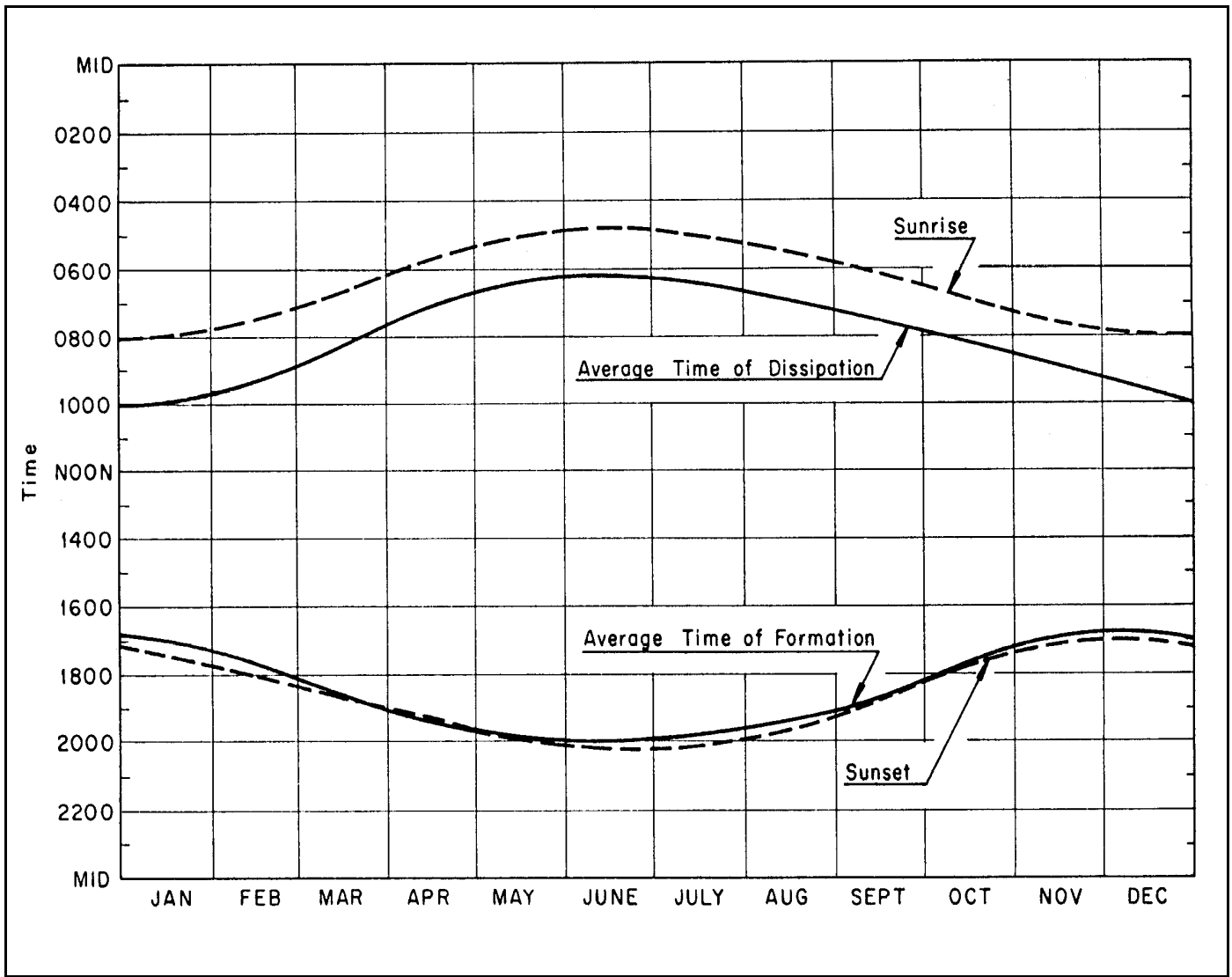


Figure B-3. Average time of onset and dissipation of the nocturnal inversion as a function of time of year.

at sunrise in the winter also shows a distinct "kink" at about 1,800 ft. AGL below which the profile appeared to become lapse, and above which the profile continued to indicate an inversion for about another 3,000 ft. This kind of trace was not indicated in the previously discussed upper air profiles (Figures B-4 through B-7) because of the limited maximum altitude of the profiles. Figure B-8 also shows that, in the summer, the inversion formed by radiation cooling only extended to about 1,300 ft.

A few other generalizations may be made from the data. First, considerable day-to-day fluctuations in the maximum height of the

the inversion were observed. Second, the height of the inversion top varied from a few hundred feet to over 5,000 ft. AGL. Third, the entire inversion usually dissipated during the daytime hours in the summer. In the winter, the inversion often did not dissipate at all or dissipated only in the lower few hundred feet of the atmosphere and the inversion frequently persisted at the higher levels for several days. Fourth, the temperature difference between the surface and the top of the inversion was as large as 40 °F. Fifth, the development of strong lapse profiles from the surface upward at midday during the summer was accompanied with upper level wind flows of light-to-moderate speeds.

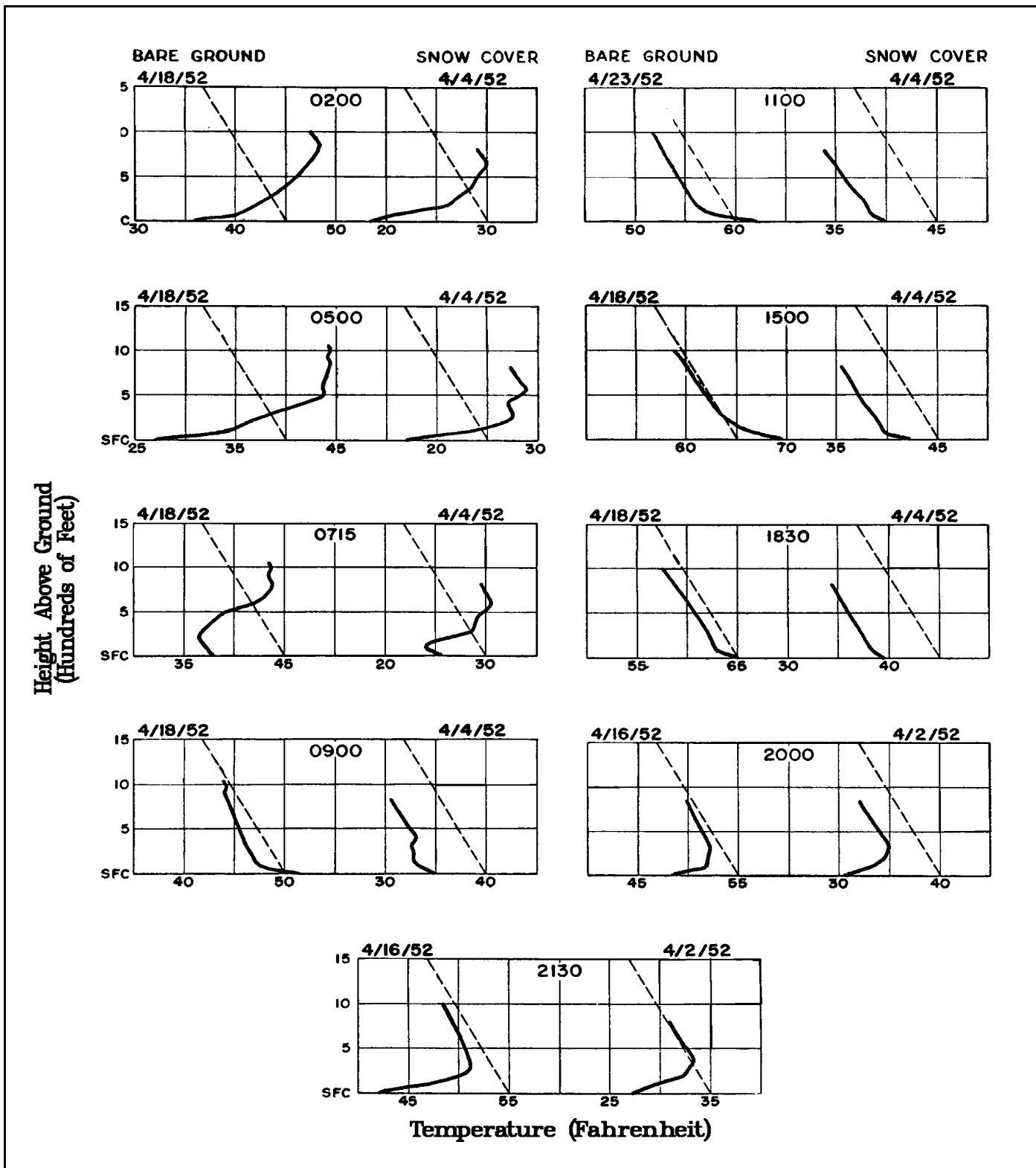


Figure B-4. Typical winter season (December-February) air temperature profiles (solid line) as a function of time of day plotted together with the dry adiabatic lapse rate (dashed line). Data were obtained above both a bare and a snow covered surface.

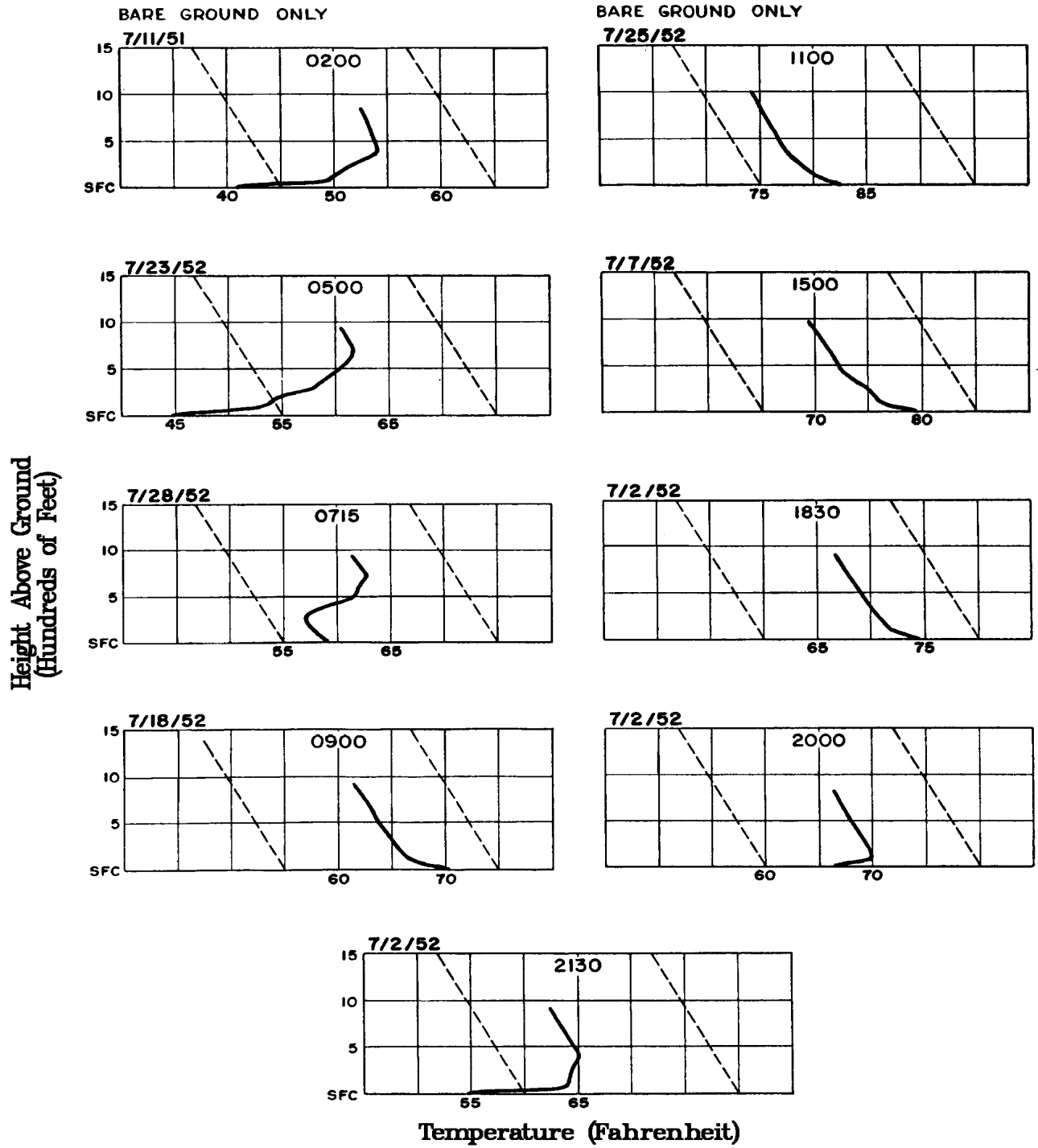


Figure B-5. Typical spring (March-May) season air temperature profiles (solid line) as a function of time of day plotted together with the dry adiabatic lapse rate (dashed line). Data were obtained above both a bare and a snow-covered surface.

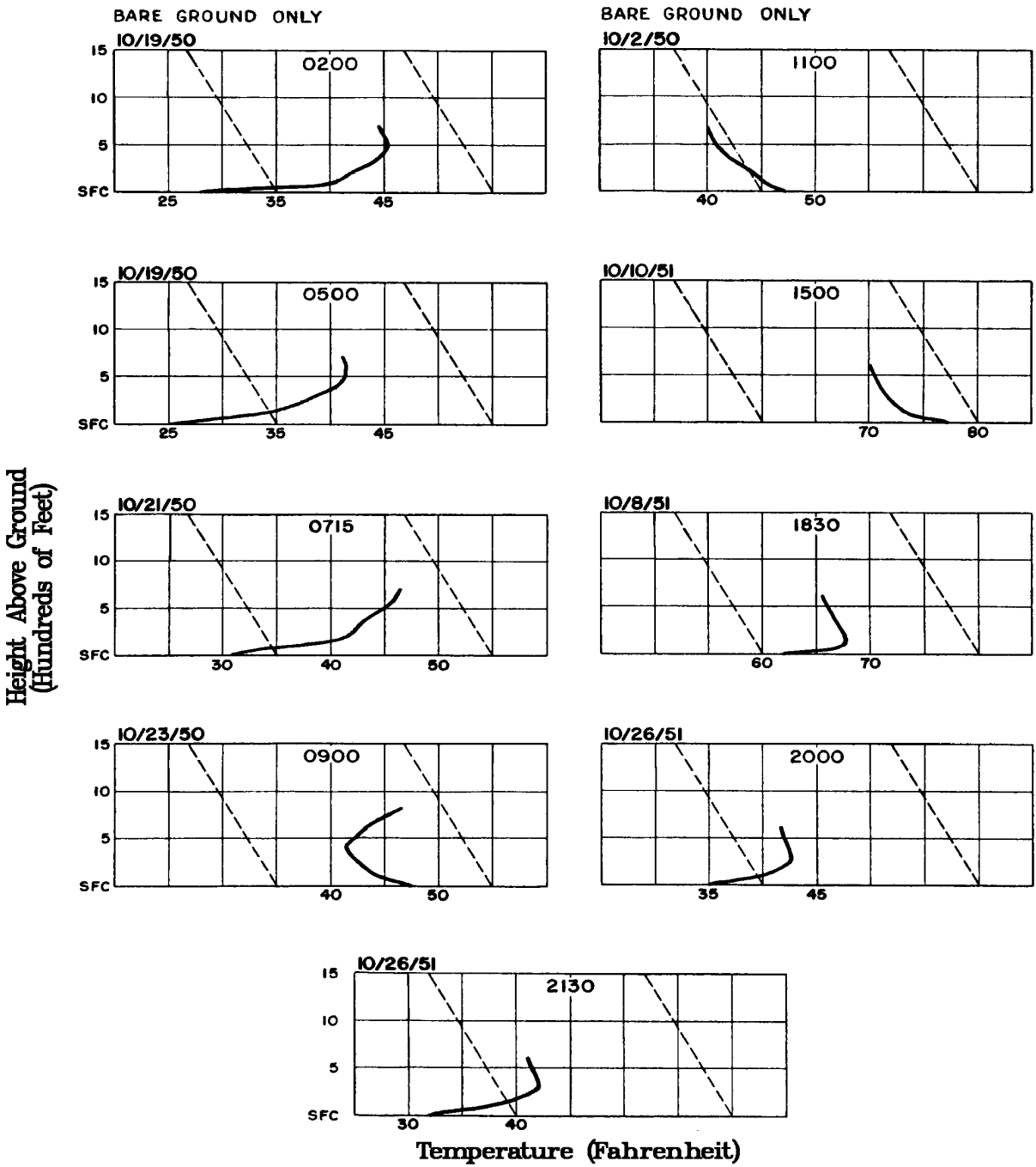


Figure B-6. Typical summer (June-August) season air temperature profiles (solid line) as a function of time plotted together with the dry adiabatic lapse rate (dashed line). Data were obtained above a bare surface.

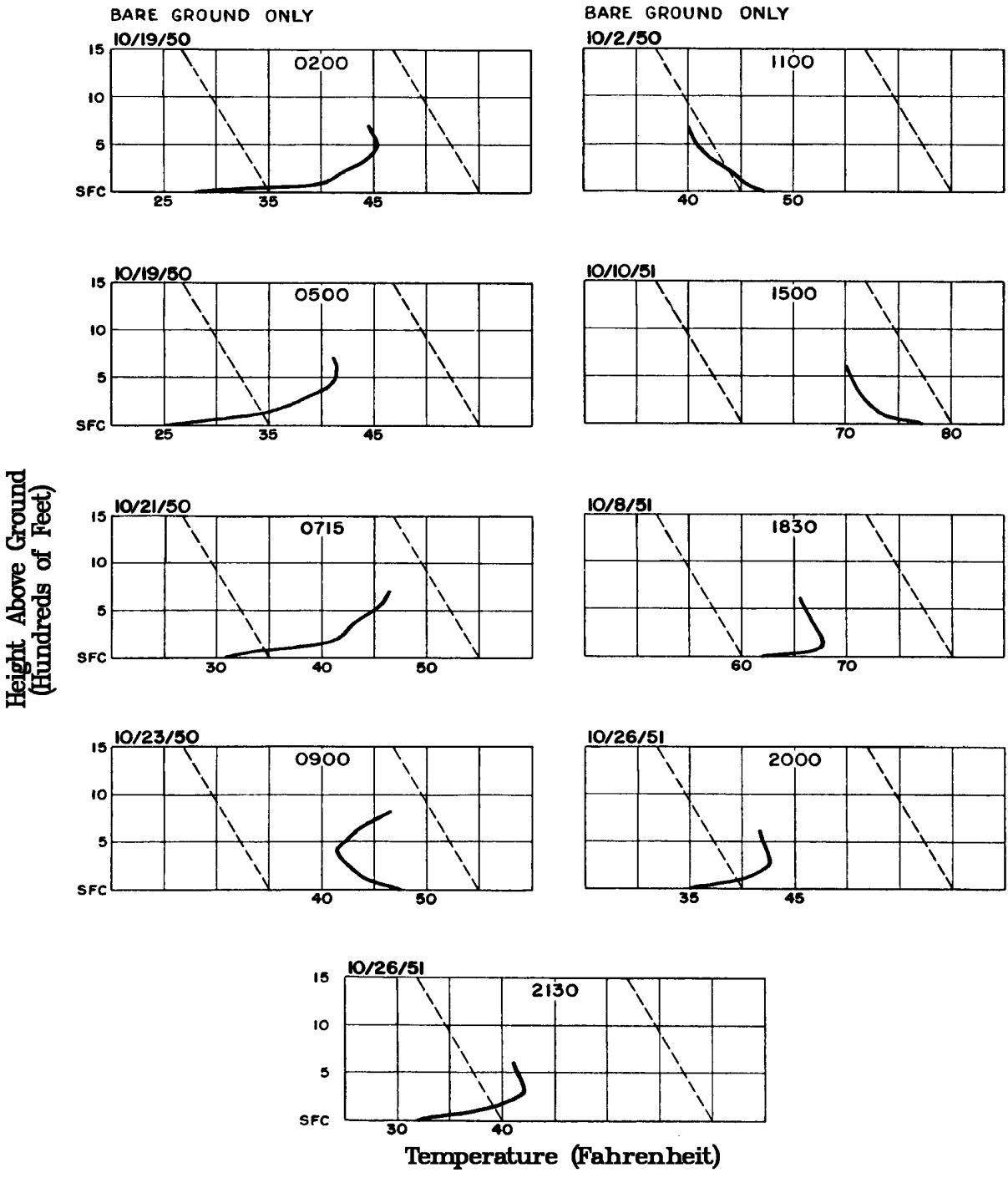


Figure B-7. Typical fall (September-October) season air temperature profiles (solid line) as a function of time of day plotted together with the dry adiabatic lapse rate (dashed line). Data were obtained above a bare surface.

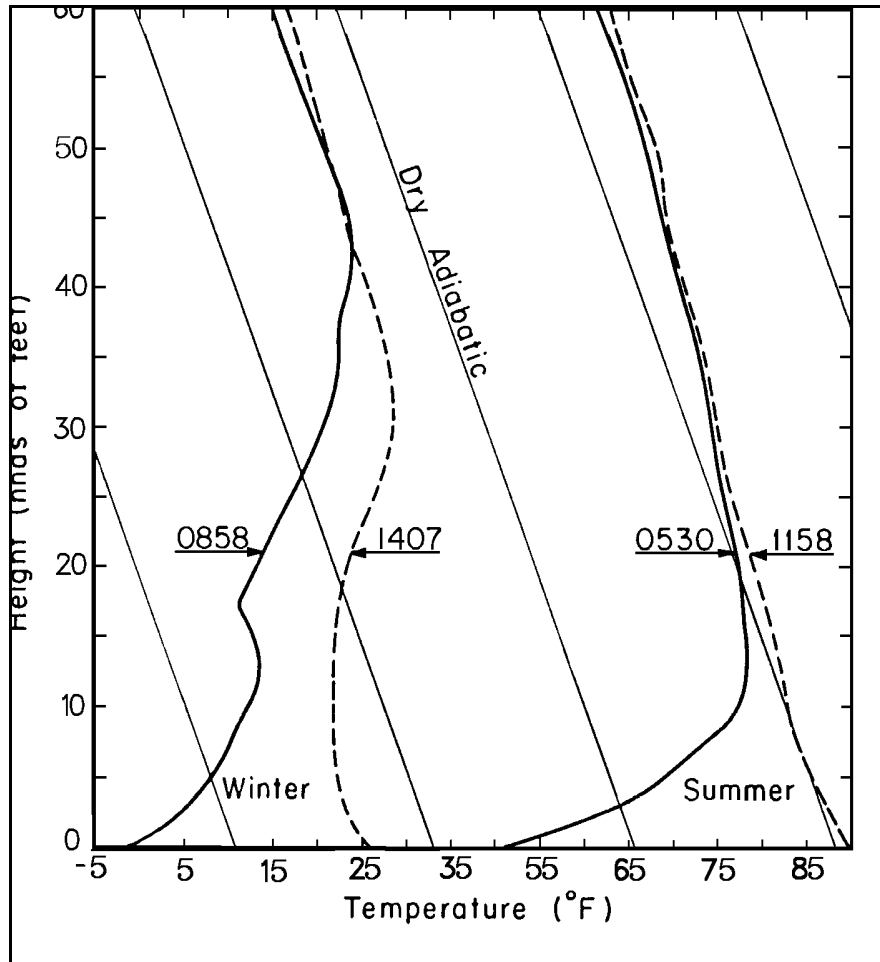


Figure B-8. Typical high-level air temperature soundings for the summer and winter seasons taken near sunrise (thick solid line) and approximately 6 hours later (dashed line) and plotted together with the dry adiabatic lapse rate (thin solid line).

Section C Soil Temperatures

Soil Surface Characteristics

Since the beginning of 1951, various soil surface temperature studies have been made. The first study was conducted for 4.25 years with a thermometer probe placed on top of a bare sandy soil or snow surface, depending on the condition of the surface. For the first 15 months of this period, the copper probe was unpainted, and thereafter it was painted black. Temperatures of exposed nonblack metallic objects are considered

to be represented by the copper-colored probe, whereas temperatures for black surfaces, i.e., asphalt roads or tarred roofs, are considered to be represented by the black-colored probe. Free air temperature was also simultaneously measured at the 5 ft. level in a shelter placed near the soil temperature probe. The results of this two-part study are listed in Table C-1.

The data show that soil surface temperatures as high as 160 °F were recorded with the black

Table C-1. Monthly averages and extremes of surface soil and air temperatures from copper and black colored probes. Paired temperatures indicate soil/air temperature. Unpaired values are soil temperature.

	Copper-Colored Thermometer Probe on Surface ^a					
	Average Daily High (°F/°F)	Average Daily Low (°F/°F)	Absolute Maximum (°F/°F)	Absolute Minimum (°F/°F)	Maximum Daily Range (°F)	Average (°F/°F)
January	39/25	3/0	61/38	-19/-26	62	NA ^b
February	48/29	7/5	63/42	-20/-26	69	NA
March	53/35	13/13	78/56	-5/-10	63	NA
April	80/59	27/29	96/74	14/15	72	NA
May	99/68	33/38	122/85	22/23	83	NA
June	103/73	35/40	127/88	24/27	98	NA
July	120/86	45/50	138/95	35/36	95	NA
August	111/81	45/48	134/93	33/35	86	NA
September	111/74	36/38	125/85	22/23	94	NA
October	81/55	27/27	105/78	13/11	81	NA
November	61/41	17/16	79/58	0/-2	60	NA
December	36/25	5/5	49/38	-10/-18	55	NA
	Black-Colored Thermometer Probe on Surface ^c					
January	47/31	17/11	81/49	-11/-24	68	NA
February	60/36	15/10	100/53	-7/-21	73	NA
March	72/42	18/16	108/66	-4/-15	89	NA
April	88/56	26/27	124/77	8/6	106	NA
May	107/67	34/35	140/91	18/18	108	NA
June	112/74	41/42	148/95	26/26	108	NA
July	133/88	47/49	160/99	32/33	115	NA
August	128/85	44/46	155/99	27/28	117	NA
September	121/78	35/36	142/92	19/18	108	NA
October	100/65	24/25	124/82	8/9	104	NA
November	75/46	16/16	102/63	-8/-13	92	NA
December	49/30	9/5	81/42	-9/-18	66	NA
	Thermometer Probe Buried 1/2 to 1 in. Below Surface					
January	27/29 ^d	19/5 ^d	43/47 ^e	3/-32 ^e	20 ^d	22.7/16.6 ^f
February	31/35	22/11	59/53	2/-31	30	27.0/22.2
March	45/44	28/20	79/63	19/-28	36	34.7/31.6
April	63/56	34/28	90/76	22/8	53	47.2/43.3
May	86/68	46/39	119/89	28/22	68	59.8/53.3
June	105/77	50/44	134/97	35/29	84	73.3/64.0
July	118/87	56/50	141/101	42/34	87	81.9/71.0
August	117/75	53/48	141/98	37/30	83	77.3/68.2
September	100/75	42/37	125/96	28/20	78	61.9/55.9
October	72/61	32/27	98/82	19/6	64	47.2/44.1
November	39/40	23/14	73/65	6/-24	43	30.3/28.4
December	30/35	21/12	50/50	1/-15	17	23.4/21.1

a. Data period of record spans January 1951 through March 1952.

b. Data not available.

c. Data period of record spans April 1952 through April 1955.

d. Data period of record spans June 1955 through May 1958.

e. Data period of record spans June 1955 through December 1961.

f. Data period of record spans January 1956 through December 1961.

probe. Temperatures as high as 138 °F were recorded with the copper probe. The painted probe showed increased average daily highs and ranges as much as 20 °F above that of the unpainted probe. The average soil surface temperatures were as much as 35 °F warmer than air temperature during the summer when measured with the copper probe. The black probe indicated differences as large as 45 °F. Little difference in the average daily lows of the two probes was observed, however, because the copper-colored and black-colored thermometers cooled at nearly the same rate at night.

A second study was conducted from June 1955 to December 1961, with the probe buried 0.5 to 1 in. below the ground surface. An exact depth was difficult to maintain due to wind erosion of the soil covering. The data from the probe at this depth was used to indicate the onset, duration, and termination of the solid freeze of winter. For the three years listed in Table C-1, the onset of the prolonged freeze usually occurred in late November, lasted three months or more, and ended in late February or early March. The maximum deviations between air and soil temperatures occurred in the winter and the summer seasons. Conversely, the smallest deviations were observed in the spring and the fall seasons.

Subsoil Characteristics

Subsurface soil temperatures were recorded from November 1956 through August 1963, with thermometer probes placed at 1 ft. intervals from 2 to 7 ft. beneath a bare sandy surface. The surface was representative of the natural terrain with the overlying vegetation removed.

Similar measurements, a short distance away, were also made under an asphalt road surface from June 1957 through August 1963. The depths under the road were the same as those under the sandy surface, except that the first level under the road was at one foot with no probe at the 2 ft. level. Soil temperatures, recorded at all six levels for both surface types, were averaged for each month.

Isotherms as a function of depth are presented in Figures C-1 and C-2 for both surfaces. To illustrate the temperature profile change throughout the year, the average vertical temperature profile beneath each surface is plotted for every other month in Figure C-3. These figures show a significant difference in temperature caused by the addition of the asphalt surface. Under the asphalt surface, soil temperatures averaged approximately 10 °F higher in the summer near the surface. In the winter, colder temperatures were observed over

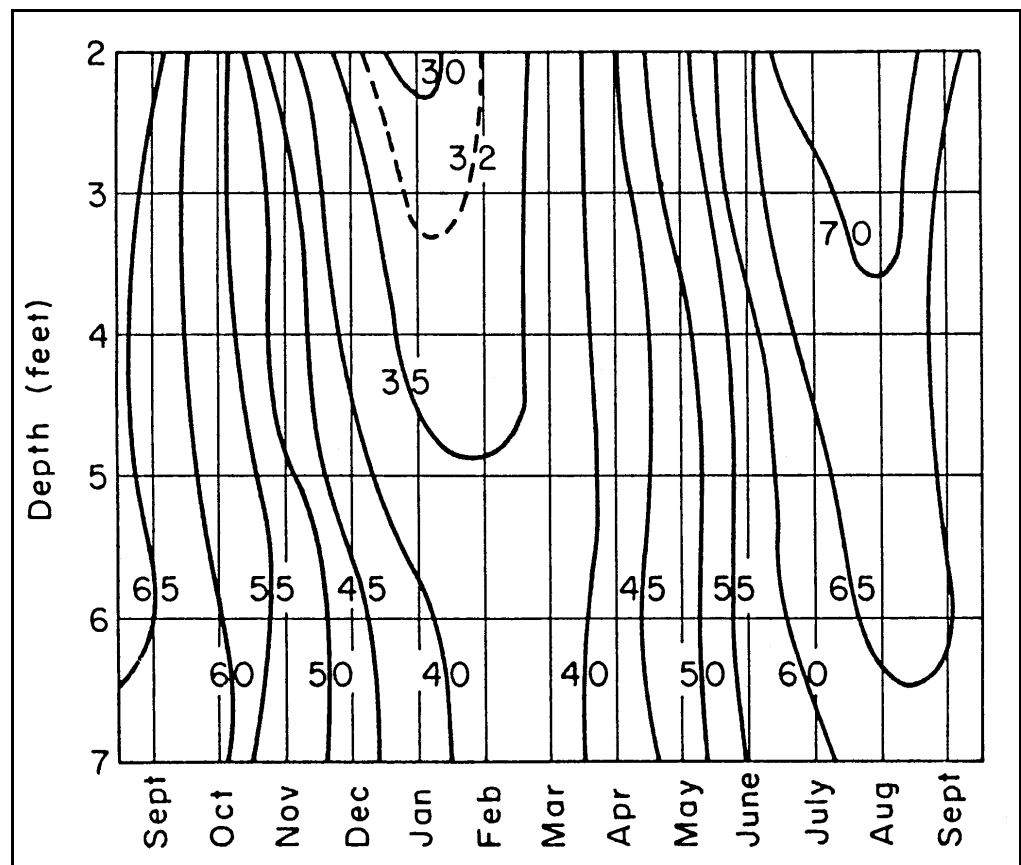


Figure C-1. Average monthly subsoil temperatures beneath a bare soil surface.

a longer period and to a greater depth. Freezing soil temperatures were observed at the 2-ft. depth for about 1 week longer under the asphalt surface than under the bare soil surface. The maximum average depth of freezing temperatures in the soil below the bare soil surface was approximately 3.3 ft. while that depth was approximately 3.8 ft. below the asphalt surface.

Monthly extreme soil temperatures recorded at each depth are found in Table C-2. Freezing temperatures were recorded near the five foot depth under the bare soil surface and near the six foot depth under the asphalt surface. Since the subsoil temperatures were taken over a relatively short period, freezing temperatures at depths slightly greater than those listed could be expected for a longer period of record.

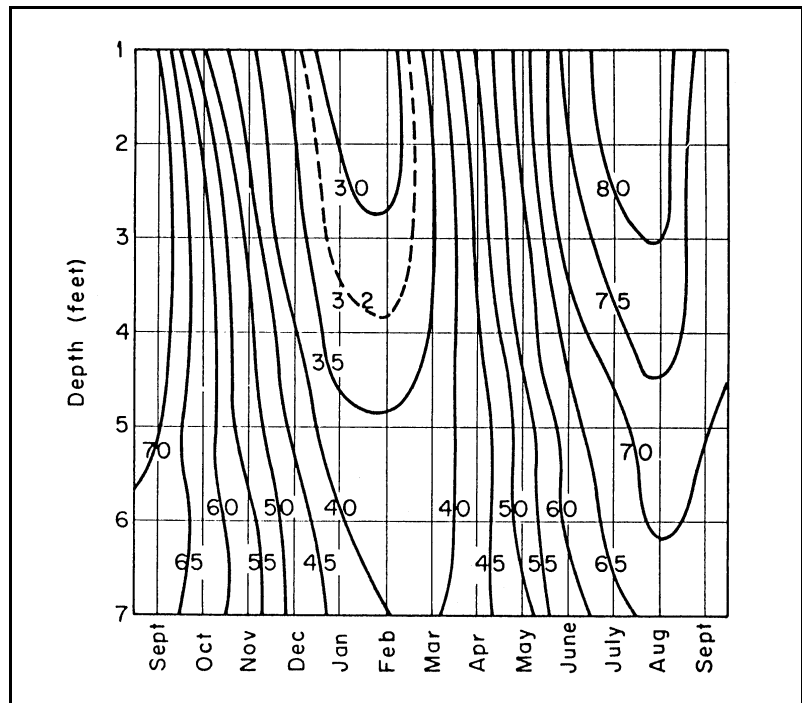


Figure C-2. Average monthly subsoil temperatures beneath an asphalt surface.

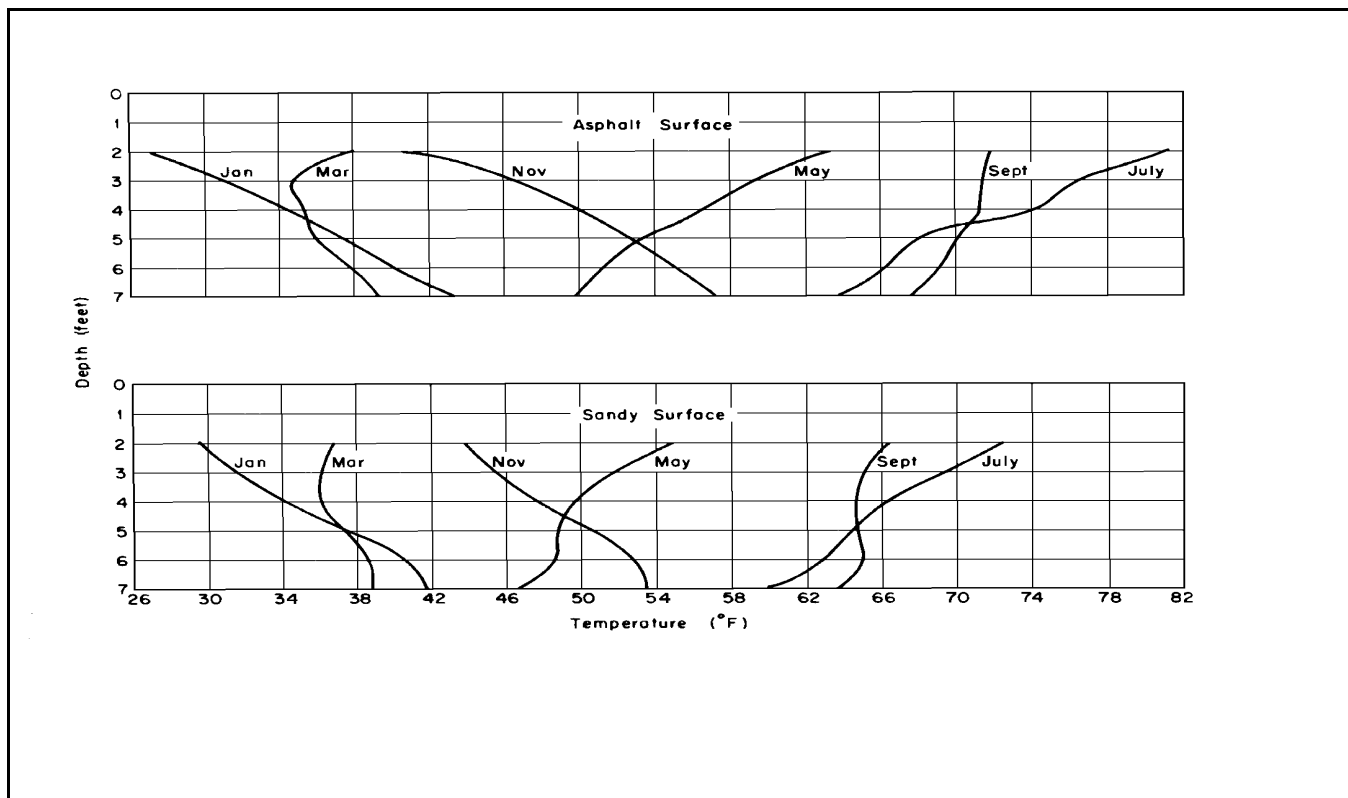


Figure C-3. Selected average monthly soil temperature profiles beneath asphalt (top) and bare sandy soil (bottom) surfaces.

Table C-2. Monthly subsoil temperature extremes (maximum/minimum) at various depths under asphalt and bare soil surfaces.

	<u>Asphalt Surface^a</u>						
	<u>1-ft</u> (°F)	<u>3-ft</u> (°F)	<u>4-ft</u> (°F)	<u>5-ft</u> (°F)	<u>6-ft</u> (°F)	<u>7-ft</u> (°F)	
January	33.0/10.0	35.5/17.8	28.6/24.6	41.6/30.6	45.0/34.3	47.7/37.7	
February	38.7/21.2	33.3/23.8	35.8/26.9	38.3/30.7	41.3/33.3	43.7/36.0	
March	50.7/19.8	44.4/21.8	43.8/25.1	42.5/29.5	42.5/32.8	43.0/35.0	
April	61.0/38.9	56.2/33.4	54.2/32.0	51.4/32.0	49.6/33.5	49.0/35.0	
May	77.1/50.3	73.0/48.9	67.8/47.4	61.7/45.8	46.9/45.1	56.1/44.4	
June	91.2/62.2	81.5/60.3	78.6/58.7	73.2/55.1	69.0/52.6	66.2/50.5	
July	94.9/70.2	87.8/68.1	85.7/63.0	80.1/59.0	75.6/56.9	72.7/55.0	
August	95.9/71.1	86.9/73.8	82.3/71.5	77.4/67.0	73.7/63.8	71.5/61.7	
September	81.6/63.4	80.9/61.4	79.9/63.4	76.5/63.4	73.7/63.4	71.0/63.4	
October	69.5/46.0	68.3/53.3	68.0/56.1	67.4/57.9	67.4/59.7	66.8/60.3	
November	52.4/33.9	55.0/37.8	58.0/41.7	59.6/45.6	61.5/49.6	62.6/52.0	
December	36.0/24.8	40.3/30.8	44.0/34.0	47.8/36.8	51.6/39.8	54.4/42.7	
	<u>Bare Soil Surface^b</u>						
	<u>2-ft</u> (°F)	<u>3-ft</u> (°F)	<u>4-ft</u> (°F)	<u>5-ft</u> (°F)	<u>6-ft</u> (°F)	<u>7-ft</u> (°F)	
January	33.4/24.7	36.4/26.4	40.0/30.0	42.7/33.0	45.0/36.6	46.0/37.9	
February	37.7/26.9	37.6/27.1	38.2/30.0	39.1/32.1	41.1/34.8	41.8/36.8	
March	42.6/30.5	41.8/30.2	41.8/31.0	41.8/32.7	42.2/35.1	42.2/36.0	
April	52.6/32.7	50.5/30.8	48.9/31.3	48.0/32.9	47.5/35.2	46.5/38.2	
May	66.3/46.2	63.5/43.9	59.8/42.0	56.7/41.9	54.2/43.1	52.4/41.4	
June	75.0/54.0	73.0/52.0	68.5/50.0	66.3/49.2	64.0/50.7	61.0/48.5	
July	81.2/64.7	79.8/62.6	75.2/60.0	73.0/57.9	70.0/57.4	67.0/53.8	
August	82.1/66.2	75.0/65.1	71.5/65.0	70.6/64.3	70.5/64.3	67.3/62.1	
September	73.7/54.6	72.3/54.4	70.7/56.0	69.6/58.0	69.3/60.5	68.1/61.0	
October	66.1/44.7	66.1/45.3	66.1/48.1	68.0/50.8	65.9/54.0	65.9/56.0	
November	53.3/35.2	53.6/37.6	56.0/40.2	57.5/42.9	58.5/46.4	58.5/48.2	
December	40.6/30.1	41.0/31.3	45.5/34.0	48.5/37.0	50.9/40.8	51.8/42.0	

a. Data period of record spans June 1957 through August 1963.

b. Data period of record spans November 1956 through August 1963.

Section D Precipitation

Precipitation has been recorded at CFA since 1950. It has also been recorded at various other locations for various periods of time. The CFA station is the only station currently in operation at which precipitation is recorded. It is also the station with the longest (approximately 40 years) period of record.

General Characteristics

The type of precipitation which occurs over the INEL is generally dictated by the season, i.e., rain showers or thundershowers in the summer, showers or periods of rain or snow in the spring and fall, and periods of snow in the winter. Although the total annual amount at CFA is light, precipitation can be expected in any month of the year. There have also been several months when no precipitation has been recorded.

Precipitation summaries for CFA and TAN are given in Tables D-1 and D-2, respectively. The data for CFA are also presented graphically in Figure D-1. A pronounced precipitation peak occurs in May and June which is due primarily to regional major synoptic conditions. The average precipitation for each of these months is approximately 1.2 in. at CFA and 1.3 in. at TAN. The precipitation observed in every other month is approximately 1/2 or less of these amounts. The annual average total precipitation is 8.71 and 7.85 in. for CFA and TAN, respectively.

Considerable precipitation variability is characteristic of the entire INEL area. As can be seen in Figure D-1, a rather large precipitation spike occurs during the twenty-third week of the year at CFA. Thunderstorms with heavy precipitation during that week have been observed in three separate years. Since the average precipitation is low, one or two severe storms can overshadow the average as illustrated in this case.

A complete listing of the extreme precipitation amounts for each day is given in Appendix 2 and summarized in Tables D-3 and D-4 together with precipitation data from TAN. The 24-hour period for CFA in these tables spans the time frame of midnight to midnight. On the other hand, the 24-hour period for TAN spans any 24-hour time frame and is not limited to the period of midnight to midnight. Precipitation amounts in excess of one inch per day (Table D-4) were recorded eight times at CFA and nine times at TAN. Maximum daily precipitation amounts of 1.64 and 1.78 in. were recorded at CFA and TAN, respectively.

Table D-4 also includes maximum observed hourly precipitation amounts. The maximum precipitation for one hour was 0.54 in. at CFA and 1.15 in. at TAN. The high hourly precipitation amounts for May and June are the result of a series of heavy thunderstorms and corresponds to the time of year when the highest monthly precipitation amounts are observed (Figure D-1).

Frequency and Duration Characteristics

In addition to precipitation amounts, the frequency of occurrence and the duration of precipitation periods are often used for planning purposes. Table D-5 lists the monthly and annual average number of days (from midnight to midnight) as a percent of occurrence during which specified amounts of precipitation fell at CFA and TAN. The data indicate that the frequency of days with a trace of precipitation was quite high during the winter and the spring months. The frequency of occurrence in the heavier categories was extremely low, even in the summer. For precipitation amounts of 0.10 in. or greater, the frequency of occurrence was less than 15% for all months and as low as 3%.

Table D-1. Average total monthly and annual precipitation (water equivalent) for CFA^a.

	Average (in.)	Highest (in.)	Lowest (in.)
January	0.69	2.56	0.00 ^b
February	0.64	2.40	0.00
March	0.60	1.44	0.07
April	0.73	2.50	0.00
May	1.20	4.42	0.07
June	1.18	3.89	0.02
July	0.53	2.29	0.00
August	0.57	3.27	0.00
September	0.63	3.52	0.00
October	0.52	1.67	0.00
November	0.68	1.74	0.00
December	0.75	3.43	0.02
ANNUAL	8.71	14.40	4.50

a. Data period of record spans January 1950 through December 1988.

b. Trace amounts are not considered as precipitation.

Table D-2. Average total monthly and annual precipitation (water equivalent) for TAN. The annual average includes only years with 12 months of observations.

	Average ^a (in.)	Highest ^b (in.)	Lowest ^b (in.)
January	0.52	0.84	Tracer ^c
February	0.57	1.83	0.08
March	0.42	1.07	Trace
April	0.58	1.85	0.01
May	1.37	5.04	0.10
June	1.19	3.35	0.09
July	0.50	1.33	Trace
August	0.64	1.81	0.06
September	0.71	2.51	0.00
October	0.29	1.14	0.00
November	0.33	1.42	0.00
December	0.59	2.43	0.07
ANNUAL	7.85	15.60	4.37

a. Data period of record spans January 1950 through December 1988.

b. Trace amounts are not considered as precipitation.

Table D-3. Occurrences of precipitation amounts equal to or greater than one inch per day for CFA^a and TAN^b.

	CFA		TAN	
	Year of Occurrence	Amount (in.)	Year of Occurrence	Amount (in.)
January	None	None	None	None
February	None	None	None	None
March	None	None	None	None
April	1981	1.51	1963	1.07
May	None	None	1962, 1963	1.24, 1.78
June	1954, 1963, 1969	1.36, 1.14, 1.64	1958	1.31
July	1979	1.25	1953	1.33
August	None	None	None	None
September	1961, 1961	1.09, 1.55	1958, 1962	1.00, 1.00
October	None	None	1964	1.12
November	None	None	None	None
December	1964	1.07	1959	1.05

- a. Data period of record spans January 1950 through December 1988.
b. Data period of record spans April 1950 through December 1964.

Table D-4. Greatest 1-hour and 24-hour precipitation amounts for CFA and TAN.

	1-hour Period		24-hour Period	
	CFA ^a (in.)	TAN ^b (in.)	CFA ^c (in.)	TAN ^b (in.)
January	0.18	0.09	0.79	0.94
February	0.16	0.18	0.79	0.70
March	0.17	0.11	0.61	0.48
April	0.18	0.24 ^d	1.51	1.07
May	0.43	1.00	0.95	1.78
June	0.54	1.15	1.64	1.31
July	0.20	0.24	1.25	1.33
August	0.40	0.45	0.80	0.89
September	0.37	0.55	1.55	1.00
October	0.34	0.21	0.74	1.12
November	0.16	0.25	0.71	0.48
December	0.23	0.15	1.07	1.05
ANNUAL	0.54	1.15	1.64	1.78

- a. Data period of record spans January 1950 through December 1964.
b. Data period of record spans April 1950 through December 1964.
c. Data period of record spans January 1950 through December 1988.
d. Hourly amounts were not available when the 24-hour record for April at TAN of 1.07 in. was recorded. The value of 0.24 in. is, therefore, probably too low.

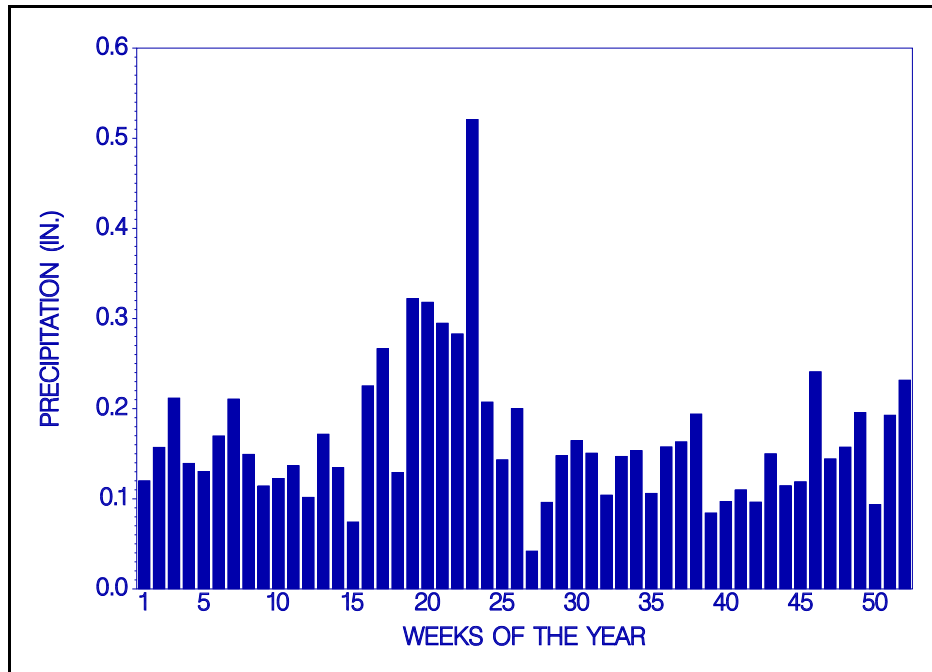


Figure D-1. Average weekly total precipitation for CFA from January 1950 through December 1988.

Table D-5. Monthly and annual average number of days (%) on which precipitation was recorded at CFA and TAN.

	Trace or More		0.01 in. or More		0.10 in. or More		0.50 in. or More		1.0 in. or More	
	CFA ^a (%)	TAN ^b (%)	CFA ^c (%)	TAN ^b (%)						
January	40	30	24	23	7	5	0.7	0.3	0.0	0.0
February	35	29	21	22	8	5	0.7	0.7	0.0	0.0
March	32	22	20	17	7	5	0.2	0.0	0.0	0.0
April	31	26	20	16	8	7	0.6	0.3	0.1	0.0
May	35	35	25	26	13	12	1.4	2.6	0.0	0.3
June	34	25	23	20	11	11	1.9	2.7	0.3	0.3
July	17	19	12	2	5	6	0.7	0.3	0.1	0.3
August	21	20	12	4	5	7	1.0	1.3	0.0	0.3
September	19	17	12	12	6	5	0.9	1.7	0.2	0.3
October	20	26	12	11	6	3	0.7	0.3	0.0	0.0
November	27	21	19	16	8	3	0.6	0.0	0.0	0.0
December	35	26	23	25	9	6	0.3	0.3	0.1	0.0
ANNUAL	28	25	19	18	8	6	0.8	0.8	0.1	0.1

a. Data period of record spans January 1950 through September 1983.

b. Data period of record spans April 1950 through December 1963.

c. Data period of record spans January 1950 through December 1988.

A listing of the probabilities of precipitation events lasting for one or more days is given in Tables D-6 and D-7 for CFA and TAN, respectively. The data have been compiled for days on which the total precipitation amount was 0.01 in. or greater. As can be seen, most of the precipitation at both CFA and TAN occurs on a single day which is both preceded and followed by a day with no measurable precipitation. The annual statistics indicate that a single day of precipitation occurs almost 2.5 times as often as a 2-day precipitation event at CFA. TAN precipitation data indicate a similar trend. The longest observed continuous period of precipitation at CFA lasted ten days from 18 December through 27 December 1955. A 14-day period of precipitation at CFA was observed from 29 May through 11 June 1963 which was broken by a trace amount and ended with a trace amount of precipitation.

A listing of the probabilities of one or more continuous days of no measurable precipitation is included in Tables D-8 and D-9 for CFA and TAN, respectively. The most common length of time with no precipitation at both CFA and TAN was one day. However, when viewed from a length of time perspective instead of from a perspective of the number of occurrences, it becomes clear that multiple days of no precipitation are the norm, rather than the exception at both CFA and TAN. The longest dry period at CFA was 61 days from 12 September through 11 November 1952. The longest dry period at TAN was 57 days from 13 September through 08 November 1958.

Snow

Snow fall and snow depth records are available only for CFA, since it has been the only manned weather station at the INEL. Snow fall is the amount of snow that falls within a given period regardless of the amount that accumulates on the ground. Since snow may melt as it falls, the snow fall amount must occasionally be estimated from the water equivalent of snow.

Average monthly and annual snow fall amounts are listed in Table D-10. Also listed are the highest daily snow falls for a given month. Daily extreme snow fall amounts are given in Appendix 3. The highest monthly average snowfall is in December with a total of 6.4 in. January also receives an amount comparable to December (6.1 in.). Snow fall as late as May and as early as September are usually observed at the INEL. Considerable snow fall variation was also noted within months, particularly December which exhibited a snow fall range of 22.3 in. Indeed, every month has recorded no snow fall at least once during the 39-year period of record. The maximum snow fall amounts in any 24-hour period were 8.5 and 8.6 in. recorded during January and March, respectively.

The annual trace of the average weekly snow fall total is illustrated in Figure D-2. A weak bimodal distribution is apparent in the data. Weekly snow fall totals range between 1 and 2 inches from about mid November through February and then gradually decline through March and part of April. The second annual snow fall maximum then occurs in the middle of April corresponding to the arrival of the spring season convective storms.

The average percentage of days (from midnight to midnight) in a given month on which a specified amount of snow fall was recorded is listed in Table D-11. Maximums and minimums are also noted. January has the largest average number of days with snow fall (20%) followed by December (19%). Snow fall has been observed on as many as 55% of the days in January and 45% of the days in December. The difference between the maximum and minimum number of snow fall days within a given month was quite large for the snow fall category of 0.1 in.

The monthly averages and extremes of snow depths are listed in Table D-12. Daily extreme snow depths are given in Appendix 4. The highest average monthly snow depth ever recorded was 20 in. The maximum snow depth for any day was 25 in. (Appendix 4). During periods when several

Table D-6. Successive days with daily precipitation total equal to or greater than 0.01 inches for CFA^a.

	1 Day (%)	2 Days (%)	3 Days (%)	4 Days (%)	5 Days (%)	6 Days (%)	7 Days (%)	8 Days (%)	9 Days (%)	10 days (%)
January	2.31	1.05	0.51	0.10	0.00	0.13	0.03	0.00	0.00	0.00
February	2.18	0.90	0.31	0.08	0.05	0.05	0.00	0.03	0.00	0.00
March	2.79	1.03	0.23	0.10	0.00	0.00	0.00	0.00	0.00	0.00
April	1.92	0.95	0.38	0.18	0.00	0.03	0.00	0.00	0.00	0.03
May	2.31	1.05	0.46	0.23	0.10	0.03	0.00	0.03	0.00	0.00
June	2.00	1.00	0.28	0.26	0.10	0.03	0.00	0.08	0.00	0.00
July	1.62	0.74	0.03	0.05	0.00	0.03	0.00	0.00	0.00	0.00
August	1.74	0.59	0.13	0.08	0.03	0.03	0.00	0.00	0.00	0.00
September	1.67	0.36	0.31	0.03	0.05	0.00	0.00	0.00	0.00	0.00
October	1.69	0.56	0.18	0.03	0.03	0.03	0.00	0.00	0.00	0.00
November	2.15	1.03	0.21	0.21	0.00	0.00	0.00	0.00	0.00	0.00
December	2.41	1.05	0.36	0.08	0.13	0.05	0.00	0.00	0.00	0.03
ANNUAL	2.07	0.86	0.28	0.12	0.04	0.03	0.00	0.01	0.00	0.01

a. Data period of record spans January 1950 through December 1988.

Table D-7. Monthly and annual probabilities of one or multiple days of continuous precipitation (amounts equal to or greater than 0.01 in.) expressed as a percent of occurrence for TAN^a.

	1 Day (%)	2 Days (%)	3 Days (%)	4 Days (%)	5 Days (%)	6 Days (%)	7 Days (%)	8 Days (%)	9 Days (%)	10Days (%)
January	2.20	1.60	0.20	0.20	0.00	0.00	0.00	0.00	0.00	0.00
February	2.10	1.10	0.10	0.10	0.00	0.00	0.00	0.00	0.10	0.00
March	1.82	1.27	0.27	0.00	0.00	0.00	0.00	0.00	0.00	0.00
April	1.55	0.73	0.09	0.27	0.09	0.09	0.00	0.00	0.00	0.00
May	2.00	0.82	0.55	0.36	0.18	0.00	0.00	0.00	0.00	0.09
June	2.00	0.73	0.18	0.36	0.00	0.09	0.09	0.09	0.00	0.00
July	1.73	0.36	0.27	0.00	0.09	0.00	0.00	0.00	0.00	0.00
August	1.82	1.09	0.00	0.00	0.00	0.00	0.00	0.00	0.00	0.00
September	1.45	0.36	0.36	0.09	0.00	0.00	0.00	0.00	0.00	0.00
October	1.70	0.70	0.20	0.00	0.00	0.00	0.00	0.00	0.00	0.00
November	2.70	1.10	0.10	0.00	0.00	0.00	0.00	0.00	0.00	0.00
December	2.30	1.10	0.30	0.00	0.10	0.00	0.00	0.00	0.00	0.00
ANNUAL	1.94	0.91	0.22	0.12	0.04	0.02	0.01	0.01	0.01	0.01

a. Data period of record spans March 1954 through September 1964.

Table D-8. Monthly and annual probabilities of one or more continuous days of no measurable precipitation (including trace amounts) expressed as a percent of occurrence for CFA^a.

	1 Day	2 Days	3 Days	4 Days	5 Days	6 Days	7 Days	8 Days	9 Days	10 Days	11 Days	12 Days	13 Days	14 Days	15 Days or More
	(%)	(%)	(%)	(%)	(%)	(%)	(%)	(%)	(%)	(%)	(%)	(%)	(%)	(%)	(%)
January	0.92	0.64	0.59	0.21	0.38	0.26	0.21	0.18	0.15	0.08	0.05	0.00	0.10	0.10	0.49
February	0.82	0.51	0.33	0.36	0.15	0.13	0.21	0.13	0.18	0.21	0.05	0.13	0.08	0.13	0.23
March	0.85	0.49	0.38	0.56	0.33	0.36	0.21	0.18	0.21	0.08	0.05	0.03	0.10	0.10	0.41
April	0.77	0.38	0.44	0.15	0.38	0.13	0.13	0.15	0.10	0.15	0.13	0.03	0.05	0.08	0.56
May	1.00	0.44	0.54	0.41	0.26	0.36	0.13	0.08	0.13	0.18	0.05	0.08	0.10	0.05	0.28
June	0.97	0.44	0.38	0.23	0.23	0.13	0.15	0.21	0.21	0.18	0.10	0.13	0.00	0.03	0.44
July	0.26	0.31	0.13	0.10	0.23	0.13	0.08	0.18	0.13	0.05	0.15	0.10	0.08	0.08	0.54
August	0.28	0.33	0.18	0.15	0.13	0.10	0.18	0.18	0.10	0.00	0.15	0.03	0.00	0.13	0.79
September	0.46	0.08	0.15	0.28	0.15	0.18	0.15	0.03	0.10	0.18	0.03	0.08	0.05	0.03	0.64
October	0.21	0.33	0.08	0.10	0.15	0.18	0.13	0.18	0.05	0.13	0.10	0.10	0.13	0.05	0.77
November	0.69	0.36	0.36	0.41	0.33	0.31	0.18	0.21	0.10	0.13	0.13	0.08	0.05	0.05	0.33
December	0.85	0.64	0.62	0.26	0.33	0.28	0.21	0.05	0.18	0.05	0.13	0.10	0.08	0.08	0.41
Annual	0.67	0.41	0.35	0.27	0.26	0.21	0.16	0.15	0.14	0.12	0.09	0.07	0.07	0.08	0.49

a. Data period of record spans January 1950 through December 1988.

Table D-9. Monthly and annual probabilities of one or more continuous days of no measurable precipitation (including also trace amounts) expressed as a percent of occurrence for TAN^a.

	1 Day	2 Days	3 Days	4 Days	5 Days	6 Days	7 Days	8 Days	9 Days	10 Days	11 Days	12 Days	13 Days	14 Days	15 Days
	(%)	(%)	(%)	(%)	(%)	(%)	(%)	(%)	(%)	(%)	(%)	(%)	(%)	(%)	(%)
January	1.00	0.78	0.56	0.67	0.67	0.22	0.22	0.22	0.22	0.22	0.22	0.00	0.00	0.00	0.22
February	0.33	0.78	0.56	0.67	0.33	0.22	0.11	0.11	0.22	0.22	0.22	0.00	0.11	0.00	0.33
March	0.40	0.70	0.20	0.80	0.40	0.20	0.40	0.20	0.30	0.10	0.00	0.30	0.10	0.00	0.30
April	0.60	0.30	0.50	0.40	0.20	0.10	0.20	0.20	0.30	0.10	0.00	0.16	0.00	0.10	0.60
May	1.40	0.70	0.30	0.50	0.20	0.30	0.20	0.40	0.10	0.00	0.20	0.10	0.10	0.00	0.30
June	1.30	0.60	0.40	0.30	0.10	0.50	0.20	0.10	0.50	0.10	0.30	0.00	0.00	0.10	0.20
July	0.50	0.60	0.30	0.10	0.30	0.10	0.30	0.00	0.10	0.00	0.30	0.10	0.30	0.10	0.50
August	0.20	0.40	0.60	0.30	0.20	0.30	0.30	0.40	0.00	0.00	0.20	0.20	0.00	0.00	0.70
September	0.70	0.10	0.20	0.10	0.20	0.20	0.40	0.00	0.20	0.10	0.10	0.30	0.00	0.00	0.90
October	0.56	0.56	0.11	0.33	0.22	0.22	0.33	0.00	0.22	0.33	0.11	0.11	0.11	0.00	0.56
November	1.22	0.89	0.44	0.67	0.22	0.44	0.11	0.56	0.00	0.11	0.22	0.11	0.00	0.11	0.22
December	1.00	0.56	0.44	0.89	0.44	0.44	0.22	0.22	0.33	0.00	0.33	0.11	0.11	0.00	0.33
Annual	0.77	0.57	0.38	0.47	0.29	0.27	0.25	0.15	0.21	0.12	0.18	0.12	0.07	0.03	0.43

a. Data period of record spans March 1954 through September 1964.

Table D-10. Monthly and annual snow fall totals and monthly and daily extreme totals for CFA^a.

	Average (in.)	Maximum (in.)	Minimum (in.)	Largest Daily Maximum (in.)
January	6.1	18.1	0.0	8.5
February	4.7	15.0	0.0	7.5
March	3.5	10.2	0.0	8.6
April	2.3	16.5	0.0	6.7
May	0.7	8.3	0.0	4.4
June	0.0	0.0	0.0	0.0
July	0.0	0.0	0.0	0.0
August	0.0	0.0	0.0	0.0
September	0.1	1.0	0.0	1.0
October	0.6	7.2	0.0	4.5
November	3.3	12.3	0.0	6.5
December	6.4	22.3	0.0	7.0
ANNUAL	27.6	59.7	6.8	8.6

a. Data period of record spans January 1950 through December 1988.

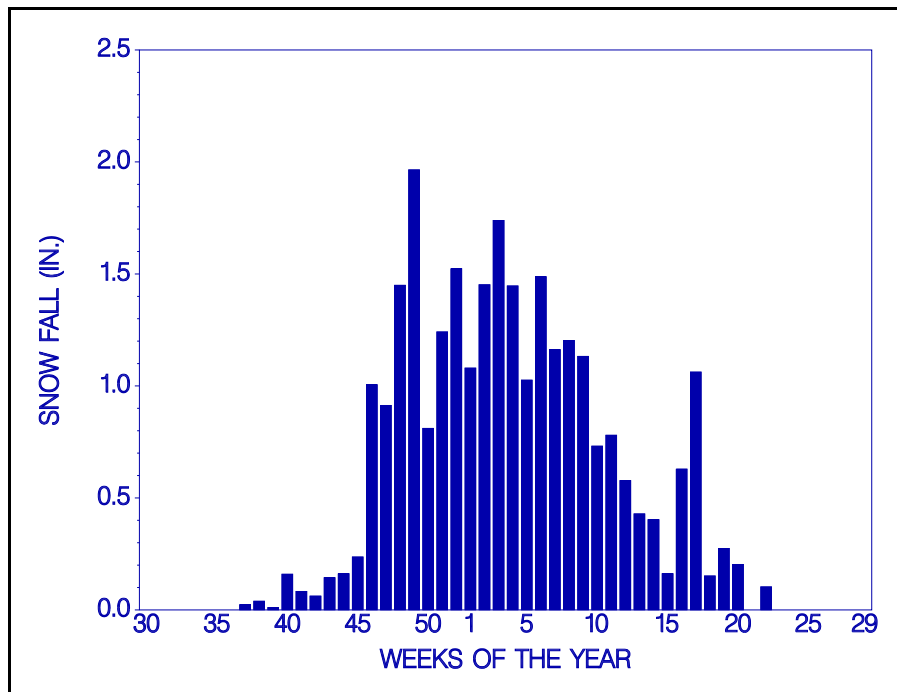


Figure D-2. Average weekly total snow fall for CFA from January 1950 through December 1988.

inches of loose snow were present along with moderate to strong surface winds, considerable blowing and drifting occurred, and drifts accumulated to a depth of several feet.

The annual trace of the average weekly snow depth is illustrated in Figure D-3. The trace is

characterized by a rapid rise from about mid-November to a single maximum of approximately 4.5 in. during the second week of February. The average snow depth then declines to near 0 in. about the second week of April. During the remainder of the year, there is no significant snow accumulation on the ground.

Table D-11. Monthly and annual average number of days (%) and extreme number of days with snow fall amounts, of equal to or greater than 0.1, 1.0, and 3.0 in. for CFA^a.

	≥ 0.1 in.			≥ 1.0 in.			≥ 3.0 in.		
	Average (%)	Maximum (%)	Minimum (%)	Average (%)	Maximum (%)	Minimum (%)	Average (%)	Maximum (%)	Minimum (%)
January	20	55	0	7	16	0	1	6	0
February	14	39	0	6	14	0	2	7	0
March	11	29	0	4	13	0	1	6	0
April	6	33	0	2	13	0	1	7	0
May	1	10	0	1	10	0	0	6	0
June	0	0	0	0	0	0	0	0	0
July	0	0	0	0	0	0	0	0	0
August	0	0	0	0	0	0	0	0	0
September	0	3	0	0	3	0	0	0	0
October	2	13	0	1	6	0	0	3	0
November	9	23	0	4	17	0	1	10	0
December	19	45	0	8	26	0	2	6	0
ANNUAL	7	13	2	3	5	1	1	2	0

a. Data period of record spans January 1950 through December 1988.

Table D-12. Monthly and annual average snow depths on the ground and extreme snow depths for CFA^a.

	Average (in.)	Maximum (in.)	Minimum (in.)
January	4.1	11.9	0.0
February	4.1	18.3	0.0
March	2.2	20.0	0.0
April	0.1	0.9	0.0
May	0.0	0.2	0.0
June	0.0	0.0	0.0
July	0.0	0.0	0.0
August	0.0	0.0	0.0
September	0.0	0.0	0.0
October	0.0	0.1	0.0
November	0.4	3.6	0.0
December	2.6	17.6	0.0
ANNUAL	1.1	5.3	0.0

a. Data period of record spans January 1950 through December 1988.

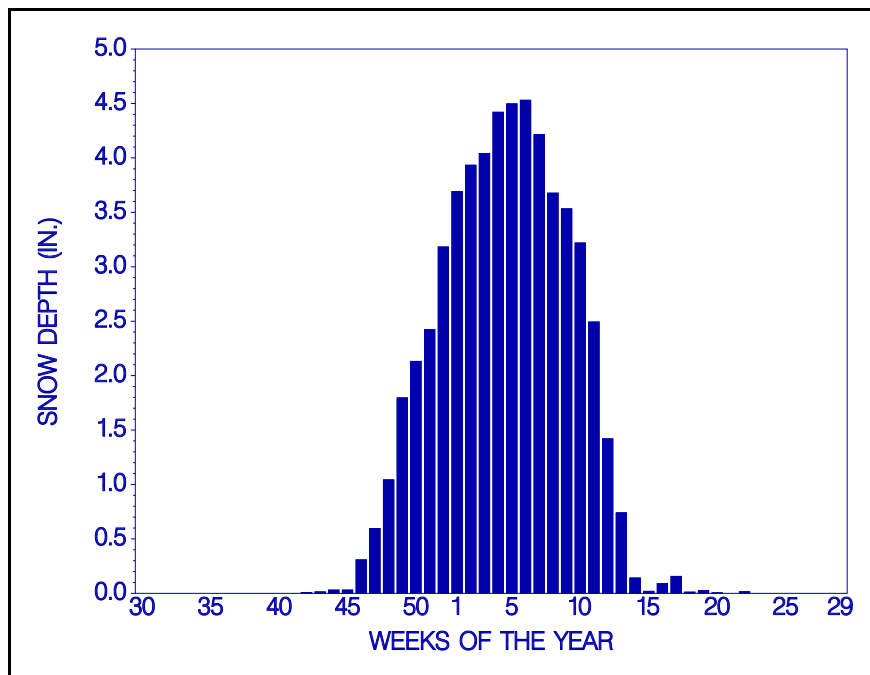


Figure D-3. Average weekly snow depths for CFA from January 1950 through December 1988.

Section E

Atmospheric Moisture

Atmospheric moisture is a meteorological parameter which is important in facility design and operation. Atmospheric moisture has been continuously monitored at the INEL since 1950. The primary observation location has been CFA. Originally, atmospheric moisture was recorded as hourly wet bulb temperatures. After discontinuing the hourly observations, atmospheric moisture was recorded as relative humidity using a hydrothermograph. Atmospheric humidity has more recently been recorded as dew point temperature with a chilled mirror. Wet bulb temperature, relative humidity, and dew point temperature are related variables, i.e., each variable can be converted into the other using an appropriate formula along with other joint variables such as pressure, temperature, etc. Each atmospheric moisture variable has a particular application in building and equipment design and engineering. Four such variables are discussed below together with a treatise on pan evaporation. The discussions pertain to the atmospheric moisture content observed at CFA. However, average atmospheric moisture varies only slightly over the local scale distances within the INEL boundaries. Hence, the moisture discussions derived from data collected at CFA are generally applicable to the entire INEL.

Wet Bulb Temperature

Wet bulb temperature is defined as the lowest temperature to which air can be cooled by evaporating water. Wet bulb temperatures are frequently used as design criteria for evaporative cooling systems.

Monthly and annual averages of hourly wet bulb temperature observations are given in Table E-1 for the time period of April 1955 through April 1961. The average monthly wet bulb temperatures range from a low of 14.7 °F in January to a high of 50.3 °F in July. The lowest single monthly average was recorded in January at

5.7 °F. The highest single monthly average was recorded in August at 52.3 °F. Table E-1 also contains absolute maximum and minimum hourly wet bulb temperatures stratified by month. The lowest hourly wet bulb temperature recorded was in January at -31.5 °F. The highest hourly wet bulb temperature recorded was in July at 67.0 °F. Although this wet bulb temperature is high, the greatest cooling efficiency is during the summer months. During this time period, the potential for cooling, i.e., the dry bulb/wet bulb temperature gradient, is the greatest.

The diurnal distribution of wet bulb temperatures is summarized in Table E-2. This table contains the monthly and annual averages of the daily maximum and minimum wet bulb temperatures. It also contains the monthly and annual extreme averages of the daily maximum and minimum wet bulb temperatures. The largest monthly average daily range was observed in January with a value of 19.8 °F. The smallest monthly average daily range was observed in May with a value of 13.5 °F.

Seasonal and annual cumulative frequency distributions of wet bulb temperatures are oftentimes of interest for design purposes. These frequencies have been calculated from the hourly data and are shown in Figure E-1. The specific wet bulb temperature at both the 2.5 and 97.5% cumulative frequency level is also given for each season and for the annual summary. The annual wet bulb temperature values at the specified frequencies are 1.0 and 57.4 °F, respectively.

Relative Humidity

Another measure of atmospheric moisture is relative humidity. This is defined as the ratio of the amount of water vapor contained in a given volume of air to the amount required for saturation at the same temperature and pressure. Pressure changes are normally small in comparison to

Table E-1. Monthly and annual averages and extremes of hourly wet bulb temperatures for CFA^a.

	Monthly Values			Hourly Extreme Values	
	Average	Highest	Lowest	Maximum	Minimum
	(°F)	(°F)	(°F)	(°F)	(°F)
January	14.7	20.8	5.7	39.6	-31.5
February	19.6	26.9	10.2	44.2	-28.0
March	26.4	28.4	24.0	47.9	-28.2
April	33.0	34.1	30.7	51.5	7.7
May	41.0	44.2	37.5	59.0	21.9
June	46.2	47.8	44.5	61.8	35.6
July	50.3	51.6	49.1	67.0	35.6
August	47.9	52.3	45.5	65.5	25.9
September	41.7	44.0	41.1	62.9	18.4
October	34.4	35.6	34.0	54.5	6.5
November	23.7	26.9	22.0	47.7	-20.2
December	19.2	22.6	15.2	43.3	-14.1
ANNUAL	33.2	34.7	32.0	67.0	-31.5

a. Data period of record spans April 1955 through April 1961.

Table E-2. Monthly and annual averages of daily maximum and minimum wet bulb temperatures for CFA^a.

	Average Maximum (°F)	Average Minimum (°F)	Highest Average		Lowest Average	
			Maximum (°F)	Minimum (°F)	Maximum (°F)	Minimum (°F)
January	24.6	4.8	28.0	13.9	18.7	-7.3
February	28.3	10.7	34.0	20.4	21.1	-0.8
March	34.1	18.6	35.5	21.2	32.5	14.8
April	40.3	25.6	42.5	27.6	37.8	23.6
May	47.7	34.2	52.1	37.7	43.9	31.1
June	53.4	39.0	54.3	41.3	52.6	36.3
July	58.2	42.4	59.9	44.1	57.3	40.8
August	56.5	39.3	60.4	44.0	53.8	37.2
September	51.0	32.4	53.3	34.7	50.5	30.5
October	43.9	24.8	44.9	27.5	43.0	22.3
November	32.9	14.4	34.3	19.6	31.2	10.1
December	28.6	9.8	30.1	15.7	26.9	3.5
ANNUAL	41.5	24.6	43.0	26.3	40.6	23.3

a. Data period of record spans April 1955 through April 1961.

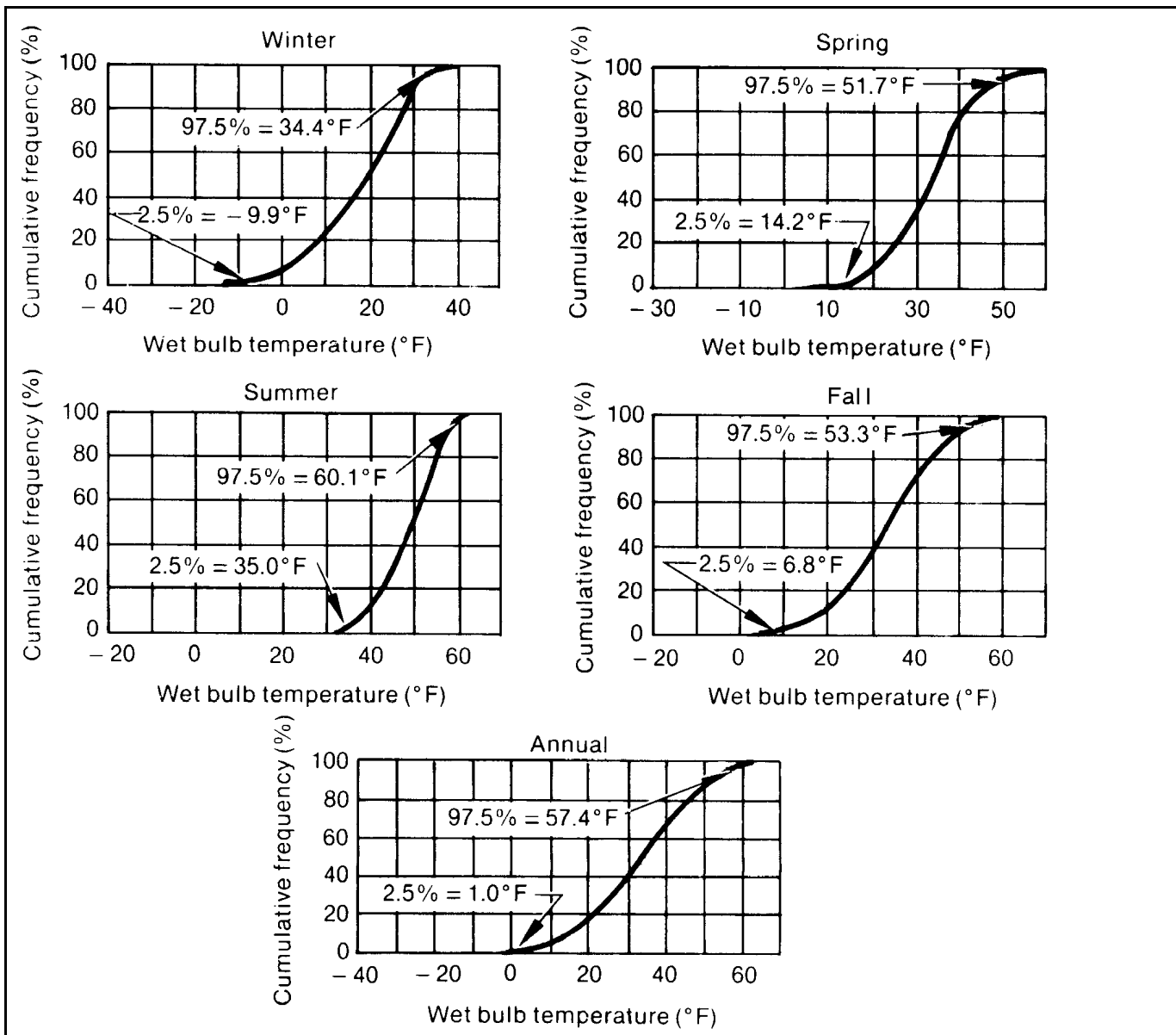


Figure E-1. Seasonal and annual cumulative frequency distributions of wet bulb temperatures.

temperature. Therefore, relative humidity is almost entirely a function of air temperature.

The average hourly relative humidity for CFA from 1956 through 1961 is shown in Figure E-2 for January, April, July, and October. Also shown are the mean maximum and minimum hourly values for the same months. These months represent the middle of each season, i.e., winter, spring, summer, and fall, respectively. The relative humidity values given here were calculated from

the wet bulb temperatures given in the previous tables. Although the absolute values change from season to season, general diurnal features still persist over the entire year. The highest diurnal values usually occur near sunrise, while the lowest values occur during mid-afternoon. The peaks and valleys always occur simultaneously with the minimum and maximum air temperatures. The highest relative humidity is observed in the winter, when the average mid-day relative humidity is about 55%. The lowest relative humidity is

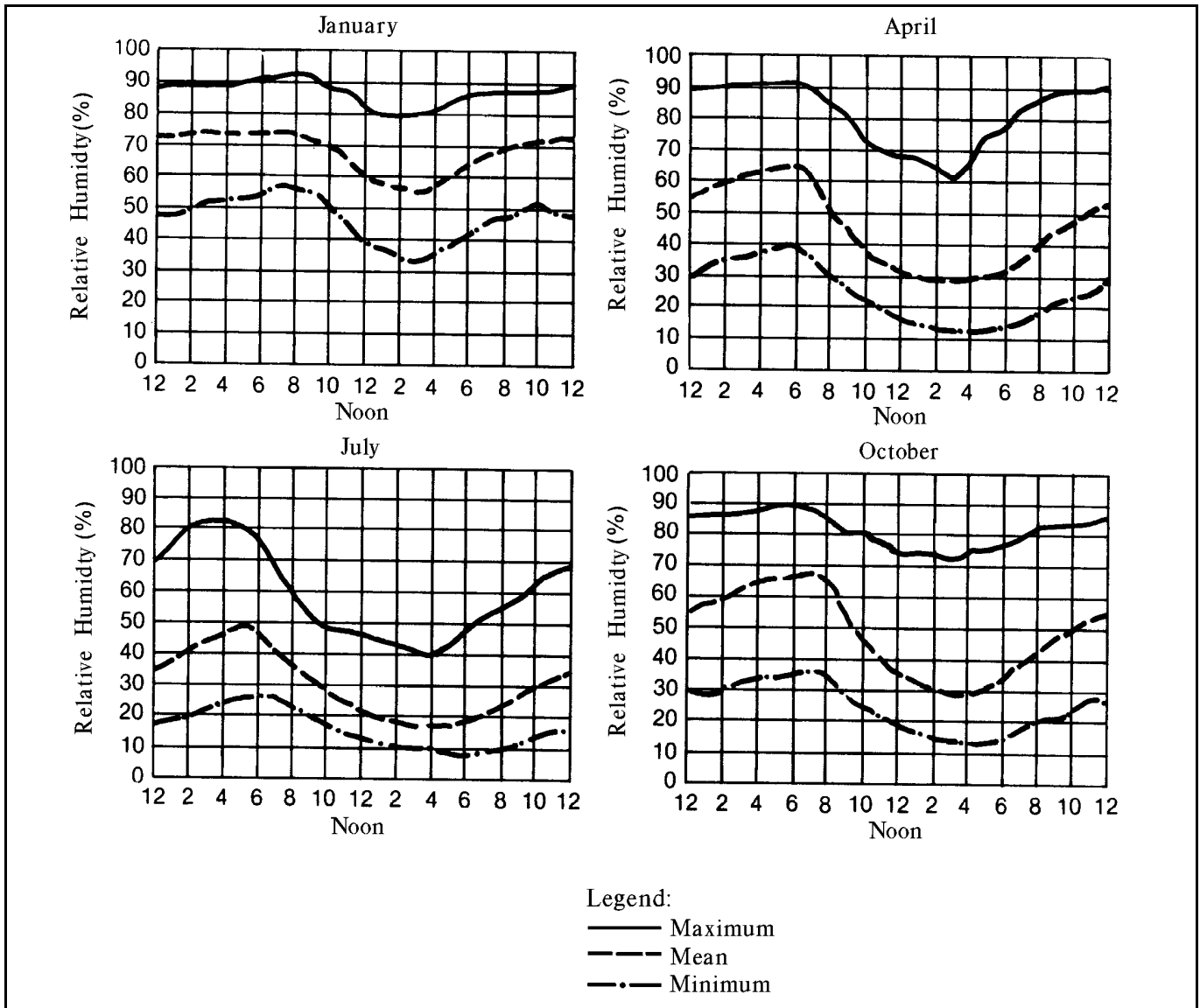


Figure E-2. Average hourly relative humidity for winter, spring, summer, and fall seasons represented by data from January, April, July, and October, respectively.

observed in the summer when the average mid-day relative humidity is about 18%. This seasonal dependence is due to the increased precipitation and the smaller daily temperature ranges observed in the winter compared to the summer.

Monthly and annual relative humidity averages, mean maximums, and mean minimums are listed in Table E-3. The average maximums and minimums were computed from hourly rather than daily values. Therefore, the indicated values will be a few percent higher for the maximums and a

few percent lower for the minimums than would be the case if average maximums and minimums were computed from daily values. Absolute maximums and minimums are also listed in Table E-3. Absolute maximum relative humidity values of 100% were observed in every month of the year except July during the 6-year time frame from 1956 through 1961. It is quite possible, although not documented, for July to also have a relative humidity observation of 100% in the future. The lowest relative humidity observed was 4% in both July and August. This is indicative of the very dry

Table E-3. Monthly and annual relative humidity averages and extremes for CFA^a.

	Average (%)	Average Maximum (%)	Average Minimum (%)	Absolute	
				Maximum (%)	Minimum (%)
January	68	87	47	100	15
February	70	89	42	100	14
March	58	84	34	100	14
April	44	81	23	100	8
May	46	83	22	100	8
June	36	73	16	100	6
July	30	59	16	92	4
August	31	65	15	100	4
September	38	74	18	100	6
October	48	82	24	100	6
November	60	86	30	100	10
December	68	89	40	100	16
ANNUAL	50	79	27	100	4

a. Data period of record spans January 1956 through December 1961.

summers experienced at the INEL in particular, and across the entire ESRP in general.

Dew Point Temperature

Yet another measure of atmospheric moisture is dew point temperature. It is defined as the temperature to which air must be cooled at a constant pressure and water vapor content in order for saturation to occur. Monthly and annual average dew point temperatures are given in Table E-4. These temperatures were computed from the monthly and annual average air and wet bulb temperatures for the time period of April 1955 through April 1961. The lowest monthly averaged dew point temperature was 7.4 °F in January. The corresponding highest monthly averaged dew point temperature is 33.5 °F in July. These dew point temperatures correspond with the lowest and highest monthly average air temperatures of 16.5 and 69.0 °F respectively.

Mixing Ratio

Still another expression of atmospheric moisture content is mixing ratio. This is the mass of water per unit mass of dry air, normally expressed in units of grams of water per kilogram of dry air. Calculated values of the mixing ratio covering the same time period as that for dew point temperature are given in Table E-5. Mixing ratios in this table include the calculated monthly and annual averages for the 6-year period and the single monthly extremes. The lowest average mixing ratio occurred in January (1.6 g/kg) and the highest average occurred in July (4.8 g/kg).

Pan Evaporation

A unique measure of atmospheric humidity not directly related through a conversion formula to the previously discussed parameters is pan evaporation. These data and/or evapotranspiration data are commonly required to support hydrologic

Table E-4. Monthly and annual averages of dew point temperatures and corresponding air (dry bulb) and wet bulb temperatures for CFA^a.

	Average Dew Point Temperature (°F)	Average Air Temperature (°F)	Average Wet Bulb Temperature (°F)
January	7.4	16.5	14.7
February	12.5	22.0	19.6
March	16.1	31.5	26.4
April	19.0	41.9	33.0
May	27.8	52.3	41.0
June	31.0	61.3	46.2
July	33.5	69.0	47.9
August	29.3	66.4	47.9
September	23.8	56.2	41.7
October	19.7	44.1	34.4
November	14.0	27.9	23.7
December	10.8	22.0	19.2
ANNUAL	20.4	42.6	33.2

a. Data period of record spans April 1955 through April 1961.

Table E-5. Monthly and annual mixing ratio averages and extremes for CFA^a.

	Average (g/kg)	Highest (g/kg)	Lowest (g/kg)
January	1.6	5.6	0.2
February	2.0	5.4	0.3
March	2.4	4.8	0.2
April	2.7	5.3	0.8
May	3.9	6.7	2.3
June	4.4	7.3	2.8
July	4.8	9.6	2.8
August	4.1	10.6	2.5
September	3.2	10.8	1.5
October	2.7	5.3	1.1
November	2.2	5.2	0.4
December	1.9	6.2	0.2
ANNUAL	2.9	10.8	0.2

a. Data period of record spans April 1955 through April 1961.

engineering, ecological, and wildlife studies. No specific measurements of this kind have been recorded at the INEL. However, the following estimates of pan evaporation were calculated in response to occasional requests for pond evaporation rates.

The first step of the analysis involved assembling Class-A pan evaporation data from the pan evaporation observation stations in southeastern Idaho. Data from 4 NCDC stations were assembled: Aberdeen Exp. Station (42° 57' N, 112° 50' W, 4405 ft. m.s.l.), Lifton Pumping Station (42° 7' N, 111° 18' W, 5926 ft. m.s.l.), Palisades (43° 22' N, 111° 14' W, 5385 ft. m.s.l.), and Twin Falls WSO (42° 33' N, 114° 21' W, 3960 ft. m.s.l.). Secondly, station altitude was adjusted by 300 ft. for each degree of latitude either south (negative) or north (positive) of CFA (43° 32' N, 112° 57' W, 4938 ft. m.s.l.). This resulted in adjusted heights of approximately 4300, 5600, 5350, and 3700 ft. m.s.l., respectively.

Thirdly, total pan evaporation amounts for the years 1950, 1951, 1958, 1959, 1963, 1964, 1969, and 1970 were collected. These years contained the most complete data record available for all 4 stations and comprised the months of May through October. The average annual pan evaporation values for those years were 47, 39, 39, and 51 in. for Aberdeen, Lifton, Palisades, and Twin Falls, respectively. Fourth, these evaporation values and adjusted heights were regressed to obtain a height vs. pan evaporation equation. Finally, the altitude for CFA was inserted in the regression equation from which an annual pan evaporation value for CFA was calculated.

Figure E-3 shows the results of the analysis. The outcome suggests an estimated total pan evaporation of about 43 in. per year for CFA with a range of approximately 40 to 46 in. This estimate is generally applicable to all INEL locations and includes year to year variability.

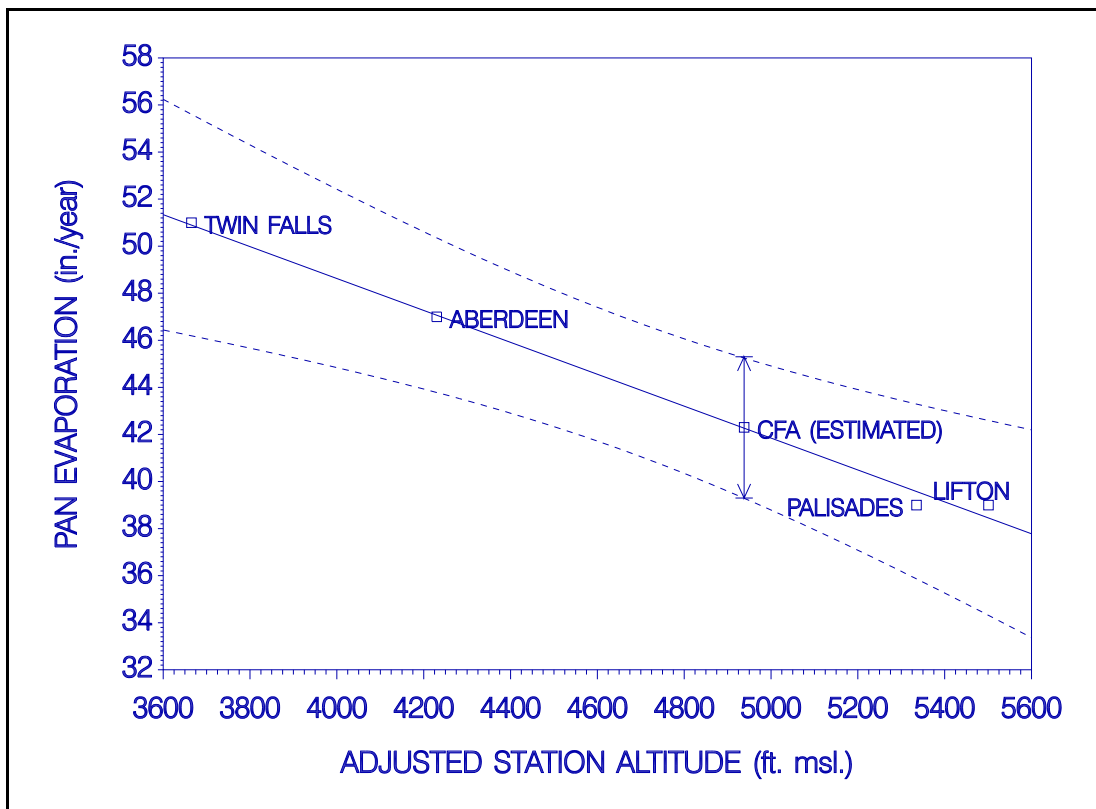


Figure E-3. Estimated CFA pan evaporation utilizing a regression analysis of data from southeastern Idaho. Dashed lines indicate the 99% confidence limit about the mean.

Section F Solar and Terrestrial Radiation

Solar radiation is the source of the energy for all movement of the atmosphere. It can be measured in terms of global, direct, diffuse, and net radiation. It can also be parameterized in terms of percent possible sunshine, percent sky cover, and day length, among others. Some of these measurements have been quantified at the INEL and are described below.

Sunrise and Sunset Times

Day length is a parameter of interest in determining the time available for reception of solar radiation. Longer days in the summer provide the opportunity for more solar heating, while shorter days bring a cooling of the earth's surface. Sunrise and sunset times for CFA are listed in Table F-1. All times listed are Mountain Standard Time (MST). The data indicate that the sun rises as early as 4:51 and sets as late as 20:17 hours MST. It also rises as late as 8:06 and sets as early as 16:56 hours MST. The longest day of the year is 15 hours, 26 minutes. The shortest day of the year is 8 hours, 56 minutes. Sunrise and sunset times on 29 February are considered to be equal to those on 28 February. The resulting uncertainty is approximately ± 1 minute. Local topographic effects and resultant shadows have a much larger influence on sunrise and sunset times than does leap year.

Solar Radiation

Solar radiation has been measured at the INEL and at several locales surrounding the INEL. The data base is small, however, and it is not suitable for a complete climatological analysis. Nevertheless, the data have been used in combination with data obtained from other regional sensors with extensive periods of record (Solar Energy Research Institute, 1981) to estimate solar radiation at the INEL. The regional solar radiation data were obtained during the years 1953-1975 from more than 200 observation stations. The

estimated for the INEL values are given in Table F-2.

The solar radiation values given in Table F-2 include global, direct, and diffuse radiation. Global radiation on a horizontal surface is comprised of the direct solar beam and diffuse sky radiation (skylight). Normal direct solar radiation represents incident direct radiation on a perpendicular surface that is continuously tracking the sun. The analysis indicates that the average daily total global radiation on a horizontal surface in July is expected to be 681 ly/day. That value drops to 131 ly/day in December. The average total daily global radiation value for the entire year is 406 ly/day. Diffuse radiation contributes about 30% of this value.

Net Radiation

Net radiation is a meteorological parameter used in the determination of the amount of solar energy available to evaporate water (latent heat flux) or to warm the air (sensible heat flux). Net radiation is defined as the balance between incoming and reflected solar and incoming and emitted terrestrial radiation.

The sign of the flux of net radiation is positive when directed toward the earth's surface (incoming) and negative when directed outward from the earth's surface to the atmosphere (outgoing).

Net radiation has been measured for a period of 5 years over natural vegetation with a Beckman and Whitley net radiometer from 1961 through 1965. The data so obtained are summarized in Figure F-1. The top two curves of the figure trace the net radiation during daylight hours only. The top curve represents the maximum total net radiation observed on any given day during the 5 year measurement period. The lower of the top two curves represents the average total daily net

Table F-1. Sunrise (S.R.) and sunset (S.S.) times at CFA.

Day	January		February		March		April		May		June	
	S.R.	S.S.	S.R.	S.S.	S.R.	S.S.	S.R.	S.S.	S.R.	S.S.	S.R.	S.S.
1	8:06	17:06	7:48	17:44	7:08	18:21	6:13	18:59	5:24	19:34	4:53	20:06
2	8:06	17:07	7:47	17:45	7:06	18:22	6:11	19:00	5:23	19:36	4:53	20:07
3	8:06	17:08	7:46	17:46	7:05	18:23	6:10	19:01	5:21	19:36	4:53	20:08
4	8:06	17:09	7:45	17:48	7:03	18:25	6:08	19:02	5:21	19:38	4:52	20:08
5	8:05	17:11	7:43	17:49	7:01	18:26	6:06	19:03	5:19	19:39	4:52	20:09
6	8:05	17:11	7:42	17:51	7:00	18:27	6:04	19:05	5:18	19:40	4:51	20:10
7	8:05	17:12	7:41	17:52	6:58	18:28	6:03	19:06	5:16	19:41	4:51	20:11
8	8:04	17:13	7:40	17:53	6:56	18:30	6:01	19:07	5:15	19:42	4:51	20:11
9	8:04	17:14	7:38	17:54	6:54	18:31	5:59	19:08	5:14	19:43	4:51	20:12
10	8:04	17:16	7:37	17:56	6:53	18:32	5:57	19:09	5:13	19:44	4:51	20:12
11	8:04	17:17	7:36	17:57	6:51	18:33	5:56	19:11	5:11	19:46	4:51	20:13
12	8:03	17:18	7:34	17:58	6:49	18:35	5:54	19:12	5:11	19:47	4:51	20:13
13	8:03	17:19	7:33	18:00	6:47	18:36	5:52	19:13	5:09	19:48	4:51	20:14
14	8:02	17:21	7:31	18:01	6:46	18:37	5:51	19:14	5:08	19:49	4:51	20:14
15	8:02	17:21	7:30	18:03	6:44	18:38	5:49	19:16	5:07	19:50	4:51	20:15
16	8:01	17:23	7:29	18:04	6:42	18:40	5:47	19:16	5:06	19:51	4:51	20:16
17	8:01	17:24	7:27	18:06	6:41	18:41	5:46	19:18	5:05	19:52	4:51	20:16
18	8:01	17:25	7:26	18:07	6:38	18:42	5:44	19:19	5:04	19:53	4:51	20:16
19	7:59	17:26	7:24	18:08	6:37	18:43	5:42	19:21	5:03	19:54	4:51	20:16
20	7:59	17:28	7:23	18:09	6:35	18:44	5:41	19:21	5:02	19:56	4:51	20:16
21	7:58	17:29	7:21	18:11	6:33	18:46	5:39	19:22	5:01	19:56	4:51	20:16
22	7:57	17:31	7:19	18:12	6:31	18:47	5:38	19:24	5:01	19:57	4:51	20:17
23	7:57	17:31	7:18	18:13	6:29	18:48	5:36	19:25	4:59	19:58	4:51	20:17
24	7:56	17:33	7:16	18:14	6:28	18:49	5:35	19:26	4:59	19:59	4:52	20:17
25	7:55	17:34	7:15	18:16	6:26	18:51	5:33	19:27	4:58	20:01	4:52	20:17
26	7:54	17:36	7:13	18:17	6:24	18:52	5:32	19:28	4:57	20:01	4:52	20:17
27	7:53	17:37	7:11	18:18	6:22	18:53	5:31	19:29	4:56	20:02	4:53	20:17
28	7:52	17:38	7:10	18:20	6:21	18:54	5:29	19:31	4:56	20:03	4:53	20:17
29	7:51	17:39	7:10	18:20	6:19	18:56	5:27	19:32	4:56	20:04	4:54	20:17
30	7:51	17:41			6:17	18:56	5:26	19:33	4:55	20:05	4:54	20:17
31	7:49	17:42			6:16	18:58			4:54	20:06		

Day	July		August		September		October		November		December	
	S.R.	S.S.	S.R.	S.S.	S.R.	S.S.	S.R.	S.S.	S.R.	S.S.	S.R.	S.S.
1	4:55	20:17	5:21	19:54	5:56	19:07	6:29	18:13	7:08	17:23	7:46	16:57
2	4:56	20:16	5:22	19:53	5:57	19:06	6:31	18:11	7:09	17:21	7:46	16:56
3	4:56	20:16	5:23	19:52	5:58	19:03	6:32	18:09	7:11	17:21	7:47	16:56
4	4:56	20:16	5:25	19:51	5:59	19:02	6:33	18:07	7:11	17:19	7:48	16:56
5	4:57	20:16	5:26	19:49	6:01	19:00	6:34	18:06	7:13	17:18	7:49	16:56
6	4:58	20:16	5:27	19:48	6:01	18:58	6:36	18:04	7:14	17:16	7:51	16:56
7	4:58	20:15	5:28	19:46	6:02	18:56	6:36	18:02	7:16	17:16	7:51	16:56
8	4:59	20:14	5:29	19:46	6:03	18:54	6:38	18:01	7:17	17:14	7:52	16:56
9	5:00	20:14	5:31	19:44	6:05	18:53	6:39	17:58	7:18	17:13	7:53	16:56
10	5:01	20:13	5:31	19:42	6:06	18:51	6:41	17:57	7:19	17:12	7:54	16:56
11	5:01	20:13	5:32	19:41	6:07	18:49	6:41	17:56	7:21	17:11	7:55	16:56
12	5:02	20:12	5:33	19:39	6:08	18:47	6:42	17:53	7:22	17:10	7:56	16:56
13	5:03	20:12	5:34	19:38	6:09	18:46	6:44	17:52	7:23	17:09	7:57	16:56
14	5:04	20:11	5:36	19:36	6:11	18:44	6:45	17:50	7:25	17:08	7:57	16:56
15	5:05	20:11	5:37	19:35	6:11	18:42	6:46	17:48	7:26	17:07	7:58	16:56
16	5:06	20:10	5:38	19:33	6:12	18:40	6:47	17:47	7:27	17:06	7:59	16:56
17	5:06	20:09	5:39	19:32	6:14	18:38	6:49	17:46	7:28	17:05	8:00	16:57
18	5:07	20:08	5:41	19:31	6:15	18:36	6:50	17:43	7:30	17:04	8:01	16:57
19	5:08	20:07	5:41	19:29	6:16	18:34	6:51	17:42	7:31	17:03	8:01	16:57
20	5:09	20:07	5:42	19:27	6:17	18:33	6:52	17:41	7:32	17:02	8:01	16:58
21	5:11	20:06	5:43	19:26	6:18	18:31	6:54	17:39	7:33	17:02	8:02	16:58
22	5:11	20:05	5:45	19:24	6:19	18:29	6:55	17:37	7:35	17:01	8:02	16:59
23	5:12	20:04	5:46	19:22	6:21	18:27	6:56	17:36	7:36	17:01	8:03	16:59
24	5:13	20:03	5:47	19:21	6:21	18:26	6:57	17:34	7:37	17:00	8:03	17:01
25	5:14	20:02	5:48	19:19	6:23	18:23	6:59	17:33	7:38	16:59	8:04	17:01
26	5:16	20:01	5:49	19:17	6:24	18:22	7:00	17:31	7:40	16:59	8:04	17:01
27	5:16	20:00	5:51	19:16	6:25	18:20	7:01	17:30	7:41	16:58	8:04	17:02
28	5:17	19:59	5:51	19:14	6:26	18:18	7:02	17:28	7:42	16:58	8:04	17:03
29	5:18	19:58	5:52	19:12	6:27	18:16	7:04	17:27	7:43	16:57	8:05	17:04
30	5:19	19:57	5:53	19:11	6:28	18:14	7:05	17:26	7:44	16:57	8:05	17:04
31	5:21	19:56	5:55	19:09			7:06	17:24			8:05	17:06

Table F-2. Estimated monthly and annual averages of total daily solar radiation (global, normally oriented direct, and diffuse) for the INEL.

Type	Jan (ly/day)	Feb (ly/day)	Mar (ly/day)	Apr (ly/day)	May (ly/day)	Jun (ly/day)
Global	143	239	370	490	549	669
Direct	239	334	418	526	645	693
Diffuse	72	96	143	179	191	191

Type	Jul (ly/day)	Aug (ly/day)	Sep (ly/day)	Oct (ly/day)	Nov (ly/day)	Dec (ly/day)	Annual (ly/day)
Global	681	597	478	311	179	131	406
Direct	776	693	621	502	311	227	454
Diffuse	155	131	119	96	72	48	119

radiation based on a 5-day running average. The bottom curve of the figure traces the average total daily net radiation during nocturnal hours only from a 5-day running average. The last remaining curve is a combination of the average daytime daylight and average nocturnal curves. It is the total amount of net radiation (incoming minus outgoing) measured during 24 hours.

The maximum total daytime net radiation recorded for a particular day (top curve of Figure F-1) is the maximum amount that would be expected on a day with completely clear skies and with a minimum amount of atmospheric turbidity. During a clear day in the summer, the INEL can be expected to receive about 625 ly/day per day during the daylight hours. The total outgoing nocturnal net radiation (bottom curve) usually averages about -75 and seldom exceeds -100 ly/day. When these two values are compared, the maximum total

24-hour net radiation expected on a clear day is about 400 ly/day.

The curves in Figure F-1 illustrate a natural seasonal dependency. In January, the daylight net radiation decreases to about 60 ly/day. The nocturnal and daytime net radiation values are

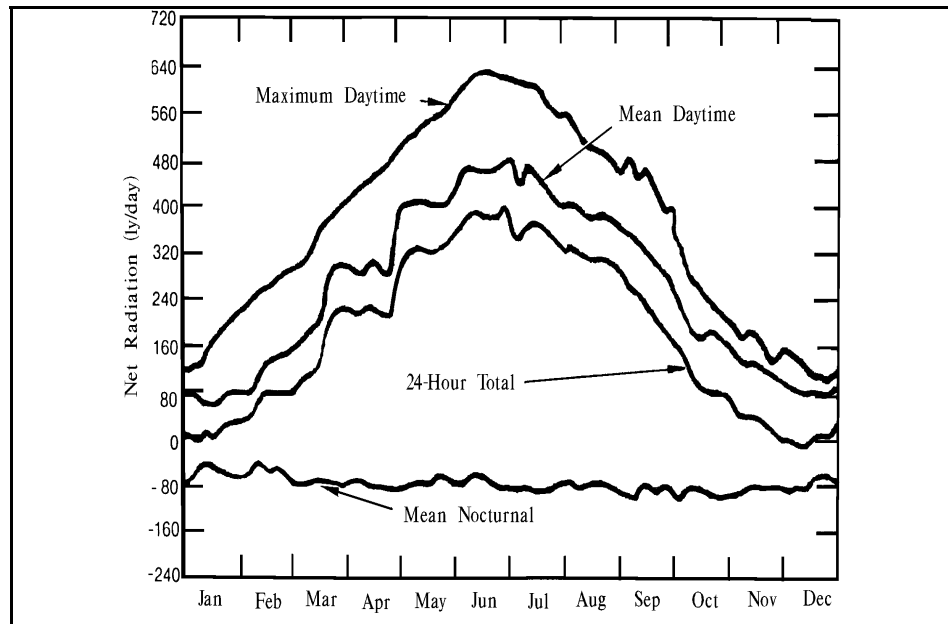


Figure F-1. Annual traces of maximum daytime, average daytime, 24-hour, and nocturnal total daily net radiation.

nearly equal but opposite in sign during the height of the winter season. The low angle of the sun combined with high reflection from clouds and snow produces the near-zero values of total daily net radiation observed in the winter. Lower net radiation values during the winter effect diminished convective activity compared to the summer months. This decrease results in a deep vertical stable layering of the atmosphere. Thus, a reduced intensity and depth of vertical dispersion of effluents is to be expected during the winter.

Sky Cover

Another meteorological parameter useful in describing solar radiation is sky cover. Observations of this type have been recorded at the INEL, but are not complete enough to permit a comprehensive analysis. Data from surrounding stations (Solar Energy Research Institute, 1981) were used to estimate sky cover at the INEL in a manner similar to that used to estimate solar radiation. These data are summarized in Table F-3. The average daily opaque sky cover for the INEL is estimated to be as high 7 tenths in December and as low as 3 tenths in July, August, and September. The annual average sky cover is 5 tenths. These estimated values are somewhat higher than actual observed values.

Table F-3. Average daily opaque sky cover for the INEL based on regional NWS observations.

	Sky Cover (Tenths of Sky)
January	6.5
February	5.5
March	5.5
April	5.5
May	5.0
June	4.0
July	3.0
August	3.0
September	3.0
October	4.0
November	5.5
December	7.0
Annual	5.0

Section G Atmospheric Pressure

Station Pressure

Measurements of atmospheric pressure are important to many phases of design and operations at the INEL. Pressure has been recorded nearly continuously at CFA since February of 1950. The record from February 1950 to August 1964 is summarized in Table G-1. A mercurial barometer was used to measure pressure during this time frame and was located at a height of 4,937.57 ft. m.s.l. Atmospheric pressure values given in Table G-1 are the actual measured values at CFA and are not adjusted to sea level.

The data indicate that the average station pressure is 25.06 in. of mercury (in. Hg). The monthly average atmospheric pressure ranges from 24.98 in. of mercury in April to 25.13 in. of mercury in December. The extreme lowest and highest atmospheric pressures ever recorded were 24.26 and 25.69 in. of mercury, respectively. This range indicates that the extreme limits of station pressure would probably be bounded by 24.00 and 26.00 in.

An examination of the average daily maximums and minimums, and the extreme daily maximums and minimums indicates the

Table G-1. Monthly and annual atmospheric pressure averages and daily pressure extremes for CFA^a.

	Monthly Average (in.Hg)	Average Daily Maximum (in.Hg)	Average Daily Minimum (in.Hg)	Extreme Daily Maximum (in.Hg)	Extreme Daily Minimum (in.Hg)
January	25.08	25.18	25.00	25.69	24.26
February	25.07	25.15	24.98	25.58	24.27
March	24.99	25.08	24.90	25.61	24.26
April	24.98	25.07	24.91	25.44	24.46
May	25.00	25.07	24.94	25.48	24.51
June	25.02	25.09	24.96	25.39	24.55
July	25.09	25.15	25.04	25.44	24.71
August	25.09	25.15	25.03	25.37	24.72
September	25.09	25.16	25.03	25.41	24.59
October	25.11	25.19	25.03	25.59	24.54
November	25.12	25.21	25.04	25.65	24.46
December	25.13	25.23	25.04	25.66	24.29
ANNUAL	25.06	25.14	24.99	25.69	24.26

a. Data period of record spans February 1950 through August 1964.

development of more intense pressure systems in the winter compared to the weaker systems prevalent in the summer months. The annual mean daily pressure range was 0.15 in, varying from near 0.10 inches in the summer to 0.20 inches in the winter.

An examination of the data records for the maximum atmospheric pressure change in a 1-hour time period has not been undertaken. However, evaluation of the synoptic and climatological records of the surrounding area indicates that the maximum expected change would be approximately 0.1 in. of mercury per hour. A similar evaluation of the records for the maximum change in a 24-hour time period yields a value of

1.0 in. of mercury per day. This is supported by the largest measured change of 0.680 in. of mercury per day.

Air Density

The average density of air at the INEL is a value of some interest and is related to atmospheric pressure. It can be computed from the equation of state using average values of air temperature, atmospheric pressure, and atmospheric moisture. Using an average air temperature and atmospheric pressure of 42.0 °F and 25.06 in. of mercury for CFA, respectively, the equation of state yields an average air density value of $1.06 \times 10^{-3} \text{ g/cm}^3$.

Section H State of the Ground

The state or condition of the ground surface, e.g., dry, wet, or snow covered, was observed daily at CFA from 1950 through 1963. The surface condition was recorded at 0800 hours MST using the coding scheme given in Table H-1. The assigned numerical value ranged from zero to nine, which resulted in ten distinct classification categories. The observation location used for state of the ground classifications 0 through 3 was an area of natural topography and vegetation. The observation location used for classifications 4 through 9 was to a cleared area which was usually grass covered. The dust or loose sand referred to in classifications 0, 8, and 9 was considered only when deposited by winds on areas having a solid soil surface.

A monthly and annual summary of the condition of the ground surface is given in Table H-2. The percent of observations in each category indicates that the ground is usually snow

Table H-1. State of the ground coding scheme.

-
- 0 = Surface of ground dry (no appreciable amount of dust or loose sand)
 - 1 = Surface of ground moist (e.g., dew)
 - 2 = Surface of ground wet (standing water in small or large pools at the surface)
 - 3 = Surface of ground frozen (at least several inches)
 - 4 = Glaze on ground, but no snow or melting snow
 - 5 = Ice, snow, or melting snow covering less than one half of the ground
 - 6 = Ice, snow, or melting snow covering more than one half of the ground (but not completely)
 - 7 = Ice, snow, or melting snow covering the ground completely
 - 8 = Loose dry snow, dust, or sand covering more than one half of the ground (but not completely)
 - 9 = Loose dry snow, dust, or sand covering ground completely
-

Table H-2. Monthly and annual classification summary of the state or condition of the ground surface (% of observations) for CFA at 0800 MST.

	0 (%)	1 (%)	2 (%)	3 (%)	4 (%)	5 (%)	6 (%)	7 (%)	8 (%)	9 (%)
January	0.0	1.0	1.5	15.7	0.5	15.4	8.5	30.1	3.5	23.8
February	2.4	4.1	3.3	19.0	1.6	8.9	17.1	27.6	1.1	14.9
March	20.8	8.9	2.2	19.1	0.5	17.1	10.2	14.1	1.0	6.1
April	71.3	14.4	3.3	0.3	0.0	4.4	3.9	2.1	0.2	0.3
May	71.7	13.9	13.6	0.0	0.0	0.0	0.5	0.3	0.0	0.0
June	77.5	14.4	8.1	0.0	0.0	0.0	0.0	0.0	0.0	0.0
July	92.3	5.5	2.2	0.0	0.0	0.0	0.0	0.0	0.0	0.0
August	86.8	7.5	5.7	0.0	0.0	0.0	0.0	0.0	0.0	0.0
September	88.6	6.1	5.0	0.0	0.3	0.0	0.0	0.0	0.0	0.0
October	82.6	8.7	3.5	3.5	0.0	0.7	0.2	0.6	0.0	0.2
November	50.6	7.2	3.8	19.8	1.2	6.6	5.5	4.1	0.2	1.0
December	13.3	0.9	0.7	17.5	2.1	13.3	10.7	31.0	2.8	7.7
ANNUAL	54.8	7.7	4.4	7.9	0.5	5.5	4.7	9.2	0.7	4.6

a. Data period of record spans 1950 through 1963.

covered in December, January, and February. The ground is usually dry from mid-April through mid-November. March and the first half of November are transition months when the surface is either frozen or covered less than 50% with snow. A significant portion of the months of January and February fall into category 9, when blowing and drifting snow is common occurrence.

The annual summary indicates that the surface of the ground is dry more than 50% of the time. Three other conditions occur with frequencies ranging in the 8 to 9 percent. The categories representing these conditions indicate that the ground is either moist, frozen, or completely covered with ice, snow, or melting snow approximately 25% of the time.

Section I Special Phenomena

Several other types of meteorological phenomena occur at the INEL which have not been addressed in the preceding sections. Among these are thunderstorms, blowing snow, and tornadoes. Each of these subjects is discussed below in the order of its frequency of occurrence.

They are, however, seldom observed during the months of November through February.

Dew

Dew forms on the surfaces of objects, e.g., vegetation or automobiles whenever the temperature of the object reaches the dew point. Dew has been observed to form on nearly any clear or mostly clear summer night. It may form as early as sunset and may not dissipate until as late as 3 to 4 hours after sunrise. Its formation and dissipation can usually be expected to approximately coincide with the formation and dissipation of the nocturnal temperature inversion.

Thunderstorms over the INEL are usually much less severe than what is normally experienced in the mountains surrounding the ESRP or east of the Rocky Mountains. This is due, in part, to high cloud-base altitudes. Hence, the precipitation from many thunderstorms evaporates before reaching the ground (virga). The frequent result is little or no measurable precipitation. Occasionally, however, rain amounts exceeding the long-term average may result from a single thunderstorm.

Thunderstorms

A thunderstorm day is defined by the NWS as a day on which thunder is heard at a given observing station. According to the definition, lightning does not have to be seen, and rain fall and/or hail is not required. Following this strict definition, the INEL may experience an average of two or three thunderstorm days during each of the summer months from June through August with considerable year to year variation. Several individual thunderstorms may occur during each of those thunderstorm days. Thunderstorms have also been observed during every month of the year.

Thunderstorms at the INEL may be accompanied by micro bursts, i.e., strong, localized, gusty winds. These micro bursts can produce dust storms and occasional wind damage. Thunderstorms may also be accompanied by cloud-to-ground as well as cloud-to-cloud lightning.

Lightning

The INEL is currently monitored by the U.S. Bureau of Land Management Interagency Fire Center lightning detection system. This system detects the location and number of lightning strikes in real time for wild fire control. Although the INEL is surveyed by the system, no historical statistics for the area have been compiled. However, the number of lightning strikes on the INEL does not appear to be very high.

Nevertheless, the lack of natural targets and the poor conductivity of the dry desert soil and underlying lava rock cause man-made structures to be susceptible to lightning strikes.

Hail

Small hail has been observed to occasionally occur in conjunction with thunderstorms. The size of the hail is usually smaller than 1/4 in. in diameter. The diameter may range up to 3/4 in., however, on very rare occasions. No hail damage has ever been reported at the INEL. Crop damage from hail is not unusual, however, on neighboring farms across the ESRP. Property damage in the city of Idaho Falls has been reported as well as in other local cities. Damage from hail still remains a possibility at the INEL.

Airborne Dust and Sand

A study of airborne dust at the INEL was made in 1952 and 1953 (Humphrey et al., 1953) in disturbed areas and areas of natural vegetation. Dust concentrations ranged from a low of $14.1 \mu\text{g}/\text{m}^3$ over a total snow cover to a high of $772 \mu\text{g}/\text{m}^3$ during the summer. In an undisturbed area, even with dust devils present, a concentration of only $151 \mu\text{g}/\text{m}^3$ was recorded. The annual average of 24-hour particulate samples was approximately $30 \mu\text{g}/\text{m}^3$. Median sizes of dust particles in undisturbed areas ranged from 0.330 to $0.425 \mu\text{m}$. Less than 1% of the particles were larger than $10 \mu\text{m}$ but these ranged in size up to several hundred μm . Petrographic examination of the dust resulted in a moderately abrasive classification of the particles.

During the daylight hours under conditions of strong winds, the concentration of dust sharply decreases with height up to approximately 70 ft. AGL. Vehicular traffic and construction equipment contribute more to high dust concentrations than do strong winds over undisturbed areas, however. It is therefore recommended that building fresh air inlets and motor vehicle air intakes should be located as high above the ground surface as possible.

Blowing dust and drifting sand can be a nuisance when the winds are strong in certain areas of the INEL. These conditions may particularly affect the activities of the construction personnel during the spring months after the winter thaw when strong frontal systems pass through the ESRP and during the summer months when thunderstorms are near.

Dust Devils

Dust devils are small atmospheric vortices which are generated over hot land surfaces. Dust devils are common in the summer at the INEL when intense solar heating of the ground makes dust devil formation possible. They usually occur on calm, sunny days. Dust devils pick up dust and pebbles, and can overturn, blow down, or carry off unsecured objects. The dust cloud may be several hundred yards in diameter and extend several thousand feet into the air.

Blowing Snow

Blowing and/or drifting snow sometimes becomes a hazard as well as a nuisance during the winter months at the INEL. Blowing snow greatly reduces visibility and slows down transportation. On rare occasions, the visibility has been reduced to zero in extreme blizzard conditions. Blowing snow usually accumulates in drifts on the leeward side of buildings, vehicles, fence posts, vegetation, etc. Drifts may occasionally render parking lots and highways on the INEL and access highways to the INEL impassable and cause traffic to be rerouted.

Icing

Rime ice occurs when fog droplets impinge upon objects at temperatures below freezing. The meteorological conditions for the formation of rime ice may persist for several days when the ground is covered with snow and accompanied by a persistent high pressure system. This makes the formation of supercooled fog or low stratus clouds and subsequent rime ice formation a distinct

possibility. The accumulation of rime ice on power lines and air intakes has not been a constraint to operations at the INEL.

Severe glaze icing, which accompanies freezing rain, rarely occurs at the INEL. The meteorological condition which most frequently permits the formation of glaze ice is the transition period from rain to snow. Glaze ice results in slippery sidewalks and roads and slows transportation. Glaze ice accumulation has been insufficient to damage power lines or communication cables.

Tornadoes

A tornado is defined as a violent local vortex in the atmosphere. When the vortex reaches the ground, it is classified as a tornado. If the vortex does not reach the ground, it is classified as a funnel cloud. The vortex is usually accompanied by a funnel shaped cloud with spiralling winds of very high velocity which may be greater than 300 mph. Tornadoes and funnel clouds always occur in association with thunderstorms, especially those which produce hail.

Most of the tornado activity in the U.S. occurs east of the Rocky Mountains. The total number of tornadoes in Idaho reported to the National Severe Storms Forecast Center (1987) for the years 1950 through 1986 was 58. Statistics indicate that tornadoes have been reported in Idaho only during the months of March through October. They occur most frequently during the month of June (31% of occurrences), but are also common in May, July and August (14, 16, and 17% of occurrences, respectively). Tornadoes occurred most frequently (53%) between the hours of 1300 to 1500 MST. The average path length was 0.92 mi., and the average path area was 0.02 mi.²

Idaho tornado statistics must be interpreted with caution. For example, during the 35-year period of 1916 through 1950, only 5 tornadoes were reported to the Idaho State Weather Service Office (Bob Glodo, personal communication). However, 10 more were sighted in the succeeding 10-year period of 1951 through 1960. This sudden increase in tornado sightings was likely an artifact of increased population density and improved communications rather than an actual increase in tornado frequency. In addition, the lack of trained spotters and poor local weather radar detection capabilities compared to midwest U.S. locations results in occasional misidentification of thunderstorm downpours as funnel clouds and tornadoes. Most tornadoes in the ESRP are not confirmed as they occur, but sightings are afterwards investigated by local National Weather Service meteorologists (Bob Glodo, personal communication). Thus, an unusually high degree of uncertainty exists in Idaho tornado statistics.

Locations of tornadoes which have been sighted in the ESRP and reported to the National Severe Storms Forecast Center (1987) are illustrated in Figure I-1. A supplemental record of funnel cloud and tornado sightings has been maintained by NOAA personnel for the INEL. This record contains the locations of both funnel cloud and tornado activity observed by or reported to NOAA personnel located at the INEL since 1950. These data are summarized in Table I-1. The NOAA record indicates that there have been

Table I-1. Funnel clouds and tornado sightings observed on the INEL by NOAA or other INEL personnel^a.

<u>Date</u>	<u>Time (MST)</u>	<u>Type of Activity</u>	<u>Location</u>
20 July 1974	12:53	2 Funnel Clouds	Within a triangle formed by Howe, TRA, and NRF
08 May 1975	M ^b	2 Funnel Clouds	Near Middle Butte
23 July 1984	12:25	1 Funnel Cloud	10 mi. west south-west of ICPP

a. Data period of record spans January 1950 through October 1989.
b. Data is missing.

a total of 5 funnel clouds and no tornados sighted within the boundaries of the INEL. Indeed, the calculated chance of a tornado developing at the INEL is extremely remote. The calculated return period for a tornado at the INEL with wind speeds exceeding 120 mph, according to Coats and Murray (1985), is 1×10^6 years. This value is

based on national tornado statistics, maximum atmospheric moisture content, surrounding geography, and other variables. Additional tornado characteristics such as typical and design basis tornadoes for the INEL can be found in Coates and Murray (1985) and in various local U. S. DOE publications.

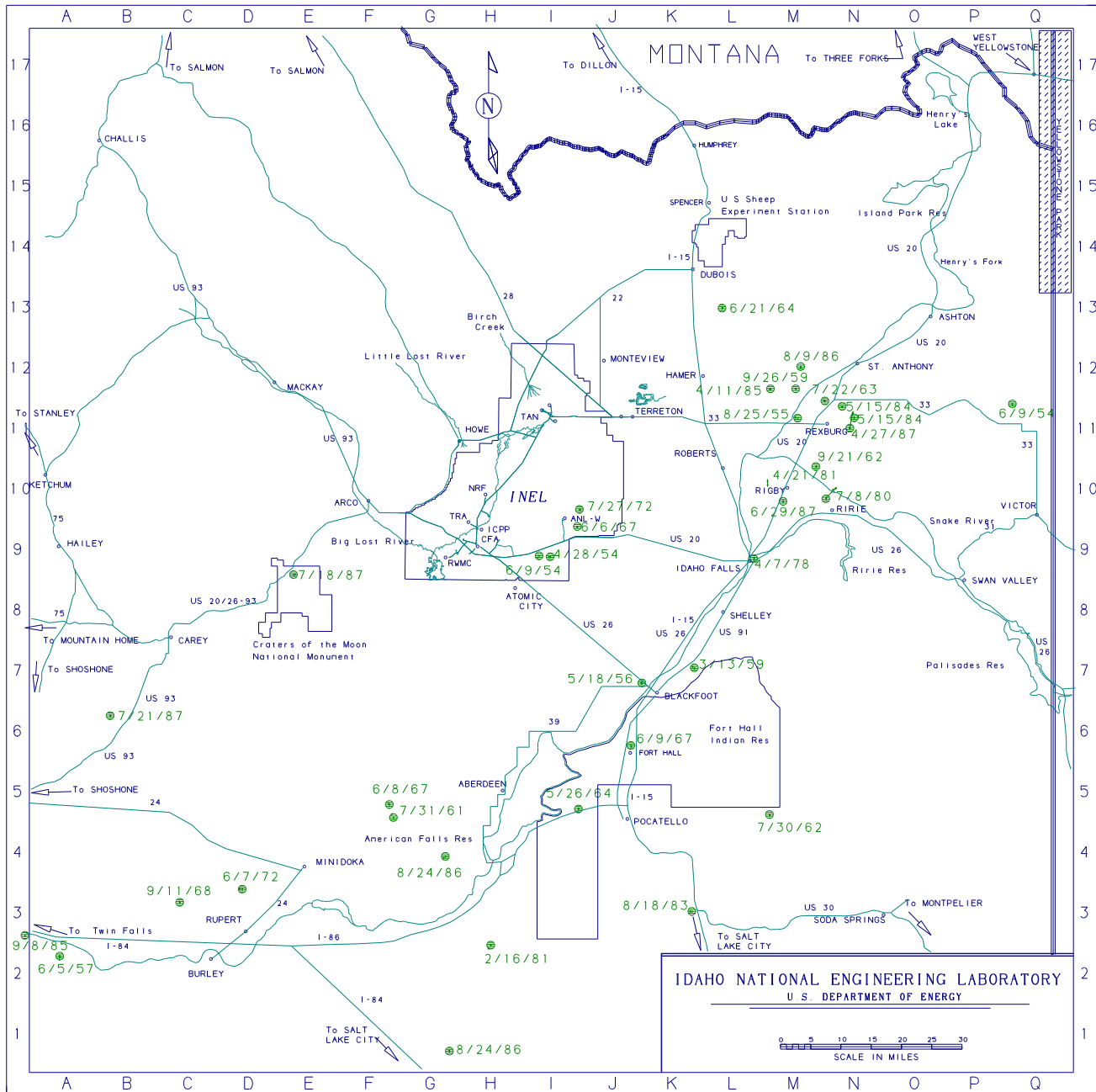


Figure I-1. Tornado sightings in the ESRP according to National Severe Storms Forecast Center Statistics from 1950 through 1987 indicated by dots and accompanied by the date of the sighting.

NOTES

Chapter VI

ATMOSPHERIC TRANSPORT AND DIFFUSION

Operations at the INEL frequently require a means of estimating potential impacts of routine or accidental effluent releases to the atmosphere. The following climatology of atmospheric dispersion at the INEL addresses factors related to both transport and diffusion. Atmospheric transport consists of that portion of dispersion which results from movement of the effluent in the wind. It is distinguished from diffusion, which involves the breakup of the coherent plume by turbulent eddies.

Atmospheric Transport

The rate of transport and diffusion of various effluents in the atmosphere is determined by the relative interactions of the effluent plume (its size scales increase with time), and the size scales of atmospheric motion which interact with it. The principles of turbulent energy transfer (continuous cascade of fluid velocity energy from largest eddy size to ever smaller sizes and eventually to viscosity, as the velocity reaches zero) are inherent in atmospheric dispersion, since the most effective eddy size for mixing is that eddy with a size nearly matching that of the effluent plume to be mixed.

Energy for atmospheric dispersion originates through solar heating which drives the global-scale (synoptic-scale) winds which, in turn, modulate the local wind circulations. At the INEL, the interaction of the synoptic-scale winds with surface winds is influenced by mountainous topography and thermal effects. They modify the wind direction and alter its temporal character in subtle, but very important ways.

Winds Aloft and Synoptic Forcing

Global temperature differences between the equator and the poles produce a pressure gradient which results in westerly winds aloft at the latitude of the INEL. Disturbances in this westerly flow in

the form of large cyclonic storm systems migrate across the continent and are enhanced or weakened by temperature and moisture fields -- a process routinely addressed in meteorological forecasting. The passing of these cyclonic disturbances alters the direction of the prevailing winds aloft, although there is usually some westerly wind component within the total wind vector.

Friction reduces the speed of the winds aloft in the layer next to the ground, and alters the balance between pressure gradient and Coriolis forces, so that the mean direction is altered as well. Over large expanses of flat terrain, the surface wind may depart 30 degrees or more from the winds aloft due to this imbalance. Where mountainous terrain intervenes, surface winds are channeled or otherwise redirected at angles determined almost wholly by the aerodynamics about the terrain. The undisturbed wind above the influence of surface terrain is termed the gradient wind, which, at the INEL, occurs at heights above 10,000 to 12,000 ft. m.s.l. Seasonal and annual upper air wind roses reflecting these influences were presented in Chapter V, Figures A-21 through A-25.

Heating of the earth's surface during the daylight hours induces elements of rising and descending air which serve to couple the winds aloft with the air next to the ground. Under these conditions, only small differences in direction and speed with altitude are seen, and surface wind direction is primarily determined by the winds aloft.

Occasionally, the pressure gradient associated with a passing storm is strong enough that winds directed by the passing weather system will dominate the surface direction regardless of the atmospheric thermal structure near the surface. This situation typically occurs during the passage of a cold front at the INEL. In that situation,

characteristics of the individual storm and aerodynamic influences of large terrain features dominate the surface wind flow.

During periods when the surface of the earth is strongly cooled, vertical motions in the atmosphere are inhibited, and the wind flow aloft becomes decoupled from the surface winds. In this situation, surface winds are often driven by density differences induced by nonuniform radiational cooling of the surface, or other factors. These weak nocturnal winds may blow at widely varying directions from the winds aloft. Examples of these situations are presented in the following section.

Topographic Influences

Energy provided by the synoptic-scale winds is transferred to smaller circulation scales bounded by topographic features of the INEL and its surroundings. One of the most interesting features observed at the INEL is the strong correlation of the wind pattern to the large fishhook-shaped depression (see Chapter II, Figure II-2) in the topography over the floor of the ESRP (Wendell, 1972).

When the contour level outlining this depression is superimposed on the wind fields, varying degrees of conformity occur during approximately 57% of the year. Incidence of this correlation varies from a high of 63% during the spring to a low of 42% during the fall. The effect of this subtle terrain feature is to direct an up-valley/down-valley diurnal flow which corresponds in direction roughly to the underlying topographic channel.

One very specific example of terrain influence is observed about 12% of the time. A circular-shaped eddy is formed that persists for a few hours in the portion of the valley northeast of the INEL. This condition occurs primarily at night and most frequently during the summer, indicating that it is most closely associated with the diurnal heating cycle and local topographic features.

The flow patterns just described are informative because they are examples of organized spatial variations in the flow pattern. These circulation patterns would be extremely difficult, if not impossible, to determine from individual wind rose plots, even if made for several locations. This type of spatial variation in the flow is very important because of its implications in the transport of material to and from the INEL.

In some cases, several topographic influences work simultaneously. Tower measurements at GRD3 have shown a 180 degree direction shear between levels 20 and 50 ft. above the ground. This strong shear has been observed many times during the early morning hours. It is attributed to the fact that the slope of the terrain in this area is opposite the general slope of the terrain over the eastern Snake River Plain. The general down slope drainage is, therefore, opposed by this local anomaly in the topography.

Another characteristic terrain effect that has been observed, but less frequently than any described previously, is channeled flow from one or more of the three valleys northwest of the INEL. A wind rose for BDM located in the valley northwest of TAN (Chapter V, Figure A-14), shows down-valley flow in excess of 6 m/s about 17% of the time.

Diurnal Wind Cycles

Solar energy incident upon local topographic features, and thermal energy radiated from the earth, provide an energy source of secondary importance to the INEL wind field. On a local scale, (especially when regional-scale pressure gradients are weak) the effects of surface heating during the day and radiational cooling at night are very evident in the INEL wind field. Under such conditions, the winds conform to a general up slope flow during the day and down slope flow at night. As noted, there is also a tendency for increased steering of the surface winds by the winds aloft during the day and a separation of those flow regimes at night.

At the INEL, several characteristic diurnal flows may be encountered -- each related to the existing terrain. During synoptic conditions in which the pressure gradient over the area is weak and the major driving force for air motion is gravity, daytime heating causes the wind direction to be from the lower terrain southwest of the INEL toward more elevated terrain to the northeast. As the cooling process begins in the evening, the tendency to reverse the direction of the flow is much stronger on the northwestern half of the INEL because of the steeper terrain in that area. Thus, the inertia of the southwesterly flow is overcome earlier over the northwestern INEL, and the flow becomes northeasterly across the portion of a broad, subtle valley depression that extends southwestward across the INEL.

Mesoscale Winds at INEL and Regional Trajectories

The combined influences of global synoptic-scale forcing, topographic channeling, and radiative heat energy exchanges near the INEL result in several characteristic trajectory patterns over the INEL. Trajectories from wind field analyses and radar-tracked balloons which originate near the INEL center are summarized in the text which follows. (NOAA meteorologists should be consulted for available information on trajectories originating at other INEL locations, since they may vary considerably from those summarized here. Climatological trajectory summaries can be developed using historical wind field data for all INEL locations).

One calendar year (1969) of hourly meteorological data from the combined INEL telemetered wind network has been analyzed (Wendell, 1972) for the trajectories reported here. An imaginary effluent plume released from PBF was modeled for the analysis. Hourly trajectories were calculated for a 12-hour to 24-hour duration beginning at noon and midnight for each day of the year. These trajectories were then sorted by type and relative frequency of occurrence. Examples of each characteristic type are presented in Figures VI-1 through VI-6. The box in each figure summarizes the relative ranking of each trajectory type by season. The number one denotes the most frequent occurrence of the trajectory type, number two is the second most frequent occurrence, etc.

Twelve different major trajectory types were derived for the INEL. Other types of patterns are recognizable, but they occur with less frequency than those shown. On an annual basis, the 12

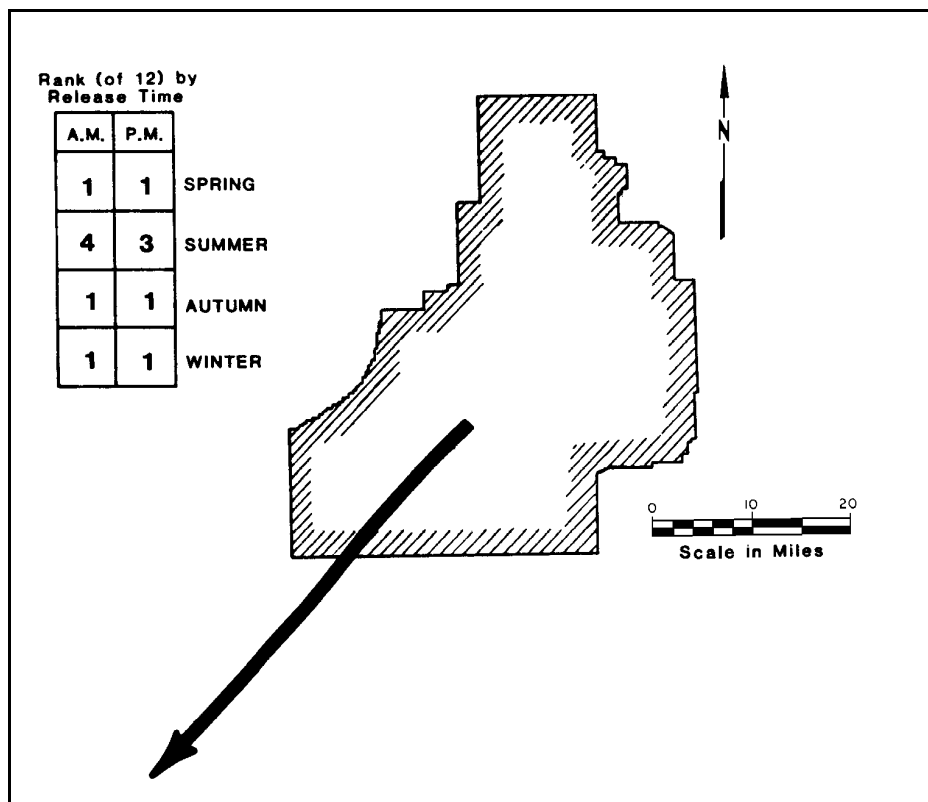


Figure VI-1. Example trajectory for type A, characterized by sustained northeasterly winds.

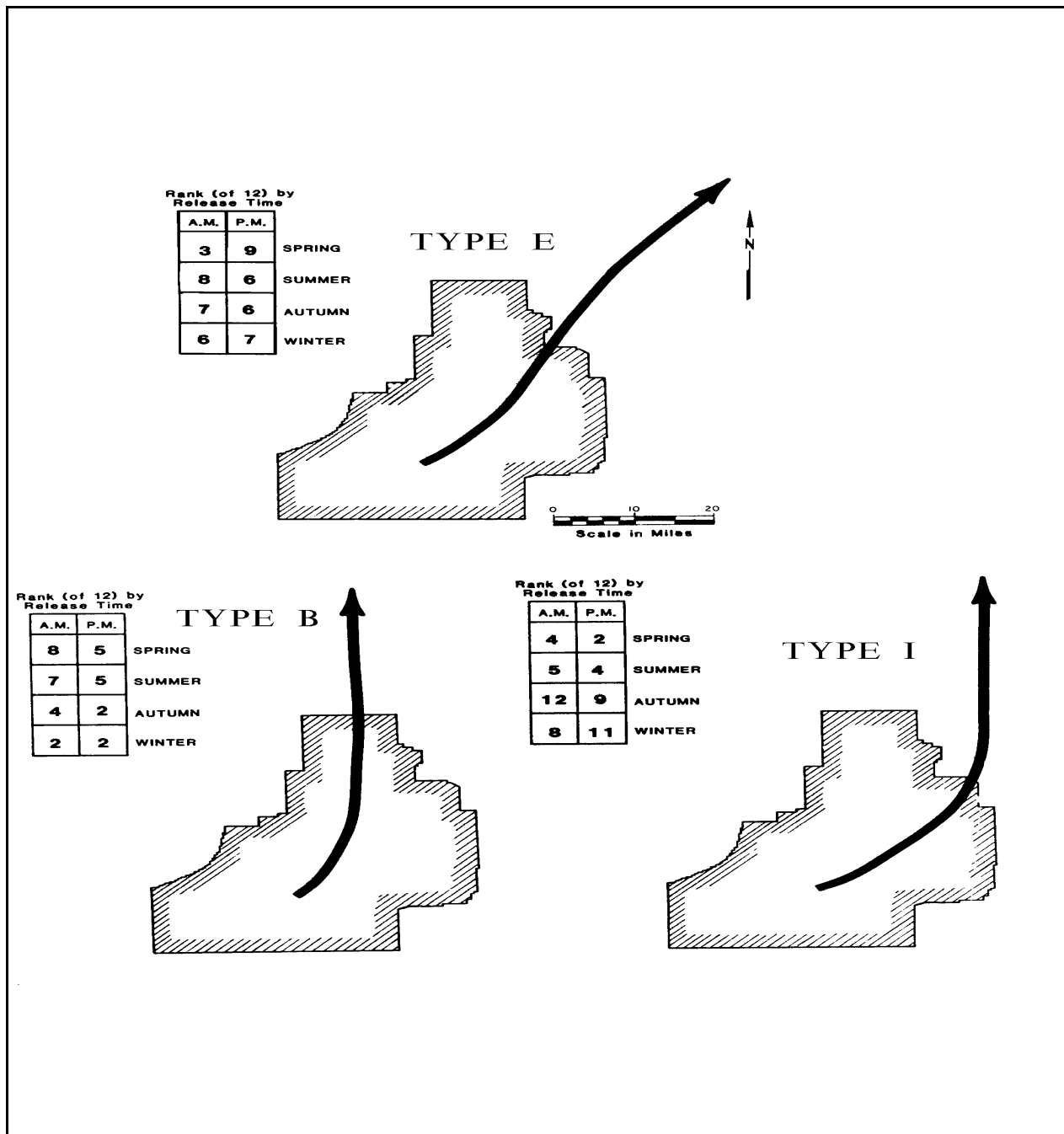


Figure VI-2. Example trajectories for types E (top), B (bottom left), and I (bottom right), characterized by sustained southerly or southwesterly winds.

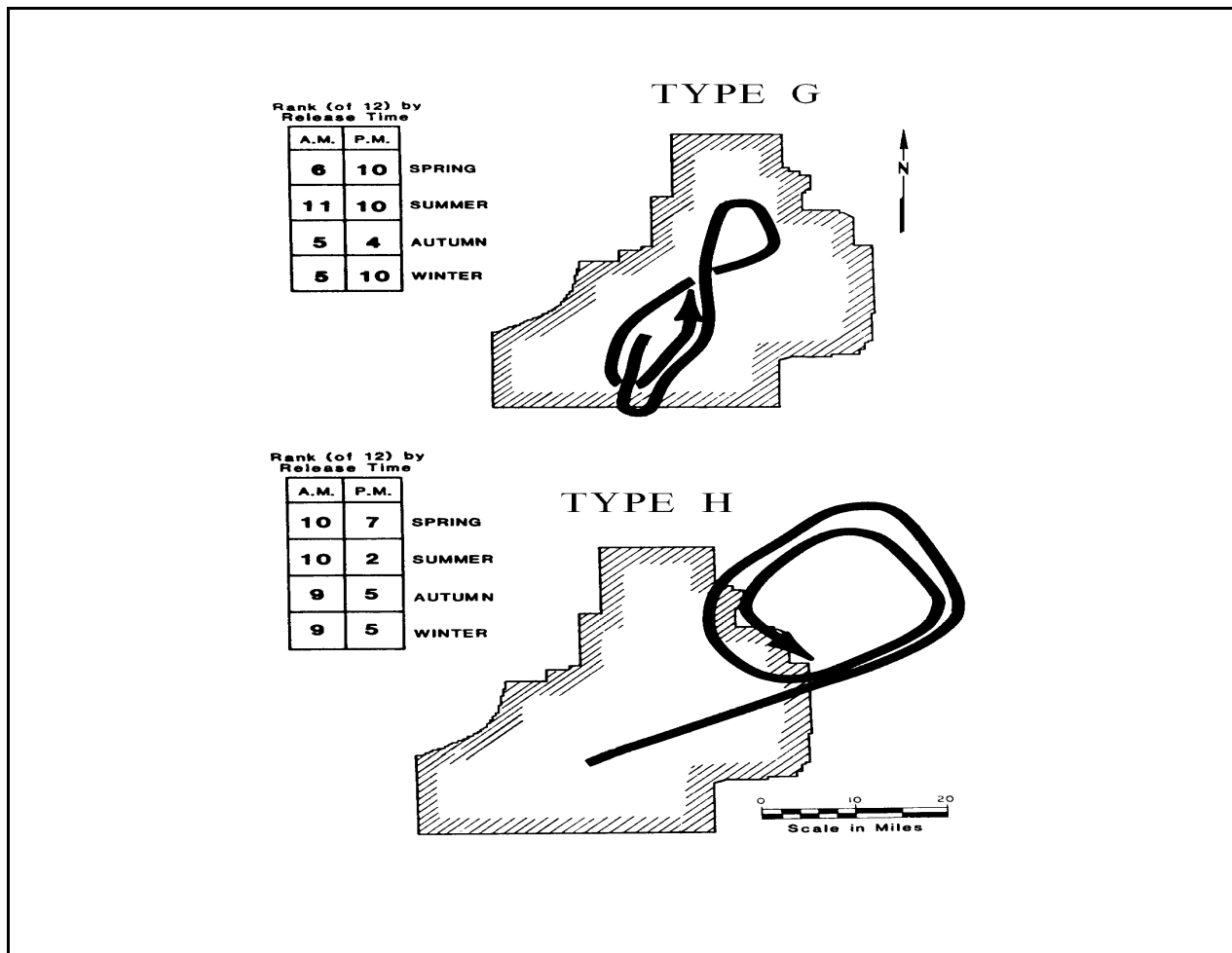


Figure VI-3. Example trajectories for types G (top) and H (bottom), characterized by localized wind recirculations.

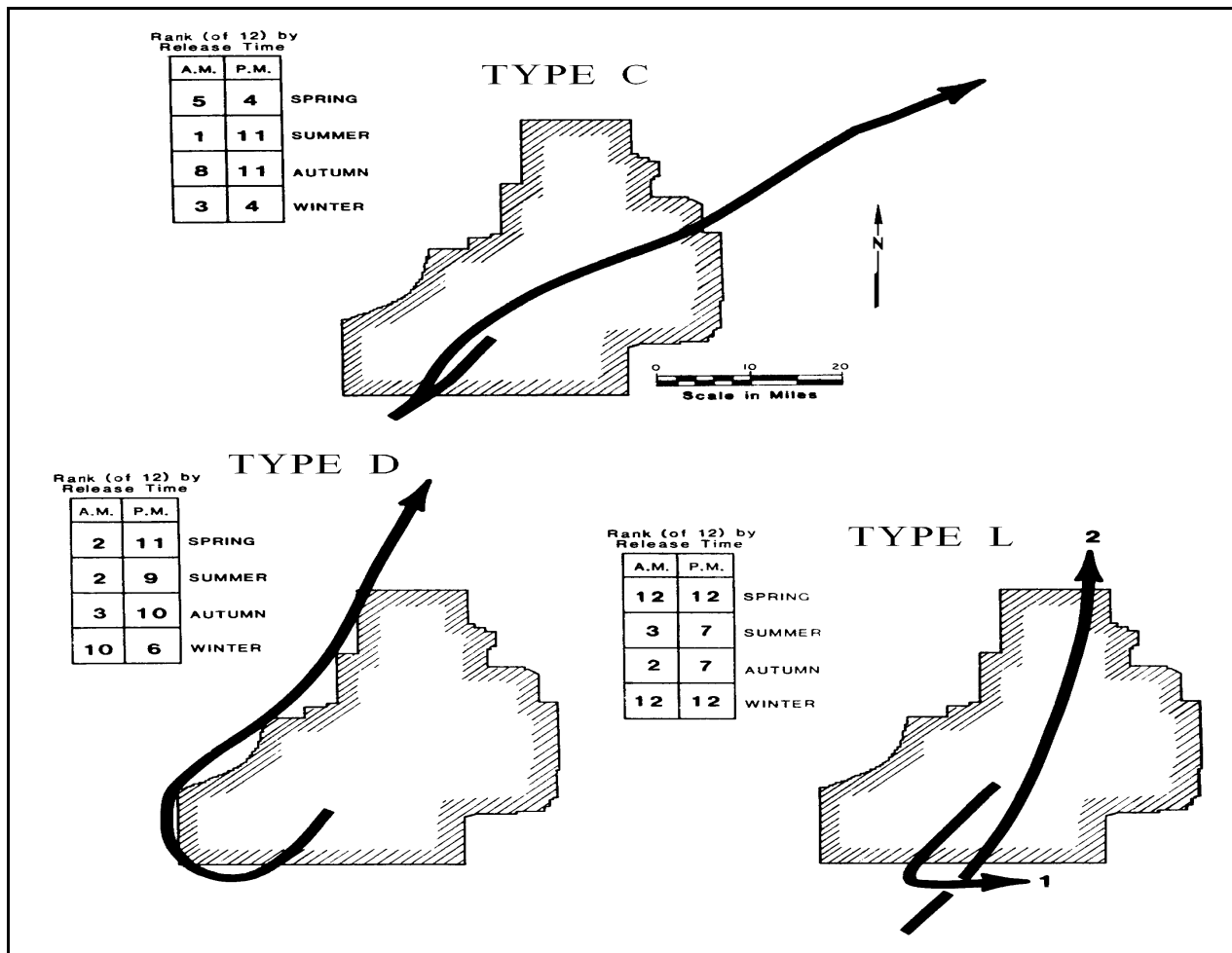


Figure VI-4. Example trajectories for types C (top), D (bottom left), and L (bottom right), characterized by diurnal wind reversals from a down-valley to an up-valley flow.

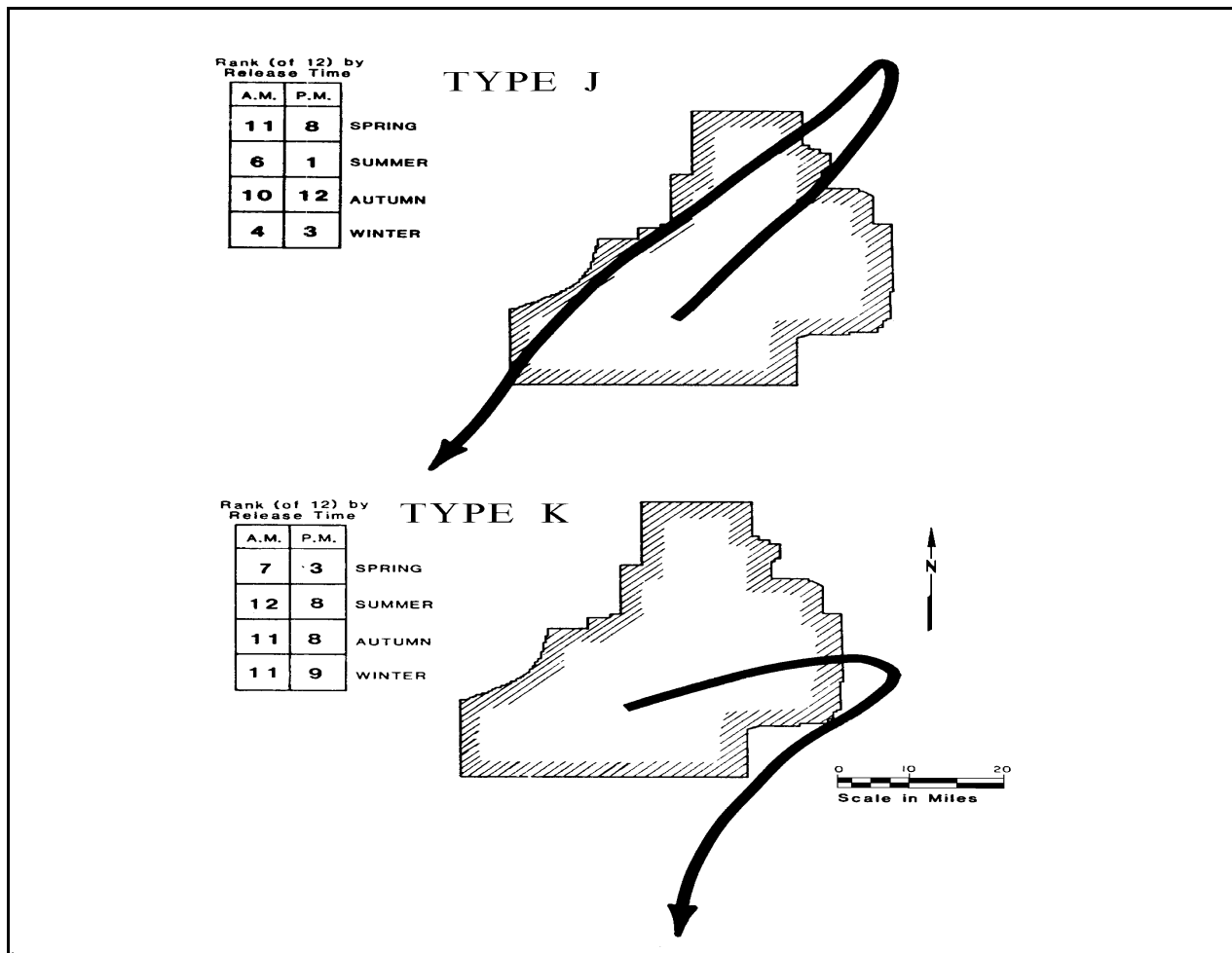


Figure VI-5. Example trajectories for types J (top) and K (bottom), characterized by diurnal wind reversals and synoptic frontal passages.

types shown account for about 74% of the flow patterns observed. The variability in the trajectory patterns seems to be greatest for the afternoon period during the spring, summer, and fall seasons. It would be during these periods that an approximation of the wind field by the indicated wind at the source would be least accurate. Indeed, an examination of each of the trajectory types and their relative frequency of occurrence indicates that, at the INEL, single station (i.e., wind rose) methodologies are not appropriate to describe transport trajectories for distances beyond about 10 miles from any on-site facility.

The most common trajectory pattern for the entire year was designated as Type A. It is characterized by a southwesterly movement of the imaginary effluent plume with little lateral deviation until it leaves the boundary of the INEL meteorological monitoring area (Wendell, 1972). The Type A trajectory results from a sustained northeasterly flow for the duration of the release period. The variation in the seasonal percentages of occurrence indicates very little preference for either a noon or midnight release. This type of transport pattern occurs most frequently in the fall, winter and spring seasons and least frequently in the summer season. During the winter of 1969, this pattern persisted for time periods as long as 8.5 days.

The next most persistent trajectory type on an annual basis was denoted Type B (Figure VI-2). It is characterized by a steady plume movement

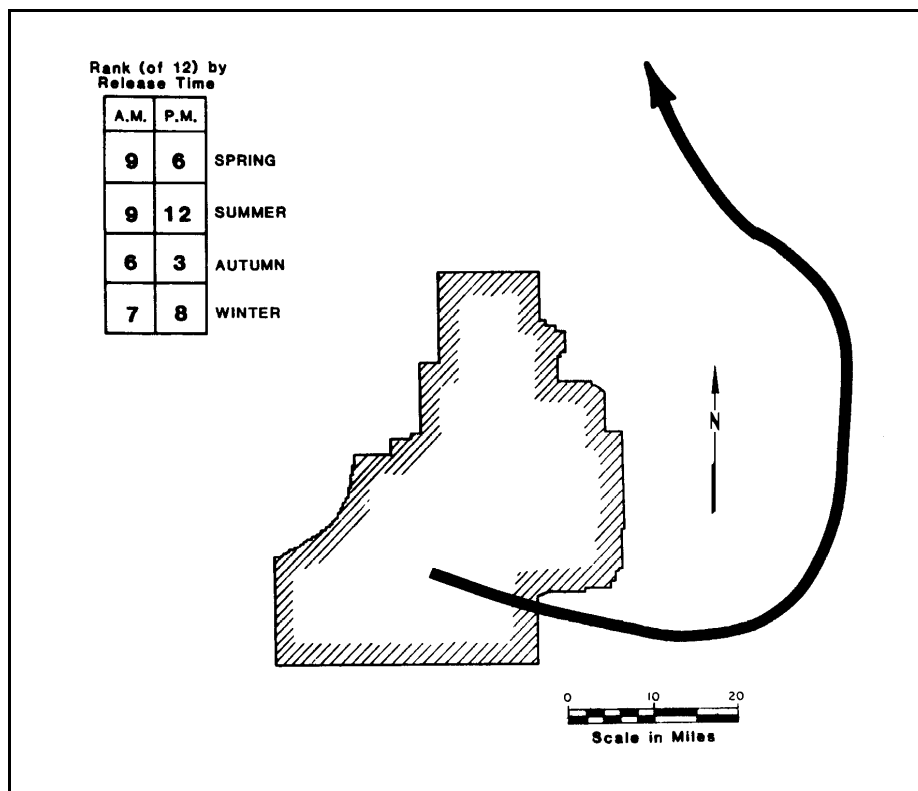


Figure VI-6. Example trajectory for type F, characterized by sustained wind flow along a shear line.

in a northerly direction directly off the INEL. This flow regime results from a sustained southerly flow lasting throughout the entire release period. This trajectory type, like Type A, shows no particular preference for either a morning or afternoon release period. It exhibits a maximum occurrence of 16% during winter, which is the second most frequent type during that season.

In Type C (Figure VI-4), the plume released at the beginning of the period moves to the southwest and away from the INEL, which indicates several hours of northeasterly flow. During the release period, however, the direction of motion of the plume suddenly reverses and streams northeastward until it leaves the valley. This trajectory pattern shows a definite preference for the morning release period during all seasons. It is the most predominant pattern during summer with a 27% frequency of occurrence. The Type C pattern is strongly related to the reversal of the winds due to the overall slope of the ESRP from

the northeast to the southwest and to the diurnal heating and cooling cycle.

The next pattern, designated Type D, (Figure VI-4), also indicates a change in the flow pattern from northerly or northeasterly flow to a southerly flow. The character of this pattern, however, indicates the change to be a gradual clockwise rotation of the wind direction instead of an abrupt reversal as in Type C. The winds near the southern INEL boundary turn before the wind at the source does. The Type D pattern also shows a preference for a morning release time, except during winter season. Its most frequent occurrence is during the spring and summer seasons, in which it ranks second. In almost every occurrence of this type, the shift in the wind direction began between 0900 and 1100 MST.

The next type of trajectory pattern is Type E (Figure VI-2). It is characterized by a northeastward movement of the plume during the entire release period. The pattern implies a sustained flow from a southwesterly direction. A review of climatological data, however, reveals that flow of this type is sustained in a relatively small percentage of total cases. Although wind rose information from individual stations implies a 30% occurrence, this flow regime is generally not sustained from the center of the INEL to the northern end of the valley. The highest frequency of occurrence for Type E is 9% for the spring season.

The next pattern shown is Type F (Figure VI-6). This trajectory pattern clearly indicates the spatial variation in wind direction which occurs in the valley. The pattern shows little variation from season to season and is characterized by west winds at the source becoming southerly toward the northern end of the valley. This pattern occurs mostly in the fall, and indicates flow conforming to the curved depression in the ESRP topography.

The next trajectory pattern, Type G (Figure VI-3), is one in which very light and variable winds are observed for over a period of at least 24 hours. In this flow regime (which occurs

primarily in summer), the released plume is not carried far from the source and even recirculates around the source. The other three seasons show a 6- to 7-% frequency of occurrence of type G for morning releases and a 2- to 6-% frequency of occurrence for afternoon releases. This indicates that a light and variable wind situation in the central INEL has a stronger tendency to persist for 24 hours if it begins in the morning than if it begins after noon.

The Type H trajectory pattern (Figure VI-3), illustrates one of the most striking examples of spatial variation in the mesoscale wind pattern across the INEL. This flow regime is a manifestation of the circular eddy discussed previously. Its occurrence shows a definite bias toward the afternoon release period, indicating that it is a late evening or early morning phenomenon. It occurs most frequently (9%) in summer with a rank of second, but it also occurs 7% of the time in the winter, when it ranks fifth. This trajectory pattern is probably the most dramatic for demonstration of the contrast between transport which might be deduced from a wind observation at the source and that projected from several observations over the entire area of interest.

The next three patterns (Types I, J, and K), demonstrate why flow Type E does not occur more often than a wind rose would imply. Type I (Figure VI-2) indicates southwesterly flow from the source becoming southerly about 45 mi. northeast of the source. This condition is most predominant in the spring. Type J (Figure VI-5) indicates southwesterly winds throughout the release period, followed by a sudden reversal to northeasterly winds. It is most predominant during the afternoon and occurs most often during the summer and winter. The relatively high frequency of occurrence (13%) in the summer is likely due to diurnal wind reversals while the correspondingly high frequency of occurrence in the winter is probably due to frontal passages. Type K (Figure VI-5) also indicates a southwesterly flow reversing to a northeasterly direction. The difference is that the direction change occurs earlier during the release period, in a gradual clockwise rotation.

This type also shows a preference for the afternoon, and occurs most frequently (8%) during the spring season.

The last trajectory type shown is Type L (Figure VI-4), which also indicates a reversal in the flow pattern. The trajectory pattern in this case indicates a light northerly flow changing to a stronger southerly flow in such a way that effluent is swept back across the INEL in a line or band-like pattern. This flow regime shows a definite bias toward the morning release period. It occurred only during the summer (11%), which resulted in a ranking of third behind Types C and D, and during the fall (9%), which resulted in a ranking of third behind types A and D.

Atmospheric Diffusion

Atmospheric diffusion is the breaking apart and dilution of an effluent plume by turbulent eddies. It is a function of the three-dimensional atmospheric turbulent wind fluctuations which interact with the airborne material. The turbulent environment varies dramatically in time (by season and diurnal cycle) and vertically (because the maximum eddy size is constrained by the surface for plumes near the ground). The theory of atmospheric turbulence and diffusion is discussed in numerous texts (e.g., Pasquill, 1961; and Slade, 1968). Over the years, efforts have been made to describe the complex atmospheric turbulence environment on the basis of readily available meteorological measurements. This has resulted in a family of alternate methodologies to describe the parameters characterizing plume spread. One of the simpler and more easily utilized methodologies is presented in the following sections.

The Diffusion Equation

Atmospheric turbulence (and, therefore, diffusion) is essentially a stationary random process over short time periods. Consequently, a Gaussian distribution of material in an effluent cloud may be assumed for relatively short travel and sampling times. Diffusion experiments, (under carefully selected conditions) with release times

from three minutes to one hour and out to distances of several kilometers from the source, have supported the Gaussian assumption for crosswind distributions of an effluent plume. It is expected, although not proven by experiment, that a Gaussian distribution will be maintained in the crosswind direction of a puff for short travel times (distances). The distribution of material in the vertical direction of a puff has not been measured as extensively as the crosswind distribution. However, the vertical distributions in both a puff and a plume have been shown to be close to Gaussian, at least for short travel times, even though vertical wind velocity fluctuations change significantly and systematically with height.

The universal diffusion equation for a receptor at ground level ($z=0$) assumes a Gaussian distribution of material in three directions relative to an effluent puff and a total reflection of the material impinging at the earth's surface as follows:

$$\chi(X,y,0) = \frac{2Q}{(2\pi)^{3/2} \sigma_x \sigma_y \sigma_z} \exp \left[-\frac{1}{2} \left(\frac{x^2}{\sigma_x^2} + \frac{y^2}{\sigma_y^2} + \frac{h^2}{\sigma_z^2} \right) \right] \quad [1]$$

where:

- χ = concentration (units/volume of air)
- Q = source strength (units)
- X = distance downwind from the source (length)
- $\sigma_x, \sigma_y, \sigma_z$ = standard deviations of effluent concentration of the puff in the along-wind, crosswind, and vertical directions, respectively (length), and are usually taken to be a function of travel time or distance
- x, y = distances from the center of the effluent puff in the along-wind and crosswind directions,

respectively (length), and $x = \bar{u}t - X$, where \bar{u} is the mean wind speed (length/time)

h = the height of release of the puff center above the ground (length).

This is the general equation for an instantaneous point source (IPS) or puff release.

The diffusion equation for a continuous point source (CPS) or plume is applicable to effluent releases on the order of a few minutes to a few hours. It can be derived from Equation [1] by integrating in the along-wind direction (with respect to X) from $-\infty$ to $+\infty$ and dividing by the mean wind speed (\bar{u}) to account for the initial dilution at the source. The resulting equation is:

$$\chi(X,y,0) = \frac{Q}{\pi \bar{u} \sigma_y \sigma_z} \exp \left[-\frac{1}{2} \left(\frac{y^2}{\sigma_y^2} + \frac{h^2}{\sigma_z^2} \right) \right] \quad [2]$$

where Q is now expressed in units/time. This equation also yields the total integrated concentration (TIC) for a puff (IPS) when Q is in units. The resultant χ for the TIC is in units-time/volume.

The diffusion equation for an infinite, crosswind-oriented, continuous line source (CLS) is derived from Equation [2] by integrating in the crosswind direction (with respect to y) from $-\infty$ to $+\infty$. The resulting equation is:

$$\chi(X,y,0) = \frac{(2/\pi)^{1/2} Q}{\bar{u} \sigma_z} \exp \left[-\frac{1}{2} \left(\frac{h^2}{\sigma_z^2} \right) \right] \quad [3]$$

where Q is now expressed in units-length/time. This equation also yields the crosswind - oriented

integrated concentration (CIC) for a plume (CPS) when Q is in units/time and χ is in units/area.

Forms of these three equations are used most commonly in diffusion calculations. Other equations for special cases have been developed from these equations by assuming a definite function of σ_y and σ_z with distance downwind.

Evaluation of Parameters in the Diffusion Equation

Traditionally, there have been three methods of evaluating the plume spread parameters (i.e., σ_y and σ_z) used in Equations [1, 2, & 3]. These are:

1. Assume a mathematical relationship (e.g., power law function) between the σ 's and meteorological parameters with distance downwind, (i.e., the Sutton, (1953), approach). This method has been discounted on the strength of theory and experimental data which show that these parameters (particularly in the stable atmosphere) do not consistently follow the assumed relationships.
2. Use the direct approach which consists of a compilation of measured diffusion data stratified into meteorological categories from which families of curves are drawn. During the past 20 years, this approach has been used extensively by the scientific community. The established curves now constitute the basis of regulatory and licensing methodologies. They have become the basis to which other, more fundamental data are referenced.
3. Use turbulent statistics of the wind. This approach remains the method of choice when defining relationships between local, close field, turbulent diffusion and the measured turbulent spectra of the wind. Costs for instrumentation and the site-specific nature of the data, however, have limited the acceptance of this approach for regulatory and licensing applications.

Because the mathematical models used by federal agencies to regulate ambient air quality from both the nuclear (i.e., NRC, and DOE) and the conventional industrial (i.e., EPA) perspectives incorporate the Gaussian assumption, and because these families of curves have found such wide acceptance, they are presented in the section which follows.

Measured Diffusion Parameters

Many diffusion experiments have been conducted during the past forty years at various sites throughout the world. Several fundamental experiments have been conducted at the INEL. These include experiments by Islitzer (1961), who studied the characteristics of effluent material released from a 45 m elevated source; Islitzer and Dumbauld (1963), who studied the characteristics of effluent material released at ground level; Sagendorf and Dickson (1974), who studied the characteristics of effluent material released into an ultra-stable, low wind speed atmosphere; Clements (1979), who studied dispersion characteristics of effluent material at extended regional and continental scales, and Start and Wendell (1974), and Start et al. (1985), who studied dispersion characteristics of effluent material in recirculating and stagnating non-steady atmospheric conditions.

A compilation and stratification of σ_y , σ_z , and the relative plume-axis concentration ($\chi\bar{u}/Q$), into representative stability categories were made for some of the early experiments. Stability categories in these cases were defined by classifying different categories of insolation (solar time), windspeed, and cloud cover. Pasquill (1961) originated this method of categorization, as an approximation scheme when direct information was lacking. This method was subsequently modified by Markee (1963) specifically for the arid to semi-arid climate at the INEL (Table VI-1).

Average curves of σ_y , σ_z , and $\chi\bar{u}/Q$ with distance downwind as a function of stability category from the early diffusion experiments are illustrated in Figures VI-7 through VI-12. The first set of curves (Figures VI-7 through VI-9) were

constructed by Hilsmeier and Gifford (1962) from Pasquill's (1961) original curves and represent effluent releases from a few minutes to 15 minutes duration. The dilution factor for the extremely stable G category has been added by extrapolation to Figure VI-9. The second set of curves (Figures VI-10 through VI-12) were derived by Markee (1963) from the INEL ground-level diffusion experiments and represent effluent releases of about 15 to 60 minutes duration. Extrapolations (dashed portions of the lines in Figures VI-10 through VI-12) to greater distances during stable conditions were based on Hanford measurements of σ_y (Fuquay et al., 1963). It should be noted that the main difference between the two sets of curves occurs during stable conditions. For the longer releases, effluent plume meander in the crosswind direction becomes a significant factor in the dispersal of effluents. σ_y increases by a factor of four, and $\chi\bar{u}/Q$ decreases by at least a factor of two for the longer releases due to meandering.

For effluent releases on the order of 3 to 15 minutes duration, the Hilsmeier-Gifford curves should be used, and for those from 15 to 60 minutes duration, the Markee curves should be used. No curves are available for puff or instantaneous point source diffusion. Reasonable estimates of the dose rate from a puff at distances greater than 1 to 2 km from the source can be made by using Hilsmeier-Gifford curves of σ_y and σ_z and assuming that $\sigma_x = \sigma_y$ for substitution into Equation [1]. For longer distances and greater travel times, the Markee curves may be more appropriate.

There are two advantages of using this direct approach: (1) the stability classification can be easily determined and (2) the diffusion downwind is allowed to depart from a power law distribution with distance, thus making the results more realistic. The accuracy of these estimates is about the same as the mathematical approach. The main disadvantage of using this approach is that no mathematical equations exist; therefore, formulae for some of the special cases are difficult to obtain. However, computer programs can perform the numerical integrations required by this approach.

Table VI-1. Atmospheric stability estimates using time of day, wind speed, and cloud cover for the INEL (Markee, 1963).

To determine the appropriate stability class for a given season, month, and time of day, work through the table in the following order:

1. Find the month of interest in one of the three columns at the left.
2. Within that column, find the time of day (MST) of interest. Times run from the morning hours at the top of the columns through noon, to midnight, and on to the morning hours again at the bottom of the columns.
3. Locate the appropriate wind speed row (1 m/sec = approximately 2 mph) range within the choices available for that time of day.
4. Adjust for cloud conditions across one of the center columns, as appropriate, and read the stability class from the table.

Time of Day (by Month)			Windspeed at 8 m (m/sec)	Cloud Cover (tenths)			Insolation ^b	Solar Altitude ^b (degrees)
November through January	February through April or August through October	May through July		0 through 5/10	5/10 through 10/10	Heavy Overcast		
10 through 12	08 through 11	06 through 09	< 6	B	C	D	Slight	15 through 35
13 through 16	14 through 18	17 through 20	6 through 9	C	C through D	D	Moderate	35 through 60
12 through 13	11 through 14	09 through 11 14 through 17	> 9	D	D	D		
			< 6	A	B	C		
			6 through 9	B	B through C	C		
			9 through 11	C	C	D		
16 through 10	18 through 08	20 through 06	> 11	D	D	D		
			< 9	A	A through B	B		
			9 through 11	B	B through C	C		
			> 11	C	C	C		
16 through 10	18 through 08	20 through 06	< 3	G	F	E	None (Night)	< 15
			3 through 9	F	E	E		
			9 through 11	E	E	D		
			> 11	D	D	D		

a. Stability class definitions are:

A - Extremely Unstable
B - Moderately Unstable

C - Slightly Unstable
D - Neutral

E - Slightly Stable
F - Moderately Stable

G - Extremely Stable

b. Data in these columns are provided for comparison to other stability categorization schemes.

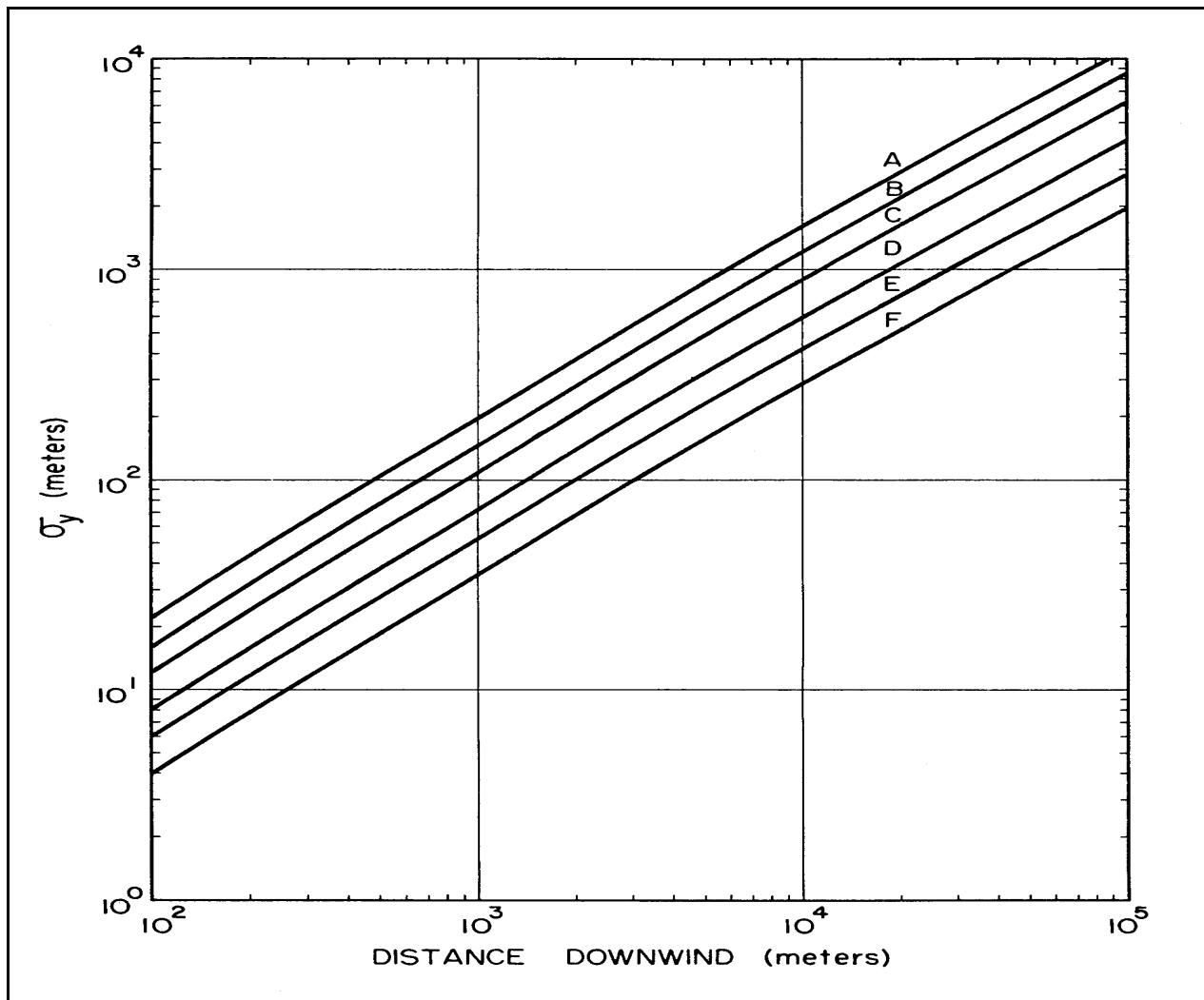


Figure VI-7. σ_y versus downwind distance as a function of stability class for a 3 to 15 minute release time (Hilsmeier and Gifford, 1962).

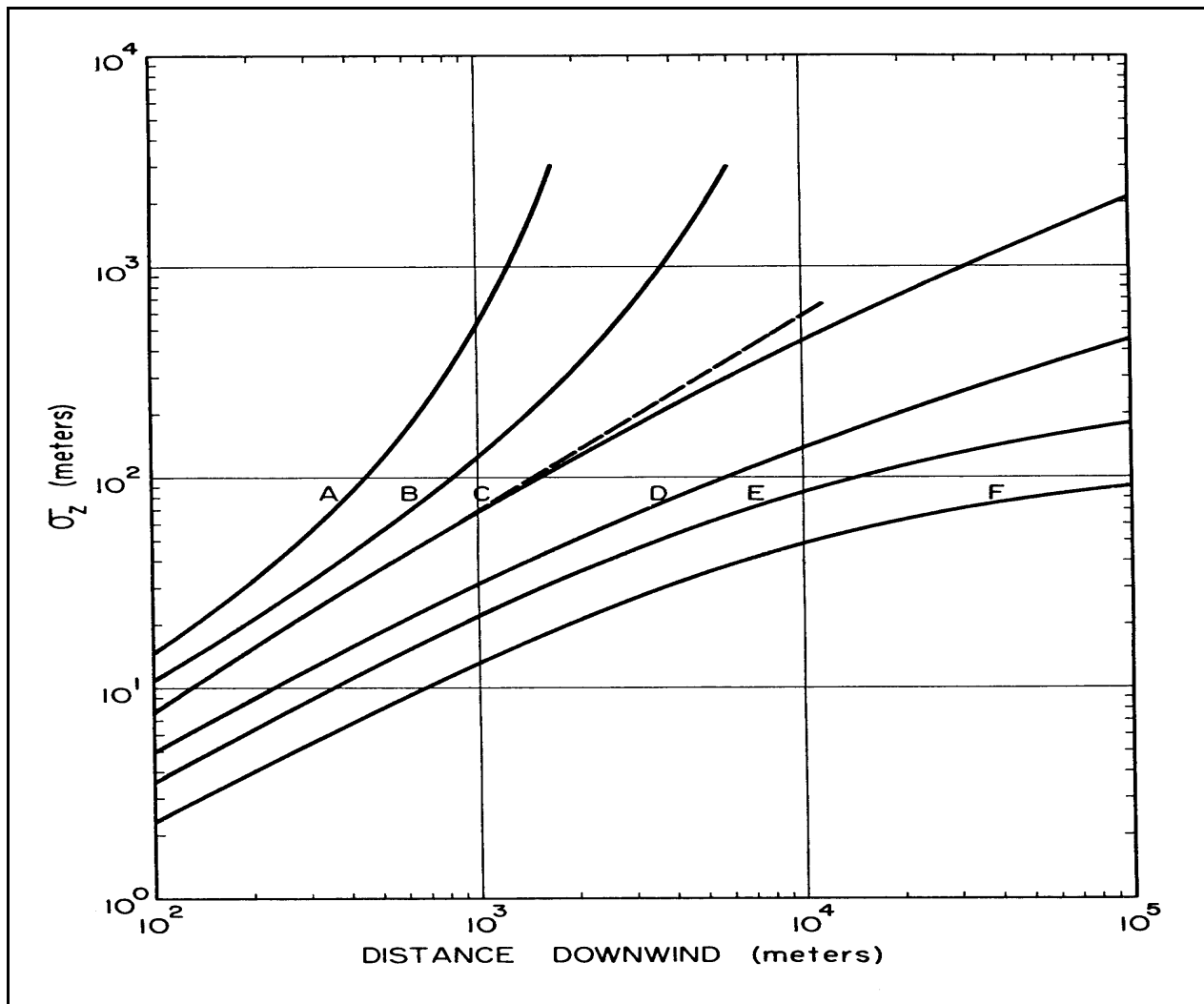


Figure VI-8. σ_z versus downwind distance as a function of stability class for a 3 to 15 minute release time (Hilsmeier and Gifford, 1962).

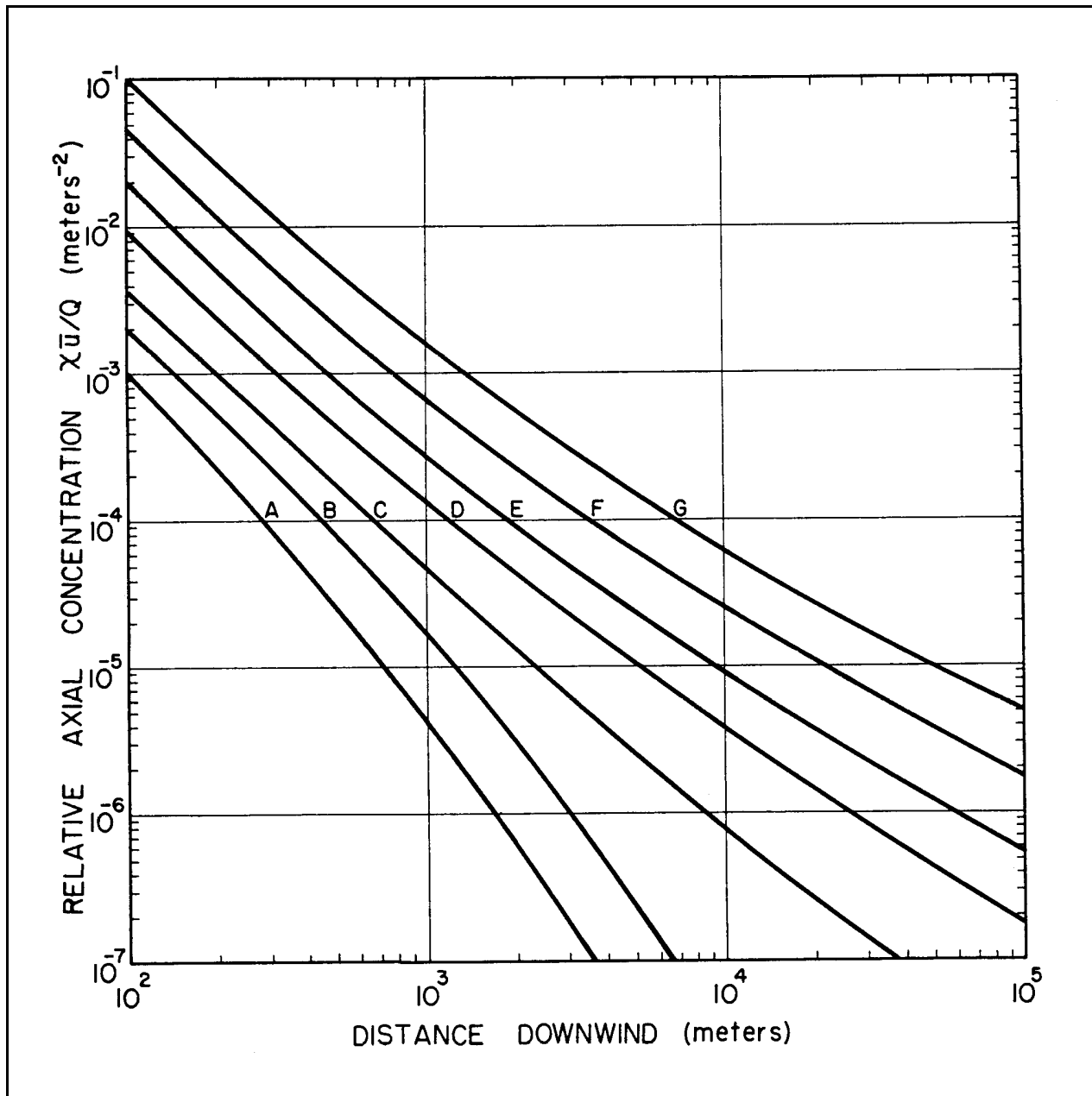


Figure VI-9. Relative axial concentration versus downwind distance as a function of stability class for a 3 to 15 minute release time (Hilsmeier and Gifford, 1962).

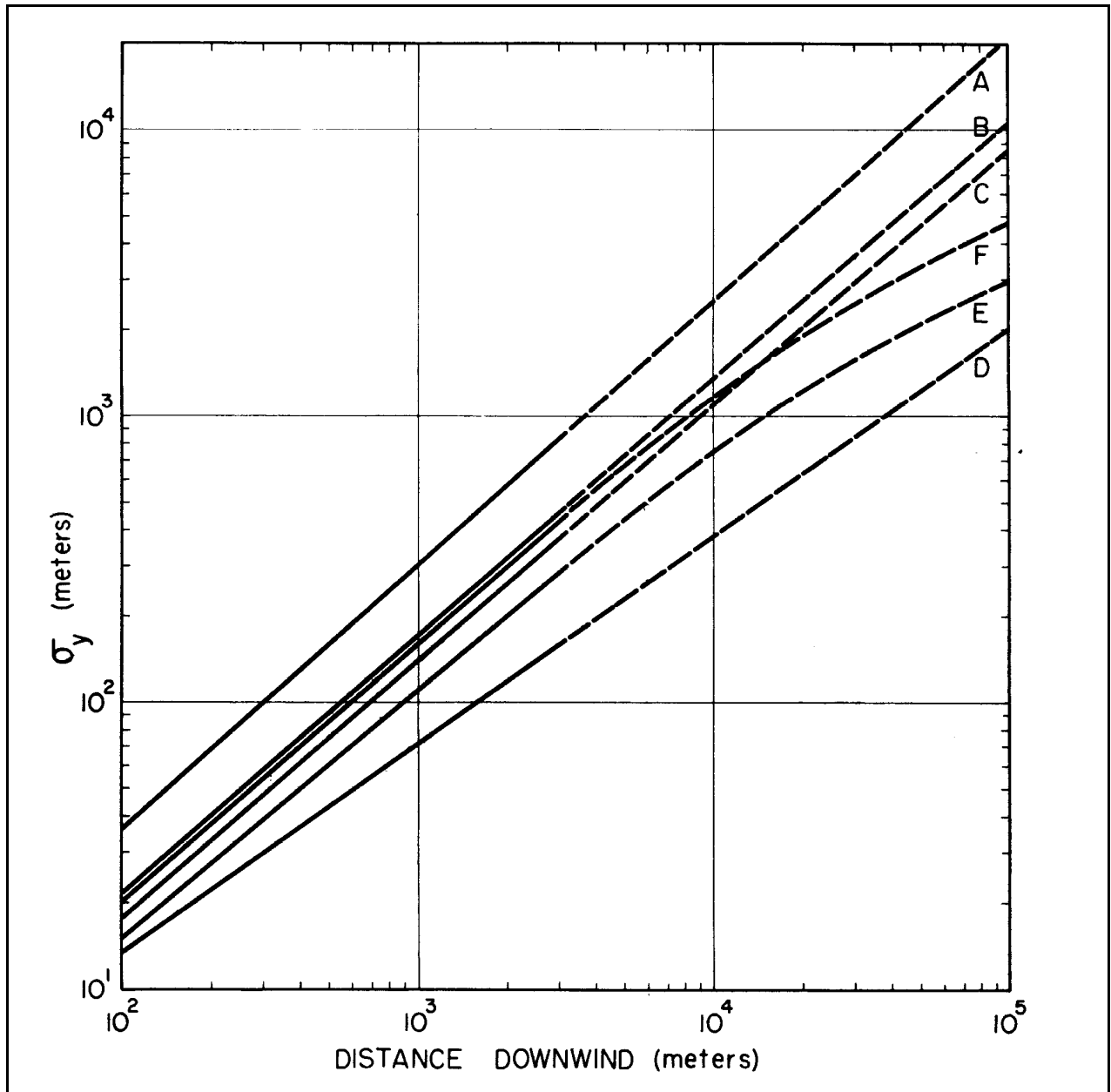


Figure VI-10. σ_y versus downwind distance as a function of stability class for a 15 to 60 minute release time (Markee 1963). The dashed portions of each line represent extrapolations according to data from Fuquay et al., 1963).

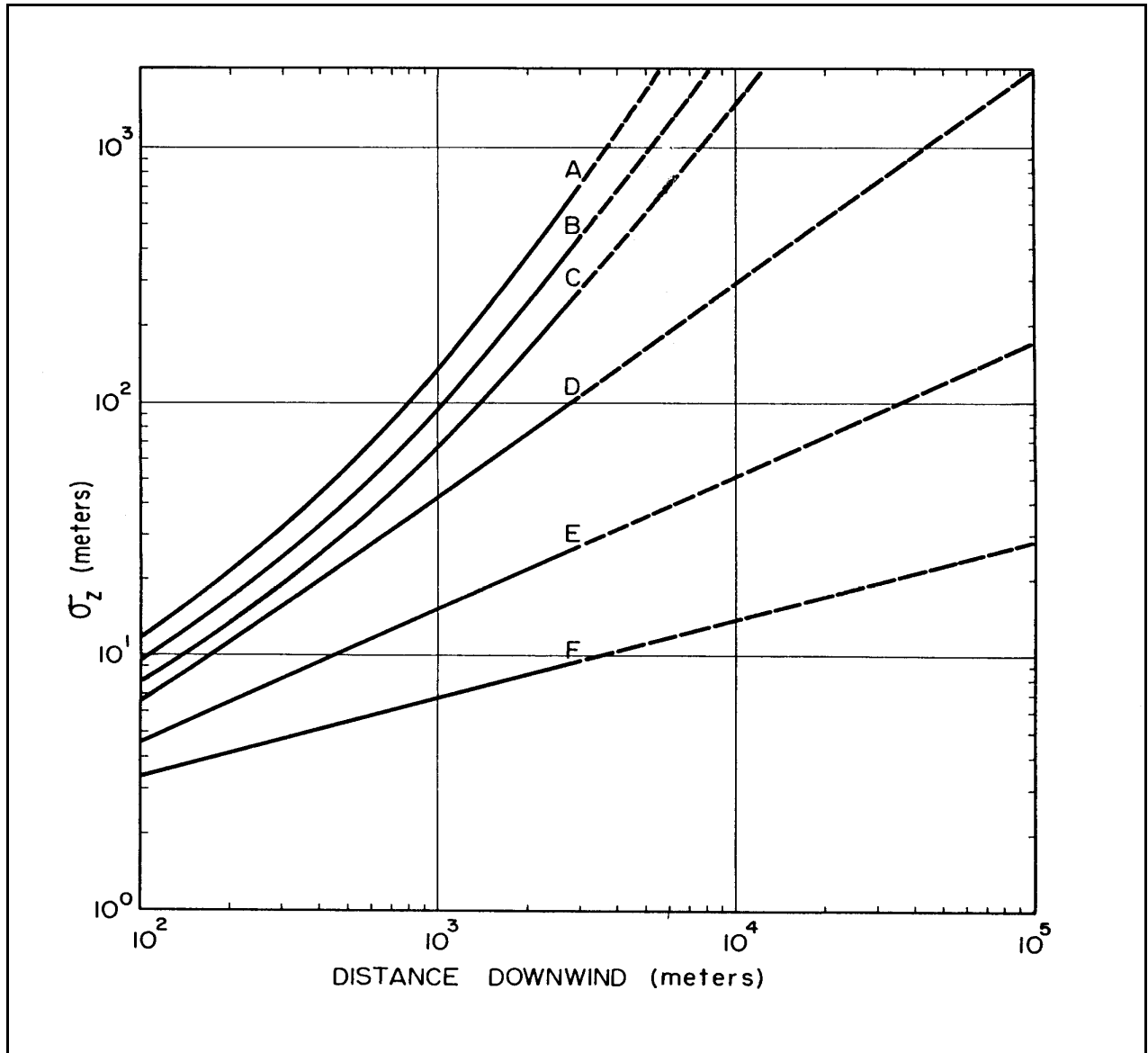


Figure VI-11. σ_z versus downwind distance as a function of stability class for a 15 to 60 minute release time (Markee, 1963). The dashed portions of each line represent extrapolations according to data from Fuquay et al., 1963).

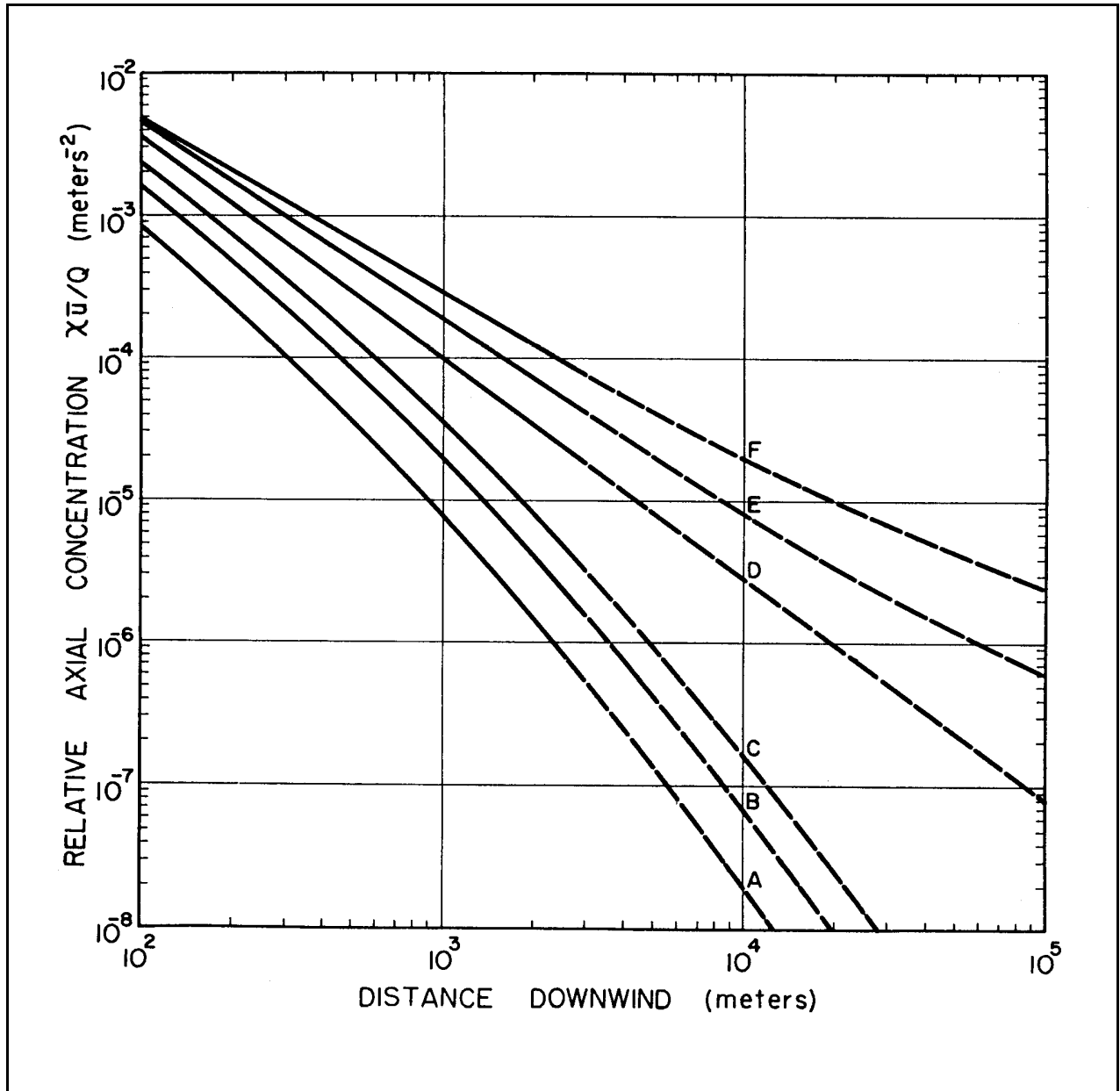


Figure VI-12. Relative axial concentration versus downwind distance as a function of stability class for a 15 to 60 minute release time (Markee, 1963). The dashed portions of each line represent extrapolations according to data from Fuquay et al., 1963).

Available Mathematical Models

Numerous mathematical models have been developed to estimate atmospheric transport and diffusion. Some have been accepted by agencies for use in regulatory assessments. Atmospheric diffusion specialists should be consulted to assist in evaluating the suitability of a model for a given application, and in assisting the user in making proper use of the available data. Important components of atmospheric transport and diffusion which must be considered in a dispersion analysis are addressed in the sections which follow.

Vertical Diffusion

The atmospheric vertical thermal structure interacts with buoyancy induced motions to enhance or restrict vertical diffusion. The atmosphere is said to be stable when warmer air overlies cooler air so that vertical motions are damped. During the day, rising currents of air heated at the surface mix vertically. Because the height to which these rising currents ascend is finite, it follows that the dispersion of an effluent will be most efficient within the thermally well-mixed portion of the atmosphere. An incorporation of this height is essential for realistic dispersion modeling.

The mixing depth can be defined as that portion of the atmosphere next to the surface through which airborne material can freely diffuse. The mixing depth is bounded above by an inversion layer where air temperature increases with height or where the rate of temperature decrease with height is less than in the air below. The depth of the mixed layer is determined by the heat energy exchange between the air and the ground, and is influenced by cloud cover, time of day, and season (solar elevation angle).

Seasonal average mixing depths, based on radiosonde data taken at selected airports throughout the contiguous United States, have been analyzed (Holzworth, 1972) to enable the prediction of mixing depths at the INEL. The results of this analysis are summarized in Table VI-2. Monthly averages of the maximum daily extent of the mixing depth are also shown in Figure VI-13. The data indicate that the mixing depth is the shallowest in the morning during the summer months. Hence, vertical dispersion is the most limited in the morning during that time of the year. The mixing depth also extends to the greatest height on summer afternoons, which results concurrently in the least restriction of vertical dispersion. The average annual mixing depth for the morning hours is 370 m and for the afternoon it is 2090 m. However, a calculated arithmetic mean of the afternoon mixing depths yields a value of approximately 1880 m. This discrepancy, combined with actual observations of the actual morning mixing depths (approximately 100 m regardless of season) indicate the amount of error inherent in this type of application of regional data to the INEL.

During clear nights, when radiational surface cooling is maximized, the inversion layer begins at the surface. Vertical diffusion within such a layer is limited due to inhibiting buoyant forces. In addition, a plume which rises above an inversion layer due to a high initial momentum, results in limited exposure to receptors on the surface until the inversion dissipates. The formation and

Table VI-2. Estimated seasonal and annual mixing depths for mornings and afternoons at the INEL.

	Morning (m AGL)	Afternoon (m AGL)
Spring	480	2330
Summer	260	2900
Autumn	330	1550
Winter	400	730
ANNUAL	370	2090

dissipation of the nocturnal inversion layer at the INEL relative to sunrise and sunset was summarized in Section B. It was shown that inversions began forming at or shortly before sunset and dissipated 1-1/2 to 2 hours after sunrise.

In addition to specifying the vertical depth through which the plume is free to diffuse, it is also necessary to calculate how the turbulent eddies will diffuse the plume vertically. This rate of diffusion is usually estimated by characterizing the existing turbulent environment on the basis of an accepted typing scheme. The plume spread prediction is subsequently applied to the modeled plume using empirical plume spread measurements made under that particular turbulence class. Measurements at the INEL (Dickson and Angell, 1968) have permitted the quantification of the variation in three-dimensional turbulent velocities as a function of season for typical buoyant plume heights of approximately 500 meters. The standard deviation of vertical velocity increases by a factor of three between January and July. To account for these effects, the U.S. Nuclear Regulatory Commission has utilized a stability classification system based on the vertical temperature gradient (U.S. NRC, 1972). This classification scheme is summarized in Table VI-3. The basic assumption behind this NRC stability classification system is that the vertical temperature lapse rate is directly related to the degree of thermal mixing induced by surface heating. The transition from a specified stability or turbulence type to plume spread parameters used in a dispersion model is commonly made via a graph specifying the vertical dispersion coefficient (σ_z) as a function of downwind distance for a given stability class. It is recommended that most modeling conducted for INEL facilities use the σ_z curves presented in Figure VI-11, since these values are based on extensive atmospheric diffusion measurements made at the INEL. These curves, therefore,

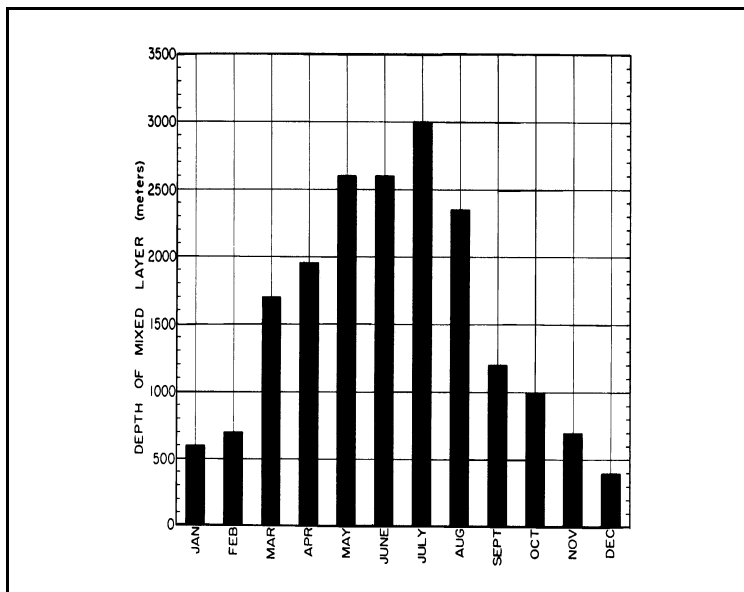


Figure VI-13. Monthly averages of the maximum daily mixed layer depth.

Table VI-3. NRC stability classification system.

Stability Class	$\frac{\Delta T}{\Delta Z}$ ($^{\circ}\text{C}/100\text{ m}$)
A	< -1.9
B	-1.9 to -1.7
C	-1.7 to -1.5
D	-1.5 to -0.5
E	-0.5 to 1.5
F	1.5 to 4.0
G	> 4.0

incorporate site specific effects such as surface roughness, surface heat energy balances, and vertical turbulent stratification which are not obtained from more generic (e.g., Turner, 1970) formulations.

Horizontal Diffusion

Effluent plumes diffuse horizontally, as well as vertically. Horizontal diffusion is resolved into crosswind (y) and along-wind (x) components. For continuous plume formulation, the along-the-

plume diffusion component (x) is assumed to be much less than the distortion caused by the wind speed and is often neglected. Plume elements or puffs are generally assumed to exhibit a symmetrical effluent distribution in both the x and y directions for convenience.

Several physical mechanisms can distort or disperse the plume in the horizontal. Wind directional shear or speed shear in the vertical will distort the plume in the horizontal because the upper portion of the plume may be carried in a different direction than the bottom portion. Modeling of this phenomenon requires elaborate vertical wind measurements over the spatial area of consideration as well as a model which can simulate a three-dimensional wind field and underlying terrain. Although important for large scale dispersion assessments, such refinements are beyond the detail utilized in many preliminary assessments and are usually not incorporated in the simpler regulatory models.

One form of shear common to surface releases at the INEL is the lateral smearing (or wind meander) of the effluent plume during low wind speeds and thermally stable conditions. In this situation, the meander of the wind considerably broadens the time-integrated horizontal plume cross-section beyond the usual spreading. This effect has been studied extensively at INEL (e.g. Sagendorf and Dickson, 1974) and should be incorporated in INEL site specific assessments.

Horizontal turbulent eddies are another mechanism which distorts and disperses the plume in its horizontal dimension. Within the atmospheric surface layer, turbulence is considered isotropic and homogeneous. In the horizontal, however, the spectrum of turbulent eddies is not constrained by the mixing depth, with the result that the horizontal and vertical plume spread parameters are not identical for a given stability.

The horizontal dispersion parameter (σ_y) recommended for modeling at INEL is the one presented in Figure VI-10. Under stable conditions, the effect of wind meander is to

increase the effective horizontal plume spread so that the stable curves cross over the curves for less stable conditions at long distances.

Facility Influences and Source Configurations

Atmospheric dispersion within the first few kilometers downwind from the effluent source is strongly influenced by the mode of effluent release and by the turbulence induced by adjacent structures and local topographic features. Because many of these influences are associated with physical facility design, they must be incorporated in the dispersion analysis on a site-specific basis. Several generic factors which influence atmospheric dispersion at the INEL are described in this section.

Structure Wake Effects

A significant phase of atmospheric transport occurs in the immediate vicinity of the plume source. It is here where the effluent plume is affected most strongly by plume rise and by facility-related turbulence and distortions of the airflows. Diffusion formulae incorporated in most assessment models make use of the assumption that the flow field has straight streamlines which are parallel to each other and to the ground. That assumption does not apply for concentration fields within a few kilometers of sources on or near buildings. Flow near buildings contains curved streamlines, sharp velocity discontinuities, and highly nonisotropic and nonhomogeneous turbulence.

Data from recent field studies of building wake effects at the INEL (Islitzer, 1965; Dickson et al., 1969; Sagendorf et al., 1980, Start et al., 1980; Start, et al., 1989) imply three characteristic zones of diffusion. The three zones are thought to represent (1) rapid diffusion in the building wake, (2) a transition zone where the plume leaves the wake of the building and where the rate of diffusion is reduced, and (3) the region where larger scale atmospheric turbulence again causes more rapid diffusion.

Figure VI-14 presents a plot of normalized concentration (χ/Q , in s/m^3) at the 95% confidence level versus scaled distance (downwind sampler distance divided by the square root of the minimum cross sectional building area) for two reactor building configurations. One is a cube-shaped bluff body (EOCR), while the second is a very large commercial nuclear generating station with a cylindrical containment vessel and large hyperbolic cooling towers (Rancho Seco facility, Sacramento, CA). The consistency in measured concentrations suggests the usefulness of this technique to estimate maximum expected concentrations near INEL reactor complexes. Significant differences between building wake diffusion near various obstacle shapes represented by INEL buildings can be addressed more specifically by diffusion meteorologists, based on additional site-specific data not included here.

Source Elevation

The location of the effluent source relative to adjacent structures, and relative to physical stack parameters and approach wind is very important in determining maximum effluent concentration fields near a facility. Given the availability of specific design data, diffusion meteorologists can assist in the evaluation of individual parameters. In many situations, numerical solutions are not available and scale model analyses or field measurements are required.

Plume Rise

At its point of release, a plume has vertical momentum due to (1) its stack exit velocity, and (2) its buoyancy if the exit gas temperature is different than the temperature of the ambient air. The magnitude of the plume momentum relative to that of

the ambient wind will determine whether the plume will rise vertically or be bent over by the wind. Even if the plume is bent over, its trajectory will continue to rise if the plume has a vertical velocity component derived from an initial exit velocity and from buoyancy momentum.

In most cases, the major plume rise variables are:

1. Stack exit velocity momentum
2. Stack exit buoyancy (sensible heat vs. ambient air temperature, and latent heat)
3. Ambient wind speed
4. Downwind distance (for bent-over plumes)

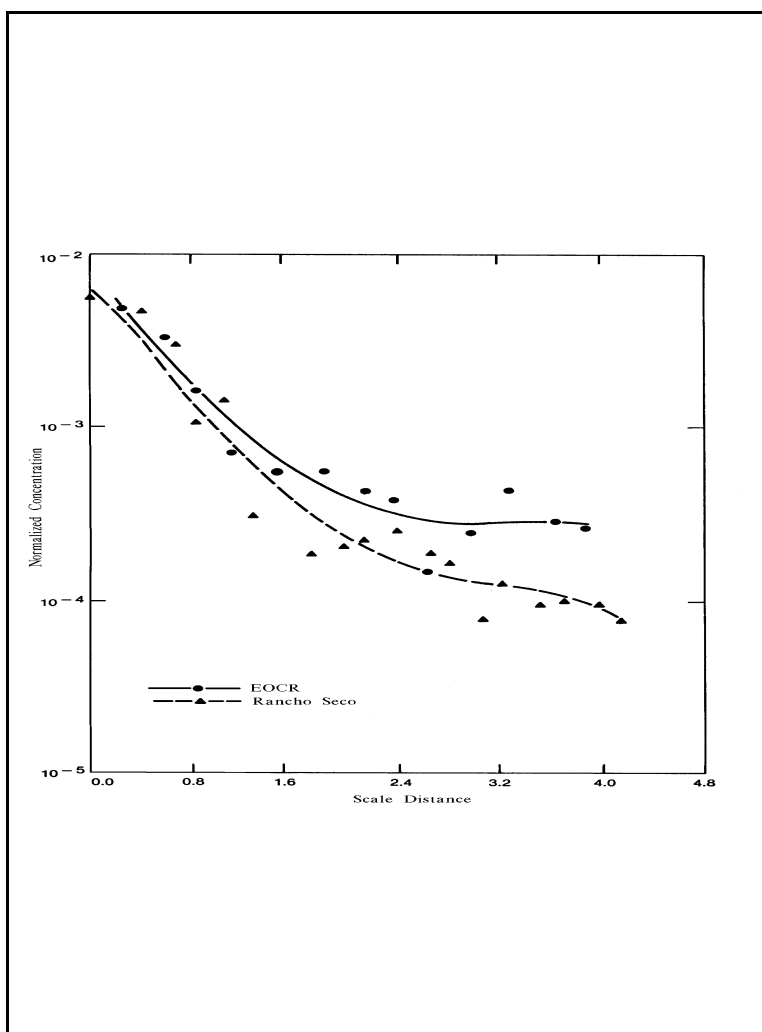


Figure VI-14. 95% level, fourth-order curves of frequency of normalized concentration versus scaled distance.

5. Atmospheric turbulence as categorized by atmospheric stability.

Briggs (1969) developed plume rise formulae for jets (cold plumes) and buoyant (heated) plumes in calm and windy conditions. For the bent-over, buoyant plume trajectory, Briggs suggests 3 different stages: 1) an "initial stage" of rise where air entrainment results mostly from self-induced turbulence, (2) a "transition stage," and (3) a "final stage" of plume rise where air entrainment results mostly from atmospheric turbulence. By convention, the maximum plume rise is assumed to be reached at a point about 3.5 times the downwind distance at which the "final stage" of plume rise begins.

Effluent plume rise and final plume height is essential to accurately predict ground level concentrations, especially near the source and in the presence of surface-based temperature inversions which are present at INEL during all seasons of the year (see Chapter V, Figures B-4 through B-7).

Effects of Cooling Towers and Ponds

Moisture released by a cooling system is important when estimating plume rise, atmospheric dispersion, plume transformation and deposition, and impacts on visibility, fogging, and icing. Meteorologists can assist with these evaluations in the context of design data for a given facility.

Removal Processes and Transformations

Rigorous analysis of atmospheric dispersion should account for changes in the concentration of effluent plume which may occur as it moves downwind and is diluted by atmospheric turbulence. Particle deposition and resuspension, wet deposition and precipitation scavenging, chemical transformations, and radioactive decay are all examples of phenomena which should be addressed by dispersion and risk assessment models.

Calculation of plume modifications due to loss by deposition, decay, or scavenging, further complicates the modeling of atmospheric transport and diffusion. Frequently, these calculations are made by separate routines using plume location, age, and concentration estimates which are products of the primary atmospheric dispersion code. For certain substances, namely particulates and soluble gases, these factors become very important. For certain facility designs and cooling system options, a thorough analysis of these factors is warranted.

Deposition

Plume depletion occurs as a result of particulate settling or absorption of effluent gases on various surfaces. Deposition of the effluent can be an important factor for some types of sources. The reader is referred to Slade (1968) for simple theoretical details and summaries of empirical deposition data. It should be emphasized that much of the existing data on deposition as a function of stability, wind speed, and ground cover has been collected at test sites on the INEL.

Decay

Accurate dose assessment modeling for INEL facilities, if applicable, should account for the facility emissions inventory and incorporate radioactive decay which will occur within the time scale considered.

In some cases deposition velocities and scavenging constants may be altered as chemical species change. A credible specification of uncertainty in final results is heavily dependent on an accurate characterization of removal processes and transformations. Great care is therefore advised in the selection and use of risk assessment models.

Precipitation Scavenging

The scavenging process has three major components:

1. Transport and dispersion of the material to the scavenging site.
2. Scavenging by cloud droplets and precipitation within the cloud.
3. Scavenging below the cloud by free falling precipitation.

The turbulence and transport environment within a cloud may differ from the near-surface winds and turbulence commonly modeled, and should be accounted for, when appropriate. The reader is again referred to the literature (e.g. Slade 1968) for an introduction to this important topic.

Emissions from certain INEL facility designs might undergo precipitation scavenging and wet deposition. In such situations, factors such as cloud location and precipitation intensity, as well as entrainment, electrical charge, and nature of the material to be scavenged (including particle size distribution and gas solubility) are extremely important and need to be specified realistically. Since precipitation occurs infrequently at the INEL, this problem is of less concern than for most locales.

Normalized Dispersion Concentration Fields

Figure VI-15 presents annual average concentration isopleths for normalized ICPP emissions using meteorological data from 1974 through 1983 (a ten year period). These long-term average isopleths exhibit several characteristics. In general, a northeast-southwest distribution of the concentration isopleths can readily be observed. Areas of higher concentration (greater than $70 \text{ h}^2/\text{m}^3 \times 10^{-9}$) are generally confined within the INEL boundaries. A secondary concentration lobe of the $10 \text{ h}^2/\text{m}^3 \times 10^{-9}$ isopleth is exhibited in the area between Blackfoot and Aberdeen.

Figure VI-16 presents concentration isopleths also calculated using normalized ICPP emissions for meteorological data from 1988. It can be seen that the concentration patterns for this year are very similar to those obtained for the ten year data

set illustrated in Figure VI-15. The southwest-northeast extensions dominate, there is little tertiary lobe development, and the maximum concentration areas near the source are generally confined and localized. This is not the case for most years, however. Comparisons of similar annual normalized concentration patterns with the 10-year pattern lead to the conclusion that 1982 and 1988 are years most representative of the long-term dispersion pattern.

Similarities are also known to exist in the concentration patterns for effluent releases from sites located in the vicinity of ICPP. The concentration patterns are similar in terms of both spatial distribution and magnitude. However, significant differences exist in the transport trajectories at locations not central to the INEL (e.g., TAN, EBR-II, RWMC and the area west of TRA). The concentration patterns presented here are not representative of those sites. Therefore, a site-specific analysis should be undertaken to obtain an accurate calculation of concentration isopleths for those locales. Diffusion meteorologists should assist in those analyses and interpretations.

Several general conclusions pertaining to local and regional-scale modeling of emissions from INEL facilities are indicated by comparing results of historical modeling analyses as follows:

1. For short-term (accidental) releases, the greatest shortcoming of single-wind rose, sector-average models (e.g., the NRC regulatory model XOQDOQ) is their failure to accurately describe the effluent trajectory, and the subregion which would be affected within the spatially variable wind field at the INEL. A multi-station, sequential wind field model (e.g., the EPA UNAMAP model MESODIF) produces annual average or multiyear total integrated concentration patterns which are significantly broader than those produced by a wind rose model. This is a result of the wind rose model's inability to incorporate short term variability in the long term average.

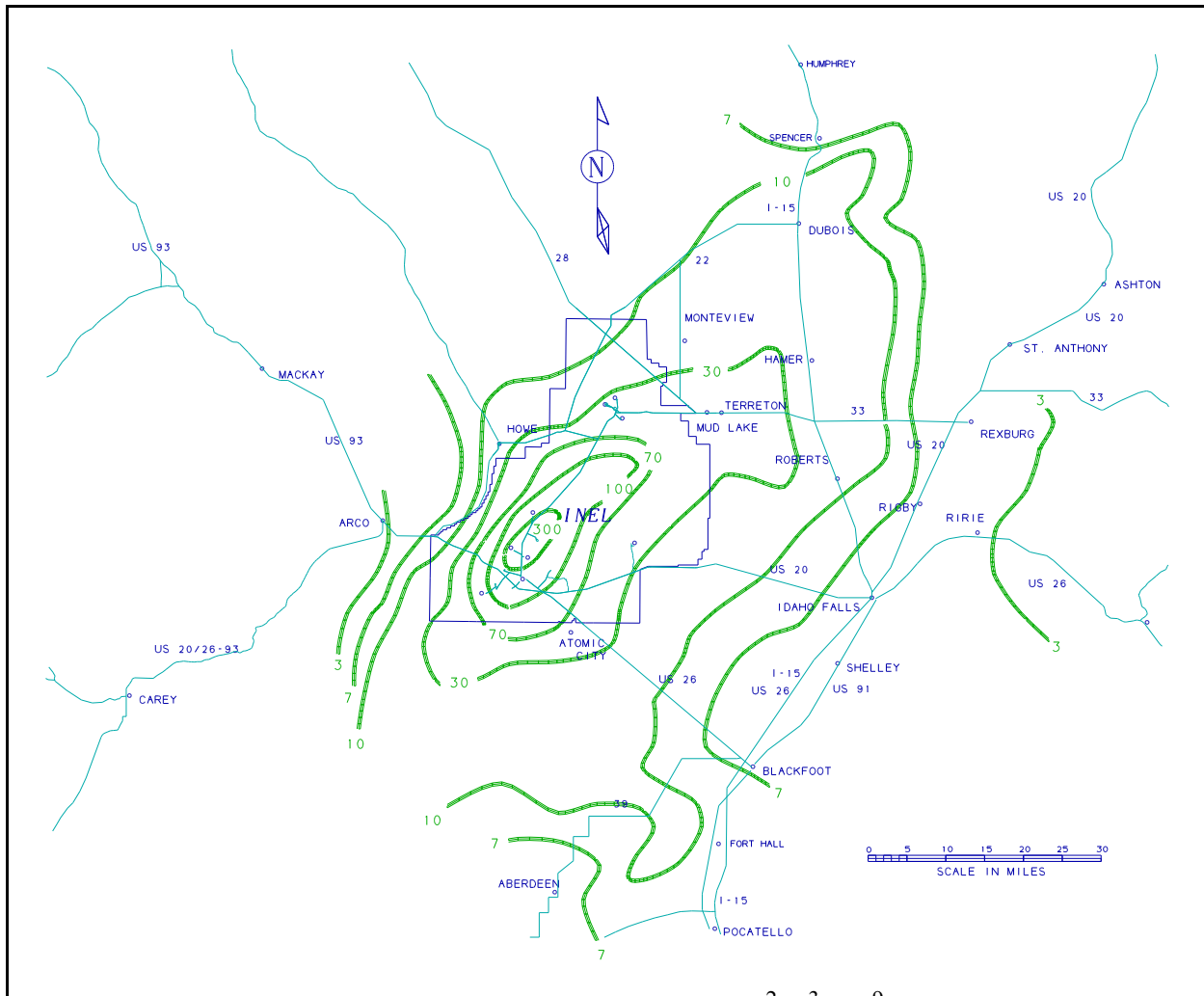


Figure VI-15. Ten year normalized total integrated concentration ($\text{h} / \text{m}^3 \times 10^{-9}$) for ICPP from 1974 through 1983.

2. Beyond 15-30 mi. from the effluent source, a wind rose model overestimates annual total integrated concentrations by about an order of magnitude. The inability of a wind rose model to accommodate time changes in stability category during effluent transport is the single most influential factor of this bias.
3. Because a sequential wind field model more realistically simulates recirculations and stagnations which occur at INEL, pockets of elevated concentration about 4.5 times the value predicted by a wind rose model are sometimes indicated during short term modeling.
4. The bimodal spatial distribution of annual concentrations is stable from year to year, and for multiyear averages, and the meteorological data for a single years 1982 or 1988 reasonably represent the long-term mean atmospheric diffusion patterns, based on the data acquired to date.
5. Normalized concentration values for sources at different locations are very similar, but some differences in annual isopleth patterns are evident. These differences increase when shorter (episode)time periods are considered.

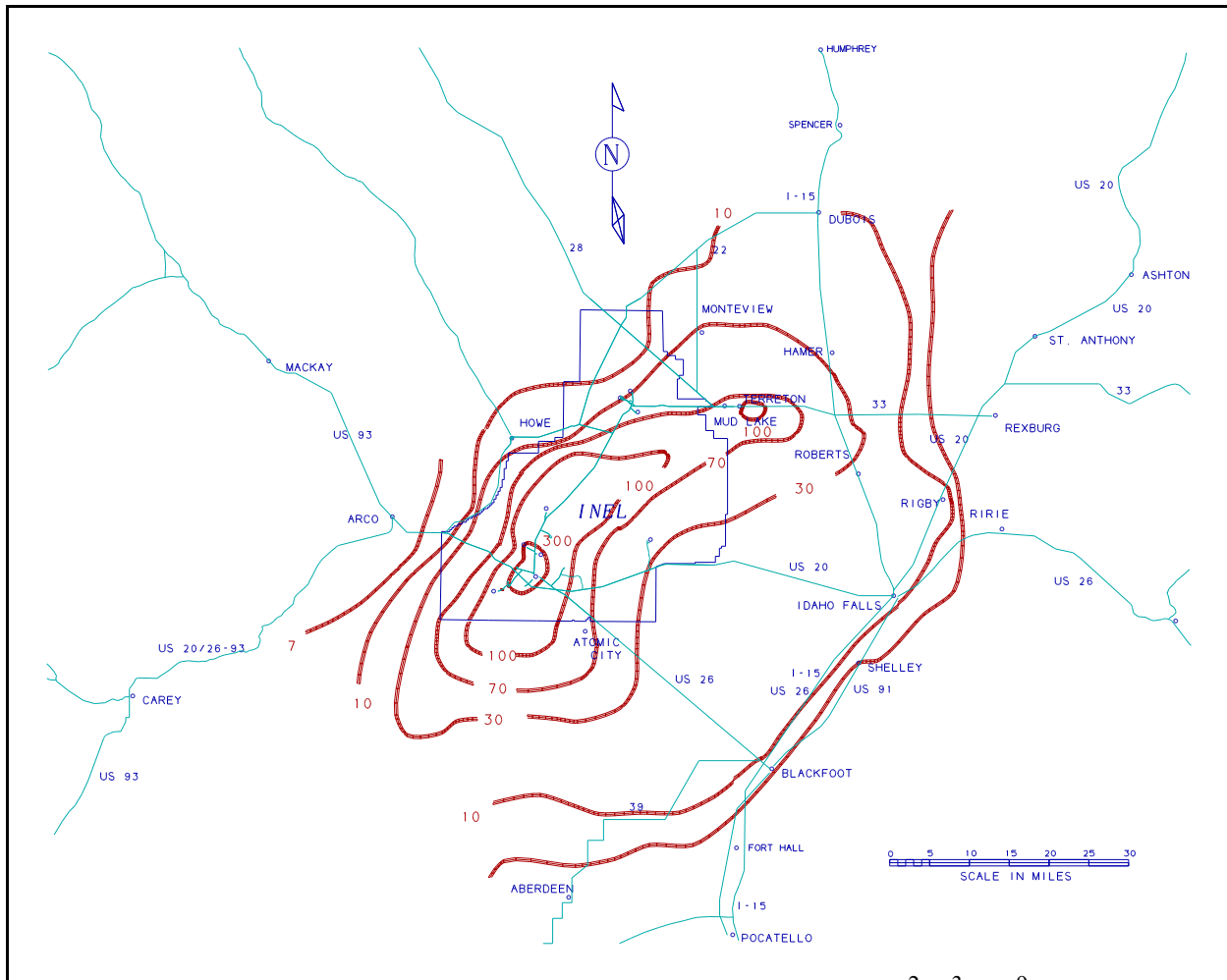


Figure VI-16. Annual normalized total integrated concentration isopleths ($\text{h}^2/\text{m}^3 \times 10^{-9}$) for ICPP during 1988.

6. Sequential wind field models (e.g., MESODIF) are based on a wind and concentration calculation grid of finite size such that resolution at subgrid scales (about five miles as generally configured) is not normally available. A wind rose model can economically simulate long term dispersion at those short distances.

NOTES

REFERENCES

- Briggs, G. A. 1969. Plume Rise. TID-25075. U.S. AEC, Washington, DC.
- Clements, W. E. 1979. Experimental design and data of the April, 1977 multitracer atmospheric experiment at the Idaho National Engineering Laboratory. LA-7795-M5. Los Alamos Sci. Lab., Los Alamos, NM.
- Coats, D. W., and R. C. Murray. 1985. Natural phenomena hazards modeling project: Extreme wind/tornado hazard models for Department of Energy sites. UCRL-53526, Rev. 1. Lawrence Livermore Nat. Lab., Livermore, CA.
- DeMarrais, G. A. 1958a. The climatology of the National Reactor Testing Station. U.S. AEC Rep. IDO-12003. U.S. Dept. of Comm., U.S. Weath. Bur., Idaho Falls, ID.
- DeMarrais, G. A. 1958b. The engineering climatology of the National Reactor Testing Station. U.S. AEC Rep. IDO-12004. U.S. Dept. of Comm., U.S. Weath. Bur., Idaho Falls, ID.
- DeMarrais, G. A., and N. F. Islitzer. 1960. Diffusion climatology of the National Reactor Testing Station. U.S. AEC Rep. IDO-12015. U.S. Dept. of Comm., U.S. Weath. Bur., Idaho Falls, ID.
- Dickson, C. R., and J. K. Angell. 1968. Eddy velocities in the planetary boundary layer as obtained from tethered flights at Idaho Falls. *J. Appl. Meteorol.* 7:986-993.
- Dickson, C. R., G. E. Start, and E. H. Markee, Jr. 1969. Aerodynamic effects of the EBR-II Reactor Complex on effluent concentration. *Nuclear Safety* 10:228.
- Fuguay, J. J., C. L. Simpson, and W. T. Hinds. 1963. Prediction of environmental exposures from sources near the ground, based on Hanford experimental data. Hanford Atomic Products Operation, General Electric Co., Richland, WA.
- Hilsmeier, W. F., and F. A. Gifford, Jr. 1962. Graphs for estimating atmospheric dispersion. U.S. AEC Rep. ORO-545. Weath. Bur., Oak Ridge, TN.
- Holzworth, G. C. 1972. Mixing heights, wind speeds, and potential for urban air pollution throughout the contiguous United States. Pub. No. AP-101. U. S. EPA, Research Triangle Park, NC.
- Humphrey, P. A., E. M. Wilkins, and D. M. Morgan. 1953. Atmospheric dust at the National Reactor Testing Station, Final Report. U. S. Dept. of Comm., Weath. Bur. Off., Idaho Falls, ID.
- Islitzer, N. F. 1961. Short-range atmospheric dispersion measurements from an elevated source. *J. Meteorol.* 443-450.
- Islitzer, N. F. 1965. Aerodynamic effects of large reactor complexes upon atmospheric turbulence and diffusion. U.S. AEC Rep. IDO-12041. U.S. Dept. of Comm., U.S. Weath. Bur., Idaho Falls, ID.

- Islitzer, N. F., and R. K. Dumbauld. 1963. Atmospheric diffusion-deposition studies over flat terrain. *Int. J. Air Wat. Poll.* 7:999-1022.
- Johnson, O. J., and C. R. Dickson. 1962. An eight year summary of the temperature gradient below 250-feet at the National Reactor Testing Station. U.S. AEC Rep. IDO-12025. U. S. Dept. of Comm., U. S. Weath. Bur., Idaho Falls, ID.
- Markee, E. H., Jr. 1963. Methods of estimating air pollutant dispersion over relatively smooth terrain from routine meteorological observations. Tech. Rep. Pres. at the 219th Nat. Mtg. of the Am. Meteorol. Soc., 20 June 1963, at Palo Alto, CA. U. S. Dept. of Comm., U. S. Weath. Bur., Idaho Falls, ID.
- Nace, R. L., P. T. Voegeli, J. R. Jones, and M. Deutsch. 1975. Generalized geologic framework of the National Reactor Testing Station, Idaho. USGS Prof. Paper 725-B. U. S. Gov. Print. Off., Washington, DC.
- Pasquill, F. 1961. The estimation of the dispersion of windborne material. *Meteorol. Mag.* 90:33-459.
- Sagendorf, J. F., and C. R. Dickson. 1974. Diffusion under low windspeed, inversion conditions. Tech. Mem. ERL/ARL-52. U.S. Dept. of Comm., NOAA, Env. Res. Lab., Air Res. Lab., Idaho Falls, ID.
- Sagendorf, J. F., N. R. Ricks, G. E. Start, and C. R. Dickson. 1980. Diffusion near buildings as determined from atmospheric tracer experiments. Tech. Mem. ERL/ARL-84. U.S. Dept. of Comm., NOAA, Env. Res. Lab., Air Res. Lab., Idaho Falls, ID.
- Slade, D. H. 1968. Meteorology and atomic energy. TID-24190. U.S. AEC, Washington, DC.
- Solar Energy Research Institute. 1981. Solar radiation energy resource atlas of the United States. SERI/SP-642-1037. U.S. Gov. Print. Off., Washington, D.C.
- Start, G. E., C. R. Dickson, J. F. Sagendorf, G. R. Ackermann, K. L. Clawson, R. C. Johnson, and N. H. Hukari. 1989. Atmospheric diffusion for airflows in the vicinity of the James Forrestal Campus, Princeton University, final report. U.S. Dept. of Comm., NOAA, Env. Res. Lab., Air Res. Lab., Idaho Falls, ID.
- Start, G. E., J. H. Cate, J. F. Sagendorf, G. R. Ackermann, C. R. Dickson, N. H. Hukari, and L. G. Thorngren. 1985. Comparisons of trajectories, tracer concentration patterns and MESODIF model calculations: Idaho Field Experiment 1981, Vol. III. NUREG/CR-3488. U.S. Dept. of Comm., NOAA, Env. Res. Lab., Air Res. Lab., Idaho Falls, ID.
- Start, G. E., N. F. Hukari, J. F. Sagendorf, J. H. Cate, and C. R. Dickson. 1980. EOCR building wake effects on atmospheric diffusion. Tech. Mem. ERL/ARL-91. U.S. Dept. of Comm., NOAA, Env. Res. Lab., Air Res. Lab., Idaho Falls, ID.
- Start, G. E. and L. L. Wendell. 1974. Regional effluent dispersion calculations considering spatial and temporal meteorological variations. Tech. Mem. ERL/ARL-44. U.S. Dept. of Comm., NOAA, Env. Res. Lab., Air Res. Lab., Idaho Falls, ID.

- Sutton, O. G. 1955. *Micrometeorology*. McGraw-Hill Book Co., Inc., New York, NY.
- Turner, D. B. 1970. *Workbook of atmospheric dispersions estimates, revised*. U. S. EPA, Research Triangle Park, NC.
- U. S. Nuclear Regulatory Commission. 1972. *Onsite meteorological programs*. Regulatory Guide 1.23. U. S. Gov. Print. Off., Washington, DC.
- Wendell, L. L. 1972. Mesoscale wind fields and transport estimates determined from a network of wind towers. *Mon. Weath. Rev.*, 100:565-578.
- Yanskey, G. R., E. H. Markee, Jr., and L. P. Richter. 1966. *Climatology of the National Reactor Testing Station*. USAEC Rep. IDO-12048. U. S. Dept. of Comm., Environ. Sci. Serv. Admin., Inst. for Atmos. Sci., Air Resour. Field Res. Off., Idaho Falls, ID.

NOTES

APPENDIX 1

SURFACE AIR TEMPERATURE EXTREMES

The following are the daily extreme surface air temperature records and corresponding year(s) observed at CFA from January 1950 through December 1988. The data include the highest and lowest maximum and the highest and lowest minimum air temperatures.

JANUARY

Day	Highest Maximum (°F)	Year of Highest Maximum	Lowest Maximum (°F)	Year of Lowest Maximum	Lowest Minimum (°F)	Year of Lowest Minimum	Highest Minimum (°F)	Year of Highest Minimum
1	50	1981	0	1979	-28	1979	21	1981
2	44	1981	6	1979	-29	1974,1978	16	1956
3	37	1956	10	1959,1974	-23	1952	21	1966
4	46	1963	0	1972	-32	1973	27	1965,1981
5	43	1954,1965	0	1971	-28	1971	32	1956
6	44	1966	3	1971	-30	1979	33	1983
7	46	1956	5	1982	-33	1979	34	1983
8	46	1961	6	1973	-26	1979	31	1983
9	44	1961	6	1977	-28	1974	32	1953
10	41	1953,1956	11	1962	-22	1977	29	1953,1980
11	44	1981	-3	1963	-30	1977	29	1956
12	47	1953	-2	1963	-35	1963	32	1953
13	48	1981	1	1963	-22	1963	34	1969,1980
14	41	1980,1981	6	1972	-19	1972	33	1980
15	42	1974	9	1984	-23	1964	35	1974
16	51	1974	10	1960	-22	1957	36	1974
17	42	1961,74,81	3	1984	-27	1960	35	1971
18	47	1981	-6	1984	-34	1984	33	1953
19	42	1953	2	1984	-32	1960	31	1953,1972
20	48	1981	0	1984	-31	1984	34	1969
21	42	1953,1981	6	1962	-40	1962	32	1969
22	49	1981	7	1962	-38	1962	31	1950,1970
23	45	1970	2	1962	-37	1962	32	1970
24	43	1959,1970	13	1957,1962	-22	1964	31	1959
25	49	1953	13	1950	-17	1962	28	1953
26	46	1987	10	1980	-28	1957	26	1970
27	43	1987	12	1979	-28	1957	27	1959
28	44	1988	2	1951	-29	1957	30	1 9 5 4
29	45	1953	8	1957	-26	1951,1979	34	1954
30	47	1961	3	1979	-28	1957	28	1981
31	47	1953	-1	1985	-35	1985	31	1986

FEBRUARY

<u>Day</u>	<u>Highest Maximum (°F)</u>	<u>Year of Highest Maximum</u>	<u>Lowest Maximum (°F)</u>	<u>Year of Lowest Maximum</u>	<u>Lowest Minimum (°F)</u>	<u>Year of Lowest Minimum</u>	<u>Highest Minimum (°F)</u>	<u>Year of Highest Minimum</u>
1	46	1987	-9	1985	-36	1985	31	1963
2	44	1987	8	1985	-29	1956	31	1987
3	53	1953	5	1985	-26	1985	37	1963
4	45	1954	3	1985	-34	1985	31	1963
5	57	1963	1	1982	-32	1982	30	1963
6	57	1963	5	1982	-29	1982	31	1978
7	54	1963	15	1982	-16	1986	26	1953,1961
8	53	1963	14	1982	-15	1956,82,86	28	1953,1961
9	50	1970	12	1982	-15	1986	35	1976
10	48	1970,1987	8	1982	-25	1981	34	1961
11	53	1961	14	1984	-24	1982	32	1962
12	52	1987	21	1984	-14	1982	33	1954
13	48	1967	20	1965,1968	-10	1955,1964	34	1979
14	47	1987	13	1952	-16	1964	33	1979
15	49	1961	16	1952	-14	1952	33	1982
16	50	1970	4	1956	-15	1956	33	1982,1986
17	48	1977	14	1956	-12	1978	33	1986
18	47	1977	15	1952	-15	1978	35	1980
19	56	1981	20	1978	-17	1955	34	1980
20	52	1958	11	1984	-21	1975	35	1980
21	53	1982	18	1952	-15	1952,71,73	31	1982
22	53	1958	11	1952	-17	1952,1975	30	1982,1986
23	49	1954,1958	18	1984	-13	1955,1960	34	1986
24	55	1963,1986	12	1960	-15	1952	32	1957,1958
25	54	1963,1986	13	1952	-20	1952	30	1957
26	55	1988	13	1960,1962	-20	1960	33	1983
27	58	1980	11	1960,1962	-25	1960	35	1976
28	59	1986	20	1960	-18	1964	35	1972
29	57	1988	9	1960	-31	1960	27	1976

MARCH

<u>Day</u>	<u>Highest Maximum (F)</u>	<u>Year of Highest Maximum</u>	<u>Lowest Maximum (F)</u>	<u>Year of Lowest Maximum</u>	<u>Lowest Minimum (F)</u>	<u>Year of Lowest Minimum</u>	<u>Highest Minimum (F)</u>	<u>Year of Highest Minimum</u>
1	59	1986	16	1960	-28	1960	35	1974
2	61	1986	21	1960	-14	1960	37	1983
3	63	1986	19	1960	-14	1964	33	1983
4	58	1968	15	1985	-14	1985	30	1980
5	59	1986	16	1955	-15	1955	30	1980,1983
6	58	1986	22	1952,1955	-10	1955	39	1987
7	55	1954,1970	21	1985	-6	1955	36	1987
8	56	1957	26	1964	-11	1964	34	1986,1987
9	65	1972	22	1969	-13	1969	36	1954
10	62	1972	23	1969	-7	1969	36	1967
11	56	1981	24	1950	-14	1969	36	1982
12	61	1972	25	1950,1952	-9	1962,1969	33	1971
13	60	1972	25	1952	-10	1969	35	1983
14	58	1981	19	1952	-12	1952	34	1984
15	60	1961	29	1952,1956	-5	1952,62,85	32	1982
16	62	1972	30	1964	-3	1962	31	1981
17	66	1972	22	1965	-1	1971	33	1974
18	60	1972	21	1965	-7	1971	31	1968
19	62	1988	25	1952	-1	1971	34	1972,1975
20	62	1988	24	1955	-13	1955	32	1981,1984
21	63	1972	29	1985	2	1952,1955	32	1988
22	69	1972	26	1952	-8	1952	34	1986
23	64	1977	29	1964	3	1964	37	1978
24	63	1956	23	1965	2	1964	32	1986
25	63	1966	29	1955	3	1965	33	1962
26	66	1966	28	1975	4	1955	34	1971,1974
27	69	1986	21	1975	8	1955	36	1974
28	73	1986	24	1975	2	1985	37	1968
29	70	1978,1986	31	1977	-3	1985	38	1986
30	70	1966,1986	32	1980	6	1985	34	1978,1983
31	70	1966	31	1975	6	1954	38	1966,1978

APRIL

<u>Day</u>	<u>Highest Maximum (°F)</u>	<u>Year of Highest Maximum</u>	<u>Lowest Maximum (°F)</u>	<u>Year of Lowest Maximum</u>	<u>Lowest Minimum (°F)</u>	<u>Year of Lowest Minimum</u>	<u>Highest Minimum (°F)</u>	<u>Year of Highest Minimum</u>
1	72	1966	34	1975	7	1952	38	1978
2	69	1961	36	1982	6	1953	36	1961,1984
3	71	1961	33	1955	9	1953	37	1988
4	72	1960,1987	35	1958	13	1966	34	1953,59,63
5	75	1960	39	1975	9	1961	37	1954
6	73	1960	38	1957	9	1983	38	1960
7	70	1960,1977	36	1953	14	1954	39	1960
8	78	1977	35	1975	7	1982	36	1986
9	73	1960	37	1975	8	1959	37	1966,74,77
10	70	1985	40	1953	9	1988	40	1960
11	72	1988	37	1970	10	1953	43	1978
12	77	1988	39	1974	11	1954	36	1976,1982
13	74	1951,1988	40	1970	14	1987	43	1954
14	76	1985	41	1970	14	1981,1983	36	1965
15	77	1985	34	1967	15	1953,1977	38	1969
16	76	1987	41	1978	11	1982	45	1987
17	76	1987,1988	43	1968	12	1963	44	1988
18	76	1962	38	1966	12	1968	43	1985
19	82	1962	35	1970	15	1982	46	1981
20	79	1980	35	1970	11	1982	44	1965
21	76	1956,80,86	34	1963	9	1982	44	1965
22	79	1969	39	1958	16	1968	48	1980
23	78	1977	37	1964	12	1972	44	1969,1980
24	81	1977	39	1964	17	1984	45	1980
25	82	1977	35	1984	14	1950	49	1959
26	82	1987	34	1976	17	1972,1988	45	1952
27	82	1987	41	1963	19	1966	44	1954
28	79	1987	39	1970	15	1966,1984	40	1979
29	80	1987	36	1967	19	1970	46	1987
30	78	1977	33	1967	16	1950	43	1959

MAY

<u>Day</u>	<u>Highest Maximum (F)</u>	<u>Year of Highest Maximum</u>	<u>Lowest Maximum (F)</u>	<u>Year of Lowest Maximum</u>	<u>Lowest Minimum (F)</u>	<u>Year of Lowest Minimum</u>	<u>Highest Minimum (F)</u>	<u>Year of Highest Minimum</u>
1	82	1985	44	1950	13	1972	45	1980
2	83	1985	42	1964	16	1973	45	1982
3	84	1966	42	1964	19	1965	48	1971
4	84	1966	36	1975	20	1953,1984	48	1962
5	83	1966	45	1975	14	1982	49	1979
6	82	1966,1987	35	1965	18	1968	47	1951,1958
7	85	1987	45	1979	19	1984	48	1962
8	85	1987	42	1979	25	1959,1968	45	1963
9	84	1954	42	1983	22	1968	49	1962
10	84	1960	45	1970	19	1953	49	1954
11	87	1960	42	1983	22	1953	45	1960,69,84
12	85	1988	46	1956,1970	24	1972	49	1984
13	82	1959	48	1970	17	1985	54	1987
14	85	1987	48	1955	21	1970	52	1984
15	86	1987	39	1955	22	1986	46	1984
16	87	1988	43	1955	16	1974	51	1987
17	83	1954,1970	49	1977	24	1984	49	1972
18	86	1954	48	1978	23	1971	47	1982
19	91	1954	47	1959	24	1950,1960	52	1956
20	89	1958	46	1974	23	1950	57	1954
21	86	1958	43	1972	26	1973	54	1958
22	87	1967	50	1986	22	1953	50	1963
23	87	1988	49	1980	17	1966	49	1963
24	85	1958,1988	48	1980	28	1966,1986	53	1979
25	84	1958,1969 1983,1988	42	1980	23	1975	54	1958
26	88	1958	54	1980,1988	20	1978	51	1961
27	88	1958	53	1959	21	1973	53	1974
28	88	1983	48	1982	23	1955,1977	50	1958,1974
29	87	1986	50	1953	28	1977	52	1961,1983
30	87	1986	44	1988	25	1974,1977	52	1969,1983
31	90	1986	52	1955	23	1978	48	1956,1960

JUNE

<u>Day</u>	<u>Highest Maximum (°F)</u>	<u>Year of Highest Maximum</u>	<u>Lowest Maximum (°F)</u>	<u>Year of Lowest Maximum</u>	<u>Lowest Minimum (°F)</u>	<u>Year of Lowest Minimum</u>	<u>Highest Minimum (°F)</u>	<u>Year of Highest Minimum</u>
1	89	1977,1986	53	1971	27	1984	52	1986
2	89	1986	50	1950,1953	26	1954	51	1960
3	89	1988	53	1962	27	1950	58	1986
4	92	1988	50	1980	30	1955	52	1952
5	93	1977	51	1954	28	1966	56	1957,1985
6	93	1977	52	1954	28	1962	57	1977
7	92	1985	44	1950	27	1951,1962	59	1977
8	87	1956	53	1968	23	1979	55	1972
9	91	1952	56	1963,68,84	27	1979	56	1977
10	91	1956	47	1984	31	1958	51	1978
11	89	1979	56	1976	30	1978	54	1961,1962
12	94	1959	51	1970	30	1984	54	1953,1961
13	93	1974	50	1976	29	1966	60	1959
14	96	1974	56	1973	25	1976	58	1959
15	97	1974	56	1957	29	1981	59	1987
16	95	1974	57	1957,1973	32	1952	58	1951,1974
17	95	1974	53	1964,1973	29	1978	55	1960
18	96	1974	51	1975	27	1973	52	1961,1986
19	97	1988	58	1964	29	1954,1973	57	1959,1961
20	95	1961	63	1956,1964	28	1978	66	1988
21	98	1988	54	1964	33	1953,1960	56	1966
22	97	1961	62	1963	30	1956	62	1971
23	97	1988	63	1967	33	1951	69	1988
24	100	1988	51	1952	32	1976	56	1988
25	100	1988	55	1969	24	1966	63	1988
26	96	1970	59	1965	32	1966,1978	60	1988
27	94	1988	58	1969	28	1976	63	1961
28	94	1966,1979	62	1969	35	1975,1976	60	1988
29	97	1976,1979	54	1959	32	1969,1971	58	1987
30	94	1950	65	1970	29	1955	56	1976,1980

JULY

<u>Day</u>	<u>Highest Maximum (F)</u>	<u>Year of Highest Maximum</u>	<u>Lowest Maximum (F)</u>	<u>Year of Lowest Maximum</u>	<u>Lowest Minimum (F)</u>	<u>Year of Lowest Minimum</u>	<u>Highest Minimum (F)</u>	<u>Year of Highest Minimum</u>
1	96	1950	63	1955	33	1984	60	1981
2	96	1985,1986	69	1983	32	1973	59	1977
3	98	1985	68	1983	36	1974	60	1986
4	99	1985	57	1982	35	1957,1971	56	1988
5	98	1985	65	1982	35	1986	61	1954
6	98	1976,1985	72	1969	28	1986	66	1981
7	95	1975,1985	68	1981	33	1988	71	1985
8	96	1975	74	1959	29	1981	60	1975,76,85
9	99	1985	78	1982	37	1959,1981	60	1960
10	98	1973	61	1951	38	1984	61	1956
11	98	1976	64	1983	37	1983	65	1985
12	99	1954	65	1952	36	1951	61	1962,1988
13	99	1954	63	1962	36	1950,1965	63	1964
14	98	1955	73	1962	38	1984	61	1954
15	99	1955	78	1982	40	1970,81,84	66	1953
16	98	1971	65	1983	34	1983	65	1987
17	98	1955	66	1987	37	1986	71	1976
18	99	1951	63	1987	40	1968,1987	62	1977
19	100	1960	73	1987	35	1987	66	1951
20	101	1960	57	1972	36	1952	59	1951
21	100	1960,1988	64	1987	34	1983	63	1956,1966
22	99	1988	64	1973	39	1952	60	1955
23	98	1959	73	1984	33	1954	66	1982
24	99	1978,1988	67	1977	35	1970	64	1959
25	99	1978,1988	73	1965	42	1964	60	1981
26	96	1959,1960	77	1963,1981	40	1953	61	1954
27	98	1975	77	1962	40	1981	64	1988
28	97	1968	75	1978	39	1963,1967	67	1960
29	98	1972	71	1950	37	1959	65	1975
30	99	1988	61	1975	35	1950	65	1960
31	98	1988	71	1975	38	1970	61	1959,1966

AUGUST

<u>Day</u>	<u>Highest Maximum (F)</u>	<u>Year of Highest Maximum</u>	<u>Lowest Maximum (F)</u>	<u>Year of Lowest Maximum</u>	<u>Lowest Minimum (F)</u>	<u>Year of Lowest Minimum</u>	<u>Highest Minimum (F)</u>	<u>Year of Highest Minimum</u>
1	95	1955,1961	74	1975	38	1975	62	1951
2	99	1954	67	1953	36	1963	65	1974
3	97	1961	66	1976	40	1970,1981	62	1980
4	98	1961,1979	73	1951	40	1980	60	1951
5	95	1975,1979	66	1950	35	1980	63	1964
6	96	1983,1986	72	1950	38	1950,1962	64	1961,1971
7	98	1983	73	1979	37	1969	62	1979
8	98	1983	71	1985	39	1956,1967	67	1983
9	98	1972	73	1968,1974	35	1970,1985	60	1963,1983
10	99	1969	78	1962	40	1985	64	1954
11	97	1958	64	1985	38	1970,1980	65	1969
12	97	1958	69	1988	38	1985	60	1963
13	97	1958	70	1978	39	1957,69,82	61	1984
14	97	1958	62	1968	38	1959,1978	58	1972
15	96	1958,1962	62	1968	32	1978	64	1958
16	96	1958	55	1978	36	1968,1987	59	1984
17	95	1981,1982	55	1968	32	1987	67	1958
18	98	1986	54	1968	28	1978	61	1977
19	96	1961	53	1968	32	1978	59	1983
20	95	1982	54	1968	33	1964	62	1961
21	95	1976,1982	58	1968	33	1974	64	1951
22	96	1969	60	1968	33	1954,1988	57	1971
23	95	1956,1967	59	1960	30	1978	57	1976
24	98	1988	63	1960	34	1971,1978	59	1961
25	99	1988	65	1977	31	1960,1978	61	1969
26	94	1969,1985	66	1977	34	1960,1973	59	1970
27	94	1981,1986	61	1956	28	1954	58	1967
28	94	1986	61	1964	31	1960	59	1958
29	93	1954	61	1964	28	1975	57	1958,1981
30	96	1954	68	1951,1965	30	1964,1975	54	1963
31	95	1955	66	1984	29	1965	57	1954

SEPTEMBER

<u>Day</u>	<u>Highest Maximum (°F)</u>	<u>Year of Highest Maximum</u>	<u>Lowest Maximum (°F)</u>	<u>Year of Lowest Maximum</u>	<u>Lowest Minimum (°F)</u>	<u>Year of Lowest Minimum</u>	<u>Highest Minimum (°F)</u>	<u>Year of Highest Minimum</u>
1	96	1950	50	1973	29	1965	53	1953
2	95	1950	61	1961,1964	29	1975	56	1954
3	96	1950	52	1971	27	1964,1975	58	1978
4	96	1950	67	1971	27	1964	58	1982
5	94	1976	48	1970	30	1964	58	1978
6	96	1955	63	1965	27	1954	63	1976
7	93	1955,77,79	64	1971	31	1972	60	1963
8	90	1979	59	1962	34	1988	58	1950
9	90	1988	59	1961	22	1962	54	1950
10	90	1959	52	1972,1978	24	1970	59	1950
11	88	1959,1963	52	1978	29	1957,1964	57	1976
12	92	1953	52	1978	27	1951,1979	51	1958,1976
13	90	1953	54	1970	27	1967	55	1953,1959
14	87	1953,1981	50	1982	21	1970	54	1973
15	87	1953	52	1982	21	1970	49	1984
16	88	1981	38	1965	20	1970	57	1953
17	90	1981	41	1965	24	1965	53	1983
18	89	1956,1981	43	1978	14	1965	49	1963
19	89	1956	48	1986	16	1965	54	1973
20	84	1966	46	1983	14	1983	50	1963
21	87	1987	44	1968	16	1983	50	1952
22	90	1987	48	1961	20	1971	50	1976
23	92	1987	49	1961	22	1955,56,85	47	1966
24	91	1987	48	1984	16	1984	46	1967
25	86	1952	48	1955	12	1970	47	1951
26	84	1952	51	1986	18	1970	55	1982
27	86	1963	47	1959	19	1964	52	1983
28	85	1967	48	1965,1985	19	1950	48	1978
29	85	1957,1967	43	1971	16	1985	53	1977
30	86	1957	38	1971	15	1985	48	1983

OCTOBER

<u>Day</u>	<u>Highest Maximum (°F)</u>	<u>Year of Highest Maximum</u>	<u>Lowest Maximum (°F)</u>	<u>Year of Lowest Maximum</u>	<u>Lowest Minimum (°F)</u>	<u>Year of Lowest Minimum</u>	<u>Highest Minimum (°F)</u>	<u>Year of Highest Minimum</u>
1	85	1987	38	1971	15	1950	45	1953,1957
2	84	1987	51	1971	19	1950	55	1976
3	84	1987	47	1957,1969	16	1973	55	1974
4	82	1980,1988	46	1957	16	1973	46	1975
5	82	1988	51	1955,62,82	16	1981	47	1963
6	81	1979	51	1970	11	1955	46	1959
7	80	1979,80,87	41	1961	15	1955	47	1960
8	81	1979,1988	31	1985	17	1974,1977	45	1956
9	80	1953	44	1985	12	1968	49	1983
10	78	1951,1953,	50	1960,77,85	14	1985	45	1962
11	78	1950	42	1960	12	1977	46	1978
12	79	1950	36	1969	12	1986	51	1962
13	79	1958	35	1969	13	1969	53	1962
14	81	1958	44	1981,1983	7	1969	44	1957
15	79	1958	44	1984	7	1970	46	1979
16	77	1973	36	1969	9	1970,1984	49	1988
17	77	1973	34	1984	11	1970	40	1950,1988
18	77	1955,1973	39	1984	12	1964	40	1986
19	75	1974	40	1984	8	1982	48	1955
20	74	1974	40	1984	7	1982	43	1986
21	71	1964	42	1951,1953	12	1958	46	1975
22	70	1954,1963	34	1975	9	1958	41	1959
23	72	1952,1965	36	1975	9	1980	44	1983
24	72	1959	32	1975	8	1980	37	1977
25	71	1977	35	1975	12	1955	41	1963
26	69	1952	38	1970	12	1954	39	1950
27	70	1977	38	1970	9	194	34	1950
28	70	1952,1987	28	1971	8	1970	36	1974
29	70	1968	38	1971	8	1971	43	1950
30	71	1962	28	1971	3	1978	42	1950
31	68	1988	33	1971	6	1972	41	1987

NOVEMBER

<u>Day</u>	<u>Highest Maximum (F)</u>	<u>Year of Highest Maximum</u>	<u>Lowest Maximum (F)</u>	<u>Year of Lowest Maximum</u>	<u>Lowest Minimum (F)</u>	<u>Year of Lowest Minimum</u>	<u>Highest Minimum (F)</u>	<u>Year of Highest Minimum</u>
1	67	1965	28	1951	7	1951	44	1987
2	66	1978	27	1973	-3	1955	45	1987
3	65	1962,65,76,81	28	1973	-4	1973	41	1987
4	62	1965,1983	31	1973	4	1973	38	1958
5	67	1980	35	1959	-1	1959	44	1983
6	64	1965	35	1971	0	1967	38	1966
7	64	1980	35	1986	3	1971	39	1980
8	65	1976	33	1984	6	1955,1977	36	1973
9	65	1958,1973	25	1950	0	1977	36	1970,1982
10	63	1954	20	1950	-6	1950	32	1973,1980
11	63	1953	26	1978	7	1950	38	1983
12	62	1953	23	1955	1	1975	39	1954
13	59	1962	25	1978	-6	1955	38	1981
14	62	1963	24	1978	-2	1959	37	1981
15	55	1953,1967	9	1955	-19	1955	39	1953
16	60	1953	7	1955	-24	1955	35	1975
17	57	1976	20	1958	-2	1958,1978	38	1983
18	55	1976	21	1958	-2	1951,1977	36	1965
19	54	1954	18	1985	-5	1953,1977	34	1955
20	59	1966	18	1977	-4	1953	39	1955
21	58	1954	16	1985	-12	1977	33	1962
22	54	1976	17	1985	-20	1985	33	1974
23	60	1959	4	1985	-21	1985	35	1961
24	55	1959	18	1985	-10	1985	34	1960
25	54	1954	24	1980	-5	1952	35	1960
26	51	1950	23	1976,1985	-12	1985	32	1961,1977
27	55	1950	20	1952	-16	1979	31	1951
28	49	1953	15	1952	-13	1952	31	1951
29	49	1986	16	1975	-19	1979	33	1966
30	49	1950,1951	16	1985	-23	1975	35	1950

DECEMBER

<u>Day</u>	<u>Highest Maximum (F)</u>	<u>Year of Highest Maximum</u>	<u>Lowest Maximum (F)</u>	<u>Year of Lowest Maximum</u>	<u>Lowest Minimum (F)</u>	<u>Year of Lowest Minimum</u>	<u>Highest Minimum (F)</u>	<u>Year of Highest Minimum</u>
1	47	1969	15	1985	-13	1967	33	1966
2	47	1972,1975	19	1984	-11	1984	35	1987
3	55	1958	18	1984	-16	1984	35	1980
4	49	1975	10	1972	-27	1972	33	1980
5	51	1987	0	1972	-37	1972	30	1974
6	52	1987	10	1972	-18	1972	32	1975
7	47	1965	10	1972	-16	1971	35	1975
8	44	1968,1976	1	1972	-24	1972	30	1975
9	41	1979,1981	0	1972	-35	1972	30	1975
10	46	1981	-6	1972	-40	1972	32	1965
11	42	1950,1977	3	1972	-34	1972	28	1975
12	41	1956,1977	5	1972	-19	1963,1985	33	1975
13	45	1956	6	1972	-26	1972	30	1977
14	43	1986	9	1984	-21	1972	36	1977
15	45	1977	9	1972	-29	1972	38	1977
16	48	1962	12	1967	-20	1964	32	1957
17	47	1962	0	1964	-33	1964	32	1957
18	43	1962,1979	12	1964,1983	-26	1964	29	1950
19	43	1979	11	1983	-21	1984	30	1952
20	44	1958	5	1983	-19	1983	30	1952,1957 1964,1969
21	45	1974	-3	1983	-38	1983	33	1955,1964
22	51	1964	6	1983	-36	1983	37	1964
23	50	1955	-8	1983	-47	1983	34	1964
24	45	1964	11	1983	-38	1983	33	1964
25	43	1980	12	1982	-18	1952	30	1980
26	49	1976	8	1988	-13	1970	31	1980
27	53	1980	3	1988	-28	1988	31	1980
28	40	1965	7	1983	-20	1983	29	1951
29	42	1965	5	1988	-25	1978	32	1965,1980
30	42	1980	0	1978	-29	1978	25	1950
31	47	1980	3	1978	-37	1978	23	1955

APPENDIX 2 PRECIPITATION EXTREMES

The following are the precipitation records and corresponding year(s) observed at CFA from January 1950 through December 1988. The data provided are the maximum total daily accumulation of precipitation (liquid equivalent in inches). A depth of zero indicates that no precipitation has been observed on that day during the 39-year period of record.

<u>Day</u>	<u>January</u>		<u>February</u>		<u>March</u>		<u>April</u>		<u>May</u>		<u>June</u>	
	<u>Depth</u>	<u>Year</u>	<u>Depth</u>	<u>Year</u>	<u>Depth</u>	<u>Year</u>	<u>Depth</u>	<u>Year</u>	<u>Depth</u>	<u>Year</u>	<u>Depth</u>	<u>Year</u>
1	0.32	1955	0.43	1963	0.42	1964	0.18	1978	0.82	1959	0.48	1961,1971
2	0.20	1951	0.44	1961	0.27	1974	0.38	1986	0.30	1960	0.56	1964
3	0.20	1977	0.16	1963	0.26	1985	0.43	1958	0.08	1973	0.29	1957
4	0.27	1977	0.17	1974	0.15	1978	0.14	1978	0.26	1975	0.44	1963
5	0.25	1976	0.13	1978	0.22	1960	0.34	1953	0.49	1986	0.49	1968
6	0.44	1965	0.26	1966	0.25	1950	0.48	1957	0.40	1965	0.63	1983
7	0.47	1965	0.22	1951	0.25	1960	0.39	1965	0.44	1965	0.66	1968
8	0.52	1975	0.77	1960	0.16	1986	0.21	1986	0.44	1957	0.55	1984
9	0.12	1970,1985	0.58	1962	0.35	1986	0.31	1984	0.61	1979	0.81	1984
10	0.18	1978	0.58	1962	0.15	1952	0.24	1966	0.44	1963	1.64	1969
11	0.25	1979	0.54	1962	0.50	1986	0.13	1972,1975	0.60	1966	0.16	1968
12	0.22	1960	0.20	1978	0.33	1967	0.18	1982	0.76	1957	0.21	1955
13	0.45	1980	0.54	1954	0.08	1987	0.24	1973	0.70	1957	0.84	1967
14	0.22	1970	0.26	1954	0.43	1983	0.11	1957	0.40	1962	0.29	1973
15	0.18	1988	0.61	1986	0.18	1958	0.12	1975	0.58	1961	0.50	1962
16	0.51	1978	0.39	1986	0.21	1970	0.19	1978	0.95	1987	0.39	1976
17	0.14	1958	0.19	1963	0.25	1950	0.04	1961,1963,1975	0.46	1987	0.32	1964
18	0.37	1974	0.79	1986	0.12	1979	0.26	1961	0.59	1957	0.09	1962,1975
19	0.79	1969	0.56	1971	0.07	1955	0.54	1970	0.33	1957	0.16	1969
20	0.61	1957	0.36	1981	0.07	1981	1.51	1981	0.30	1970	0.31	1977
21	0.65	1985	0.15	1979	0.39	1958	0.37	1958	0.48	1972	0.25	1967
22	0.14	1982	0.16	1977	0.61	1973	0.42	1958	0.16	1965,1971	0.18	1987
23	0.40	1954	0.43	1957	0.15	1978	0.39	1964	0.56	1959	0.47	1972
24	0.25	1965	0.47	1969	0.11	1958	0.27	1960	0.70	1953	0.26	1950
25	0.11	1958	0.30	1958	0.18	1957,1972	0.67	1975	0.30	1956	0.79	1965
26	0.32	1969	0.21	1957	0.45	1975	0.57	1963	0.32	1964	0.65	1965
27	0.25	1968	0.15	1965	0.35	1981,1985	0.88	1963	0.28	1960	0.55	1959
28	0.52	1987	0.10	1976,1983	0.37	1963	0.38	1970	0.65	1964	0.20	1959
29	0.21	1981	0.40	1976	0.45	1982	0.24	1983	0.85	1971	0.47	1962
30	0.25	1981			0.20	1951	0.18	1954	0.23	1957	0.08	1957
31	0.72	1963			0.18	1951			0.14	1954		

Day	July		August		September		October		November		December	
	Depth	Year	Depth	Year	Depth	Year	Depth	Year	Depth	Year	Depth	Year
1	0.79	1987	0.24	1952	0.36	1973	0.60	1971	0.23	1987	0.46	1982
2	0.09	1980	0.15	1953	0.14	1985	0.51	1976	0.16	1987	0.25	1962
3	0.46	1980	0.43	1951	0.56	1971	0.32	1957	0.60	1968	0.41	1980
4	0.12	1961	0.41	1963	0.01	1960	0.01	1951	0.19	1963	0.44	1974
5	0.10	1950	0.28	1951	0.12	1970	0.25	1967	0.19	1973	0.34	1966
6	0.03	1960	0.54	1951	0.45	1978	0.00	ALL	0.43	1969	0.10	1971,1972,1982
7	0.16	1978	0.11	1964	0.73	1971	0.32	1961	0.57	1969	0.30	1950
8	0.05	1975	0.41	1961	0.66	1980	0.58	1973	0.12	1986,1988	0.27	1985
9	0.02	1980	0.56	1982	1.09	1961	0.39	1983	0.24	1984	0.33	1970
10	0.71	1983	0.01	1978	0.27	1985	0.30	1972	0.20	1958	0.26	1964
11	0.40	1970	0.72	1950	0.14	1956	0.18	1981	0.38	1985	0.15	1958
12	0.24	1985	0.21	1954	0.82	1976	0.38	1981	0.48	1973	0.29	1983
13	0.53	1962	0.59	1968	0.44	1982	0.11	1975	0.34	1988	0.16	1974
14	0.28	1964	0.41	1968	0.34	1986	0.31	1968	0.34	1971	0.30	1977
15	0.38	1985	0.13	1979	0.31	1959	0.35	1953	0.48	1954	0.14	1977
16	0.23	1958	0.31	1960	0.10	1977	0.42	1980	0.31	1972	0.16	1984
17	0.40	1987	0.29	1961	0.45	1961	0.17	1984	0.51	1964	0.23	1973
18	0.15	1985	0.14	1965	1.55	1961	0.17	1986	0.20	1973	0.39	1967
19	0.42	1973	0.70	1959	0.27	1963	0.14	1972,1979	0.29	1982	0.20	1964
20	0.35	1973	0.74	1959	0.70	1962	0.11	1955	0.21	1950	0.17	1981
21	0.83	1987	0.37	1968	0.49	1962	0.52	1975	0.13	1966	0.62	1964
22	0.73	1973	0.80	1960	0.08	1968	0.17	1985	0.70	1977	1.07	1964
23	1.25	1979	0.65	1976	0.29	1973	0.33	1970	0.36	1988	0.59	1982
24	0.35	1977	0.18	1987	0.01	1973	0.30	1974	0.58	1981	0.52	1959
25	0.15	1982	0.07	1977	0.21	1960	0.11	1975	0.50	1984	0.44	1959
26	0.18	1951	0.03	1970	0.20	1982	0.15	1956,1975	0.33	1964	0.24	1955
27	0.78	1984	0.09	1970	0.22	1983	0.74	1956	0.10	1951	0.27	1964
28	0.13	1951,1978	0.08	1964	0.37	1983	0.13	1967	0.28	1984	0.30	1974
29	0.70	1984	0.37	1971	0.06	1971	0.04	1964,1973	0.71	1970	0.15	1973
30	0.40	1985	0.23	1986	0.68	1971	0.65	1964	0.27	1970	0.29	1977
31	0.56	1985	0.40	1963			0.11	1982			0.17	1959

APPENDIX 3 SNOW FALL EXTREMES

The following are the snow fall records and corresponding year(s) observed at CFA from January 1950 through December 1988. The data provided are the maximum daily total accumulation of snow fall (in inches). A depth of zero indicates that no snow fall has been observed on that day during the 39-year period of record.

Day	January		February		March		April		May		June	
	Depth	Year	Depth	Year	Depth	Year	Depth	Year	Depth	Year	Depth	Year
1	3.5	1955	2.5	1952	4.9	1964	0.7	1967	0.0	ALL	0.0	ALL
2	2.8	1951	5.0	1961	3.0	1979	3.0	1955	0.0	ALL	0.0	ALL
3	2.5	1973	0.5	1975	3.0	1985	0.9	1958	0.0	ALL	0.0	ALL
4	5.0	1977	1.0	1976	2.0	1956	1.0	1980	0.0	ALL	0.0	ALL
5	3.0	1976	3.5	1975	2.3	1960	0.9	1964	2.0	1978	0.0	ALL
6	1.5	1959	3.0	1966	1.3	1962	3.4	1957	3.9	1965	0.0	ALL
7	2.0	1960	1.5	1962	1.8	1960	2.4	1965	4.4	1965	0.0	ALL
8	3.0	1975	7.5	1960	0.5	1951	0.2	1982	1.0	1979	0.0	ALL
9	1.4	1970	4.0	1978	1.3	1962	1.0	1984	2.0	1979	0.0	ALL
10	5.0	1978	5.0	1984	2.0	1952	0.4	1955	0.0	ALL	0.0	ALL
11	4.0	1971	5.6	1973	2.7	1954	1.0	1975	1.7	1966	0.0	ALL
12	3.3	1960	2.1	1969	3.3	1967	0.5	1975	0.7	1970	0.0	ALL
13	3.1	1957	6.4	1973	1.1	1956	0.5	1975	0.2	1951,1970	0.0	ALL
14	2.5	1970	3.0	1954	0.3	1988	0.2	1955,70,73	0.2	1955	0.0	ALL
15	2.0	1952,1988	3.2	1962	3.6	1958	0.5	1970	1.8	1955	0.0	ALL
16	5.0	1978	4.0	1952	1.9	1971	0.3	1959,1975	2.7	1955	0.0	ALL
17	1.0	1958,1988	2.1	1955	3.0	1982	0.4	1968	0.0	ALL	0.0	ALL
18	2.2	1973	2.0	1961	1.0	1977,1982	0.4	1963	1.1	1960	0.0	ALL
19	4.4	1969	7.2	1971	1.1	1955	6.5	1970	1.2	1959	0.0	ALL
20	8.5	1957	3.2	1956	0.9	1964	1.0	1963	0.0	ALL	0.0	ALL
21	5.0	1985	2.0	1979	1.0	1980,1981	3.0	1958	0.0	ALL	0.0	ALL
22	4.0	1982	1.0	1974,1977 1980,1984	8.6	1973	3.4	1958	0.0	ALL	0.0	ALL
23	5.0	1972	2.0	1987	1.0	1975	3.9	1964	0.0	ALL	0.0	ALL
24	2.6	1967	5.1	1969	0.7	1954	2.2	1961	0.0	ALL	0.0	ALL
25	3.4	1956	2.4	1966	3.0	1975	3.0	1984	0.0	ALL	0.0	ALL
26	3.5	1956	0.7	1964	0.6	1958	1.5	1976	0.0	ALL	0.0	ALL
27	2.5	1968	2.0	1979	5.0	1985	4.7	1963	0.0	ALL	0.0	ALL
28	2.0	1981	2.5	1983	0.7	1960	6.7	1970	0.0	ALL	0.0	ALL
29	2.5	1981	2.0	1976	2.0	1970	2.0	1967	4.0	1979	0.0	ALL
30	3.0	1981			1.2	1959	0.0	ALL	0.0	ALL	0.0	ALL
31	2.6	1967			1.0	1982			0.0	ALL		

<u>Day</u>	<u>July</u>		<u>August</u>		<u>September</u>		<u>October</u>		<u>November</u>		<u>December</u>	
	<u>Depth</u>	<u>Year</u>	<u>Depth</u>	<u>Year</u>	<u>Depth</u>	<u>Year</u>	<u>Depth</u>	<u>Year</u>	<u>Depth</u>	<u>Year</u>	<u>Depth</u>	<u>Year</u>
1	0.0	ALL	0.0	ALL	0.0	ALL	4.5	1971	0.0	ALL	6.5	1982
2	0.0	ALL	0.0	ALL	0.0	ALL	1.5	1969	0.0	ALL	1.9	1952
3	0.0	ALL	0.0	ALL	0.0	ALL	0.2	1969	0.7	1961	5.0	1972
4	0.0	ALL	0.0	ALL	0.0	ALL	0.0	ALL	1.8	1956	7.0	1983
5	0.0	ALL	0.0	ALL	0.0	ALL	0.0	ALL	0.0	ALL	3.4	1966
6	0.0	ALL	0.0	ALL	0.0	ALL	0.0	ALL	0.0	ALL	2.5	1972
7	0.0	ALL	0.0	ALL	0.0	ALL	3.0	1961	0.8	1969	3.6	1950
8	0.0	ALL	0.0	ALL	0.0	ALL	0.0	ALL	1.5	1986	3.0	1963
9	0.0	ALL	0.0	ALL	0.0	ALL	0.0	ALL	0.0	ALL	3.0	1970
10	0.0	ALL	0.0	ALL	0.0	ALL	0.2	1985	2.0	1975	2.6	1964
11	0.0	ALL	0.0	ALL	0.0	ALL	0.0	ALL	3.0	1985	0.7	1952
12	0.0	ALL	0.0	ALL	0.0	ALL	0.0	ALL	3.1	1964	3.0	1971,1983
13	0.0	ALL	0.0	ALL	0.9	1970	0.0	ALL	3.5	1988	2.5	1974
14	0.0	ALL	0.0	ALL	0.0	ALL	0.8	1981	1.5	1957,1971	0.6	1964,1972
15	0.0	ALL	0.0	ALL	0.0	ALL	0.0	ALL	1.1	1971	0.6	1957
16	0.0	ALL	0.0	ALL	0.0	ALL	0.2	1969	2.0	1972	2.0	1984
17	0.0	ALL	0.0	ALL	0.5	1965	0.0	ALL	5.1	1964	2.1	1973
18	0.0	ALL	0.0	ALL	0.0	ALL	1.0	1984	0.6	1956	6.0	1967
19	0.0	ALL	0.0	ALL	0.0	ALL	0.0	ALL	2.5	1979	1.5	1964
20	0.0	ALL	0.0	ALL	0.0	ALL	0.0	ALL	1.5	1950	1.2	1963
21	0.0	ALL	0.0	ALL	1.0	1961	1.5	1975	0.5	1983	3.0	1973
22	0.0	ALL	0.0	ALL	0.0	ALL	0.0	ALL	6.0	1977	4.5	1971
23	0.0	ALL	0.0	ALL	0.0	ALL	2.8	1970	5.0	1963	2.0	1979
24	0.0	ALL	0.0	ALL	0.0	ALL	0.0	ALL	6.5	1981	3.7	1968
25	0.0	ALL	0.0	ALL	0.0	ALL	0.0	ALL	4.0	1983	3.0	1968
26	0.0	ALL	0.0	ALL	0.0	ALL	0.1	1970	3.0	1964	2.6	1968
27	0.0	ALL	0.0	ALL	0.0	ALL	0.7	1961	1.0	1951	2.7	1964
28	0.0	ALL	0.0	ALL	0.0	ALL	0.0	ALL	4.0	1975,1984	4.1	1972
29	0.0	ALL	0.0	ALL	0.0	ALL	0.0	ALL	2.0	1970	0.8	1966
30	0.0	ALL	0.0	ALL	0.2	1959,1971	2.0	1971	2.5	1970	4.0	1977,1981
31	0.0	ALL	0.0	ALL	0.0	ALL	0.6	1956			2.0	1 9 5 9

APPENDIX 4 SNOW DEPTH EXTREMES

The following are the extreme snow depth records and corresponding year(s) observed at CFA from January 1950 through December 1988. The data provided are the daily maximum observed snow depths (in inches). A depth of zero indicates that no significant snow depth has been observed on the ground on that day during the 39-year period of record.

<u>Day</u>	<u>January</u>		<u>February</u>		<u>March</u>		<u>April</u>		<u>May</u>		<u>June</u>	
	<u>Depth</u>	<u>Year</u>	<u>Depth</u>	<u>Year</u>	<u>Depth</u>	<u>Year</u>	<u>Depth</u>	<u>Year</u>	<u>Depth</u>	<u>Year</u>	<u>Depth</u>	<u>Year</u>
1	13	1984	14	1952,1985	20	1985	12	1985	0	ALL	0	ALL
2	13	1984,1986	15	1952	21	1985	8	1985	0	ALL	0	ALL
3	13	1984,1986	15	1952	24	1985	5	1985	0	ALL	0	ALL
4	13	1986	15	1952	24	1985	3	1952	0	ALL	0	ALL
5	14	1986	14	1952,1985	24	1985	1	1952,1958	2	1978	0	ALL
6	14	1986	14	1952,1985	25	1985	2	1957	0	ALL	0	ALL
7	13	1986	14	1985	25	1985	1	1957,1965	5	1965	0	ALL
8	13	1986	18	1985	24	1985	0	ALL	0	ALL	0	ALL
9	13	1986	20	1985	24	1985	1	1984	2	1979	0	ALL
10	13	1986	20	1985	23	1985	0	ALL	0	ALL	0	ALL
11	13	1986	20	1985	23	1952,1985	1	1975	0	ALL	0	ALL
12	13	1986	20	1985	23	1985	1	1975	0	ALL	0	ALL
13	13	1986	20	1985	23	1985	2	1975	0	ALL	0	ALL
14	13	1986	20	1985	23	1985	0	ALL	0	ALL	0	ALL
15	13	1986	19	1985	22	1985	0	ALL	1	1955	0	ALL
16	13	1986	19	1985	22	1952,1985	1	1970,1971	0	ALL	0	ALL
17	12	1984	19	1985	21	1952,1985	0	ALL	0	ALL	0	ALL
18	12	1984	19	1985	21	1952	0	ALL	0	ALL	0	ALL
19	12	1984	19	1985	21	1952	1	1957,1963	0	ALL	0	ALL
20	12	1984	21	1985	21	1952	6	1970,1971	0	ALL	0	ALL
21	14	1985	22	1952	20	1952	3	1970,1971	0	ALL	0	ALL
22	14	1985	22	1952	20	1952	1	1958	0	ALL	0	ALL
23	14	1985	22	1952	19	1952	5	1964	0	ALL	0	ALL
24	14	1985	21	1952	18	1952	2	1960,1961	0	ALL	0	ALL
25	14	1985	21	1952	16	1952	3	1984	0	ALL	0	ALL
26	14	1985	20	1952,1985	14	1952	2	1976	0	ALL	0	ALL
27	14	1985	20	1952,1985	17	1985	6	1976	0	ALL	0	ALL
28	14	1985	20	1952,1985	17	1985	6	1970,1971	0	ALL	0	ALL
29	14	1985	19	1952	16	1985	2	1970,1971	4	1979	0	ALL
30	14	1985			15	1985	1	1967	0	ALL	0	ALL
31	14	1985			14	1985			0	ALL		

<u>Day</u>	<u>July</u>		<u>August</u>		<u>September</u>		<u>October</u>		<u>November</u>		<u>December</u>	
	<u>Depth</u>	<u>Year</u>	<u>Depth</u>	<u>Year</u>	<u>Depth</u>	<u>Year</u>	<u>Depth</u>	<u>Year</u>	<u>Depth</u>	<u>Year</u>	<u>Depth</u>	<u>Year</u>
1	0	ALL	0	ALL	0	ALL	0	ALL	1	1956,1971	9	1985
2	0	ALL	0	ALL	0	ALL	0	ALL	1	1956,1971	10	1985
3	0	ALL	0	ALL	0	ALL	0	ALL	0	ALL	13	1985
4	0	ALL	0	ALL	0	ALL	0	ALL	1	1956	12	1983
5	0	ALL	0	ALL	0	ALL	0	ALL	1	1956	14	1983
6	0	ALL	0	ALL	0	ALL	0	ALL	0	ALL	14	1983
7	0	ALL	0	ALL	0	ALL	0	ALL	0	ALL	14	1983
8	0	ALL	0	ALL	0	ALL	0	ALL	1	1986	13	1985
9	0	ALL	0	ALL	0	ALL	0	ALL	1	1960,1986	12	1985
10	0	ALL	0	ALL	0	ALL	0	ALL	2	1975	12	1985
11	0	ALL	0	ALL	0	ALL	0	ALL	3	1985	12	1985
12	0	ALL	0	ALL	0	ALL	0	ALL	3	1985	13	1983
13	0	ALL	0	ALL	0	ALL	0	ALL	3	1978,1985	13	1983
14	0	ALL	0	ALL	0	ALL	1	1981	5	1988	13	1983
15	0	ALL	0	ALL	0	ALL	0	ALL	4	1988	13	1983
16	0	ALL	0	ALL	0	ALL	0	ALL	4	1988	13	1983
17	0	ALL	0	ALL	0	ALL	0	ALL	6	1964	13	1983
18	0	ALL	0	ALL	0	ALL	1	1984	7	1988	13	1983
19	0	ALL	0	ALL	0	ALL	0	ALL	7	1988	13	1983
20	0	ALL	0	ALL	0	ALL	0	ALL	6	1964,1985,1988	13	1983
21	0	ALL	0	ALL	0	ALL	2	1975	6	1964,1985,1988	13	1983
22	0	ALL	0	ALL	0	ALL	1	1975	6	1964,1977,1985	13	1983
23	0	ALL	0	ALL	0	ALL	1	1975	6	1985	13	1982,1983
24	0	ALL	0	ALL	0	ALL	0	ALL	6	1981,1985	13	1983
25	0	ALL	0	ALL	0	ALL	0	ALL	8	1985	13	1983
26	0	ALL	0	ALL	0	ALL	0	ALL	8	1985	13	1983
27	0	ALL	0	ALL	0	ALL	0	ALL	8	1985	13	1983
28	0	ALL	0	ALL	0	ALL	0	ALL	8	1985	13	1983
29	0	ALL	0	ALL	0	ALL	0	ALL	8	1985	13	1983
30	0	ALL	0	ALL	0	ALL	0	ALL	9	1985	13	1983
31	0	ALL	0	ALL			2	1971			13	1983

NOTES